

9-1-2015

DESIGN, SYNTHESIS AND EVALUATION OF BIVALENT INHIBITORS OF TREHALOSE-6-PHOSPHATE PHOSPHATASE

Chunliang LIU

Follow this and additional works at: https://digitalrepository.unm.edu/chem_etds

 Part of the [Physical Chemistry Commons](#)

Recommended Citation

LIU, Chunliang. "DESIGN, SYNTHESIS AND EVALUATION OF BIVALENT INHIBITORS OF TREHALOSE-6-PHOSPHATE PHOSPHATASE." (2015). https://digitalrepository.unm.edu/chem_etds/1

This Dissertation is brought to you for free and open access by the Electronic Theses and Dissertations at UNM Digital Repository. It has been accepted for inclusion in Chemistry ETDs by an authorized administrator of UNM Digital Repository. For more information, please contact disc@unm.edu.

Chunliang Liu

Candidate

Chemistry and Chemical Biology

Department

This dissertation is approved, and it is acceptable in quality and form for publication:

Approved by the Dissertation Committee:

Debra Dunaway-Mariano, Chairperson

Patrick S. Mariano

Fu-Sen Liang

Karen N. Allen

**DESIGN, SYNTHESIS AND EVALUATION OF BIVALENT
INHIBITORS OF TREHALOSE-6-PHOSPHATE
PHOSPHATASE**

by

CHUNLIANG LIU

B.S., Biotechnology, Lanzhou University, 2008

M.S., Biochemistry and Molecular Biology, Lanzhou University, 2011

DISSERTATION

Submitted in Partial Fulfillment of the
Requirements for the Degree of

**Doctor of Philosophy
Chemistry**

The University of New Mexico
Albuquerque, New Mexico

June, 2015

ACKNOWLEDGEMENTS

I would like to express my deepest gratitude and respect to my advisors, Dr. Debra Dunaway-Mariano and Dr. Patrick S. Mariano, for guiding my research for the past several years and for helping me to develop my background in biochemistry, and carbohydrate synthesis. I also appreciate their understanding, patience, and providing me with an excellent atmosphere for doing research, without their guidance and persistent help this dissertation would not have been possible.

My sincere thanks must also go to Dr. Fu-Sen Liang and Dr. Karen N Allen, members of my doctoral committee. I wish to thank them for reading and evaluating my dissertation. I would also like to thank all of the past and present members in Dr. Debra Dunaway-Mariano's group for their help and friendship.

I would also like to extend my thanks Dr. Jeremiah Farelli, a postdoctoral in Dr. Karen N. Allen's Lab, for his many contributions to T6PP structure determination and high throughput screening for T6PP inhibitors.

Finally, I would like to thank two other people who are very important in my life: My wife, Qin Zhou and my son, Kevin Josiah Liu. I thank Qin for everything. I thank my little son for making me so happy with his cute smile.

**DESIGN, SYNTHESIS AND EVALUATION OF BIVALENT
INHIBITORS OF TREHALOSE-6-PHOSPHATE
PHOSPHATASE**

BY

CHUNLIANG LIU

ABSTRACT OF DISSERTATION

Submitted in Partial Fulfillment of the
Requirements for the Degree of

**Doctor of Philosophy
Chemistry**

The University of New Mexico
Albuquerque, New Mexico

June, 2015

DESIGN, SYNTHESIS AND EVALUATION OF BIVALENT INHIBITORS OF TREHALOSE-6-PHOSPHATE PHOSPHATASE

Chunliang Liu

B.S., Biotechnology, Lanzhou University, 2008

M.S., Biochemistry and Molecular Biology, Lanzhou University, 2011

Ph.D., Chemistry and Chemical Biology, University of New Mexico, 2015

ABSTRACT

The D-glucose disaccharide α, α' -D-trehalose is synthesized by a variety of bacteria, fungi, plants and invertebrates to support cell survival by functioning as a fuel, a metabolic regulator or a protectant against environmental stress. Five different trehalose biosynthetic pathways are known to exist, one of which, the OtsA/OtsB pathway is common among pathogenic bacteria and fungi and is also found in parasitic nematodes. Previously reported otsA and otsB gene knockout (or knockdown) experiments have shown that both pathway enzymes are essential for *M. tuberculosis* cell growth and host colonization. RNAi gene silencing carried out in the nematode model system *Caenorhabditis elegans* revealed that the T6P phosphatase is essential. Based on these findings we concluded that trehalose-synthesizing pathogens are likely to be vulnerable to the action of small molecule inhibitors of T6P phosphatase. We designed a bi-module inhibitor prototype. Accordingly, the phosphate group of the trehalose 6-phosphate moiety was replaced by a phosphate mimetic for targeting the active site of the catalytic domain, and the glucose unit was modified for

targeting the cap domain for induced cap closure over the active site. Sulfate proved to be the most effective warhead for the substrate-binding site. T6S binding was shown by using Single Angle X-ray Scattering (SAXS) analysis to induce cap closure. Using glucose-6-sulfate as the platform, a series of synthetic derivatives possessing “drug-like” functions tethered to the glucose ring were evaluated. Of these first generation inhibitors 4-n-octylphenyl- α -D-glucopyranoside 6-sulfate proved to be the tightest binding T6PP competitive inhibitor. In parallel, we have used the glucose-6-sulfate as the scaffold in the design of active site-directed, irreversible inhibitors. From the adducts which were synthesized and tested for T6PP inactivation, 4-n-octylphenyl-2-(3-(fluorosulfonyl)benzoylamino)-2-deoxy- α -D-glucopyranoside-6-sulfate was selected for further characterization, and subsequently shown to inactivate the T6PPs with stoichiometric covalent modification and reasonable efficiency. Bioinformatic analysis and site-directed mutagenesis methods were used to identify the modified residue, a stringently conserved lysine residue was identified. Based on this result, the design and synthesis of the second generation of irreversible inhibitors that are optimized this target site is planned for future work.

TABLE OF CONTENTS

ABBREVIATIONS	xiii
Chapter One	
Trehalose-6-Phosphate Phosphatase as a New Candidate Drug Target in Filarial Nematodes and Pathogenic Bacteria	1
References	8
Chapter Two	
Cloning, Expression, Purification and Kinetics of Trehalose-6-Phosphate Phosphatase Homologues	
2.1 Introduction	11
2.2 Materials and Methods	11
2.2.1 General Methods	11
2.2.2 Preparation of Recombinant Wild-type T6PPs	12
2.2.2.1 Preparation of Recombinant Wild-type Mycobacterium tuberculosis T6PP	12
2.2.2.2 Preparation of Recombinant Wild-type Shigella boydii T6PP	15
2.2.2.3 Preparation of Recombinant Wild-type Ascaris suum T6PP	16
2.2.2.4 Preparation of Recombinant Wild-type Salmonella typhimurium T6PP	17
2.2.3 T6PPs Molecular Weight Determination	19
2.2.4 Steady-state kinetic constant determinations	19
2.2.4.1 Method for determination of Mt-T6PP steady-state kinetic constants	19

2.2.4.2 Method for determination of Sb-T6PP Steady-state kinetic constants	20
2.2.4.3 Method for determination of As-T6PP steady-state kinetic constants	20
2.2.4.4 Method for determination of St-T6PP steady-state kinetic constants	21
2.2.4.5 Method for determination of Bm-T6PP steady-state kinetic constants	21
2.3 Results and Discussion	22
2.3.1 Preparation of the recombinant T6P Phosphatases	22
2.3.2 ES-MS Determination of the exact mass of the purified proteins	24
2.3.3 T6PPs Substrate Specificity Profile	28
2.3.4 Quaternary structure determination	31
2.3 Conclusion	31
2.4 References	32

Chapter Three

Trehalose-6-Phosphate Phosphatase Inhibitor Design, Synthesis and Evaluation

3.1 Background	33
3.2 Research Strategy	34
3.3 Inhibitor Selection and Synthesis	34
3.4 Results and Discussion	36
3.4.1 Determination of the Source(s) of T6PP Substrate Binding Energy	36
3.4.2 Analysis of the T6PP Active Site	38
3.4.3 Binding Affinities of Inert T6P Analogs: Evaluation of Phosphate Mimetic Groups	41
3.4.3 Synthetic Routes to the T6P Analogs 1-4	44

3.4.4 Examination of Substrate (Analog) Induced Conformational Changes in T6P Phosphatases Using SAXS	45
3.5 Material and Methods	53
3.5.1 Inhibitor Synthesis	53
3.5.2 References for synthesis	66
3.5.3 SAXS measurements and data analysis	67
3.5.4 KI measurement	68
3.5.5 EnzChek Phosphate Assay	69
3.5.6 Site-Directed Mutagenesis	69
3.6 References	70

Chapter Four

Synthesis and Evaluation of First Generation Trehalose-6-Phosphate Phosphatase

Reversible Biomodular Inhibitors

4.1. Background	75
4.3 Results and Discussion	77
4.3.1. Substrate Recognition: Diversity in the T6PP Cap Domain Residue Usage and Function.....	77
4.3.2 Synthesis	86
4.3.3 Catalytic hydrolysis of Compound 7 by T6PP	90
4.3.4 Inhibition measurement using High Throughput Screening.....	91
4.3.4 Competitive inhibition test.....	94
4.3.6 Inhibition Constants	95

4.3.7 SAXS studies	97
4.3.8 Inhibition Specificity	103
4.3.9 Molecular Modeling.....	105
4.4 Material and Methods	108
4.4.1 Inhibitor Synthesis	108
4.4.2 References for Inhibitor Synthesis.....	121
4.5 References.....	128

Chapter Five

Irreversible Inhibition of HAD Family Member Trehalose-6-Phosphate Phosphatase with Active Site Directed Biomodular Inhibitors

5.1 Abstract	132
5.2. Introduction.....	132
5.3. Results	137
5.3.1 Synthesis of T6PP irreversible inhibitors	137
5.3.2 Biological activity of irreversible inhibitors	139
5.3.2.1 Screening the irreversible inhibitors' inactivation and inhibition activities on T6PPs	139
5.3.2.2 Kinetic analysis of T6PPs inactivation by 26	141
5.3.2.3 Mass spectrometry analysis of T6PPs inactivation by 26.....	144
5.3.3. Identification of modified residues by compound 26	147
5.3.4. Molecular Modeling.....	149
5.3.4 Inactivation specificity of 26	152

5.5 Conclusion	153
5.5 Material and Methods	154
5.5.1 Inhibitor Synthesis	154
5.5.2 Reference for synthesis	173
5.5.3 Expression and Purification of T6PPs	174
5.5.4 Kinetic Characterization of T6PPs Inactivation by 26.....	174
5.5.5 ES-MS Analysis of T6PP Modification by Inhibitor 26	176
5.6 References.....	176
APPENDIX	180
A.1 Published Collaborative Work	180
A.1.1 Covalent docking predicts substrates for haloalkanoate dehalogenase superfamily phosphatases	180
A.1.2 Structure of the trehalose-6-phosphate phosphatase from <i>Brugia malayi</i> reveals key design principles for anthelmintic drugs	181
A.1.3 An improved method for the large scale preparation of α , α' -trehalose-6- phosphate	183
A.1.4 Panoramic view of a superfamily of phosphatases through substrate profiling	184
A.2 Plots in Chapter Two.....	185
A.3 Plots in Chapter Three.....	188
A. 4 Plots in Chapter Four	203
A.4.1 Bm-T6PP kinetic Plots in Table 4.1	203

A.4.2 Bm-T6PP kinetic Plots in Table 4.4	210
A.5 ESI mass spectra In Chapter Five	220
A.5.1 ESI mass spectra of Bm-T6PP treated with 26	220
A.5.2 ESI mass spectra of Sb-T6PP treated with 26	221
A.5.3 ESI mass spectra of Mt-T6PP treated with 26	222
A.5.4 ESI mass spectra of St-T6PP treated with 26	223
A.5.5 ESI mass spectra of Mt-T6PP-K253A	225
A.5.6 ESI mass spectra of Mt-T6PP-K253A treated with 26	226
A.5.7 ESI mass spectra of Bm-T6PP-K334A.....	227
A.5.8 ESI mass spectra of Bm-T6PP-K334A treated with 26	228
A.5.9 Sequence alignments of nematode and bacteria T6PP enzymes	229
A.5.10 Plots of <i>pseudo-first order rate</i> constant for inactivation (k_{obs})	230
A.5.10.1 Plots of k_{obs} for 26 mediated As-T6PP inactivation	230
A.5.10.2 Plots of k_{obs} for 26 mediated Bm-T6PP inactivation.....	231
A.5.10.3 Plots of k_{obs} for 26 mediated Mt-T6PP inactivation.....	231
A.5.10.4 Plots of k_{obs} for 26 mediated Sb-T6PP inactivation	232
A.5.10.5 Plots of k_{obs} for 26 mediated St-T6PP inactivation	232

ABBREVIATIONS

A	Alanine
AA	Amino Acid
Arg/R	Arginine
Asn/N	Asparagine
Asp/D	Aspartic acid
ATCC	American Type Culture Collection
Bp	Base-Pair
Blast	Basic Local Alignment Search Tool
C	Cysteine
cDNA	Complementary Deoxyribonucleic acid
Da	Dalton
DNA	Deoxyribonucleic acid
DI H ₂ O	Distilled and deionized water
3-D	Three dimensional
DMSO	Dimethyl sulfoxide
DTT	Dithiothreitol
E	Enzyme
EC	Enzyme Commission
E.coli	Escherichia Coli
EDTA	Disodium ethylenediamine tetraacetate

ESI-MS	Electrospray ionization Mass spectrometry
EXPASY	Expert protein analysis system
F-6-P	Fructose-6-phosphate
FPLC	Fast Protein Liquid Chromatography
g	Gram
Gln/Q	Glutamine
Glu/E	Glutamate
Gly/G	Glycine
β G1P	β -D-Glucose-1-Phosphate
β G1,6bisP	β -D-Glucose 1,6-(bis)phosphate
GDH	α -Glycerophosphate dehydrogenase
GmhB	D-glycero-D-manno-heptose 1,7-bisphosphate phosphatase
h	Hour
HADSF	Haloalkanoic acid dehalogenase superfamily
H-bond	Hydrogen bond
HEPES	4-(2-Hydroxyethyl)-1-piperazineethanesulfonic acid
His/H	Histidine
HPLC	High Performance Liquid Chromatography
Ile/I	Isoleucine
IPTG	Isopropylthio- β -galactoside
k	Rate constant

k_{cat}	Enzyme turnover rate
Kd	Dissociation constant
Km	Michaelis-Menten constant
Ki	Inhibition Constant
kobs	Observed rate constant
kDa	Kilo-Dalton
KDN	2-Keto-3-deoxy-D-glycero-D-galacto-nononic acid
KDN9P	2-Keto-3-deoxy-D-glycero-D-galacto-nononate 9-phosphate
KDO	2-Keto-3-deoxy-D-manno-octulosonic acid
KDO8P	2-Keto-3-deoxy-D-manno-octulosonate 8-phosphate
L	Liter or Leucine
LB	Luria-Bertani
Lys/K	Lysine
mg	Milligram
min	Minute
ml	Milliliter
mmole	Millimole
MS	Mass spectrum
MW	Molecular Weight
mRNA	Messenger Ribonucleic acid
Met/M	Methionine

ng	Nanogram
NADH	β -Nicotinamide adenine dinucleotide, reduced form
NCBI	National Center for Biotechnology Information
OD	Optical density
ORF	Open reading frame
pfu	Plaque forming units
PDB	Protein Data Bank
PCR	Polymerase Chain Reaction
PAGE	Polyacrylamide gel electrophoresis
PEP	Phosphoenolpyruvate
Phe/F	Phenylalanine
Pi	Inorganic phosphate
PPi	Pyrophosphate
pI	Isoelectric point
PNPP	p-nitrophenyl phosphate
Pro/P	Proline
RNA	Ribonucleic acid
RT	Room Temperature
rpm	Rotation per minute
s	Second
S	Substrate/Serine

SDS	Sodium dodecyl sulfate
SN	Nucleophilic substitution
T6P	Trehalose-6-hosphate
T6PP	Trehalose-6-phosphate Phosphatase
Thr/T	Threonine
Tris	Tris[hydroxymethyl]aminomethane
Trp/W	Tryptophan
Tyr/Y	Tyrosine
U	Uridine
μM	Micromolar
UDP	Uridine diphosphate
UV	Ultraviolet
Val/V	Valine
V _{max}	Maximum Velocity
V	Volume
WT	Wild type

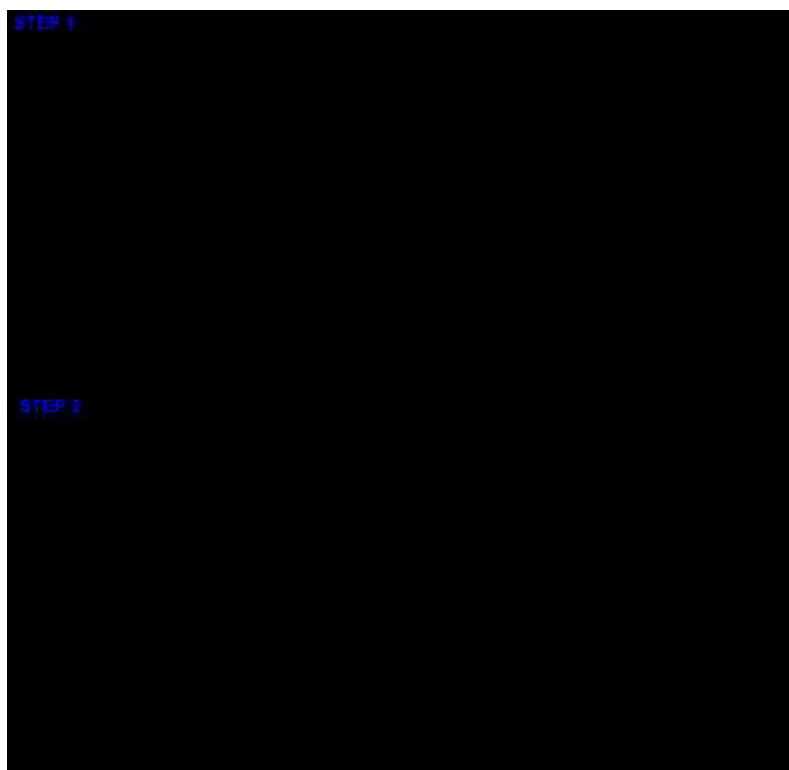
CHAPTER ONE

TREHALOSE-6-PHOSPHATE PHOSPHATASE AS A NEW CANDIDATE DRUG TARGET IN FILARIAL NEMATODES AND PATHOGENIC BACTERIA

Some of the most chronically debilitating diseases caused by parasitic nematodes plague the low-income populations of Africa, Asia, and the Americas. One of these diseases is Lymphatic filariasis, a mosquito borne disease caused by *Brugia malayi*, *Wuchereria bancrofti* and *Brugia timori*. This disease affects around 120 million people worldwide in tropical and sub-tropical countries putting 1.3 billion people at risk (WHO, 2009) [1, 2]. Filarial infections are responsible for extreme infirmity, distress, and social stigma. In fact, lymphatic filariasis is a major cause of permanent and longterm disability in people worldwide [3]. Because of the nature of infection and the impact on people suffering from this disease, the Global Program for the Elimination of Lymphatic Filariasis (GPELF) was established in 1999 with the main goal of ending the transmission of this disease by 2020. Currently, the recommended treatment for lymphatic filariasis is the administration of albendazole together with ivermectin or diethylcarbamazine citrate. Even though these treatments are effective in community-wide treatment programs, they are not without drawbacks. One problem is the fact that these drugs can only kill microfilariae, leaving the adult worms intact. Consequently, the treatment must be continued during the entire reproductive life span of the adult worm (about 5 years) [4]. The other issue is that the drug

combination can prove lethal if administered to individuals with high microfilarial loads caused by a co-infection by *Loa loa* [5]. Therefore, new drugs which are not subject to these limitations are in demand.

Parasitic nematode model systems are needed to facilitate the drug-discovery programs. The laboratory-based investigation is difficult because of the complicated life cycle of nematodes. *C. elegans* has served as a model system for research on free-living nematodes for decades [6-8]. Fortunately, *B. malayi* can be maintained in a *jird* host, which is amenable to in vitro studies at different stages of its life-cycle [9, 10]. Presently, both *C. elegans* and *B. malayi* serve as plausible models for research on lymphatic filarial nematodes. Trehalose-6-phosphate phosphatase (T6PP) (UniProt: A8NS89) is one of the highest-ranking targets in the top drug target candidates identified in *B. malayi* using a ranking system [11]. Trehalose-6-phosphate phosphatase participates in the OtsAB biosynthetic pathway, which is the dominant pathway leading to the disaccharide trehalose. The two-step pathway consists of the trehalose-6-phosphate synthase (OtsA)-catalyzed reaction of α -UDP-glucose and glucose-6-phosphate to generate α,α' -D-trehalose-6-phosphate, which is then hydrolyzed to α,α -D-trehalose by trehalose-6-phosphate phosphatase (OtsB) (**Scheme 1.1**). Trehalose, a sugar found in many species of plants, bacteria, fungi and invertebrate animals, but not in vertebrates, is a non-reducing disaccharide composed of two glucose moieties. Apart from its function as a reserve carbohydrate, trehalose is known for its role as a stress protectant in many organisms across all three Kingdoms wherein it protects the organism from damage via desiccation, freezing, starvation, and osmotic stress.

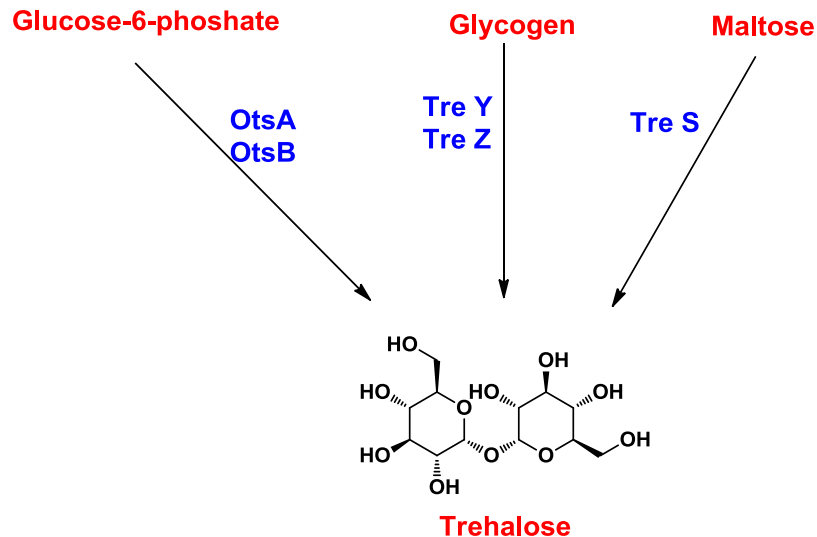


Scheme 1.1 OtsAB biosynthetic pathway.

Although trehalose performs important functions in nematodes, the reduction in T6PP activity in *C. elegans* by gene knockdown is lethal not because of the absence of trehalose but rather because of the accumulation of trehalose-6-phosphate (T6P). One theory is that T6P acts as a toxic anti-metabolite, leading to organism death [12]. In *Saccharomyces cerevisiae*, T6P acts as an important signal for metabolic regulation. Specifically it regulates the first steps in glycolysis through the inhibition of hexokinase II, and its accumulation is detrimental to the organism [13]. Finally, silencing of the T6PP-encoding *tpp* gene in *B. malayi* caused the arrested growth of the larvae [14]. We therefore concluded that trehalose phosphate phosphatase (T6PP) is essential to *B. malayi* and other

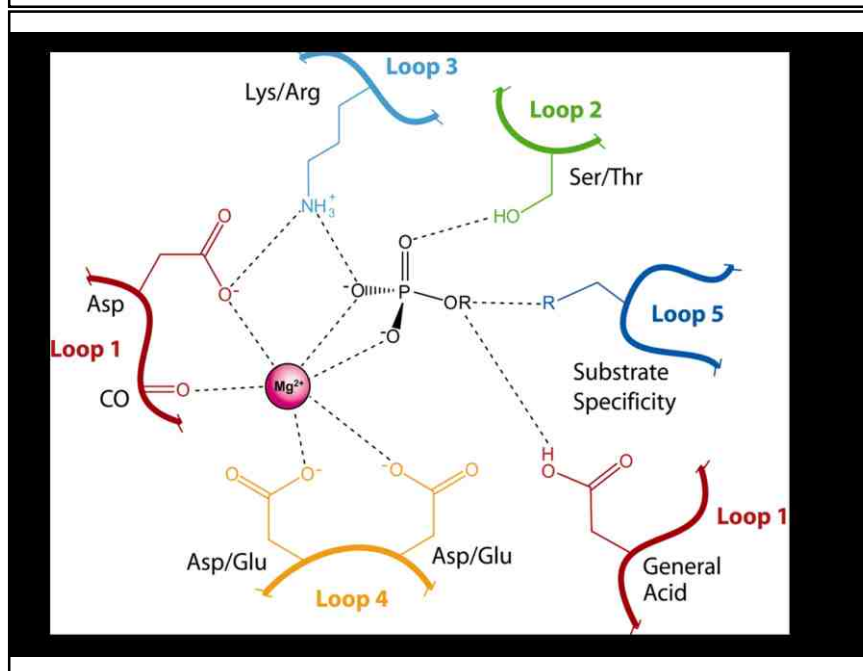
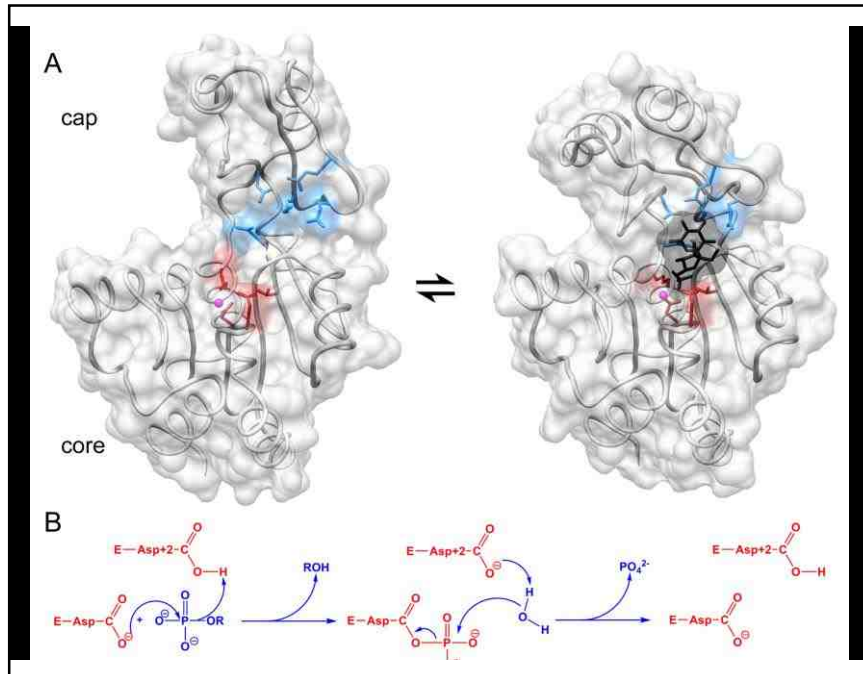
T6P-producing organisms, and that inhibition by a small drug-like molecule could be an effective strategy for the development of a therapeutic agent.

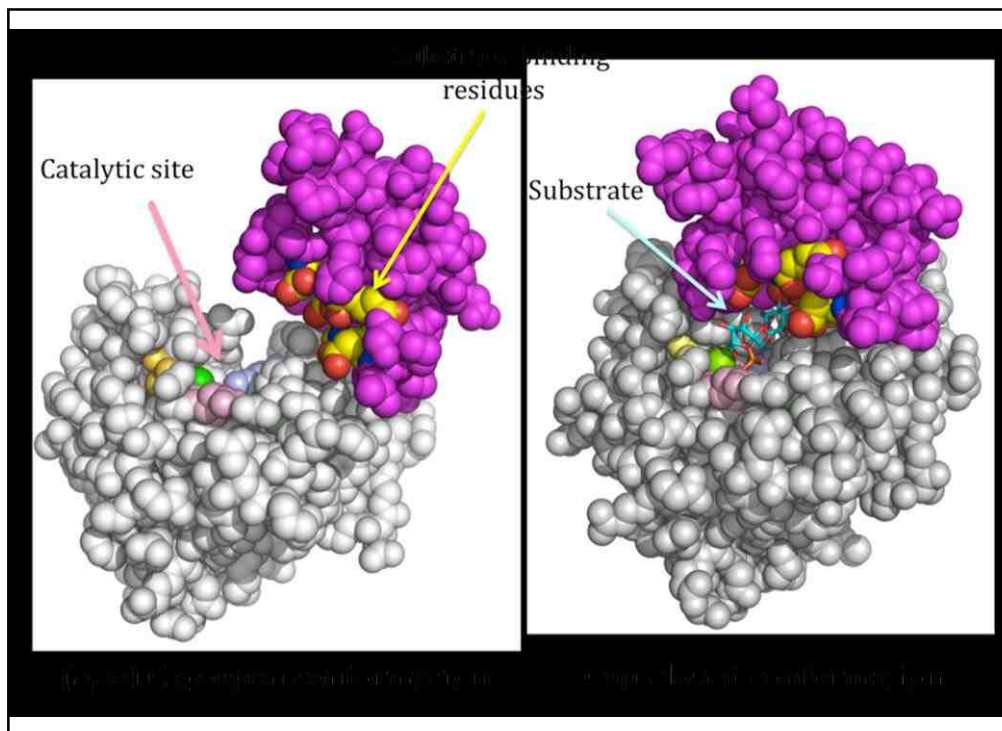
In *Mycobacterium tuberculosis*, trehalose is the major free sugar in the cytoplasm; it is a constituent of cell wall glycolipids, and it is required for the transport of mycolic acid during cell wall biogenesis. *Mycobacterium tuberculosis* causes Tuberculosis (TB), an infectious disease. In 2010, there were an estimated 8.5–9.2 million cases of TB and 1.2–1.5 million deaths. TB is the second leading cause of death from an infectious disease worldwide (WHO, 2011) [15]. Resistance to anti-TB drugs, a problem recognized in the very early days of the chemotherapeutic era, has become a global threat. New drugs which act on new drug targets can counteract existing drug resistance. There are three potential pathways to synthesize trehalose in mycobacteria, the previously mentioned OtsAB pathway (which utilizes glucose and glucose-6-phosphate to generate T6P catalyzed by trehalose synthase, then hydrolyzed to trehalose by T6PP), the TreYZ pathway (which makes trehalose from the hydrolysis of glycogen), and the TreS enzyme (which can convert maltose to trehalose) (**Scheme 1.2**) [16]. However, the OtsAB pathway is the dominant pathway required for *M. tuberculosis*'s growth in laboratory culture and for its virulence in a mouse model [17]. Trehalose-6-phosphate phosphatase (TPP) is an essential enzyme for growth of mycobacteria, which has been identified to be a potential anti-tuberculosis drug target.



Scheme 1.2 Three pathways for trehalose biosynthesis in *M. tuberculosis*

T6PP is a member of the haloalkanoate dehalogenase (HAD) superfamily of phosphatases. HAD phosphatases catalyze the hydrolysis of organophosphate esters using a two-step reaction sequence, which employs nucleophilic catalysis by one active site Asp residue and acid/base catalysis by a second Asp nucleophile (**Figure 1.1**). The phosphoryl group is activated for transfer by a Mg^{2+} cofactor and by an active site Thr/Ser and Lys residue (**Figure 1.1**). Based on the known structure of the close structural homolog sucrose 6-phosphate phosphatase (S6PP) (**Figure 1.2**) it is evident that the T6PP is comprised of a Rossmann-fold catalytic domain and an α,β -fold cap domain. The catalytic domain contains the catalytic scaffold (represented in Figure 1.1) that mediates the two phosphoryl transfer steps, whereas the cap domain binds the organic leaving group (trehalose in the case of T6P) that is displaced in the first step.





The goal of the work reported herein was to carry out structure-function analysis to define the T6PP substrate binding for inhibitor targeting which will provide the foundation for future drug design. The working hypothesis is that small molecule inhibitors will block T6PP activity in vivo and this in turn will lead to the accumulation of the T6P and result in death of the host organism. My first objective is to identify the steric and electrostatic features of the T6PP substrate binding site region and my second objective is to use this information to guide the design of tight binding inhibitors. The X-ray structure

determinations will be carried out in Karen Allen's laboratory at Boston University. To facilitate the structure determinations I will supply recombinant wild-type and mutant T6PP and synthetic substrate analogs (inhibitors) for co-crystallization. I will use the structural data obtained in combination with the K_i values measured for the inhibitors to locate the residues that can provide the largest amount of favorable binding energy. These results will be used to refine inhibitor design.

References:

1. Martin, J., Abubucker, S., Heizer, E., Taylor, C.M., Mitreva, M. Nematode.net update 2011: addition of data sets and tools featuring next-generation sequencing data. *Nucleic Acids Res*, **2012**, *40*, D720–8.
2. Ottesen, E. A., Hooper, P.J., Bradley, M., Biswas, G. The global programme to eliminate lymphatic filariasis: health impact after 8 years. *PLoS Negl Trop Dis*, **2008**, *2*, e317.
3. WHO (2009) World Health Organization Global Program to Eliminate Lymphatic Filariasis. Available: http://www.who.int/lymphatic_filariasis/disease/en/. Accessed 2 June 2014.
4. Gyapong, J.O., Kumaraswami, V., Biswas, G., Ottesen, E. A. Treatment strategies underpinning the global programme to eliminate lymphatic filariasis. *Expert Opin Pharmacother*, **2005**, *6*, 17–200.
5. Kamgno, J., Boussinesq, M. Encephalopathy after Ivermectin Treatment in a Patient Infected with *Loa Loa* and *Plasmodium* spp. *Am J Trop Med Hyg*, **2008**,

- 78, 546–551.
6. Aboobaker, A.A., Blaxter, M.L. Use of RNA interference to investigate gene function in the human filarial nematode parasite *Brugia malayi*. *Mol. Biochem. Parasitol.* **2003**, *129*, 41–51.
 7. Lustigman, S., Zhang, J., Liu, J., Oksov, Y., Hashmi, S. RNA interference targeting cathepsin L and Z-like cysteine proteases of *Onchocerca volvulus* confirmed their essential function during L3 molting. *Mol. Biochem. Parasitol.*, **2004**, *138*, 165–170.
 8. Pfarr, K., Heider, U., Hoerauf, A. RNAi mediated silencing of actin expression in adult *Litomosoides sigmodontis* is specific, persistent and results in a phenotype. *Int. J. Parasitol.*, **2006**, *36*, 661–669.
 9. Ash, L.R., Riley, J.M. Development of Subperiodic *Brugia malayi* in the Jird, *Meriones unguiculatus*, with notes on infections in other rodents. *J. Parasitol.*, **1970**, *56*, 969–973.
 10. Falcone, F.H., Schlaak, M., Haas, H. In vitro cultivation of *Brugia malayi*, a parasitic nematode that causes human lymphatic filariasis. *ALTEX*, **1995**, *12*, 179–187.
 11. Kumar, S., Chaudhary, K., Foster, J.M., Novelli, J.F., Zhang, Y., et al. Mining predicted essential genes of *Brugia malayi* for nematode drug targets. *PLoS One*, **2007**, *2*, e1189.
 12. Kormish, J.D., McGhee, J.D. The *C. elegans* lethal gut-obstructed *gob-1* gene is trehalose- 6-phosphate phosphatase. *Dev. Biol.*, **2005**, *287*, 35–47.

13. Blazquez, M. A., Lagunas, R., Gancedo, C., and Gancedo, J. M. Trehalose-6-phosphate, a new regulator of yeast glycolysis that inhibits hexokinases. *FEBS Lett.*, **1993**, 329,51–54.
14. Kushwaha, S., Singh, P.K., Shahab, M., Pathak, M., Bhattacharya, S.M. In vitro silencing of *Brugia malayi* trehalose-6-phosphate phosphatase impairs embryogenesis and in vivo development of infective larvae in jirds. *PLoS Negl. Trop. Dis.*, **2012**, 6(8):e1770.
15. WHO, Global Tuberculosis Control. 2011.
16. De Smet, K.A.L., Weston, A., Brown, I.N., Young, D.B. and Robertson, B.D. Three pathways for trehalose biosynthesis in mycobacteria. *Microbiology*, **2000**, 146, 199–208.
17. Murphy, H.N., Stewart, G.R., Mischenko, V.V., Apt, A.S., Harris, R. and McAlister, M.S., et al. The OtsAB pathway is essential for trehalose biosynthesis in *Mycobacterium tuberculosis*. *J Biol Chem*, **2005**, 280, 14524–14529.

CHAPTER TWO

CLONING, EXPRESSION, PURIFICATION AND KINETICS OF TREHALOSE-6-PHOSPHATE PHOSPHATASE HOMOLOGUES

2.1 Introduction

The T6PPs that I have selected for study (based on availability of genomic DNA for T6PP gene cloning) are *Mycobacterium tuberculosis* (bacterial causative agent of tuberculosis), *Shigella boydii* (bacterial causative agent of dysentery), *Salmonella typhimurium* (causative agent of Salmonellosis), *Ascaris suum* (pig roundworm). We assumed that by generating recombinant T6PP from several different pathogens for examination we might increase our chances for successful crystallization and structure determination. Furthermore, each of the chosen T6P phosphatase orthologs can serve as a unique subject for inhibitor development and for in vivo inhibition. The gene encoding the T6PP from *Brugia malayi* (parasitic human roundworm causative agent of elephantiasis) was cloned by our collaborators (the Carlow laboratory at New England Biolabs). They have provided wild-type and mutant *B. malayi* T6PP for X-ray structure determination and for inhibitor evaluation.

2.2 Materials and Methods

2.2.1 General Methods

All chemicals and buffers were purchased from Sigma-Aldrich. The sources of the gene cloning materials are as follows: primers (Invitrogen); T7 Express I^q Competent *E. coli* (High Efficiency) competent cells, T4 DNA ligase, restriction enzymes (New England

biolabs) and *Pfu*, Turbo polymerases (Stratagene); pET23a and pET28a vector kits (Novagen); Qiaprep Spin Miniprep Kit (Qiagen). DEAE Sepharose was from Amersham Biosciences. Butyl and Phenyl-Sepharose resins were purchased from Sigma-Aldrich, whereas the Ni-NTA resin was from Qiagen. Snakeskin pleated dialysis tubing was purchased from Thermo Scientific. SDS-PAGE analysis was performed with a 12% -16% acrylamide running gel and a 4% stacking gel (37.5:1 acrylamide:biacrylamide ratio) (BioRad, Hercules, CA). Protein solutions were concentrated using a 10K Amicon Ultra Centrifugal filter (Millipore). The nucleotide sequence of each cloned gene or mutant gene was determined by GENEWIZ, Inc. Electro-spray mass-spectrometry (ES-MS) determinations were carried out by the University of the New Mexico Mass Spectrometry Facility. Protein concentrations were determined using the Bradford assay kit from Sigma-Aldrich.

2.2.2 Preparation of Recombinant Wild-type T6PPs

2.2.2.1 Preparation of Recombinant Wild-type *Mycobacterium tuberculosis* T6PP

The gene encoding Mt-T6PP was amplified by using the polymerase chain reaction (PCR). The reaction mixture contained *M. tuberculosis* genomic DNA (ATCC 25177), Deep Vent DNA Polymerase and with the forward (5'-GTGAGAGG GTGGCATATGCGCAAGTTGGGC-3') and reverse (5'-CATGGCCGTCCTCCTC GAGGACGGTCGGAG-3') oligonucleotide primers containing NdeI and XhoI restriction sites, respectively. Gene amplification was carried out under the following conditions: 50 μ L reactions contained 5 μ L 10 \times Pfu buffer, 4 μ L dNTP mix (2.5mM), 1 μ L Deep Vent DNA Polymerase, 2 μ L forward primer (50 μ M), 2 μ L reverse primer

(50 μ M), 2 μ L template/genomic DNA (20ng/ μ L) and 34 μ L DI H₂O. The initial denaturation was carried out at 94°C for 10 min followed by 25 cycles of denaturation at 94 °C for 1 min, annealing at 51.5 °C for 2 min and extension at 72 °C for 5 min. The final extension was carried out at 72 °C for 10 min. The PCR products were digested with *NdeI* and *XhoI* restriction enzymes at 37 °C for 3 h, and the digested products were harvested by agarose gel electrophoresis. At the same time, pET-15b (+) tev (Boston University) and pET-23a (+) vectors were digested by *NdeI* and *XhoI* restriction enzymes at 37 °C for 3h, and the digested products were harvested in the same manner. Digested DNA was ligated to corresponding digested pET-15b (+) tev and pET-23a (+) vectors at room temperature for 5-7 h, and the cloned products were verified by DNA sequencing. Both of the pET-15b (+) tev-T6PP and pET-23a (+) -T6PP constructs were transformed into T7 Express I^q Competent E. coli (High Efficiency) cells from New England BioLabs. Over-expression of Mt-T6PP was induced with 0.4 mM IPTG (isopropyl β -D-thiogalactoside) overnight at 37 °C and 175 rpm in LB cultures at logarithmic phase growth (OD₆₀₀=0.4-0.6).

Cells containing Mt-T6PP were harvested at 6500 rpm for 15 min and the collected pellet was suspended in 20 mM HEPES buffer (pH =7.5) containing 100 mM NaCl, 5 mM MgCl₂ and 2 mM DTT. The suspended cells were lysed by disruption using a French Pressure Cell and the lysate was centrifuged at 20,000 rpm for 15 min. For the His-tagged Mt-T6PP (from pET15b (+) tev-T6PP), the supernatant was loaded onto a nickel nitrilotriacetic acid (Ni-NTA) agarose affinity column, which was pre-equilibrated with 20 mM HEPES buffer (pH =7.5) containing 100 mM NaCl, 5 mM

MgCl₂, 2 mM DTT and 40 mM imidazole. The column was subsequently washed with the same buffer for 3-5 column volumes before the recombinant protein was eluted with similar buffer containing 500 mM imidazole. The purity of eluted protein was analyzed by 12% SDS-PAGE (Coomassie blue staining). Recombinant Mt-T6PP protein was dialyzed against 20 mM HEPES buffer (pH 7.5) containing 5 mM MgCl₂, 100 mM NaCl and 2 mM DTT in order to remove imidazole. The dialyzed protein was subjected to steady-state kinetic analysis. For protein that was used for crystallization, the concentrated, dialyzed protein was loaded onto a HiPrep Sephacryl S200 HR size-exclusion column that had been equilibrated with 20 mM HEPES buffer (pH=7.5) containing 5 mM MgCl₂ and 2 mM DTT, and eluted with the same buffer. Protein concentration was determined using the Bio-Rad protein assay with bovine serum albumin as the standard

For purification of native Mt-T6PP, the protein was first precipitated from the supernatant derived from centrifugation of the lysed cells using ammonium sulfate. The fraction containing Mt-T6PP was then resuspended using 20 mM HEPES (pH=7.5) buffer containing 5 mM MgCl₂, 100 mM NaCl, 2 mM DTT and 17 % (NH₄)₂SO₄, and applied to a Butyl sepharose (BS) column with a binding buffer containing 20 mM HEPES (pH=7.5), 5 mM MgCl₂, 100 mM NaCl, 2 mM DTT and 17 % (NH₄)₂SO₄. The column was eluted with a linear gradient of 17%-0% (NH₄)₂SO₄ in buffer (10 column volumes). The fraction containing Mt-T6PP was collected and dialyzed against 20 mM HEPES buffer (pH=7.5) containing 5 mM MgCl₂ and 2 mM DTT to remove the ammonium sulfate. The protein solution was then loaded onto a DEAE column and

eluted with 0-1 M KCl in buffer (10 column volume). The Mt-T6PP-containing fraction was then loaded onto a BS column, running the same gradient as before to obtain pure protein. Lastly, the fraction containing pure Mt-T6PP was collected and dialyzed against 20 mM HEPES buffer (pH=7.5) containing 5 mM MgCl₂ and 2 mM DTT. The protein solution was then chromatographed on a Sephacryl S-200 HR column using 20 mM HEPES buffer (pH=7.5) containing 5 mM MgCl₂ and 2 mM DTT as eluant.

2.2.2.2 Preparation of Recombinant Wild-type *Shigella boydii* T6PP

The gene encoding the Sb-T6PP protein was amplified by PCR using DNA synthesized by GenScript, Deep Vent DNA polymerase, along with a gene-specific oligonucleotide forward primer (5'CCTCGCGAATGCATCTAGATCCCAT3') and reverse primer (5'CAGGCCTCTGCAGTCGACGG3') containing *NdeI* and *XhoI* restriction sites, respectively. The pET-28a and pET-23 vectors, digested by *NdeI* and *XhoI* restriction enzymes, were ligated to the PCR product previously digested with the same restriction enzymes. For pET-15b-TEV vector, it was digested by *NdeI* and BamHI restriction enzymes and ligated to the PCR product previously digested with the same restriction enzymes. The ligation product was used to transform T7 Express I^q Competent *E. coli* cells (High Efficiency) that were then grown on an agar plate containing kanamycin for the pET-28a construct and an agar plate containing ampicillin for the pET-23a construct. A selected colony was checked for T6PP expression and the isolated plasmid was sequenced to verify the correct gene sequence. Sb-T6PP was further prepared using the same method described for Mt-T6PP preparation.

For the purification of His-tagged and native Sb-T6PP, the same methods as

described previously in Mt-T6PP purification were used. For the purification of His-tag removed As-T6PP, TEV protease was used to cut the tag from the His-tagged As-T6PP. Mass spectrometry was used to confirm cleavage of the tag.

2.2.2.3 Preparation of Recombinant Wild-type *Ascaris suum* T6PP

The DNA coding the As-T6PP protein was amplified by PCR using template DNA synthesized by GenScript in PUC-57 with Deep Vent DNA polymerase and an oligonucleotide forward primer (5'CGCGAATGCATCTAGATCCCATATGACT3') and reverse primer (5'GATCGGATCCAATTTATTCAGTGGCTCGTT3') containing *NdeI* and *XhoI* restriction sites. The pET-15b-tev and pET-23a vectors, digested by *NdeI* and *XhoI* restriction enzymes, were ligated to the PCR product that had been purified and digested with the same restriction enzymes. The ligation product was used to transform T7 Express I^q Competent *E. coli* (High Efficiency) cells that were then grown on an agar plate containing kanamycin for the pET-15B-tev construct and an agar plate containing ampicillin for the pET-23a construct. A selected colony was checked for T6PP expression, and the isolated plasmid was sequenced to verify the correct gene sequence. Cells were cultured for protein production using the same method previously described for Mt-T6PP.

For the purification of His-tagged As-T6PP, the same method described previously for Mt-T6PP purification was used. For the purification of native As-T6PP, TEV protease was used to cut the tag from the His-tagged As-T6PP. Mass spectrometry was used to confirm cleavage of the tag.

2.2.2.4 Preparation of Recombinant Wild-type *Salmonella typhimurium* T6PP

The gene encoding St-T6PP was amplified by using the polymerase chain reaction (PCR). The reaction mixture contained *Salmonella typhimurium* genomic DNA (ATCC 700720D), PfuTurbo DNA Polymerase and with the forward (5'-AGACCCATATGGCAGAACCGTTA-3') and reverse (5'-CACAACCCTCGAGCCGCTTT-3') oligonucleotide primers containing *NdeI* and *XhoI* restriction sites, respectively. Gene amplification was carried out under the following conditions: 50 μ L reactions contained 5 μ L 10 \times Pfu buffer, 4 μ L dNTP mix(2.5mM), 1 μ L Deep Vent DNA Polymerase, 2 μ L forward primer (50 μ M), 2 μ L reverse primer (50 μ M), 2 μ L template/genomic DNA (20ng/ μ L) and 34 μ L DI H₂O. The initial denaturation was carried out at 94°C for 2 min followed by 30 cycles of denaturation at 95 °C for 30 s, annealing at 55.2 °C for 30 s and extension at 72 °C for 1.5 min. The final extension was carried out at 72 °C for 10 min. The PCR products were digested with *NdeI* and *XhoI* restriction enzymes at room temperature overnight, and the digested products were harvested by agarose gel electrophoresis. At the same time, pET-15b (+) tev (Boston University) was also digested by *NdeI* and *XhoI* restriction enzymes at room temperature overnight, and the digested products were harvested in the same manner. Digested DNA was ligated to corresponding digested pET-15b (+) tev vector at room temperature for 5-7 h, and the cloned products were verified by DNA sequencing. The pET-15b (+) tev-T6PP construct was transformed into T7 Express I^q Competent *E. coli* (High Efficiency) cells from New England BioLabs. Over-expression of St-T6PP was induced with 0.4 mM IPTG (isopropyl β -D-thiogalactoside) overnight at 37 °C and 175

rpm in LB cultures at logarithmic phase growth ($OD_{600}=0.4-0.6$).

Cells containing St-T6PP were harvested at 6500 rpm for 15 min and the collected pellet was suspended in 25 mM HEPES buffer (pH =8.0) containing 25 mM NaCl, 5 mM MgCl₂. The resuspended cells were lysed by disruption using a French Pressure Cell and the lysate was centrifugated at 20,000 rpm for 15 min. For the His-tagged St-T6PP (from pET15b (+) tev-T6PP), the supernatant was loaded onto a nickel nitrilotriacetic acid (Ni-NTA) agarose affinity column, which was pre-equilibrated with 25 mM HEPES buffer (pH =8.0) containing 25 mM NaCl, 5 mM MgCl₂, and 10 mM imidazole. The column was subsequently washed with the same buffer for 3-5 column volumes before the recombinant protein was eluted with similar buffer containing 500 mM imidazole. The purity of eluted protein was analyzed by 16% SDS-PAGE (Coomassie blue staining). Recombinant St-T6PP protein was dialyzed against 25 mM HEPES buffer (pH 8.0) containing 5 mM MgCl₂, 25 mM NaCl in order to remove free phosphate. The dialyzed protein was subjected to steady-state kinetic analysis. For protein that was used for crystallization, the concentrated, dialyzed protein was loaded onto a HiPrep Sephacryl S200 HR size-exclusion column that had been equilibrated with 25 mM HEPES buffer (pH=8.0) containing 5 mM MgCl₂, and eluted with the same buffer. Protein concentration was determined using the Bio-Rad protein assay with bovine serum albumin as the standard.

2.2.3 T6PPs Molecular Weight Determination

The theoretical subunit molecular mass of each recombinant T6PP was calculated

from the amino acid composition using the ExPASy Molecular Biology Server program Compute pI/MW (http://web.expasy.org/compute_pi/). The approximate subunit mass of each recombinant T6PP was determined by SDS-PAGE analysis (**Figure 2.1, Figure 2.2**) using protein molecular weight standards from New England Biolabs Inc. The exact subunit mass was determined by MS-ES mass spectrometry. The molecular mass of the native T6PP was determined by FPLC gel filtration column chromatography against protein standards (13.7-220 kDa from GE Healthcare). The 1.6 cm x 60 cm Sephacryl S-200HR column (GE Healthcare) was eluted at 4 °C with the same type of buffer solution that used for purification. The native molecular weight was derived from the measured elution volume by extrapolation of the plot of the elution volume of the molecular weight standard *versus* log molecular weight.

2.2.4 Steady-state kinetic constant determinations

2.2.4.1 Method for determination of Mt-T6PP steady-state kinetic constants

Phosphatase activity was measured using the EnzChek Phosphate Assay Kit. Reactions solutions 500 μ L in volume contained 25 μ L 20 \times reaction buffer, 5 μ L purine nucleoside phosphorylase (0.5 U) and 28 nM of purified enzyme. The Absorbance at 360 nm was measured to determine the amount of free phosphate produced, which was linear in the range of 0.05– 1 mM trehalose-6-phosphate. The steady-state kinetic parameters (K_m and k_{cat}) were determined by fitting the initial velocity data measured at varying substrate concentration (varied in the range $K_m - 10K_m$) to the equation:

$$V_0 = (V_{\max}[S])/([S]+K_m)$$

Where V_0 is the initial velocity, V_{\max} the maximum velocity, $[S]$ the substrate concentration, and K_m the Michaelis constant for the substrate, using the SigmaPlot Enzyme Kinetics Module. The k_{cat} values were calculated from V_{\max} and $[E]$ according to the equation $k_{\text{cat}} = V_{\max}/[E]$, where $[E]$ is the enzyme concentration.

2.2.4.2 Method for determination of Sb-T6PP Steady-state kinetic constants

To test for Sb-T6PP phosphatase activity, the EnzChek Phosphate Assay kit (as described previously) was used. Reactions with a final volume of 500 μL contained 25 μL 20 \times reaction buffer, 5 μL purine nucleoside phosphorylase (0.5 U) and 28 nM of purified enzyme. The absorbance at 360 nm was measured to determine the amount of free phosphate produced, which was linear in the range of 0.5– 3 mM trehalose-6-phosphate. The kinetic parameters K_m , k_{cat} and k_{cat}/K_m were determined by using the same method previously described for Mt-T6PP.

2.2.4.3 Method for determination of As-T6PP steady-state kinetic constants

To test for Sb-T6PP phosphatase activity, the EnzChek Phosphate Assay kit (as described previously) was used. Reactions with a final volume of 500 μL contained 25 μL 20 \times reaction buffer, 5 μL purine nucleoside phosphorylase (0.5 U) and 28 nM of purified enzyme. The absorbance at 360 nm was measured to determine the amount of free phosphate produced, which was linear in the range of 50– 500 mM trehalose-6-

phosphate. The kinetic parameters K_m , k_{cat} and k_{cat}/K_m were determined by using the same method previously described for Mt-T6PP.

2.2.4.4 Method for determination of St-T6PP steady-state kinetic constants

To test for St-T6PP phosphatase activity, the EnzChek Phosphate Assay kit (as described previously) was used. Reactions with a final volume of 300 μ L contained 15 μ L 20 \times reaction buffer, 3 μ L purine nucleoside phosphorylase (0.3 U) and 33 nM of purified enzyme. The absorbance at 360 nm was measured to determine the amount of free phosphate produced, which was linear in the range of 0.13– 1.2 mM trehalose-6-phosphate [1]. The kinetic parameters K_m , k_{cat} and k_{cat}/K_m were determined by using the same method previously described for Mt-T6PP.

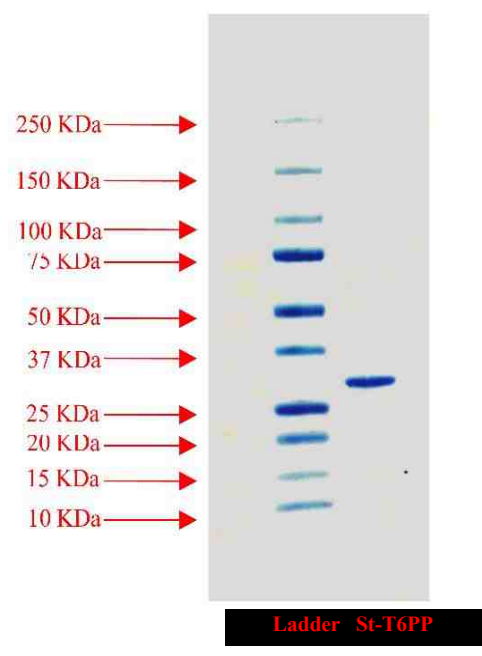
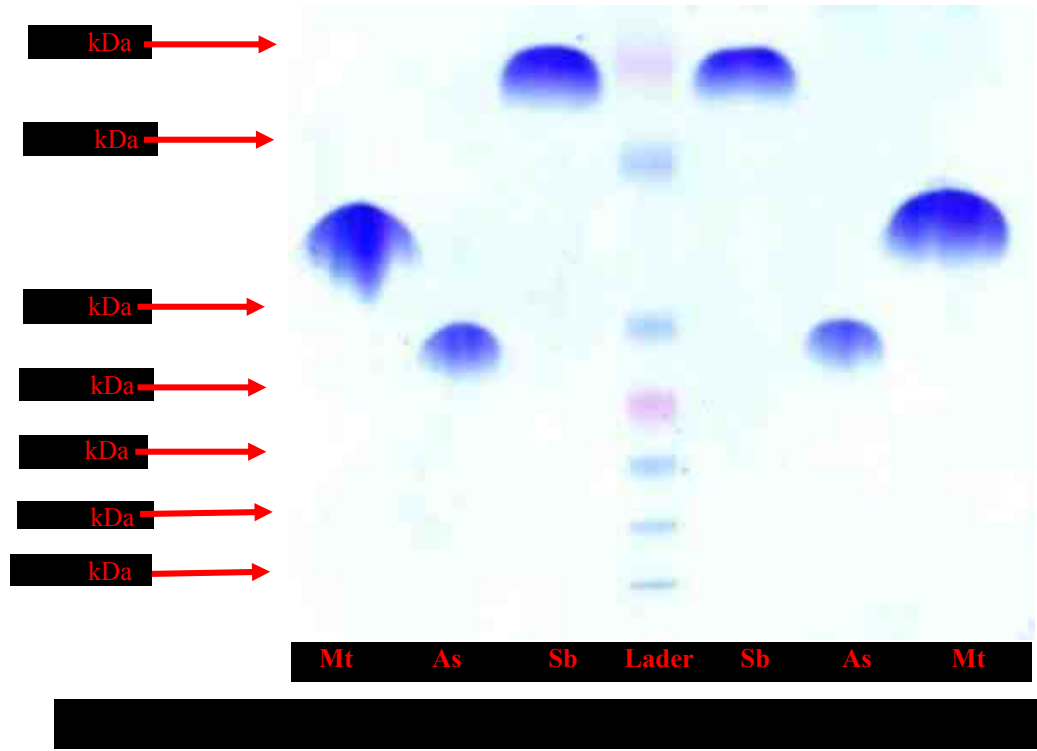
2.2.4.5 Method for determination of Bm-T6PP steady-state kinetic constants

To test for Bm-T6PP phosphatase activity, the EnzChek Phosphate Assay kit (as described previously) was used. Reactions with a final volume of 500 μ L contained 25 μ L 20 \times reaction buffer, 5 μ L purine nucleoside phosphorylase (0.5 U) and 8 nM of purified enzyme. The absorbance at 360 nm was measured to determine the amount of free phosphate produced, which was linear in the range of 0.0625-5 mM trehalose-6-phosphate. The kinetic parameters K_m , k_{cat} and k_{cat}/K_m were determined by using the same method previously described for Mt-T6PP.

2.3 Results and Discussion

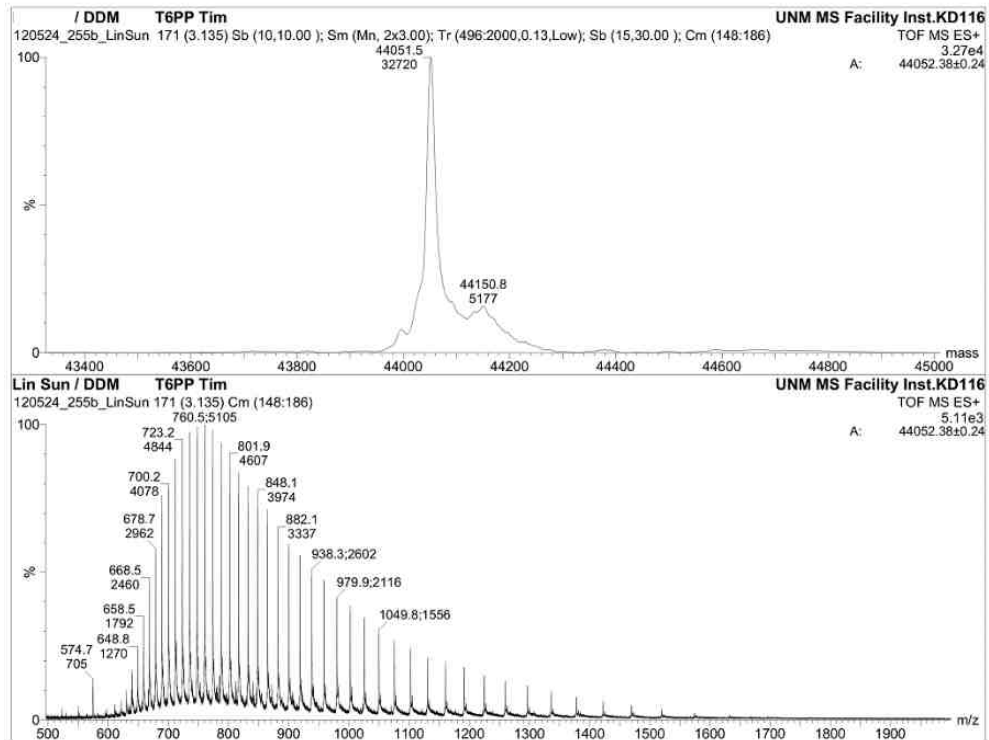
2.3.1 Preparation of the recombinant T6P Phosphatases

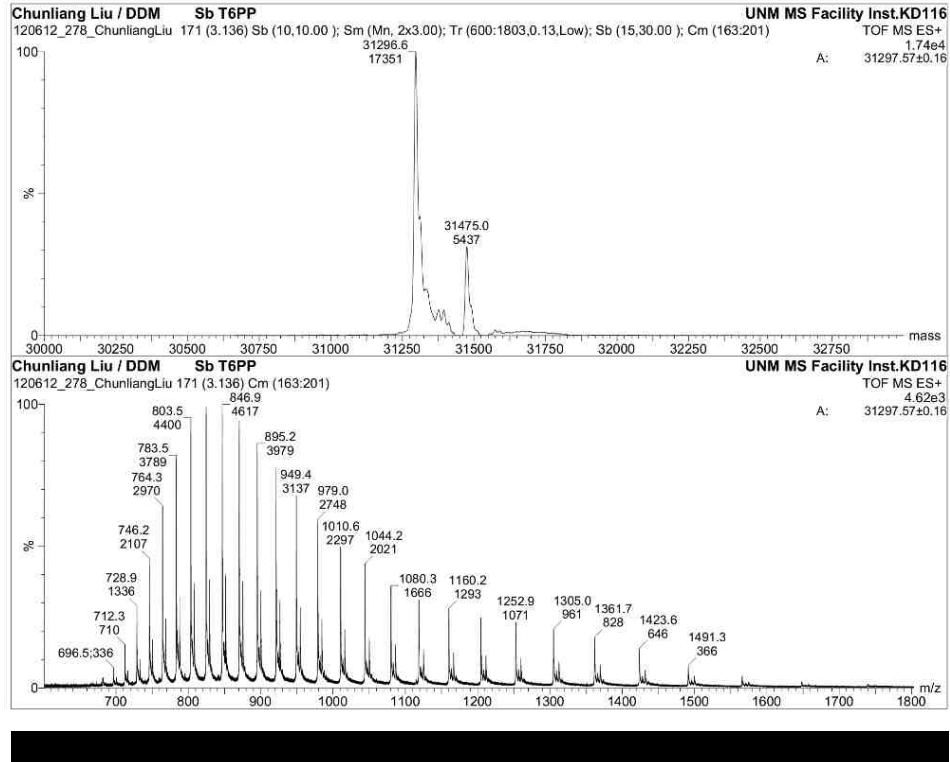
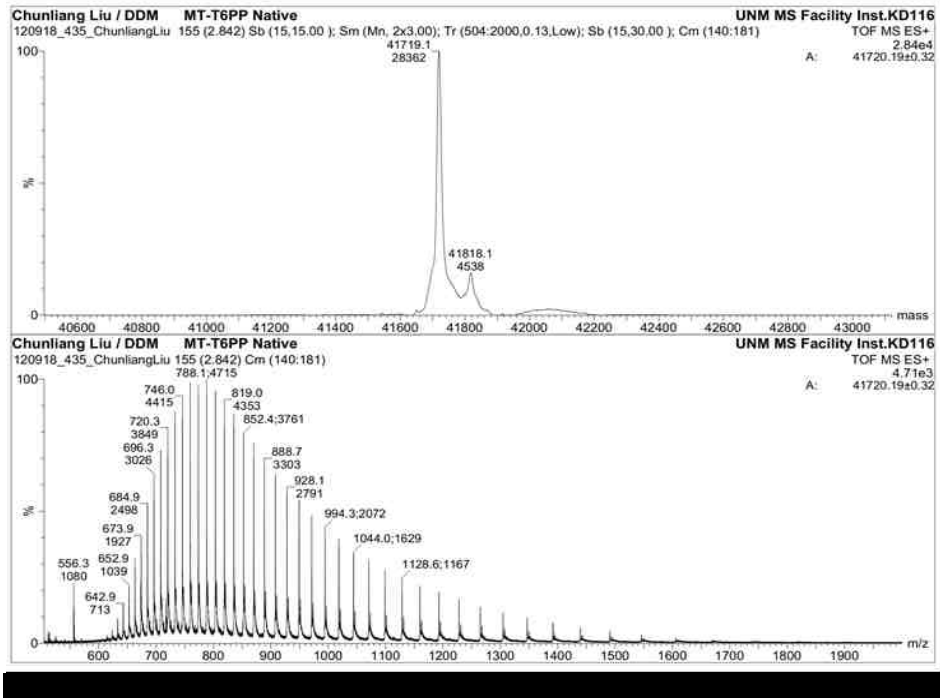
His₆-tagged T6P phosphatases were expressed in *E. coli* and purified by affinity chromatography. The SDS-PAGE gels of the purified proteins are shown in Figure 2.3.1 and 2.3.1. Typical yields (mg protein/g cell pellet) are as follows: As-T6PP 2.7, Mt-T6PP 5.3, Sb-T6PP 3.7, St-T6PP 11.7.

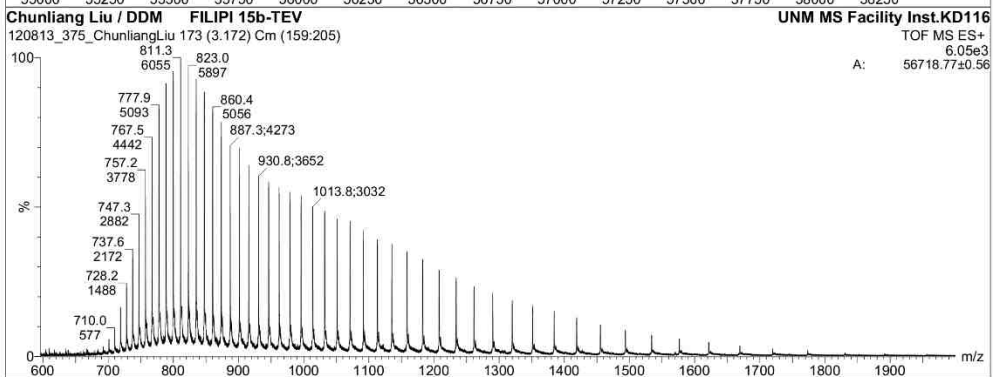
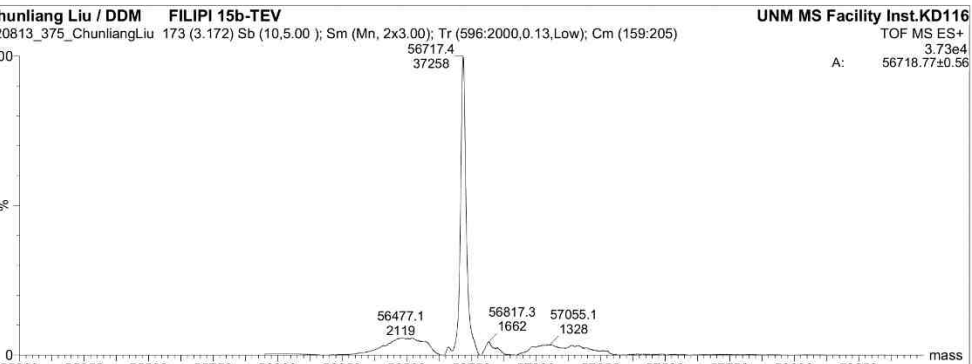
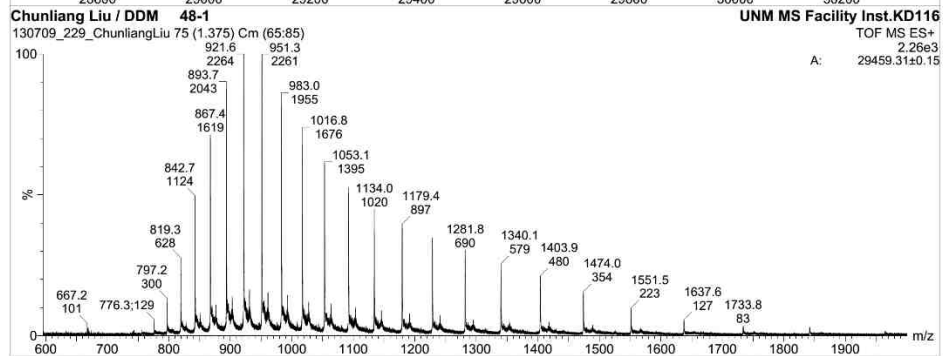
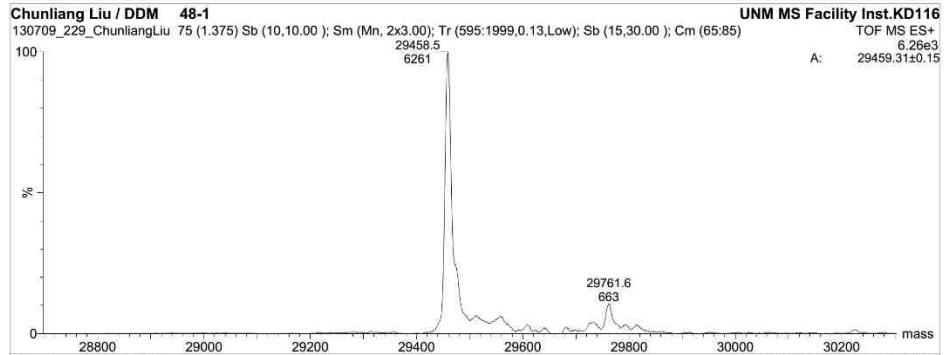


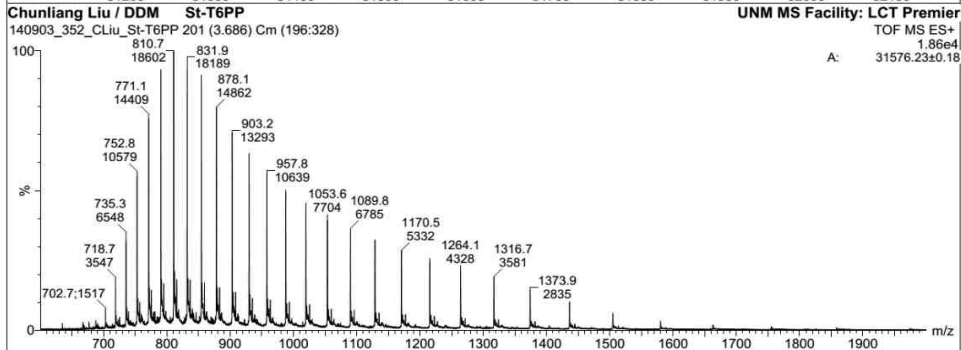
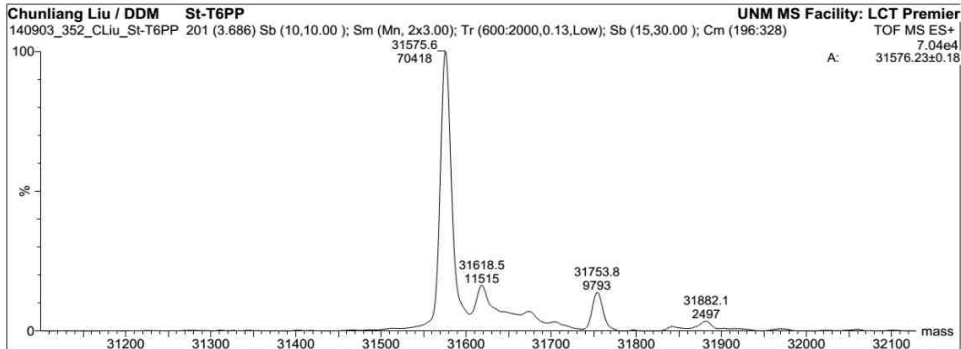
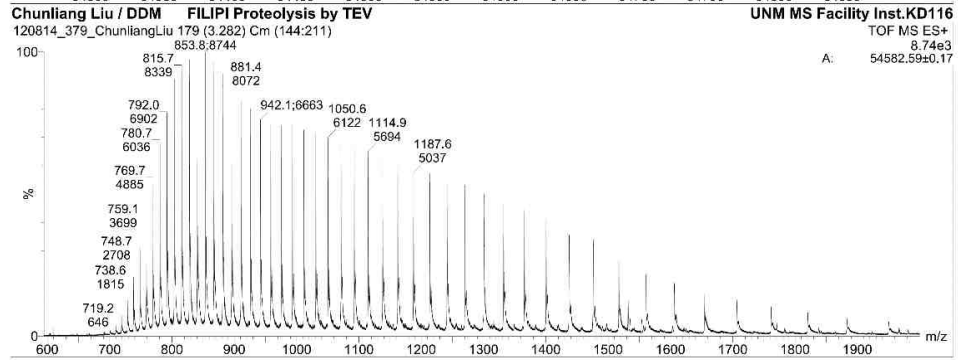
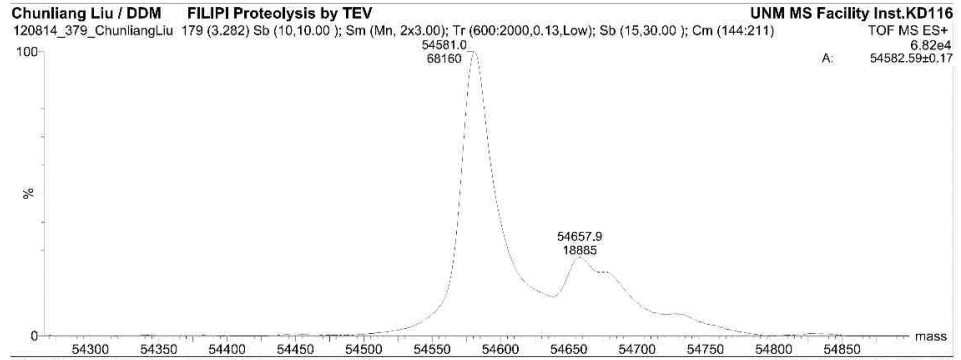
2.3.2 ES-MS Determination of the exact mass of the purified proteins

ES-MS analysis of the purified proteins yielded the following results: His-tagged Mt-T6PP (theoretical 44.051 kDa) 44.052 kDa; Native Mt-T6PP (theoretical 41.720 kDa) 41.720 kDa; His-tagged Sb-T6PP (theoretical 31.297 kDa) 31.297 kDa; Tev cleaved His-tagged Sb-T6PP (theoretical 29.459 kDa) 29.459 kDa; His-tagged As-T6PP (theoretical 56.717 kDa) 56.718 kDa; Tev cleaved His-tagged As-T6PP (theoretical 54.581 kDa) 54.582 kDa. His-tagged St-T6PP ((theoretical 31.576 kDa) 31.576 kDa. The mass spectra are shown in the figures below.









2.3.3 T6PPs Substrate Specificity Profile

The ability of purified T6PPs to catalyze the conversion of some similar monosaccharide (glucose-6-phosphate) and disaccharide phosphates (sucrose-6-phosphate) and *p*-nitrophenyl phosphate (a generic substrate for HAD phosphatases) were tested. Under the reaction conditions employed (10 mM phosphate ester substrate, 1 mM MgCl₂, 0.1 Mm sodium azide and 50 μM Mt-T6PP mM in 50 mM Tris buffer at pH 7.5 and 25 °C), No activity was observed above the detection limit of one catalytic turnover per hour. The one exception is Mt-T6PP which displayed marginal activity towards α-D-glucose-1-phosphate ($k_{\text{cat}} = 0.0022 \pm 0.0002 \text{ s}^{-1}$ and $K_m = 8 \pm 1 \text{ mM}$. Earlier, Mt-T6PP was reported to display activity with α-D-glucose-1-phosphate, α-D-mannose-1-phosphate and mannose-6-phosphate [2].

In general, the T6PPs show stringent substrate specificity which is unusual for HAD phosphatases. Even the disaccharide sucrose-6-phosphate, which is highly similar to trehalose-6-phosphate, both of them are disaccharide and have phosphate at one of the 6 positions of the monosaccharide moiety. Trehalose-6-phosphate has 1,1, α, α linkage, but sucrose -6-phosphate has 2,1, α-linkage, besides, Trehalose-6-phosphate was formed by two glucose, but sucrose-6-phosphate has a glucose and a fructose [Figure 4]. However, none of the T6PPs shows activities on it. Besides, *p*-nitrophenyl phosphate is a widely used “activated” substrate for detecting phosphatase activity in HAD phosphatases, yet remarkably none of the T6PPs showed activities with it.

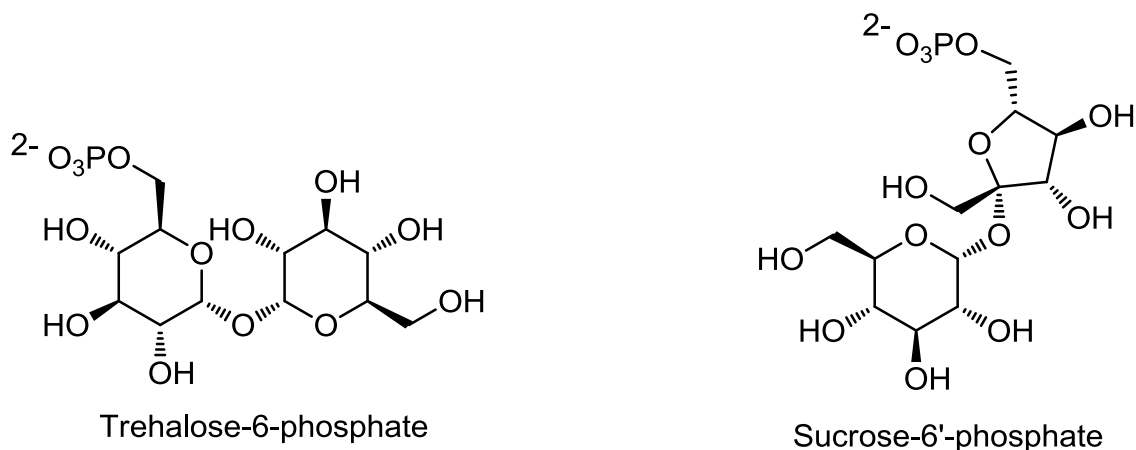


Figure 2.10. Structures of trehalose-6-phosphate and sucrose-6'-phosphate

Next, the T6PPs phosphatase activities were tested using their biological substrate trehalose-6-phosphate [Figure 2.10]. Their k_{cat} , K_m and k_{cat}/K_m values were determined at pH 7.5 and 25 °C [Table 2.1]

Table 2.1 Steady-state kinetic constants for wild-type T6PPs-catalyzed hydrolysis of trehalose 6-phosphate at pH 7.5 and 25 °C. See Materials and Methods for details

<u>T6PP Source</u>	<u>k_{cat} (s^{-1})</u>	<u>K_m (μM)</u>	<u>k_{cat}/K_m ($M^{-1}s^{-1}$)</u>
<i>Brugia malayi</i> ⁵	24±2	360±60	6.9×10 ⁴
<i>Mycobacterium tuberculosis</i>	10±0.9	500±100	1.9×10 ⁴
<i>Shigella boydii</i>	16±0.8	690±70	2.3×10 ⁴
<i>Ascaris suum</i>	3.6±0.5	230±70	1.6×10 ⁴
<i>Salmonella typhimurium</i>	6.2±0.3	310±40	1.9×10 ⁴

The k_{cat} value is governed by the two partial reactions: the first is the phosphoryl transfer from the bound substrate (T6P) to the Asp nucleophile, and the second step is the hydrolysis of the aspartyl-phosphate intermediate by the attack of a water molecule [3]. A second Asp residue (denoted Asp + 2 because it is positioned two residues from the Asp nucleophile) functions as a general acid/base residue to protonate the leaving group in the first partial reaction and deprotonate the water nucleophile in the second partial reaction [Figure 2.11] [4].

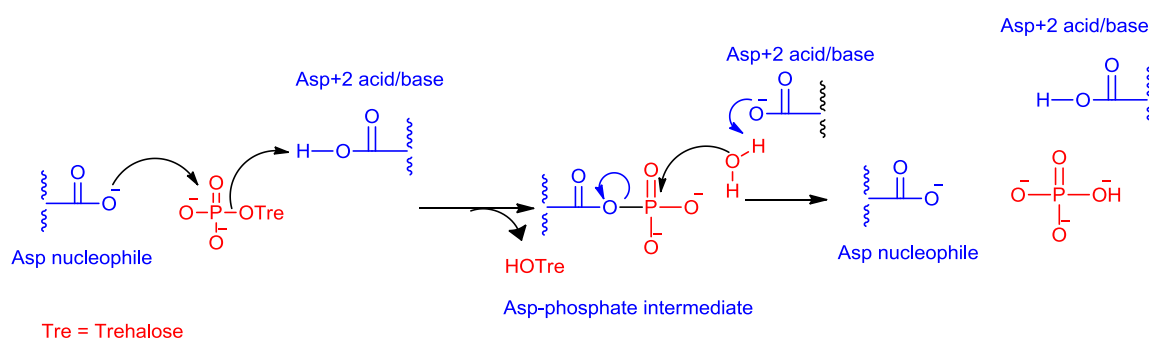


Figure 2.11. Catalytic mechanism for T6PP.

The $k_{\text{cat}}/K_{\text{m}}$ value, the substrate specificity constant, is determined by both the substrate binding affinity and the efficiency that the bound substrate (aspartyl-phosphate intermediate) is converted to the product (phosphate). The $k_{\text{cat}}/K_{\text{m}}$ value is very useful for identifying substrates that have physiologically relevant activities since the concentration of the substrate in the cell is likely to be sub-saturating. HAD phosphatases that function as regulators of the level and composition of organophosphate metabolite pools typically have K_{m} values in the milli-molar range and $k_{\text{cat}}/K_{\text{m}}$ values in the 1×10^3 to $1 \times 10^4 \text{ M}^{-1} \text{ s}^{-1}$ range, where those that target single physiological substrate typically display a $k_{\text{cat}}/K_{\text{m}}$ value in the range of 1×10^5 to $1 \times 10^7 \text{ M}^{-1} \text{ s}^{-1}$. The k_{cat} values typically fall in the range of

1-20 s⁻¹ range and the K_m values from low micromolar to low millimolar. Accordingly, the T6PPs display a moderate, but certainly a physiologically relevant level of catalytic efficiency towards T6P. It is the high level of substrate specificity displayed each of the T6PPs that stands-out.

2.3.4 Quaternary structure determination

The native masses were determined by using size exclusion (HiPrep Sphacryl S200 HR) column chromatography in conjunction with protein molecular weight standards. The results are as follows: native Mt-T6PP 39.1 kDa (monomer); native Sb-T6PP 28.8 kDa (monomer); native As-T6PP 61.9 kDa (monomer)

2.3 Conclusion

There is an urgent need to discover novel antifilarial and antibacterial drug targets to assail the parasite especially when the risk of development of resistance to mainstay drugs is mounting. In trehalose biosynthesis, T6PP seems to be novel drug target as gene-knockout experiments have shown that it is the pathway trehalose-6-phosphate phosphatase (T6PP) that is essential (owing to build-up of toxic levels of T6P) to the survival of the host organism (parasitic nematodes and bacteria). Thus, in the present study we have cloned, expressed, purified and characterized four orthologs of trehalose-6-phospahte phosphatase from different organisms, *A. suum*, and *B. malayi* T6PPs are from nematodes, *M. tuberculosis* T6PP is form mycobacteria, and *S. boydii*, *S. typhimurium* T6PPs are from bacteria, which will be used for further characterization and inhibition studies.

2.4 References

1. Liu, C.; Mariano, P.S. An improved method for the large scale preparation of α , α' -trehalose-6-phosphate. *Tetrahedron Lett*, **2015**, 56(23), 3008–3010.
2. Edavana, V. K.; Pastuszak, I.; Carroll, J.D.; Thampi, P.; Abraham, E. C.; Elbein, A. D. Cloning and expression of the trehalose-phosphate phosphatase of *Mycobacterium tuberculosis*: comparison to the enzyme from *Mycobacterium smegmatis*. *Archives of Biochemistry and Biophysics*, **2004**, 426, 250-257.
3. Collet, J.F., Stroobant, V., Van, Schaftingen, E. Evidence for phosphotransferases phosphorylated on aspartate residue in N-terminal DXDX(T/V) motif. *Methods Enzymol*, **2002**, 354, 177-188.
4. Lahiri, S.D., Zhang, G., Dunaway-Mariano, D., Allen, K.N. Caught in the act: the structure of phosphorylated betaphosphoglucomutase from *Lactococcus lactis*. *Biochemistry*, **2002**, 41(26), 8351-8359.
5. Farelli, J. D.; Galvin, B. D.; Li, Z.; Liu, C.; Aono, M.; Garland, M.; Hallett, O. E.; Causey, T. B.; Ali-Reynolds, A.; Saltzberg, D. J.; Carlow, C. K.; Dunaway-Mariano, D.; Allen, K.N. *PLoS Pathog.*, **2014**, 10(7), e1004245.

CHAPTER THREE

TREHALOSE-6-PHOSPHATE PHOSPHATASE INHIBITOR DESIGN, SYNTHESIS AND EVALUATION

3.1 Background

Although the HADSF fold is dominant among eukaryotic and prokaryotic phosphatases, it has yet to be fully exploited for drug discovery. This stands in contrast to the phosphotyrosine phosphatase (PTP) family of phosphatases, for which great progress has been made in drug-like lead-inhibitor design and focused library-screening-based drug discovery [1-7]. To date only two reports of HADSF phosphatase inhibitor discovery have been described. First, the human small C-terminal domain phosphatase (Scp), which catalyzes the dephosphorylation of the C-terminal domain of eukaryotic RNA polymerase II, was screened against a pilot library of the NIH clinical collection (400 compounds) and the spectrum collection (2000 compounds). Among the hits, the drug Rabeprazole was found to have the tightest binding ($IC_{50} = 5 \mu M$) [8]. X-ray structural analysis revealed that this inhibitor binds to a shallow hydrophobic pocket adjacent to the catalytic site. In a second instance, the structure of the HADSF eyes absent-2 phosphatase was subjected to virtual screening of the InterBioScreen library and the top hits were shown by *in vitro* assay to have IC_{50} values ranging from 4-66 μM [9]. *In-silico* modeling suggests Mg^{2+} coordination of a chelating substituent augmented by favorable electrostatic interactions with substituents that occupy the catalytic site. Notably, both Scp and the eyes absent-2

phosphatase belong to a subclass of HADSF phosphatases that do not possess cap domains. Importantly, the potential for targeting a larger region of the protein contributed by the catalytic domain and the cap domain has yet to be explored.

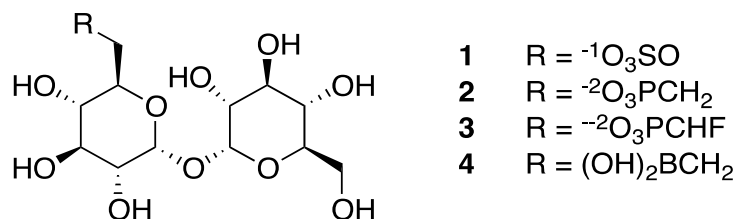
3.2 Research Strategy

The initial strategy used for T6PP inhibitor design is based on the expectation catalysis by this enzyme might be prevented by binding a substance to the catalytic domain, to the cap domain, or to both domains in either a cap-open or cap-closed conformations. Thus, in this effort we have focused on the selection of potential inhibitors that might target the binding sites of the cap-closed and cap-open T6PP conformers. Specifically, the initial inhibitor approach centers substances that contain phosphate-mimetic groups, which can bind to the active site of the catalytic domain, tethered to organic moieties, which can ligate with the binding site of the cap domain. “Bivalent” inhibitors of this type have the potential of being high affinity and high specificity T6PP targeting agents [10]. In this chapter, we focus on the selection and evaluation of phosphate-mimetic groups to replace the C(6)phosphate group of trehalose. The corresponding inert substrate analogs were synthesized and then used as inhibitors of T6PP-catalyzed T6P hydrolysis.

3.3 Inhibitor Selection and Synthesis

As described above, in the active sites of HAD phosphates the substrate phosphoryl substituent coordinates the Mg^{2+} cofactor and forms a number (>10) of hydrogen bonds with donors located in the active site of the catalytic domain. Crystallographic snapshots

of liganded active sites posed in the trigonal bipyramidal phosphorane transition-state



configuration suggest that favorable binding interactions are maximized when the ligand conforms to the active site mold [11]. As a consequence of this analysis, we have designed several T6P analogs that contain the trehalose skeleton, which should be appropriate for binding to the cap domain of T6PPs. In addition these potential inhibitors contain groups that possess charge and Mg^{2+} and hydrogen bonding characteristics that are analogous to those of the phosphate moiety in T6P. Specifically, the inhibitors explored in this investigation, including the trehalose-6-sulfate **1**, -methylenephosphonate **2**, and -fluoromethylenephosphonate **3** [Scheme 3.1], contain groups that have been shown to resemble phosphate moieties present in substrates for kinases and phosphatases [12-21]. In addition, in this study we have tested the ability of trehalose-6-methyleneboronate **4** and its in situ derived hydroxide adduct to target the T6PP catalytic sites. To our knowledge, boronates have not been tested as phosphomimetics. However, their ability to act as mechanism-based inhibitors of arginase and β -lactamase [22, 23] suggest that they might participate in formation of stable complexes with HAD catalytic sites. In the case of arginase, the trigonal boronate group plays the role of the Arg guanidinium moiety in reaction with the metal-ion bridged hydroxide to form a stable transition-state analog

complex. In the case of β -lactamase, the active site Ser nucleophile forms a covalent adduct with the boronate group in a peptide-mimetic [24, 25]. We reasoned that by analogy the T6PP Asp nucleophile might form a covalent adduct with the boronate group in **4**.

3.4 Results and Discussion

3.4.1 Determination of the Source(s) of T6PP Substrate Binding Energy

The five T6P phosphatases were compared for their ability to bind substrate analog (sucrose-6-phosphate), substrate fragments (trehalose and glucose-6-phosphate), tetrahedral P_i analog (tungstate) and metavanadate, a potential trigonal bipyramidal-forming transition ligand). The abilities of the respective ligands to bind to the respective T6PP active sites were determined by testing them as inhibitors of catalyzed T6P hydrolysis by using steady-state kinetic techniques. The results are reported in Table 3.1. HAD phosphatases differ in the ability to form the (nucleophilic) Asp carboxylate adduct with the vanadate and/or with the vanadate complex of the alcohol complex. With the exception of As-T6PP, the T6P phosphatase is not inhibited by vanadate. Tungstate binding is also variable among HAD phosphatases. Based on the results reported in Table 3.1 we can conclude that tungstate binds tightly to Bm-T6PP and Mt-T6PP, moderately to As-T6PP and does not bind with significant affinity to Sb-T6PP and St-T6PP.

The absence of significant binding affinity observed for sucrose-6-phosphate with all five T6P phosphatases accounts for its lack of substrate activity, as was first reported in Chapter 2. Clearly, overall fit is important for substrate binding as well as catalysis. The

absence of significant binding of trehalose to the T6P phosphatases suggests that the trehalose moiety, alone, does not make a sizable contribution to the substrate binding affinity as reflected in K_i values too large to measure using steady-state kinetic techniques. Yet, it must be kept in mind that the trehalose moiety is required for productive binding, or in other words, for formation of the catalytically active enzyme-substrate complex (i.e., for turnover) (viz., glucose-6-phosphate is not turned over).

Table 3.1. Inhibition constant (K_i) of product, product analog or substrate analog measured for T6PPs from various organisms.

Inhibitor	SbT6PP K_i	SfT6PP K_i	MtT6PP K_i	BmT6PP K_i	AsT6PP K_i
Sucrose-6-P	ND ^a	ND ^a	ND ^a	ND ^a	ND ^a
Glucose-6-P	ND ^a	ND ^a	ND ^a	ND ^a	ND ^a
K_2WO_4	ND ^b	ND ^b	19±2 μ M	4.0±0.6 μ M	120±20 μ M
Trehalose	ND ^a	ND ^a	ND ^a	ND ^a	ND ^a
Na_3VO_4	ND ^a	ND ^a	ND ^a	ND ^a	55±9 μ M
20 mM Trehalose + 1.3 mM Na_3VO_4	-	-	-	~1.3 mM	-

^a No Inhibition detected for catalyzed hydrolysis of [T6P] = K_m in the presence of 10 mM inhibitor.

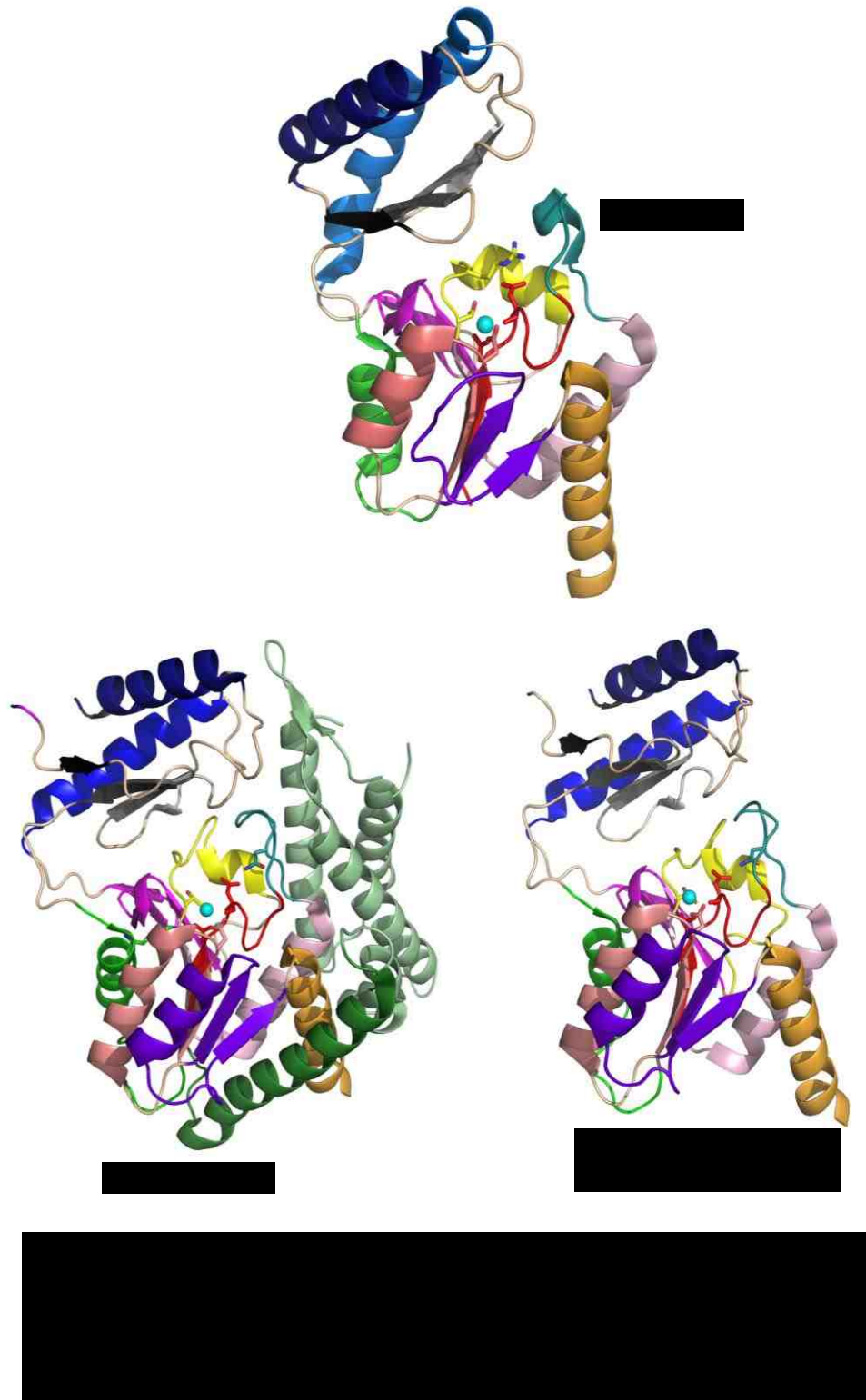
^b No inhibition detected for catalyzed hydrolysis of 600 μ M T6P in the presence of 2 mM inhibitor

^cThis value was calculated, when the initial velocity is half of that without trehalose and Na_3VO_4 in the presence of 200 μ M T6P.

Likewise, the T6P fragment glucose-6-P does not bind with significant affinity to the five T6P phosphatases. This observation suggests that binding to the individual substrate fragments is not strong enough to overcome the loss in entropy associated with complex formation. As will be developed further in the following section, this deduction lead us to design inert substrate analog inhibitors having a phosphate mimetic group located at the C(6) position of trehalose.

3.4.2 Analysis of the T6PP Active Site

As described in Chapter 1, the phosphoryl group of the HADSF phosphatase substrate engages in coordination bond formation with the Mg^{2+} cofactor, in hydrogen bond formation between the bridging oxygen and the (acid/base) Asp in its protonated state, in ion pair formation with the conserved Lys, and hydrogen bond formation with the conserved Thr/Ser. At the outset of my work the only known T6PP X-ray structure was that of (Archeae) *Thermoplasma acidophilum* T6PP complexed with the Mg^{2+} cofactor, but recently our collaborators at Boston University (Karen Allen and co-workers) solved the structure of the (nematode) *Brugia malayi* T6PP complexed with Mg^{2+} [26] (see Figure 3.1). Despite the addition of the N-terminal MIT domain to the *Bm*-T6PP, the (HADSF) phosphatase cap and core domains are quite similar in fold to those of *Tm*-T6PP. (Figure 3.1).



Likewise, the phosphate binding sites are conserved as illustrated in Figure 3.2. The T6P phosphate group can be manually docked into position making favorable electrostatic contacts with the Mg^{2+} , Thr, Lys and possibly the protonated Asp (acid/base).

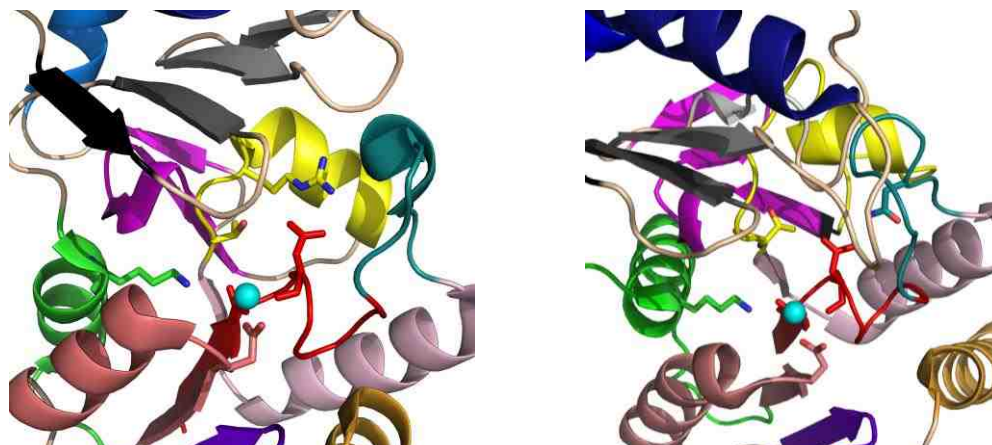


Figure 3.2 Cartoon representation *Ta*-T6PP (left panel) and *Bm*-T6PP (right panel) phosphate binding site generated in Pymol. The N-terminal MIT domain of the *Bm*-T6PP is not shown. Conserved elements of secondary structure are colored the same in the two structures, as are the phosphate binding residues whose side chains are shown in stick, and Mg^{2+} the cyan sphere.

How then to orient the trehalose? The trehalose moiety should fit snugly within the substrate binding pocket formed by the interfaced cap and catalytic domains. The trehalose binding sites of the T6P phosphatases will be described in Chapter 4. Instead, in this chapter I focus on the route to identification of stable functional groups that bind to the phosphate binding site with high affinity. Ms. Christine Harvey, a graduate student in the Dr. Karen Allen lab at BU created T6P-docked structures (manual) for *Ta*-T6PP and (*Bm*-T6PP model looks the same) shown in Figure 3.3, highlighting the phosphate binding site.

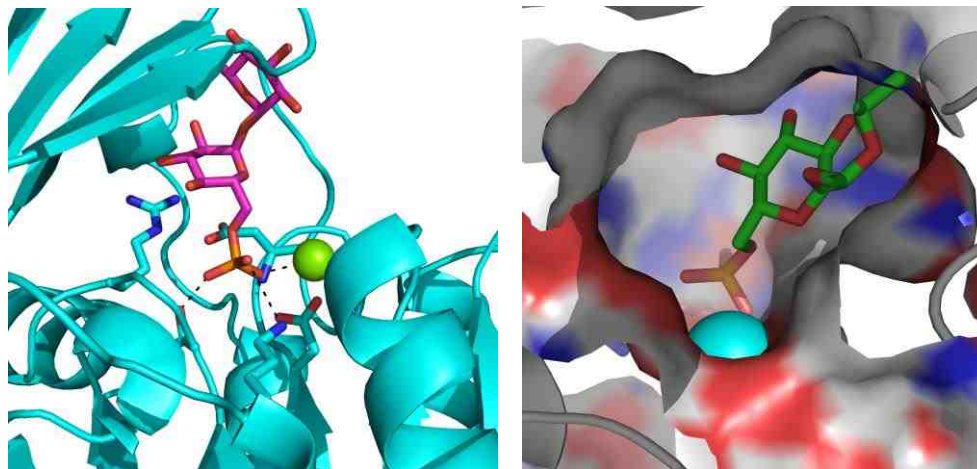


Figure 3.3 Two representations of the X-ray structure of *Ta*-T6PP manually docked with T6P.

3.4.3 Binding Affinities of Inert T6P Analogs: Evaluation of Phosphate Mimetic Groups.

Inert T6P analogs, **1-4** in which the C(6)phosphate is replaced with an approximate isosteric and isoelectronic functional group (resistant to hydrolytic cleavage), were prepared as outlined in Scheme 3.2 and described in Section 3.4.3 and tested as competitive inhibitors (vs. T6P) of the five T6P phosphatases. The steady-state competitive inhibition constants (K_i) determined for these substrate analog inhibitors are reported in Table 3.2. The plots of the kinetic data sets obtained for each inhibitor-T6PP pair are provided in the Appendix (page 187-201).



Inhibitor	<i>Bm</i> -T6PP	<i>Mt</i> -T6PP	<i>Sb</i> -T6PP	<i>As</i> -T6PP	<i>St</i> -T6PP
1	82 ± 7 μM	130 ± 20 μM	330 ± 40 μM	49 ± 5 μM	180 ± 10 μM
2	490 ± 90 μM	500 ± 100 μM	>2 mM	520 ± 80 μM	>2 mM
3	280 ± 50 μM	470 ± 90 μM	>2 mM	490 ± 70 μM	>2 mM
4	No Inhibition	No Inhibition	No Inhibition	No Inhibition	No Inhibition

The K_i values varied between inhibitors tested with the same T6PP and between T6P phosphatases tested with the same inhibitor. The results show that the sulfate group is superior overall in attracting favorable binding energy from the phosphate binding sites of T6P phosphatases. The results also show that subtle differences exist between the binding sites of the T6PP orthologs which impact inhibitor binding affinity.

The sulfate group, like the phosphate group, has tetrahedral geometry and like the phosphate group monoanion, it carries a single negative charge. The S-O-C(6) bridging oxygen atom of trehalose-6-sulfate (T6S) **1** can potentially serve as a hydrogen bond

acceptor in analogy to the P-O-C(6) bridging oxygen atom of the T6P. The methylene group of the trehalose-6-methylene phosphate **2** inhibitor of course cannot engage in such interaction, thus accounting at least in part for lower binding affinity. The substitution of the methylene hydrogen atom(s) for fluorine(s) is known to enhance the binding of the phosphonate inhibitor to tyrosine phosphate phosphatases. The trehalose-6-monofluoromethylene phosphonate **3** did indeed show improved binding affinity, yet still not enough and my attempts to prepare the trehalose-6-difluoromethylene phosphonate for testing were not successful.

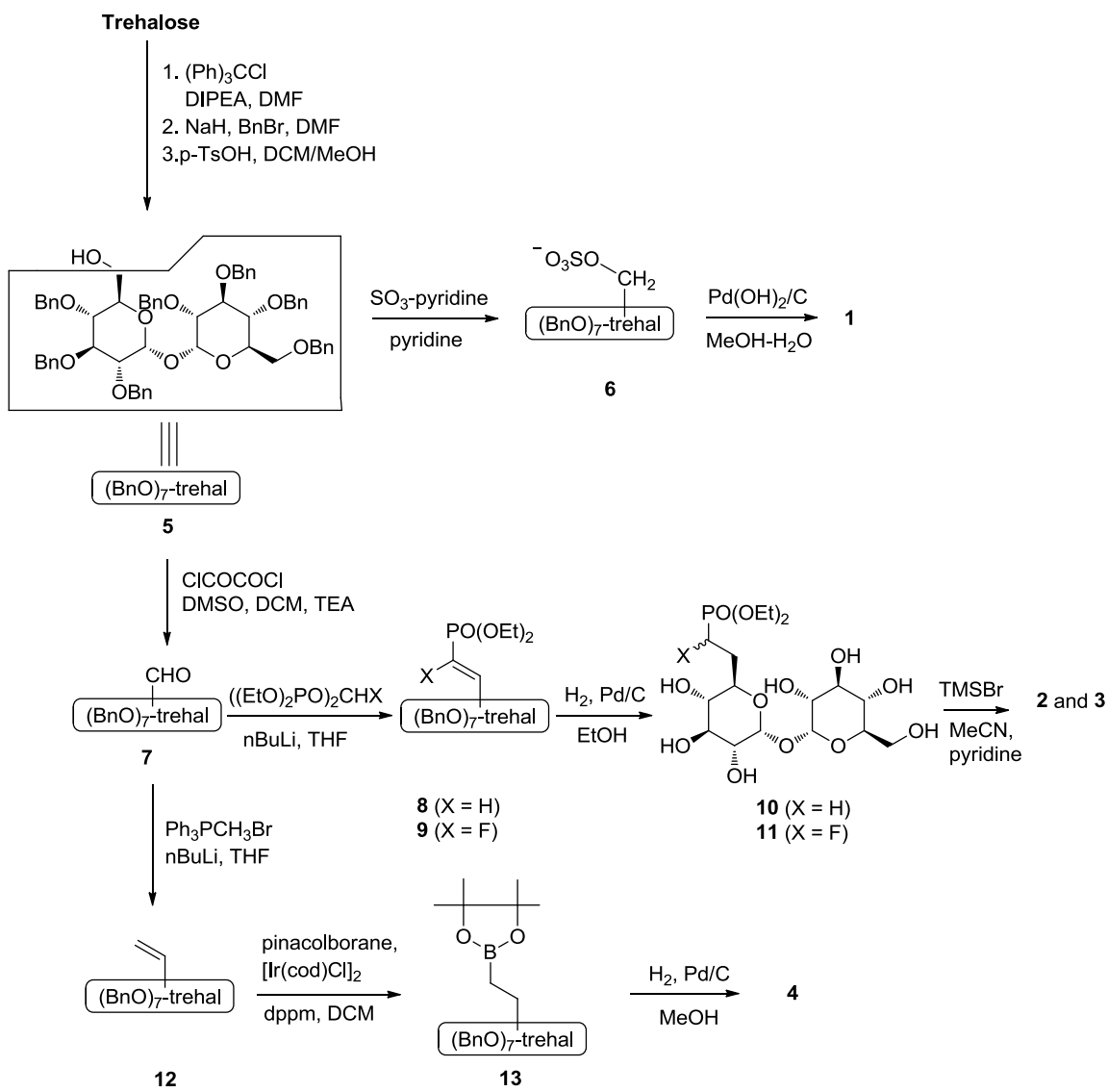
Also during this work I have tested the ability of trehalose-6-methyleneboronate **4** and its in situ derived hydroxide adduct to target the T6PP catalytic sites. Disappointingly, no inhibition was found.

In summary, T6S proved to be a moderately tight binding substrate analog inhibitor which we exploited as the “ligand of choice” in X-ray structure determinations, Structure-Activity Relationship (SAR) analysis and Small Angle X-ray Scattering (SAXS) analysis. The SAR studies are reported in Chapter 4 whereas the SAXS studies are reported in this Chapter.

3.4.3 Synthetic Routes to the T6P Analogs 1-4.

The synthetic routes utilized for preparation of **1-4**, potential inhibitors of T6PP, are displayed in **Scheme 3.2**. The key intermediate employed in all of the pathways is the selectively protected and desymmetrized trehalose derivative **5**, generated by using the

route described earlier by Berndt and his coworkers [28]. For example, **5** was transformed to trehalose-6-sulfate (**1**) by treatment with the pyridine sulfur trioxide complex to produce the benzyl-protected derivative **6**, which was then subjected to hydrogenolysis to form **1**. Similar methods, involving Swern oxidation of **5** to form aldehyde **7** followed by phosphono-olefination with methylene bis-phosphonate esters $((\text{EtO})_2\text{OP})_2\text{CH}_2$ and $((\text{EtO})_2\text{OP})_2\text{CHF}$, hydrogenation/hydrogenolysis, and phosphonate ester cleavage, were employed to produce the respective methylene- and fluoromethylene-phosphonate derivatives **2** and **3**. Finally, boronate derivative **4**, was prepared by using a sequence that began with Wittig olefination of aldehyde **7**, iridium promoted hydroboration with of the resulting olefin **12** with pinacolborane, and hydrogenolysis/boronate hydrolysis.



Scheme 3.2. Synthesis of reversible inhibitors.

3.4.4 Examination of Substrate (Analog) Induced Conformational Changes in T6P Phosphatases Using SAXS

As was described in Chapter 1, a catalytic cycle for a HADSF phosphatase involves a sequence of conformational changes in which the cap and core domains move relative to

one another in order to allow substrate to bind (open), catalysis to occur (closed) and products to disassociate (open). If the T6P binds to the T6PP in the open conformation, and additional binding energy is gained from the ligand in the closed conformation, the T6P acts to stabilize the enzyme in its catalytically active closed conformation. This is an example of substrate-induced fit. For the purpose of testing domain-scale conformational changes in the T6PP, the T6S inhibitor was used in place of T6P as titrant in SAXS solution-based experiments.

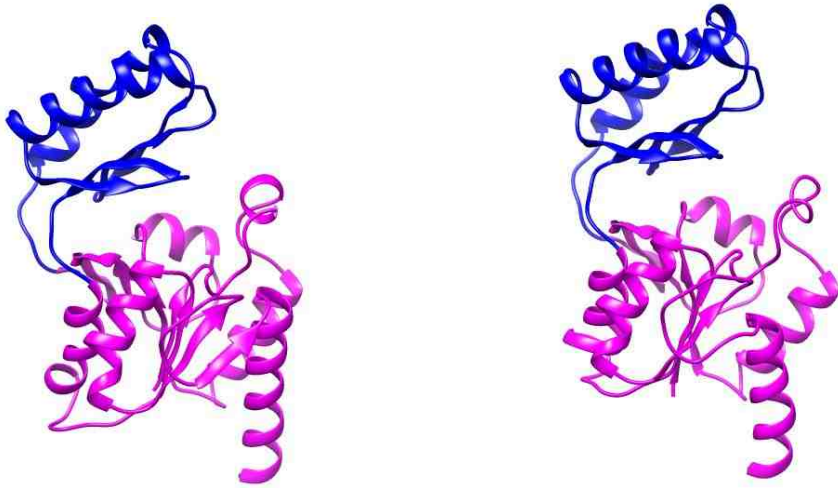
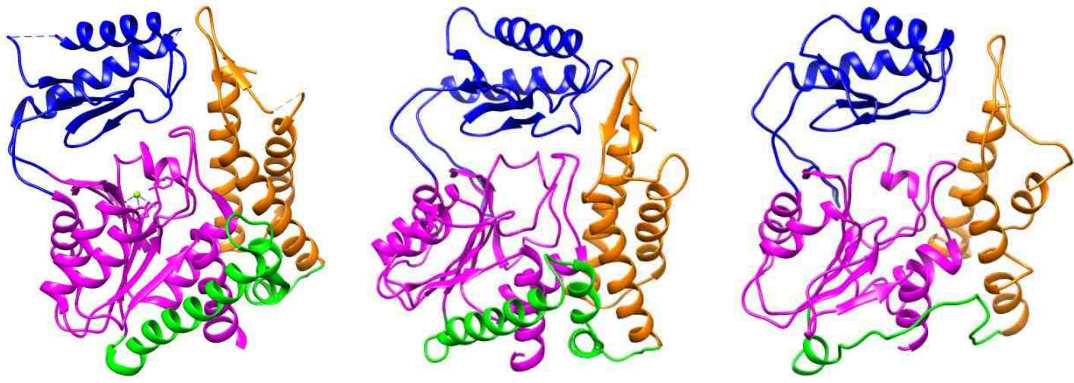
The SAXS data collection and analysis were carried out by my labmate Dr. Tyrel Bryan. The maximum diameter was determined using the $p(r)$ distribution and R_g values calculated for each protein with and without inhibitor T6S (**Table 3.3**). These values among the scattering and Kratky plots were used to investigate the predisposition to close the cap due to ligand binding. Because the T6PP proteins tested are C2 HAD proteins; theoretical scattering profiles representing the two conformers of a different C2 HAD protein were generated to investigate differences among the scattering profiles due to cap position relative to core domain (**Figure 3.5**). The two nematode T6PP proteins (*A. suum*, and *B. malayi*) displayed no evidence of change in structure due to binding T6S. In each case the proteins scattering curves look identical between the native protein and protein in the presence of inhibitor (**Figure 3.6, 3.7**). To further support no change in domain position, the d_{max} values and R_g values are the same between the two samples in both cases. This result can be accredited to the addition of the MIT-domain in the nematode structures compared to the smaller orthologs with a significantly smaller sequence addition to the N-terminus (*M. tuberculosis* T6PP) and the absence of “extra” N-terminal sequence in the

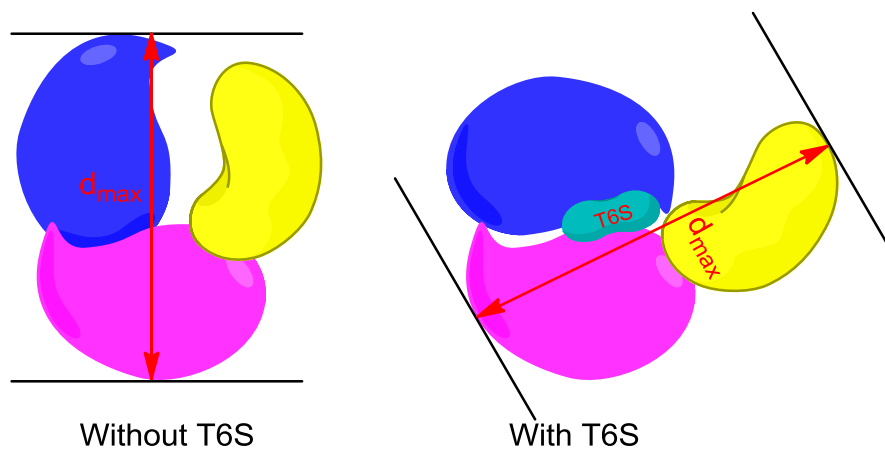
case the two T6PP orthologs from *S. boydii* and *S. typhimurium*.

As expected with a significantly smaller insert or without the additional domain, movement can be observed in the presence of T6S when compared to the native samples (**Figure 3.9, 3.10**). Although the change in d_{\max} in each case are small, the change in R_g and the presence of distinct scattering patterns suggest closure of the cap.

Table 3.3 $p(r)$ distribution and R_g values calculated for each protein with and without the inhibitor T6S

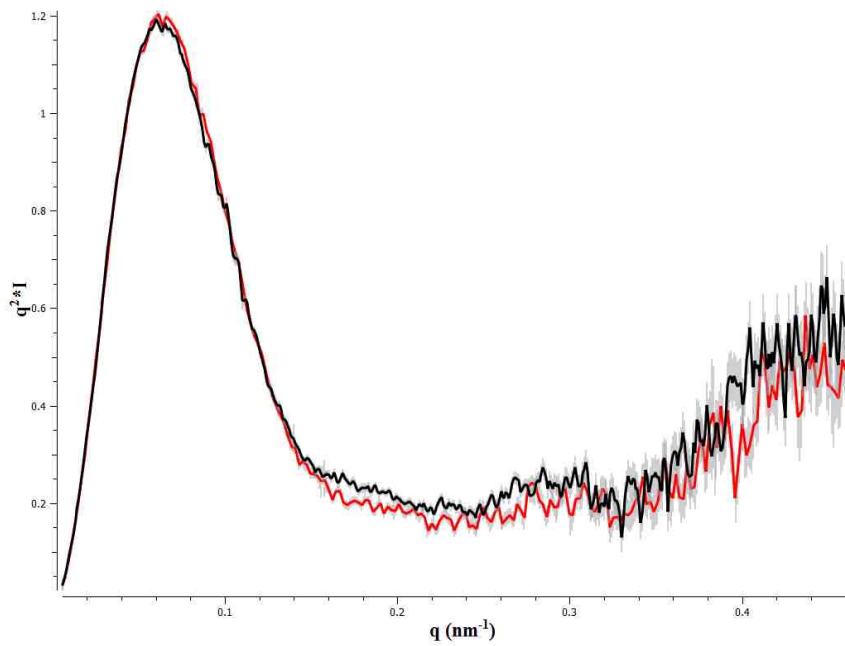
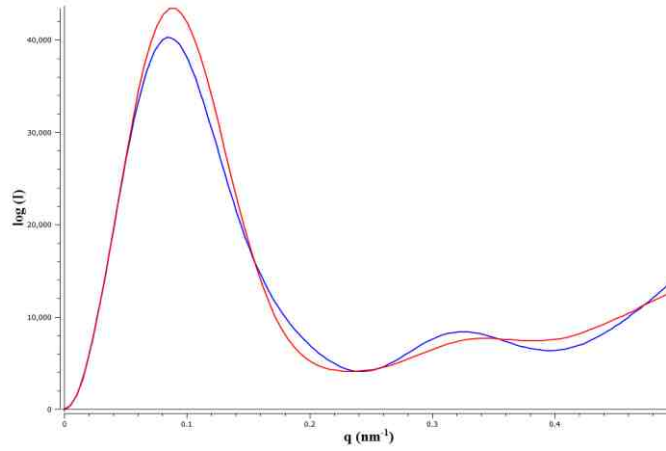
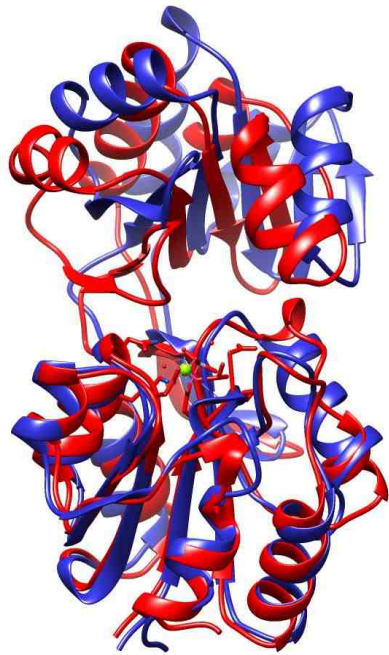
Protein	Ligand	Guinier Region R_g	$P(r)$ Distribution R_g	d_{\max} (Å)	
A. suum	---	30.60 ± 0.07	31.5	107	DNM
	T6S	30.50 ± 0.10	31.5	107	
B. Malayi	---	27.20 ± 0.22	26.6	89	DNM
	T6S	27.28 ± 0.18	27.4	89	
S. boydii	---	23.50 ± 0.28	23.7	82	
	T6S	22.30 ± 0.13	22.9	80	MOVE
M. tuberculosis	---	32.51 ± 0.37	32.9	114	
	T6S	34.62 ± 0.22	35.0	119	MOVE
S. typhimurium	---	23.96 ± 0.09	24.8	84	
	T6S	23.18 ± 0.16	23.2	81	MOVE

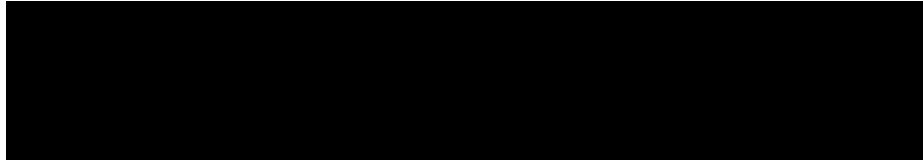
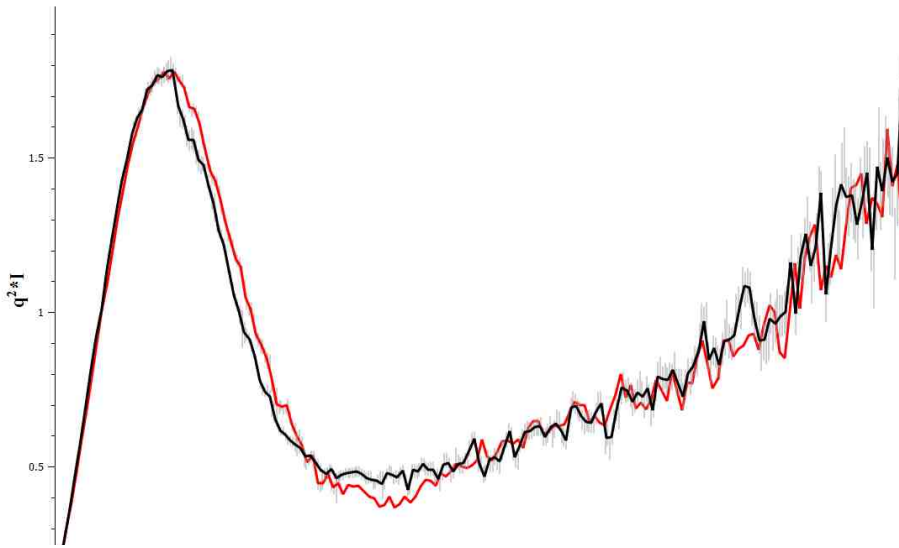
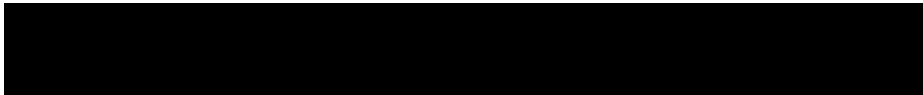
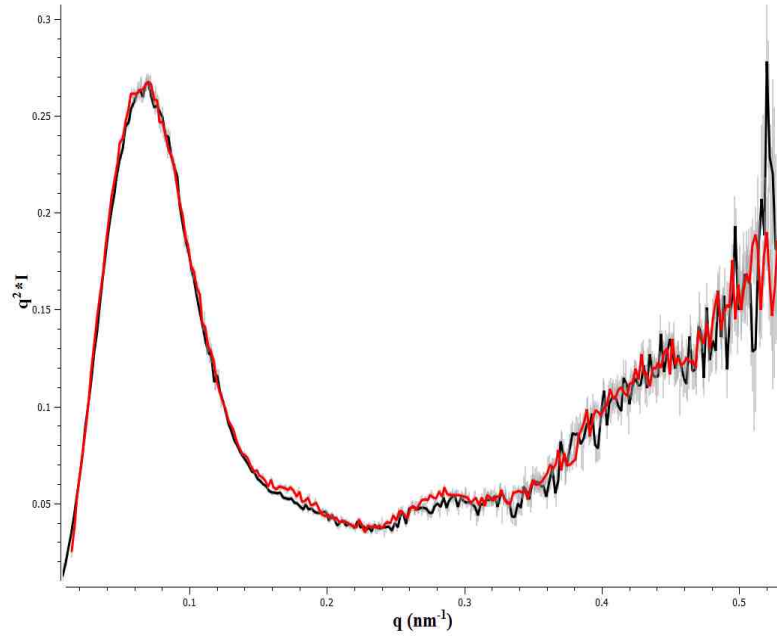


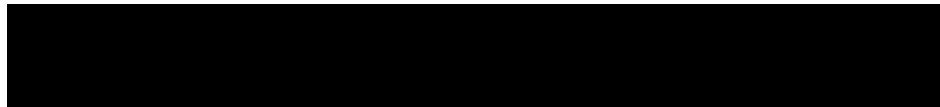
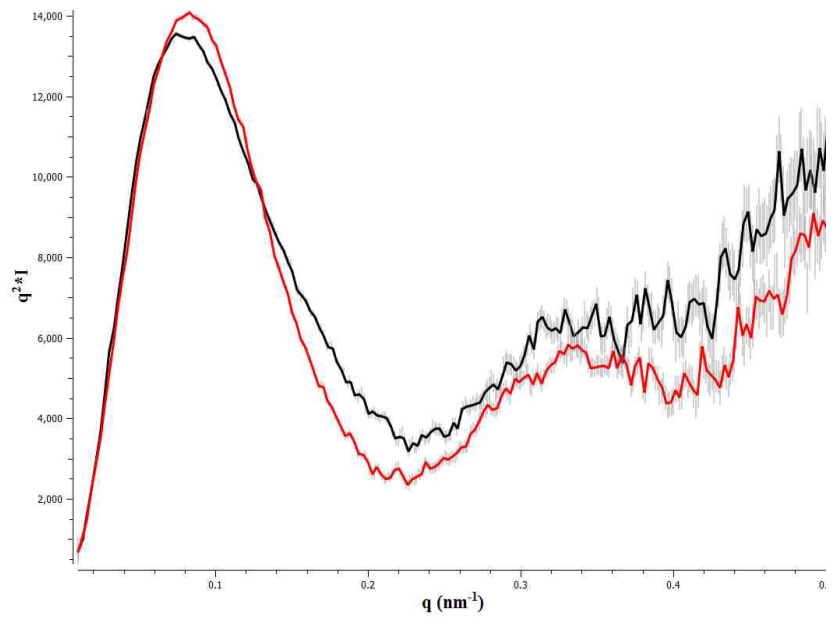
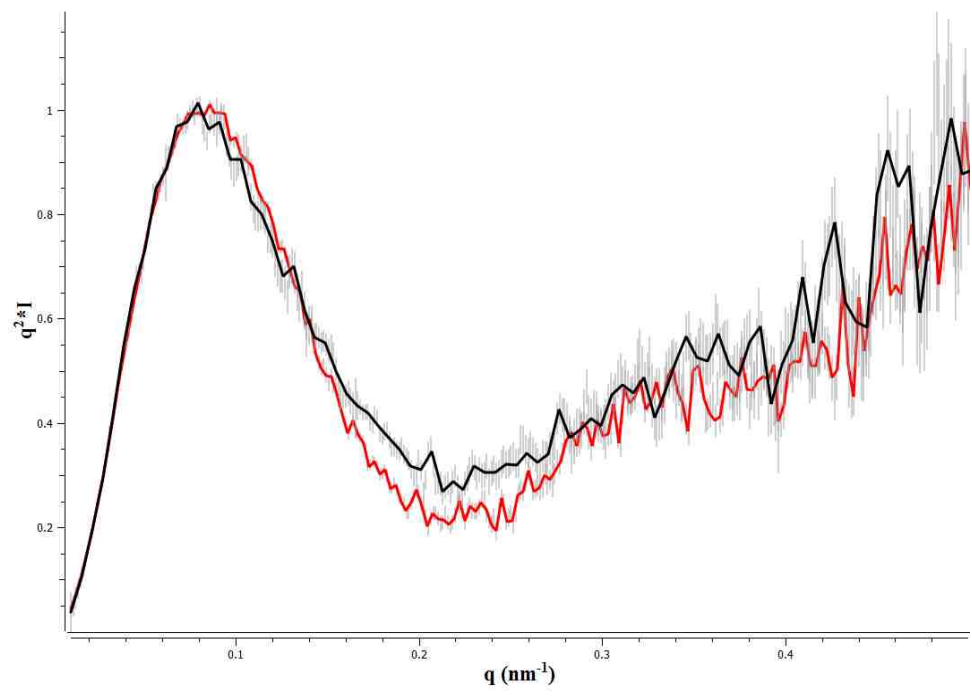


Scheme 3.3. Simulation of Mt-T6PP domain movement. Blue: HAD cap domain; Magenta: HAD core domain; Orange: N-terminal “domain”; Cyan: T6S. Left: Mt-T6PP without inhibitor T6S, cap open Right: Mt-T6PP with inhibitor T6S, cap closure.

In the case of Mt-T6PP, It has bigger d_{\max} when binding with T6S inhibitor (increased by 5 Å). We hypothesize that its extra N-terminal “domain” was pushed away when inhibitor T6S induces the cap closure of Mt-T6PP (**Scheme 3.3**).





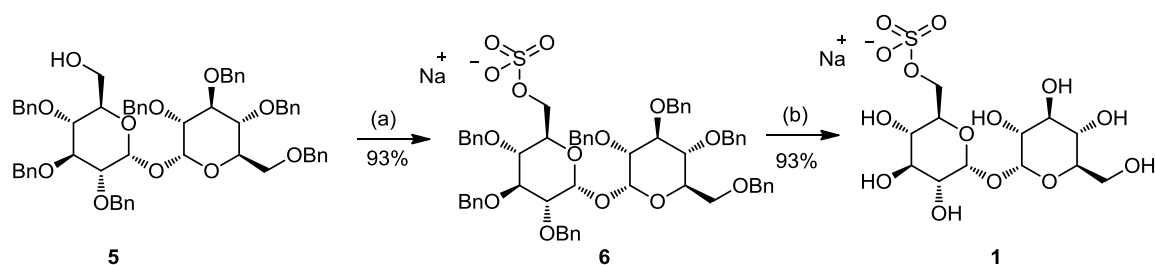


3.5 Material and Methods

3.5.1 Inhibitor Synthesis

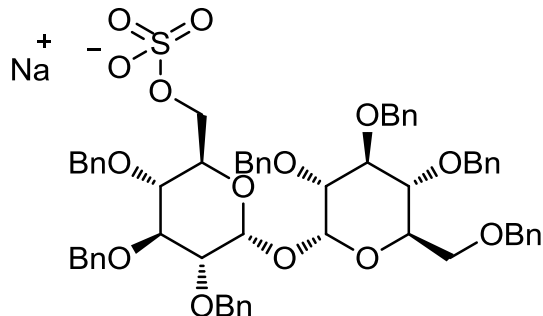
General information: Except specified, all commercial solvents and reagents were purchased from Sigma-Aldrich and used without further purification. Analytical thin-layer chromatography (TLC) was performed on Sorbent Technologies silica gel plates with fluorescence F₂₅₄ indicator and column chromatography was performed using the indicated solvent on Merck 60 silica gel (230-400 mesh). ¹H (300 and 500 MHz), ¹³C NMR (75 MHz and 125 MHz), and ³¹P (121.5 MHz) NMR spectra were recorded on Bruker Avance 500 and Bruker Avance III 300 spectrometers. ¹H, ¹³C and ³¹P NMR data are reported as follows: for ¹H NMR chemical shifts are reported in ppm relative to HDO and multiplicities are given as s = singlet, d = doublet, t = triplet, q = quartet, m = multiplet, coupling constant (*J*); ¹³C NMR chemical shifts are reported in ppm using NH₄HCO₃ as standard; for ³¹P NMR chemical shifts are reported in ppm using 50% aq H₃PO₄ as standard.

Synthesis of 6-O-sulfonato- α,α -D-trehalose



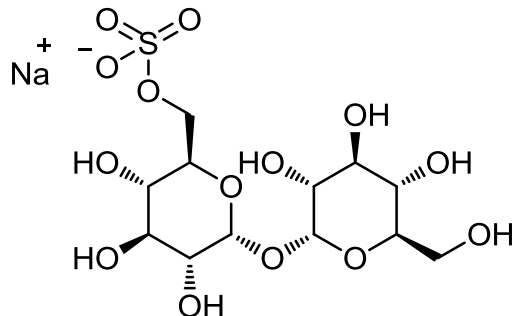
Scheme 1. Reagents and conditions. (a) SO₃/C₅H₅N, C₅H₅N, 5 h (b) Pd(OH)₂/C, MeOH/H₂O, r.t. 24 h.

Compound 6¹



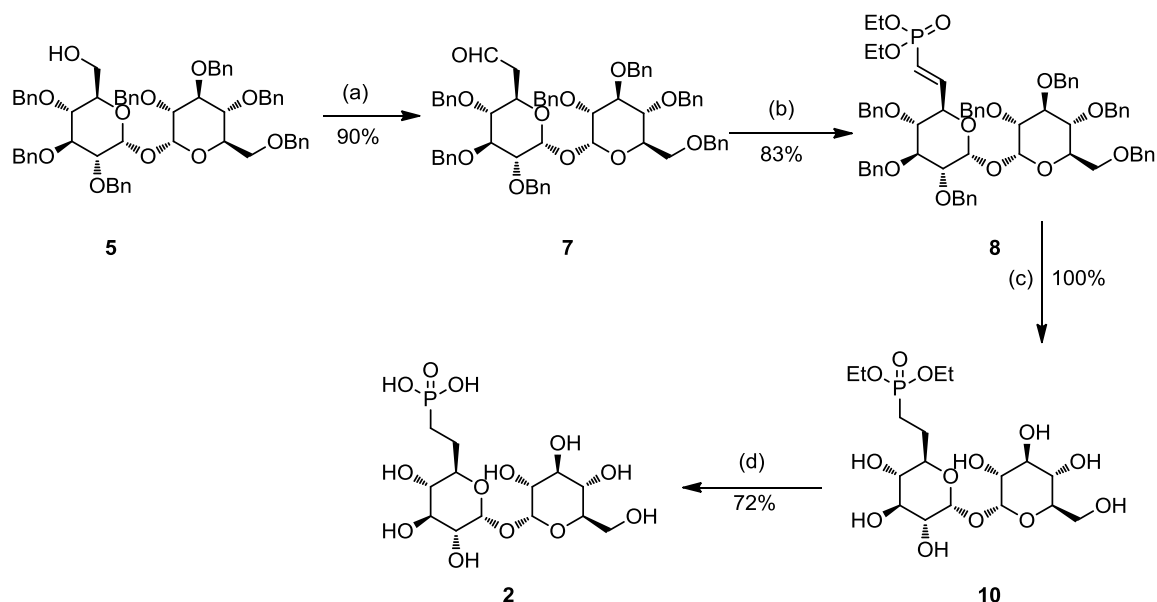
To a solution of SO₃/C₅H₅N complex (432 mg, 2.7 mmol) in freshly distilled pyridine (5mL), a solution of **5**² (1.345g, 1.35 mmol) in freshly distilled pyridine (5 mL) was added. The mixture was stirred for 5 h at room temperature, then the reaction mixture was neutralized with Na₂CO₃(aq) (1 M, 10 mL) and concentrated under reduced pressure. The salts were triturated with anhydrous MeOH and filtered. The filtrate was concentrated in vacuo and the crude product was purified by silica gel column chromatography (30:1 MeOH/EtOAc) affording **6** (1.35g, 93%) as a white powder. TLC (MeOH:EtOAc, 30:1, v/v): R_f=0.30; ¹H NMR (MeOD): 3.50-3.58(3H, m), 3.62(1H, t, *J*=9.45 Hz), 4.00-4.07(2H, m), 4.09-4.12(2H, m), 4.14-4.18(2H, m), 4.34-4.37(1H, m), 4.42-4.45(2H, m), 4.61-4.80(9H, m), 4.87-4.90(2H, m), 5.26-5.27(2H, m), 7.10-7.30(35H, m); ¹³C NMR (MeOD): 68.19, 70.6, 71.9, 72.8, 74.8, 75.0, 75.2, 76.4, 76.6, 77.2, 796, 80.0, 81.7, 81.8, 83.3, 83.4, 94.9, 129.3, 129.4, 129.53, 129.59, 129.6, 129.7, 129.80, 129.88, 130.0, 130.1, 130.2, 130.3, 140.1, 140.2, 140.4, 140.6, 140.7, 141.0; HRMS(ES) m/z: [M-Na]⁻ calcd. for C₆₁H₆₃O₁₄S⁻, 1051.3939; found, 1051.4022.

Compound 1¹



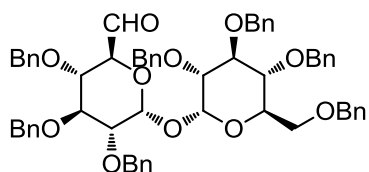
6 (0.96g, 0.89 mmol) was dissolved in MeOH/H₂O (1:1, V/V, 40 mL) and to this was added 20% Pd(OH)₂/C (1.26g) and palladium was activated by repeat purge flush cycles with hydrogen. The mixture was stirred under 1 atm pressure at room temperature for 24 h. Then the mixture was filtered through a Celite pad, the filtrate was concentrated in vacuo and the crude product was purified by column chromatograph (1:4:4, water/isopropanol/ethyl acetate) to give the desired, fully deprotected sugar, as white powder (366 mg, 93%). TLC (water/isopropanol/ethyl acetate, 1:4:4, v/v/v): R_f=0.40; ¹H NMR (D₂O): 3.39-3.52(2H, m), 3.60-3.67(2H, m), 3.72-3.86(5H, m), 3.97-4.02(1H, m), 4.23-4.26(2H, m), 5.16-5.18(2H, m); ¹³C NMR (D₂O): 60.3, 66.7, 69.1, 69.5 70.0, 70.68, 70.74, 72.0, 72.19, 72.25; HRMS(ES) m/z: [M-Na]⁻ calcd. for C₁₂H₂₁O₁₄S⁻, 421.0652; found, 421.0648.

Synthesis of Trehalose-6-phosphonate



Scheme 1. Reagents and conditions. (a) oxalyl chloride, DMSO, DCM, -60°C, TEA; r.t., 3 h; (b) n-BuLi, THF, -78°C, 2 h. (c) H₂, Pd/C, EtOH, rt; (d) TMSBr, MeCN/C₅H₅N, r.t. 4 h; H₂O, overnight.

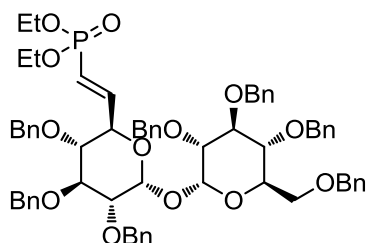
Compound 7³



To a solution of oxalyl chloride (490 mg, 3.86 mmol) in freshly distilled DCM (10 ml) at -60°C under argon, was added dimethyl sulfoxide (603 mg, 7.72 mmol) dropwise. After stirring for 30 min at -60°C, a solution of **5** (2.4g, 2.57 mmol) in 5ml freshly distilled DCM was added dropwise, the resulting mixture was stirred at -60°C for 1 h, then TEA (1.04 g, 10.3 mmol) was added, and the mixture was allowed to reach to room temperature over a

period of 30 min, then stirred at room temperature for 3 h. The solvent was concentrated in vacuo and the crude product was purified by silica gel column chromatography (20:1 DCM/MeOH) affording **7** (2.15g, 90%). TLC (DCM): R_f=0.20; ¹H NMR (CDCl₃): 3.41-3.45(2H, m), 3.55-3.61(3H, m), 3.65(1H, dd, *J*₁=3.5 Hz, *J*₂=9.5 Hz), 3.75(1H, t, *J*= 9.65), 4.07(1H, t, *J*=9.3 Hz), 4.14(1H, t, *J*=9.7 Hz), 4.20(1H, dd, *J*₁=3.5 Hz, *J*₂=9.8 Hz), 4.44(1H, d, *J*=11.8 Hz), 4.52(1H, d, *J*=10.4 Hz), 4.59-4.63(2H, m), 4.71-4.78(4H, m), 4.86-4.97(4H, m), 5.05-5.08(2H, m), 5.20(1H, d, *J*=3.4 Hz), 5.28(1H, d, *J*=3.0 Hz), 7.26-7.45(35H, m), 9.39(1H, s); ¹³C NMR (CDCl₃): 61.0, 63.9, 64.0, 65.7, 66.2, 66.5, 67.6, 68.0, 68.1, 68.6, 68.8, 70.6, 71.3, 71.7, 72.3, 74.5, 74.8, 87.4, 88.1, 120.4, 120.6, 120.6, 120.7, 120.8, 120.9, 121.0, 121.1, 121.2, 121.3, 121.4, 121.4, 121.4, 121.5, 130.4, 130.8, 131.2, 131.3, 131.4, 131.7, 190.7; HRMS(ES) m/z: [M+Na]⁺ calcd. for C₆₁H₆₂O₁₁Na⁺, 993.4190; found, 993.4256.

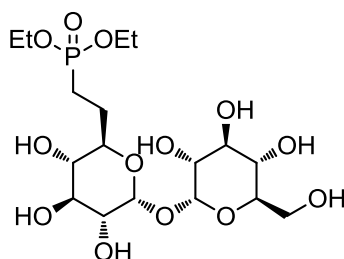
Compound 8



n-BuLi (371 μL, 2.5M in hexanes) was added to a suspension of tetraethyl methylenediphosphonate (294 mg, 1.02 mmol) in anhydrous THF (4 ml) at -78°C. The mixture was allowed to warm to -20°C over a period of 1 h, then the mixture was cooled to -78°C, and a solution of the aldehyde **7** (600 mg, 0.619 mmol) in THF (2 ml) was added dropwise. After stirring for 30 min at -78°C, the reaction mixture was allowed to warm to

room temperature slowly, and kept stirring at room temperature overnight. Then saturated $\text{NH}_4\text{Cl}(\text{aq})$ was added, the aqueous phase was extracted with Et_2O , and the combined organic extracts were dried using anhydrous Na_2SO_4 , the solvent was removed in vacuo, and the crude product was purified by silica gel column chromatography (20:1 DCM/MeOH) affording **8** (2.15g, 90%). TLC (DCM): $R_f=0.20$; ^1H NMR (CDCl_3): 1.32(6H, t, $J=8.1\text{Hz}$), 3.43(1H, dd, $J_1=3.4\text{ Hz}$, $J_2=10.25\text{ Hz}$), 3.55(1H, dd, $J_1=3.4\text{ Hz}$, $J_2=10.25\text{ Hz}$), 3.60-3.63(2H, m), 3.72(1H, t, $J=9.6\text{ Hz}$), 4.03-4.21(8H, m), 4.42-5.06(14H, m), 5.16(1H, d, $J=3.35\text{Hz}$), 5.29(1H, d, $J=3.3\text{Hz}$), 5.99-6.07(1H, m), 6.92-7.00(1H, m), 7.27-7.43(35H, m); ^{13}C NMR (CDCl_3): 9.31, 9.35, 54.6, 61.1, 63.4, 63.6, 63.7, 65.8, 65.9, 66.5, 68.1, 68.5, 68.6, 68.7, 70.7, 71.8, 72.3, 74.4, 74.8, 74.9, 86.8, 87.4, 110.1, 111.6, 120.4, 120.5, 120.6, 120.9, 121.0, 121.2, 121.3, 121.5, 130.6, 130.7, 130.9, 131.0, 131.3, 131.6, 131.8, 141.3; ^{31}P NMR(CDCl_3): 18.6; HRMS(ES) m/z : $[\text{M}+\text{Na}]^+$ calcd. for $\text{C}_{66}\text{H}_{73}\text{O}_{13}\text{PNa}^+$, 1127.4687; found, 1127.4668.

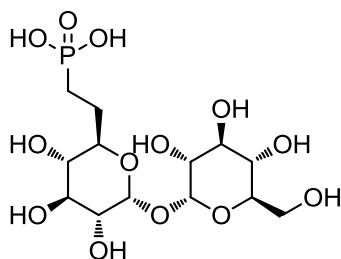
Compound **10**⁴



A mixture of compound **8** (413.4 mg, 0.38 mmol), and Pd/C (10%) (161 mg, 0.16 mmol) in ethanol (5 mL) was stirred under H_2 (1 atm) for 24 h. After completion, the catalyst was removed by filtration through Celite, and filtrate was concentrated in vacuo. The crude product was purified by silica gel column chromatography to give **10** (180 mg, 100%).

TLC (water/isopropanol/ethyl acetate, 1:4:20, v/v/v): Rf=0.20; ^1H NMR (MeOD): 1.32(6H, t, $J=7.1\text{Hz}$), 1.56-1.66(1H, m), 1.77-1.87(1H, m), 1.96-2.06(1H, m), 2.09-2.16(1H, m), 3.07(1H, t, $J=9.4\text{ Hz}$), 3.33(1H, t, $J=9.2\text{ Hz}$), 3.35(1H, dd, $J_1=2.5\text{ Hz}$, $J_2=8.9\text{ Hz}$), 3.68(1H, dd, $J_1=4.9\text{ Hz}$, $J_2=11.4\text{ Hz}$), 3.75(1H, t, $J=9.4\text{ Hz}$), 3.78-3.84(4H, m), 4.05-4.12(4H, m), 5.05(1H, d, $J=3.5\text{ Hz}$), 5.08(1H, d, $J=3.6\text{ Hz}$); ^{13}C NMR (MeOD): 17.5, 17.6, 21.9, 26.6(d, $J_{C,P}=18.7\text{ Hz}$), 63.4, 64.1, 72.7, 73.0, 73.2, 4.0, 74.2, 74.7 75.4, 76.5, 96.0, 96.2; ^{31}P NMR(D_2O): 34.2; HRMS(ES) m/z: $[\text{M}+\text{Na}]^+$ calcd. for $\text{C}_{17}\text{H}_{33}\text{O}_{13}\text{PNa}^+$, 499.1556; found, 499.1544.

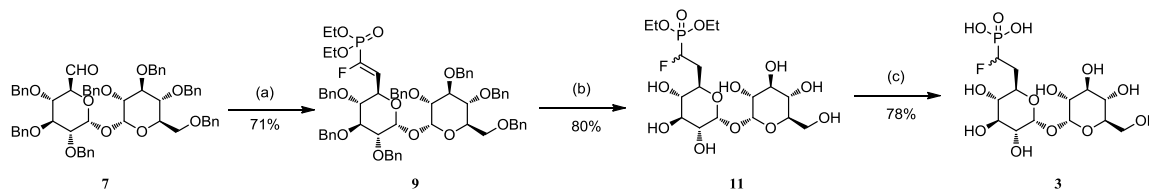
Compound 2 ⁵



To a solution of **10** (77 mg, 0.16 mmol) in anhydrous acetonitrile (2.5 ml) was added pyridine (25 μl) and bromotrimethylsilane (495 mg, 3.24 mmol) under N_2 . After stirring at room temperature for 4 h, the solvent and bromotrimethylsilane were removed in vacuo, then 3 ml of DI H_2O was added and stirring was continued at room temperature overnight. The aqueous phase was washed with CH_2Cl_2 , and the aqueous phase was lyophilized, the crude product was purified by silica gel column chromatography to give **2** (49 mg, 72%). TLC (water/isopropanol/ethyl acetate, 1:2:4, v/v/v): Rf=0.20; ^1H NMR (D_2O): 1.40-1.62(2H, m), 1.70-1.87(2H, m), 3.04(1H, t, $J=9.4\text{ Hz}$), 3.22(1H, t, $J=9.5\text{ Hz}$), 3.38-3.45(2H, m), 3.47-3.66(6H, m), 4.90(1H, d, $J=1.4\text{ Hz}$), 4.91(1H, d, $J=1.4\text{ Hz}$); ^{13}C NMR (D_2O): 23.6,

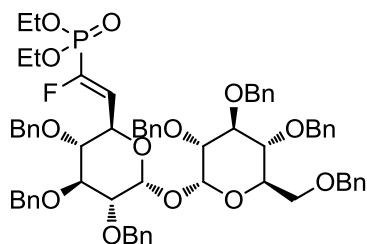
24.4, 60.5, 69.6, 69.9, 70.9, 71.1, 71.3, 72.1, 72.4, 73.1, 93.0, 93.3; ^{31}P NMR(D_2O): 29.3; HRMS(ES) m/z: $[\text{M}-\text{H}^+]^-$ calcd. for $\text{C}_{13}\text{H}_{25}\text{O}_{13}\text{P}$, 419.0955; found, 419.0941.

Synthesis of compound 3:



Scheme 3. Reagents and conditions. (a) $((\text{EtO})_2\text{PO})_2\text{CHF}$, n-BuLi, THF, -78°C , 2 h; r.t. overnight (b) H_2 , $\text{Pd}(\text{OH})_2$, 24 h. (c) TMSBr, MeCN/ $\text{C}_5\text{H}_5\text{N}$, r.t. 4 h; H_2O , overnight.

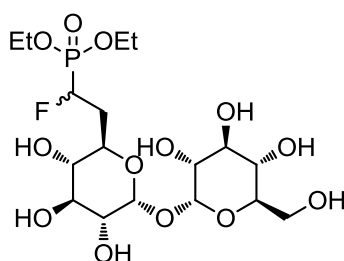
Compound 9⁶



To a solution of $((\text{EtO})_2\text{PO})_2\text{CHF}$ (1.4 g, 1.4 mmol) in anhydrous THF (8 ml) at -78°C was added a solution of n-butyl lithium (0.4 ml, 2.5 M in THF). The mixture was allowed to stir at -78°C for 1 h and then a solution of **7** (337 mg, 1.1 mmol) in anhydrous THF (2 ml) was added and the reaction mixture was stirring at -78°C for 1 h, then it was allowed to slowly warm to room temperature in a period of 1 h. The mixture was allowed to stir at room temperature overnight and the next day the reaction was quenched with aqueous ammonium chloride and then the aqueous layer was extracted with EtOAc, then the organic layer was extracted with brine, the organic layer was then dried with anhydrous sodium sulfate, filtered, and then the filtrate was concentrated in vacuo. The crude product was

purified by silica gel column chromatography to give **9** (1.3 g, 71%). TLC (hexane/ethyl acetate, 1:1, v/v): Rf=0.3; ¹H NMR (CDCl₃): 1.20-1.27(6H, m), 3.37-3.71(7H, m), 3.97-4.20(7H, m), 4.38-5.08(14H, m), 5.15(1H, d, *J*=3.5 Hz), 5.24(1H, d, *J*=3.5 Hz), 6.00-6.19(1H, m), 7.28-7.40(35H, m); ¹³C NMR (CDCl₃): 9.1, 56.2, 61.1, 63.5, 65.3, 66.4, 68.0, 68.7, 70.6, 70.8, 72.3, 74.1, 74.6, 74.8, 86.9, 87.7, 120.3, 120.5, 120.6, 120.9, 121.3, 130.7, 131.0, 131.1, 131.6, 131.9, 156.0; ³¹P NMR(CDCl₃): 4.8 (d, *J*_{F,P}=245 Hz);

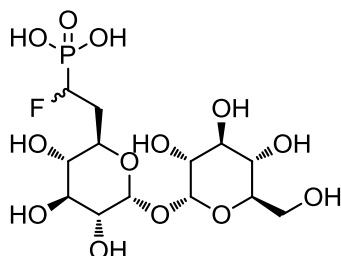
Compound **11** ⁶



To a solution of **9**(1.14g, 1.02 mmol) in ethanol (15 ml)was added a catalytic amount of 20% palladium hydroxide on carbon(432mg, 0.408 mmol) and 3 drops of acetic acid; the reaction was then subjected to a hydrogen atmosphere (1 atm) and was allowed to stir for 24 h. Then the reaction mixture was filtered through a pad of Celite to remove all palladium using methanol as the eluent followed by removal of all solvent in vacuo. The crude product was purified by flash chromatography to give **11** (403 mg, 80%). TLC (water/isopropanol/ethyl acetate, 1:4:4, v/v/v): Rf=0.40; ¹H NMR (D₂O): 1.35-1.40(6H, m), 1.81-2.05(1H, m), 2.40-2.56(1H, m), 3.31(1H, t, *J*=9.4 Hz), 3.45(1H, t, *J*=9.4 Hz), 3.62(1H, dd, *J*₁=3.8 Hz, *J*₂=9.9 Hz), 3.69(1H, dd, *J*₁=3.8 Hz, *J*₂=9.9 Hz), 3.74-3.88(6H, m), 4.00(1H, t, *J*=9.9 Hz), 4.23-4.34(4H, m), 5.15(1H, dd, *J*=3.8 Hz), 5.19(1H, dd, *J*=3.8 Hz) ; ¹³C NMR (D₂O): 15.6, 15.7, 31.5, 31.7, 60.5, 64.9(d, *J*_{C,P}=27.8 Hz), 65.1(d, *J*_{C,P}=26.9 Hz),

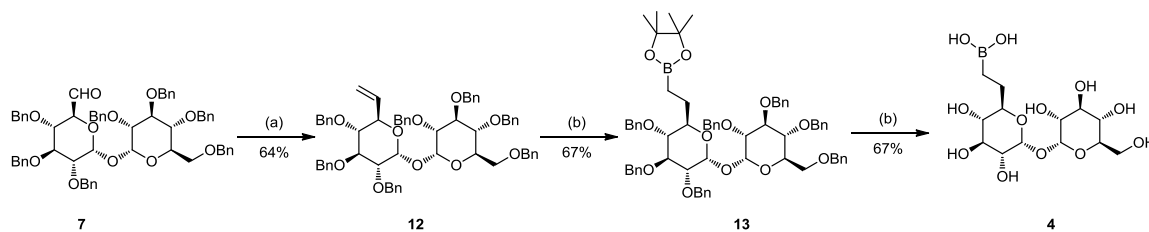
66.4, 66.6, 69.9, 70.9, 71.1, 72.1, 72.5, 72.6, 73.4, 93.1, 93.4; ^{31}P NMR(D_2O): 20.8 (d, $J_{\text{F,P}}=187.5$ Hz).

Compound 3



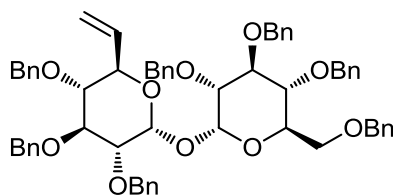
To a solution of **11** (57 mg, 0.116 mmol) in anhydrous acetonitrile (2 ml) was added pyridine (20 μl) and bromotrimethylsilane (353 mg, 2.3 mmol) under N_2 . After stirring at room temperature for 4 h, the solvent and bromotrimethylsilane were removed in vacuo, then 3 ml of DI H_2O was added and stirring was continued at room temperature overnight. The aqueous phase was washed with CH_2Cl_2 , and the aqueous phase was lyophilized, the crude product was purified by flash chromatography to give **3** (40 mg, 78%). TLC (water/isopropanol/ethyl acetate, 1:1:1, v/v/v): $R_f=0.40$; ^1H NMR (D_2O): 1.72-1.96(1H, m), 2.26-2.41(1H, m), 3.30(1H, t, $J=9.4$ Hz), 3.43(1H, t, $J=9.3$ Hz), 3.58-3.68(2H, m), 3.72-3.86(5H, m), 3.96(1H, t, $J=9.8$ Hz), 4.62-4.67(1H, m), 5.15(1H, dd, $J=3.9$ Hz), 5.17(1H, dd, $J=4.0$ Hz); ^{13}C NMR (D_2O): 32.69(d, $J=82.4$ Hz), 60.5, 67.6(d, $J=45.3$ Hz), 69.7, 70.9, 71.1, 71.2, 72.1, 72.5, 73.4, 93.0, 93.4. ^{31}P NMR (D_2O): 13.2 (d, $J_{\text{F,P}}=155.2$ Hz). HRMS (ES) m/z : $[\text{M}-\text{H}^+]^-$ calcd. for $\text{C}_{13}\text{H}_{24}\text{FO}_{13}\text{P}$, 437.0860; found, 437.0861.

Synthesis of trehalose-6-boronate



Scheme 4. Reagents and conditions. (a) Ph_3PMeBr , $n\text{-BuLi}$, THF, -78°C ; $-78^\circ\text{C} - -20^\circ\text{C}$, 1 h; $-78^\circ\text{C} - \text{r.t.}$, 40 min; r.t. overnight (b) Pinacoborane, $[\text{Ir}(\text{cod})\text{Cl}]_2$, dppm, CH_2Cl_2 , 24 h. (c) H_2 , Pd/C, MeOH, 24 h.

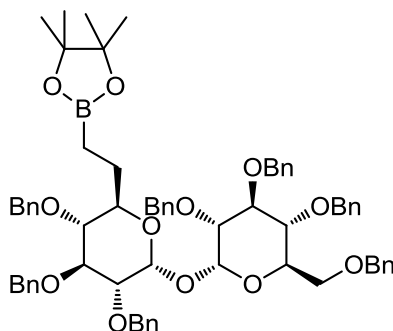
Compound 12



$n\text{-BuLi}$ (240 μL , 2.5 M in hexanes) was added to a suspension of methyltriphenylphosphonium bromide (250 mg, 0.7 mmol) in THF (2 ml) at -78°C . The reaction mixture was slowly warmed to -20°C over a period of 1 h, then it was cooled back to -78°C , and a solution of compound **7** (194 mg, 0.2 mmol) was added dropwise. After 40 min, the reaction mixture was allowed to warm to room temperature slowly, and kept stirring at room temperature overnight. Then saturated NH_4Cl (aq) was added, the aqueous phase was extracted with Et_2O , and the combined organic extracts were dried using anhydrous Na_2SO_4 , the solvent was removed in vacuo, and the crude product was purified by silica gel column chromatography (5:1 hexane/ethyl acetate) affording **12** (124 mg, 64%). TLC

(hexane/ethyl acetate, 7:1): Rf=0.20; ^1H NMR (CDCl_3): 3.35(1H, t, $J=9.6$ Hz), 3.45(1H, dd, $J_1=2.6$ Hz, $J_2=10.6$ Hz), 3.58(1H, dd, $J_1=2.7$ Hz, $J_2=10.6$ Hz), 3.65-3.68(2H, m), 3.76(1H, t, $J=9.5$ Hz), 4.11-4.18(2H, m), 4.25-5.12(16H, m), 5.28-5.37(4H, m), 7.32-7.47(35H, m); ^{13}C NMR (CDCl_3): 61.2, 63.6, 64.8, 65.7, 65.8, 66.5, 68.0, 68.3, 68.6, 68.7, 70.7, 72.1, 72.5, 74.4, 74.8, 75.6, 87.0, 87.4, 110.5, 120.4, 120.5, 120.7, 120.8, 120.9, 121.1, 121.3, 121.4, 128.3, 130.8, 131.2, 131.2, 131.4, 131.8, 131.9; HRMS(ES) m/z: $[\text{M}+\text{Na}]^+$ calcd. for $\text{C}_{62}\text{H}_{64}\text{O}_{10}\text{Na}^+$, 991.4397; found, 991.4424.

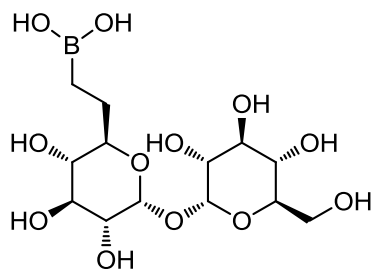
Compound 13 ⁷



A round-bottom flask charged with $[\text{Ir}(\text{cod})\text{Cl}]_2$ (7.3 mg, 1.5 mol%) and bis(diphenylphosphino) methane (8.4 mg, 3 mol%) was flushed with argon. CH_2Cl_2 (2.5 ml), pinacolborane (112 mg, 0.874 mmol), and **12** (707 mg, 0.728 mmol) were added successively at room temperature. The mixture was then stirred at room temperature for 24 h. The reaction was quenched with methanol and water, the product was extracted with ether, and dried over MgSO_4 . The solvent was removed in vacuo, and the crude product was purified by silica gel column chromatography (10:1 to 5:1, Hexane/Ethyl acetate) affording **13** (531 mg, 67%). TLC (Hexane/Ethyl acetate, 6:1): Rf=0.30; ^1H NMR (CDCl_3): 0.68-0.91(2H, m), 1.26(6H, s), 1.27(6H, s), 1.58-1.71(1H, m), 1.89-2.00(1H, m), 3.34(1H,

t, $J=9.3$ Hz), 3.44(1H, dd, $J_1=1.5$ Hz, $J_2=10.4$ Hz), 3.53-3.60(2H, m), 3.63-3.73(2H, m), 4.02-4.16(3H, m), 4.18-4.23(2H, m), 4.41- 5.04(14H, m), 5.22(1H, d, $J=3.5$ Hz), 5.33(1H, d, $J=3.5$ Hz), 7.16-7.39(35H, m); ^{13}C NMR (CDCl_3): 24.9, 24.9, 25.8, 68.4, 70.6, 71.9, 72.7, 73.0, 73.5, 75.0, 75.1, 75.6, 77.3, 79.2, 80.0, 81.6, 81.7, 81.8, 82.9, 92.9, 93.3, 127.5, 127.6, 127.7, 127.9, 128.0, 128.3, 138.0, 138.3, 138.4, 138.6, 138.7, 138.9, 139.0; HRMS(ES) m/z : $[\text{M}+\text{Na}]^+$ calcd. for $\text{C}_{68}\text{H}_{77}\text{BO}_{12}\text{Na}^+$, 1119.5406; found, 1119.5450; $[\text{M}+\text{K}]^+$ calcd. for $\text{C}_{68}\text{H}_{77}\text{BO}_{12}\text{K}^+$, 1135.5145; found, 1135.5183.

Compound 4



A mixture of compound **13** (300 mg, 0.27 mmol), and Pd/C (10%) (116 mg, 0.11 mmol) in methanol (5 mL) was stirred under H_2 (1 atm) for 24 h. After completion, the catalyst was removed by filtration through Celite, and filtrate was concentrated in vacuo. The crude product was purified by flash chromatography to give **4** (107 mg, 100%). TLC (water/isopropanol/ethyl acetate, 1:4:4, v/v/v): $R_f=0.80$; ^1H NMR (D_2O): 0.83-1.05(2H, m), 1.65-1.82(2H, m), 3.41-3.47(2H, m), 3.61-3.69(2H, m), 3.74- 3.78(6H, m), 5.15(1H, d, $J=4.1$ Hz), 5.17(1H, d, $J=4.0$ Hz); ^{13}C NMR (CDCl_3): 23.5, 24.5, 60.2, 69.3, 70.6, 70.7, 70.9, 71.8, 71.9, 72.2, 75.3, 92.9, 93.0; HRMS(ES) m/z : $[\text{M}+\text{Na}]^+$ calcd. for $\text{C}_{13}\text{H}_{25}\text{BO}_{12}\text{Na}^+$, 407.1337; found, 407.1344.

3.5.2 References for synthesis

1. Vidal S., Garcia M., Montero J.L., Morere A. Synthesis and Biological Evaluation of New Mannose 6-Phosphate Analogues. *Bioorganic & Medicinal Chemistry*, **2002**, *10*, 4051–4056.
2. Berndt F., Sajadi M., Ernsting N. P., Mahrwald R., Covalent linkage of N-methyl-6-oxyquinolinium betaine to trehalose. *Carbohydrate Research*, **2011**, *346*, 2960–2964.
3. Omura K., Swern D. Oxidation of alcohols by "activated" dimethyl sulfoxide. A preparative, steric and mechanistic study. *Tetrahedron*, **1978**, *34*, 1651.
4. Belakhov V., Dovgolevsky E., Rabkin E., Shulami S., Shoham Y., Baasov T. Synthesis and evaluation of a mechanism-based inhibitor of KDO8P synthase. *Carbohydrate Research*, **2004**, *339*, 385–392.
5. Vidil C., Morère A., Garcia M., Barragan V., Hamdaoui B., Rochefort H., Montero J. L. Synthesis and Biological Activity of Phosphonate Analogs of Mannose 6-Phosphate (M6P) *Eur. J. Org. Chem.*, **1999**, *2*, 447-450.
6. Cui P., McCalmont W. F., Tomsig J. F., Lynch K. R., Macdonald T. L. α - and β -Substituted phosphonate analogs of LPA as autotaxin inhibitors *Bioorg. Med. Chem.*, **2008**, *16*, 2212-2225.

7. Yamamoto Y., Fujikawa R., Umemoto T., Miyaura N. Iridium-catalyzed hydroboration of alkenes with pinacolborane *Tetrahedron*, **2004**, *60*, 10695–10700.

3.5.3 SAXS measurements and data analysis

Synchrotron X-ray scattering data were collected at the SSRL 4-2 BioSAXS beamline (SLAC, Menlo Park CA). Data were collected with a MarCCD225 detector at wavelength of 1.3 Å, at a distance of 1.7 m at 10 °C, which corresponds to a scattering vector range of $0.007 \text{ \AA}^{-1} < q < 0.55 \text{ \AA}^{-1}$, where $q = 4\pi\sin\theta/\lambda$; 2θ is the scattering angle. Samples were placed into a cooled 96-well plate (40 μL sample volume), sample injection was automated and data collection was done in a quartz capillary tube. For each sample 15 exposure frames of 1 sec were collected for each sample and corresponding buffer. Frames were carefully inspected for aggregation and radiation damage induced by the X-ray source. Scattering profiles were generated either by automated buffer subtraction using beamline automated data processing software (SAXSpipes) or manually using beamline software SasTool.

For each protein sample (five different orthologs) scattering profiles were collected on at least four protein concentrations ranging between 0.5 - 10 mg/mL. To experimentally investigate cap closure, data were collected on each protein w/wo protein inhibitor T6S. Inhibitor concentration was dependent on calculated K_i constants for each protein, to ensure saturation T6S concentration were $10\times K_i$. Scattering was tested and corrected (if necessary) for moderate intermolecular interaction. During each collection period both water and lysozyme (50 mM HEPES, 150 mM NaCl pH 7.0) scattering patterns were

collected for calibration of MW. For each sample the radius of gyration (R_g) was calculated using Guinier approximation (Guinier and Fournet, 1955) and using GNOM (Svergun, 1992), which provides the distant distribution function $p(r)$. The $p(r)$ function displays a histogram or the distances within the particle, whereas d_{\max} is represented as the maximum dimension of the particle.

3.5.4 K_I measurement

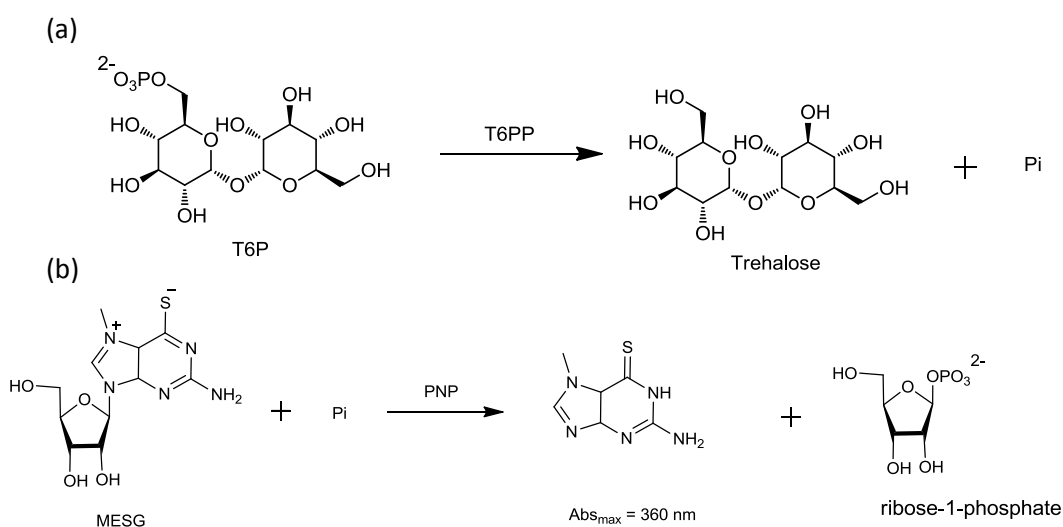
The steady-state competitive inhibition constant K_I was determined for inhibitors by fitting the initial velocity data, measured as a function of trehalose 6-phosphate ($0.5 K_m$ to $5K_m$) [29] and inhibitor ($0, K_I, 2K_I$) concentration to the following using SigmaPlot Enzyme Kinetics Module:

$$v_o = \frac{v_{\max} [S]}{K_m \left(1 + \frac{[I]}{K_I} \right) + [S]}$$

where v_o is the initial velocity, v_{\max} the maximum velocity, $[S]$ the substrate concentration and K_m the Michaelis-Menten constant calculated for trehalose 6-phosphate, $[I]$ is the inhibitor concentration and K_I is the inhibition constant.

3.5.5 EnzChek Phosphate Assay

T6PP-catalyzed T6P hydrolysis was monitored continuously by using the EnzChek Phosphate Assay kit. In this assay phosphate formation is coupled to the phosphorylase reaction of MESG catalyzed by purine nucleoside phosphorylase.



Scheme 3.4. T6PP –coupled enzyme assay utilizing PNP; (a) T6PP-catalyzed hydrolysis of trehalose 6-phosphate; (b) Enzymatic conversion of MESG to ribose 1-phosphate and 2-amino-6-mercapto-7-methylpurine by purine ribonucleoside phosphorylase(PNP). Conversion of MESG to 2-amino-6-mercapto-7-methylpurine shifts absorbance from 330 to 360 nm, respectively. The accompanying change in the absorption maximum at 360 nm allows quantitation of inorganic phosphate (Pi) consumed in the reaction.

3.6 References

1. Vang, T., Xie, Y., Liu, W. H., Vidović, D. i., Liu, Y., Wu, S., Smith, D. H., Rinderspacher, A., Chung, C., Gong, G., Mustelin, T., Landry, D. W., Rickert, R. C., Schürer, S. C., Deng, S.-X., and Tautz, L. (2010) Inhibition of Lymphoid Tyrosine Phosphatase by Benzofuran Salicylic Acids, *Journal of Medicinal Chemistry* 54, 562-571.
2. Barr, A. J. (2010) Protein tyrosine phosphatases as drug targets: strategies and challenges of inhibitor development, *Future Med Chem* 2, 1563-1576.
3. Zhang, S., Chen, L., Luo, Y., Gunawan, A., Lawrence, D. S., and Zhang, Z.-Y. (2009) Acquisition of a Potent and Selective TC-PTP Inhibitor via a Stepwise Fluorophore-Tagged Combinatorial Synthesis and Screening Strategy, *Journal of the American Chemical Society* 131, 13072-13079.
4. He, R., Yu, Z., He, Y., Zeng, L.-F., Xu, J., Wu, L., Gunawan, A. M., Wang, L., Jiang, Z.-X., and Zhang, Z.-Y. (2010) Double Click Reaction for the Acquisition of a Highly Potent and Selective mPTPB Inhibitor, *ChemMedChem* 5, 2051-2056.
5. Kim, S.-E., Bahta, M., Lountos, G. T., Ulrich, R. G., Burke, T. R., Jr, and Waugh, D. S. (2011) Isothiazolidinone (IZD) as a phosphoryl mimetic in inhibitors of the

- Yersinia pestis* protein tyrosine phosphatase YopH, *Acta Crystallographica Section D* 67, 639-645.
6. He, Y., Zeng, L.-F., Yu, Z.-H., He, R., Liu, S., and Zhang, Z.-Y. (2012) Bicyclic benzofuran and indole-based salicylic acids as protein tyrosine phosphatase inhibitors, *Bioorganic & Medicinal Chemistry* 20(6), 1940-6.
 7. Yu, Z.-H., Chen, L., Wu, L., Liu, S., Wang, L., and Zhang, Z.-Y. (2011) Small molecule inhibitors of SHP2 tyrosine phosphatase discovered by virtual screening, *Bioorganic & Medicinal Chemistry Letters* 21, 4238-4242.
 8. Zhang, M., Cho, E. J., Burstein, G., Siegel, D., and Zhang, Y. (2011) Selective inactivation of a human neuronal silencing phosphatase by a small molecule inhibitor, *ACS Chem Biol* 6, 511-519.
 9. Park, H., Jung, S.-K., Yu, K. R., Kim, J. H., Kim, Y.-S., Ko, J. H., Park, B. C., and Kim, S. J. (2011) Structure-Based Virtual Screening Approach to the Discovery of Novel Inhibitors of Eyes Absent 2 Phosphatase with Various Metal Chelating Moieties, *Chemical Biology & Drug Design* 78, 642-650.
 10. Profit, A. A., Lee, T. R., and Lawrence, D. S. (1998) Bivalent Inhibitors of Protein Tyrosine Kinases, *Journal of the American Chemical Society* 121, 280-283.
 11. Lu, Z., Dunaway-Mariano, D., and Allen, K. N. (2008) The catalytic scaffold of the haloalkanoic acid dehalogenase enzyme superfamily acts as a mold for the trigonal bipyramidal transition state, *Proc Natl Acad Sci U S A* 105, 5687-5692.

12. Burke, T. R., Kole, H. K. & Roller, P. P. (1994) Potent inhibition of insulin receptor dephosphorylation by a hexamer peptide containing the phosphotyrosyl mimetic F2Pmp. *Biochem. Biophys. Res. Commun.* 204, 129–134.
13. Jia, Z. et al. (2001) Structure of protein tyrosine phosphatase 1B in complex with inhibitors bearing two phosphotyrosine mimetics. *J. Med. Chem.* 44, 4584–4594.
14. Bayly, C. & Ohkubo, M. (2001) Sulfur substituted aryldifluoromethylphosphonic acids as PTP1B inhibitors. Patent WO 01/70754.
15. Leblanc, Y., Dufresne, C., Gauthier, J. Y. & Young, R. (2001) Aromatic phosphonates as protein tyrosine phosphatase 1B (PTP1B) inhibitors. Patent WO 01/46204.
16. Shen, K. et al. (2001) Acquisition of a specific and potent PTP1B inhibitor from a novel combinatorial library and screening procedure. *J. Biol. Chem.* 276, 47311–47319.
17. Leblanc, Y., Dufresne, C., Roy, P. & Wang, Z. (2000) Phosphonic and carboxylic acid derivatives as inhibitors of protein tyrosine phosphatase-1B. Patent WO 00/69889.
18. Ala, P.J. et al. (2006) Structural basis for inhibition of protein-tyrosine phosphatase 1B by isothiazolidinone heterocyclic phosphonate mimetics. *J. Biol. Chem.*, 281(43), 32784-95.

19. Kim, S.H. et al. (2013) Design, synthesis, functional and structural characterization of an inhibitor of N-acetylneuraminase-9-phosphate phosphatase: observation of extensive dynamics in an enzyme/inhibitor complex. *Bioorg Med Chem Lett.*, 23(14), 4107-11.
20. Subramanian, T., Ren, H., Subramanian, K.L., Sunkara, M., Onono, F.O., Morris, A.J., Spielmann, H.P. (2014) Design and synthesis of non-hydrolyzable homoisoprenoid α -monofluorophosphonate inhibitors of PPAPDC family integral membrane lipid phosphatases. *Bioorg Med Chem Lett.*, 24(18), 4414-17.
21. Tran, K.L., Aronov, P.A., Tanaka, H., Newman, J.W., Hammock, B.D., Morisseau, C. (2005) Lipid sulfates and sulfonates are allosteric competitive inhibitors of the N-terminal phosphatase activity of the mammalian soluble epoxide hydrolase. *Biochemistry*, 44 (36), 12179–12187.
22. Di Costanzo, L., Sabio, G., Mora, A., Rodriguez, P. C., Ochoa, A. C., Centeno, F., and Christianson, D. W. (2005) Crystal structure of human arginase I at 1.29-Å resolution and exploration of inhibition in the immune response, *Proc Natl Acad Sci U S A* 102, 13058-13063.
23. Usher, K. C., Blaszczyk, L. C., Weston, G. S., Shoichet, B. K., and Remington, S. J. (1998) Three-Dimensional Structure of AmpC β -Lactamase from *Escherichia coli* Bound to a Transition-State Analogue: Possible Implications for the Oxyanion Hypothesis and for Inhibitor Design, *Biochemistry* 37, 16082-16092.

24. Usher, K. C., Blaszczyk, L. C., Weston, G. S., Shoichet, B. K., and Remington, S. J. (1998) Three-Dimensional Structure of AmpC β -Lactamase from *Escherichia coli* Bound to a Transition-State Analogue: Possible Implications for the Oxyanion Hypothesis and for Inhibitor Design, *Biochemistry* 37, 16082-16092.
25. Strynadka, N. C., Adachi, H., Jensen, S. E., Johns, K., Sielecki, A., Betzel, C., Sutoh, K., and James, M. N. (1992) Molecular structure of the acyl-enzyme intermediate in beta-lactam hydrolysis at 1.7 Å resolution, *Nature* 359, 700-705.
26. Farelli, J. D.; Galvin, B. D.; Li, Z.; Liu, C.; Aono, M.; Garland, M.; Hallett, O. E.; Causey, T. B.; Ali-Reynolds, A.; Saltzberg, D. J.; Carlow, C. K.; Dunaway-Mariano, D.; Allen, K.N. *PLoS Pathog.*, **2014**, 10(7), e1004245.
27. Berndt, F., Sajadi, M., Ernsting, N. P., Mahrwald, R., (2011) Covalent linkage of N-methyl-6-oxyquinolinium betaine to trehalose. *Carbohydrate Research*, **346**, 2960–2964.
28. Webb, M. R. *Proc. Natl. Acad. Sci. U.S.A.* 1992, 89, 4884–4887.
29. Liu, C.; Mariano, P.S. An improved method for the large scale preparation of α , α' -trehalose-6-phosphate. *Tetrahedron Lett*, **2015**, 56(23), 3008–3010.

CHAPTER FOUR

SYNTHESIS AND EVALUATION OF FIRST GENERATION TREHALOSE-6-PHOSPHATE PHOSPHATASE REVERSIBLE BIOMODULAR INHIBITORS

4.1. Background

Carbohydrates play an important role in biological systems, including serving as precursors for building diverse polymers, storing short-term energy, providing structural building materials, serving as molecular "tags" to allow recognition of specific cells and molecules. Many diseases are associated with malfunctioning biochemical processes involving carbohydrates, and the ability to interfere in such processes by targeting the enzyme catalyst, is of great biomedical importance.

Trehalose, a natural alpha-linked disaccharide formed by an α,α -1,1-glucoside bond between two α -glucose units, is synthesized by a variety of bacteria, plants, fungi and invertebrates to support cell survival by functioning as a fuel, a metabolic regulator or a protectant against environmental stress. Five different trehalose biosynthetic pathways are known to exist (OtsA/B or TPS/TPP pathway, TS pathway, TreY/TreZ pathway, TreP pathway, TreT pathway) [1], one of which, the OtsA/B pathway is common among pathogenic bacteria and fungi as well as in parasitic nematodes. The OtsA/B pathway, which utilizes glucose and glucose-6-phosphate to generate trehalose-6-phosphate catalyzed by trehalose synthase, then hydrolyzed to trehalose by trehalose-6-phosphate

phosphatase (T6PP). Previously reported *otsA* and *otsB* gene knockout (or knockdown) experiments have shown that both pathway enzymes are essential for growth of *M. tuberculosis* in laboratory culture, and for its virulence in a mouse model [2]. The T6P synthase and phosphatase are also required for trehalose production in the filamentous fungus *Fusarium graminearum*, however only the T6PP proved to be indispensable for development and virulence [3]. RNAi gene silencing carried out in the nematode model system *Caenorhabditis elegans* revealed that the T6PP is essential, however only when the T6P synthase-encoding gene is functional [4].

Based on these findings we concluded that trehalose-synthesizing pathogens are likely to be vulnerable to the action of small molecule inhibitors of their T6PPs. In Chapter Three trehalose-6-sulfate (T6S) was identified as an inert T6P analog having moderate binding affinity and the ability to induce cap-domain closure in the bacterial T6P phosphatases. In the study described below, a structure-guided search for inhibitors of T6PPs from important target pathogens was carried out. The effort was aimed at uncovering a versatile T6PP inhibitor prototype that could be modified to target specific T6PPs of pathogens from various taxonomic groups. For this purpose, I selected several members of different structural families of potential T6PP inhibitors. These were designed and synthesized, and determination of binding affinities of these substances was carried out.

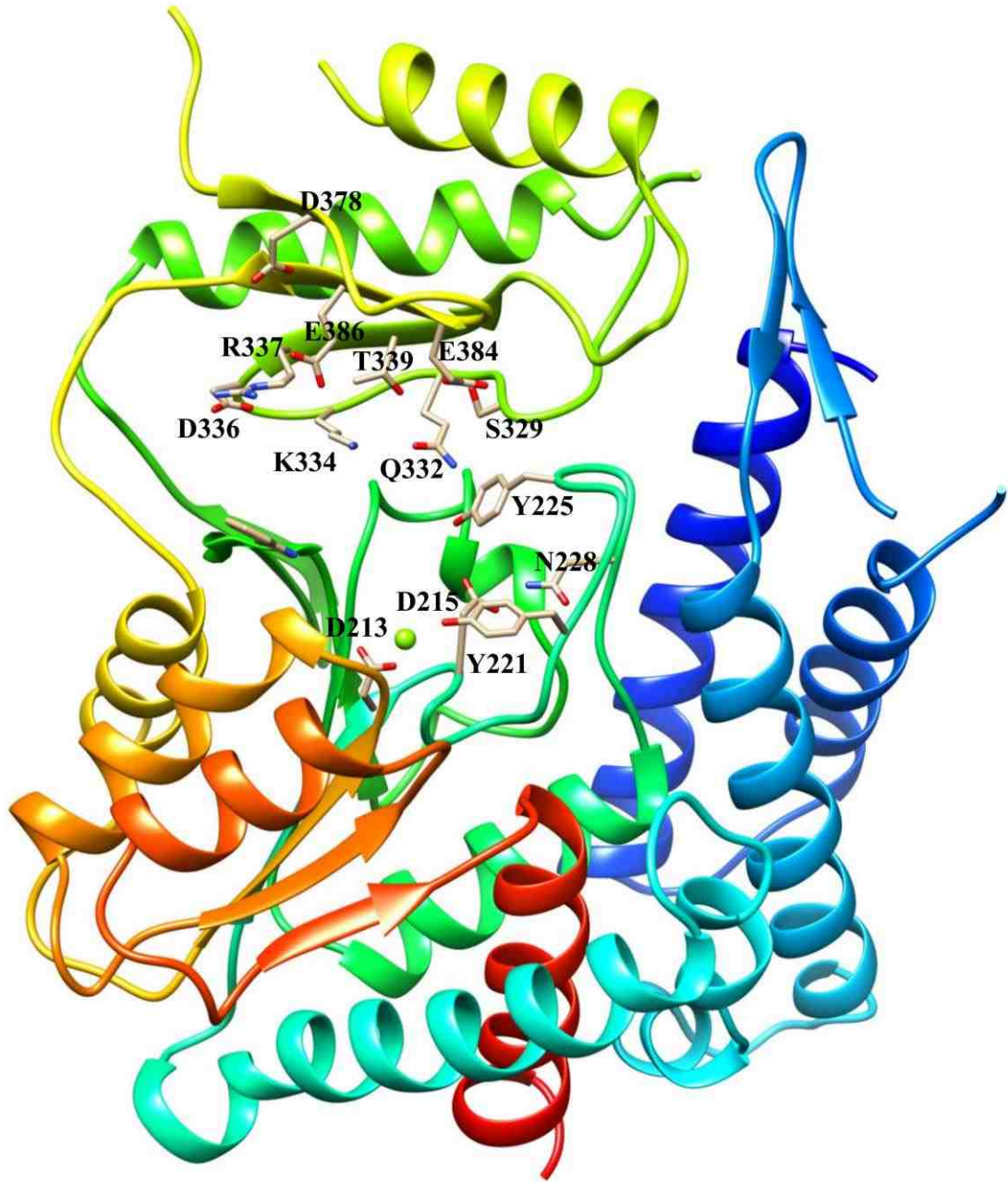
In parallel, the residues forming the substrate binding region at the T6PP cap domain were compared and probed for contributions to substrate binding by kinetic analysis of residue-directed mutants.

4.3 Results and Discussion

4.3.1. Substrate Recognition: Diversity in the T6PP Cap Domain Residue Usage and Function

Following the determination of the structure of the Bm-T6PP (with the Mg^{2+} cofactor bound), the residues which form the substrate-binding region of the cap domain could be identified. This work was carried out in collaboration with Dr. Karen Allen and co-workers at Boston University and Dr. Tilde Carlow and co-workers of New England BioLabs. My role was to measure the steady-state k_{cat} and K_m for wild-type and mutant *Bm*-T6PP-catalyzed hydrolysis of T6P and the K_i for T6S inhibition.

The conserved fold of the Ta-T6PP and Bm-T6PP structures provided more confidence in the threading models that could be generated from the T6PP ortholog sequences. Of the bacterial T6PP orthologs, *Mt*-T6PP proved to be the only one that is sufficiently robust to withstand amino acid replacement. Therefore, the SAR analysis carried out on Bm-T6PP was also carried out on Mt-T6PP. This work was carried out in collaboration with my labmate Dr. Tyrel Byran, who helped generate the mutant genes and gene products.



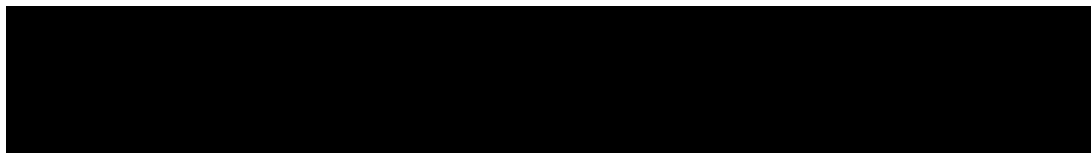
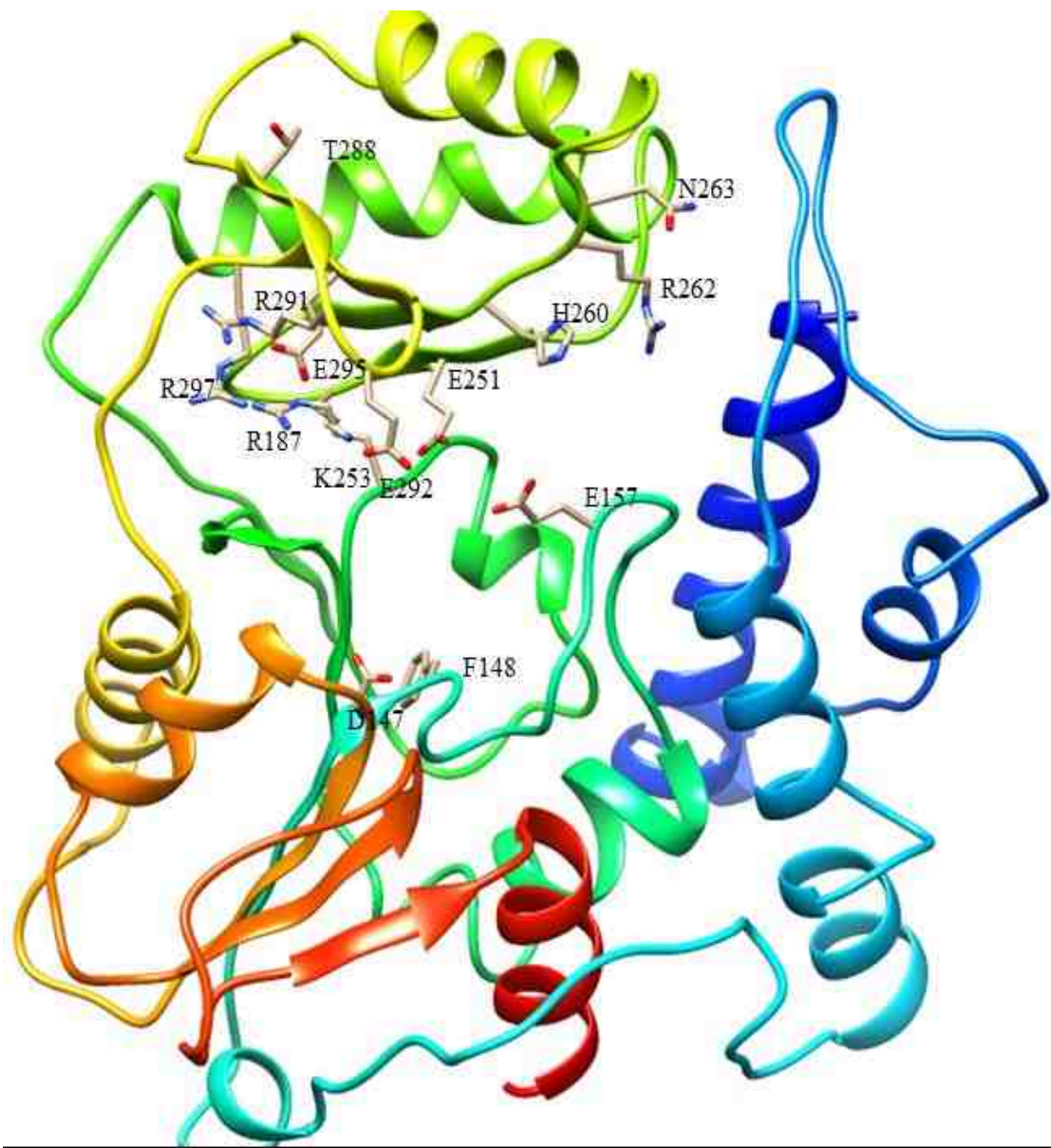


Table 4.1. Steady-state kinetic constants and dissociation constants for inhibitors for wild-type and variant *M. tuberculosis* or *B. malayi* T6PP-catalyzed hydrolysis of trehalose 6-phosphate.

<i>M. tuberculosis</i> T6PP					<i>B. malayi</i> T6PP				
Construct	k_{cat} (s^{-1})	K_m (μM)	k_{cat}/K_m ($M^{-1}s^{-1}$)	K_i trehalose-6-sulfate(μM)	Construct	k_{cat} (s^{-1})	K_m (μM)	k_{cat}/K_m ($M^{-1}s^{-1}$)	K_i trehalose-6-sulfate(μM)
wild type	10±1	540±110	1.9×10 ⁴	130±20	wild type	24 ± 2	360 ± 60	6.9 x 10 ⁴	82 ± 7
					Δ59	28 ± 1	260 ± 20	1.1 x 10 ⁵	-
Catalytic Asp residues					Catalytic Asp residues				
D147A	NA ^a	—	—	—	D213A	NA ^a	-	-	-
					D215A	~0.0004	-	-	-
Catalytic domain residues					Catalytic domain residues				
F148A	0.28±0.02	2200±400	1.3×10 ²	360±70					
					Y221A	1.0 ± 0.05	330 ± 50	3.0 x 10 ³	1,300 ± 100
E157A	25±0.6	230±20	1.1×10 ⁵	71±6					
					Y225A	5.5 ± 0.1	150 ± 10	3.6 x 10 ⁴	400 ± 40
R187K	0.11±0.01	3800±400	29	>4 mM ^b					
					N228A	18 ± 0.8	40 ± 8	4.5 x 10 ⁵	16 ± 2
					W280A	19 ± 2	150 ± 30	1.2 x 10 ⁵	270 ± 50
Cap residues					Cap residues				
E251A	0.99±0.06	1500±200	6.4×10 ²	>4 mM ^b	Q332A	0.22 ± 0.001	200 ± 40	5.5 x 10 ²	1,000 ± 200
					R337A	0.28 ± 0.03	400 ± 100	1.5 x 10 ³	700 ± 100
K253A	0.098±0.002	6800±300	14	>4 mM ^b	K334A	0.06 ± 0.007	500 ± 120	1.1 x 10 ²	150 ± 20
H260A	0.28±0.03	1100±300	2.5×10 ²	780±170					
					S329A	4 ± 0.2	250 ± 50	1.5 x 10 ⁴	240 ± 30
R262A	0.13±0.01	2100±300	63	2400±500					
					E384A	2.9 ± 0.2	100 ± 20	3.0 x 10 ⁴	200 ± 30
N263A	23±0.7	890±70	2.6×10 ⁴	320±40					
					E386A	2.3 ± 0.1	82 ± 15	2.8 x 10 ⁴	150 ± 20
T288A	11±0.6	1400±200	8.2×10 ³	1700±200					
					T339A	15.3 ± 1.0	200 ± 40	7.7 x 10 ⁴	35 ± 5
R291A	0.39±0.07	2900±900	1.3×10 ²	>4 mM ^b					
					D336A	0.094 ± 0.004	46 ± 6	2.0 x 10 ²	33 ± 5
E292A	15±0.5	540±60	2.7×10 ⁴	380±50					
E295A	0.16±0.01	1500±200	1.1×10 ²	190±20					
R297A	3±0.2	730±90	4.1×10 ³	460±40	D378A	10.6 ± 0.6	270 ± 30	3.9 x 10 ⁴	320 ± 30

Note: The residues in Bm-T6PP and Mt-T6PP are at the same position base on sequence alignment if they are in the same row.

The structure of the *Bm*-T6PP and threading model of the *Mt*-T6PP are shown in Figures 4.1 and 4.2, respectively. In each figure the residues identified for alanine replacement by mutagenesis are highlighted. The change in steady-state k_{cat} value observed for the mutant reflects the impact that the alanine substitution has on the efficiency that bound T6P is converted to product and released. Nonproductive binding (orientation of the reaction center is not optimized for catalysis) and/or disruption of the cap closure over the catalytic site and/or alteration of the electrostatic environment of the catalytic site can result in reduction in the k_{cat} value compared to that of the wild-type T6PP. The k_{cat}/K_m value reflects substrate binding and catalysis. If the magnitude of reduction in k_{cat} value and k_{cat}/K_m value is the same then it follows that the T6P binding affinity has been unaltered. On the other hand, if the k_{cat}/K_m value is decreased x -fold over the decrease observed in the k_{cat} value, then it follows that the substrate binding affinity is decreased x -fold. An independent measure of the change in substrate binding affinity upon Ala mutagenesis is the change in the inhibition constant for the inert substrate analog trehalose-6-sulfate (T6S). The k_{cat} and k_{cat}/K_m values for wild-type and mutant and *Bm*-T6PP and *Mt*-T6PP are listed in Table 4.1 along with the competitive inhibition constants (K_i) measured for T6S vs T6P.

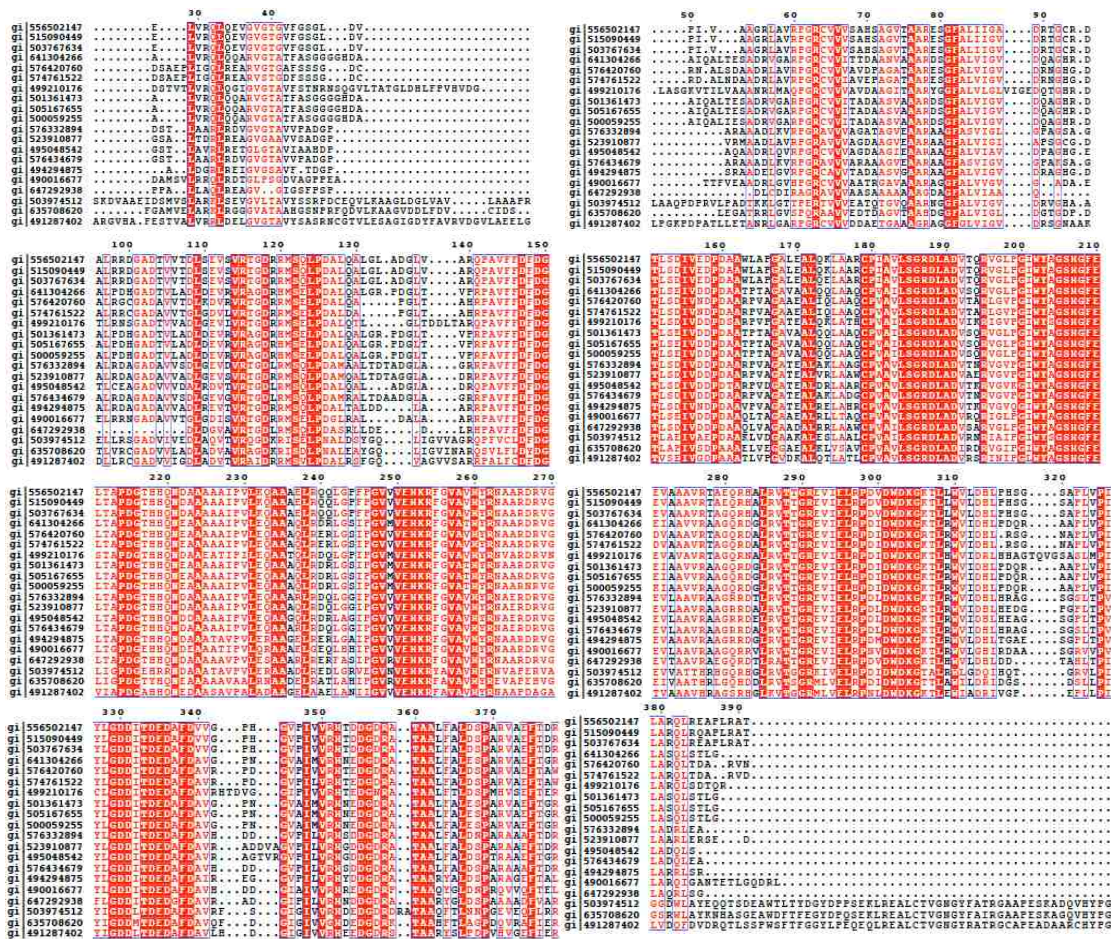


Figure 4.3. Alignment of Mycobacterium T6PP sequences

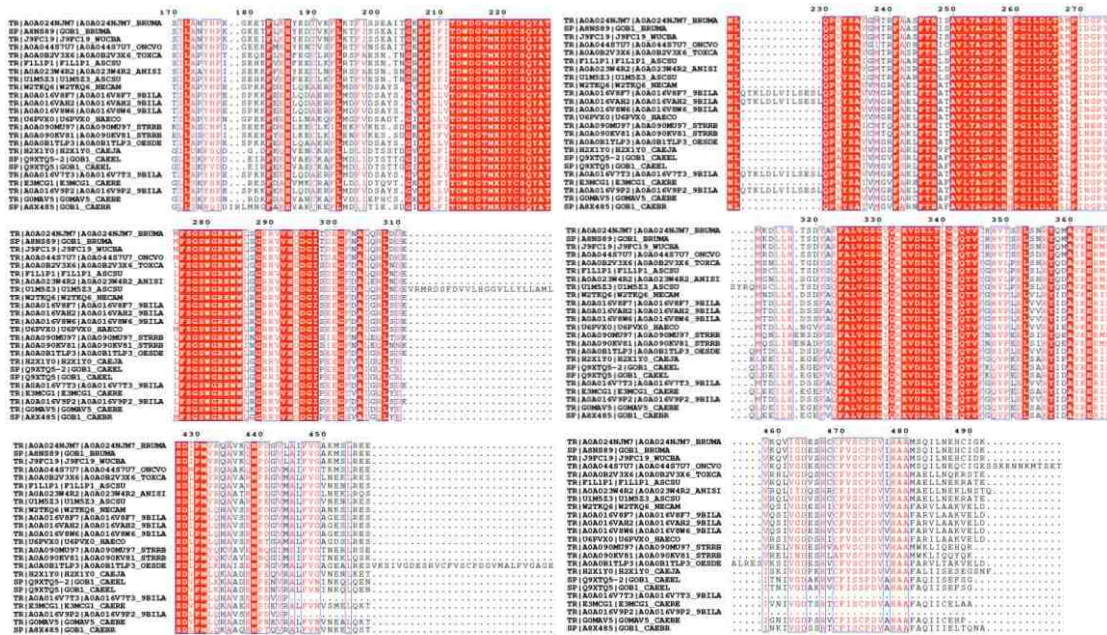


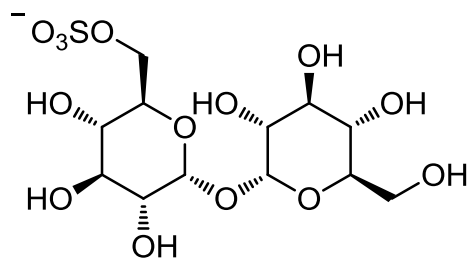
Figure 4.4 An alignment of nematode T6PP sequences.

As expected, replacement of the catalytic Asp147 resulted in the loss of all detectable activity (**Table 4.1**). The replacements of Phe148, Arg187, Glu251, Lys253, Arg262, Thr288, Arg291, Glu295 resulted in a dramatic change in K_m for T6P suggesting a role in substrate binding. Mutations in Phe148, Arg187, Glu251, Lys253, His260, Arg262, Arg291, E295 resulted in large decreases in k_{cat} (36-, 91-, 10-, 100-, 36-, 77-, 26-, 77-fold, respectively) suggesting a role in catalysis. Each of these residues except for Phe148 are found in the cap domain (**Figure 4.2**) and may interact with the sugar moiety in order to orient the substrate for catalysis.

We also used inhibitor binding studies to test if any of the protein variants differed in their affinity for substrate. To assess substrate affinity, the substrate analogue trehalose

6-sulfate was used to measure K_I for all of the T6PP variants (**Table 4.1**). Trehalose 6-sulfate was shown by steady-state inhibition kinetics to be a competitive inhibitor of wild type T6PP with a K_I of 130 μ M against trehalose 6-phosphate as substrate. The variants except E295 that have dramatic increased K_m showed dramatic increases in K_I for trehalose 6-sulfate: Phe148, Arg187, Glu251, Lys253, Arg262, Thr288, Arg291 (**Table 4.1, Figure 4.2**). From these experiments, Phe148, Arg187, Glu251, Lys253, Arg262, Thr288, Arg291 are likely to be involved in binding trehalose 6-phosphate, while E295 and His260 may play other roles in catalysis. These roles may include desolvation, steric restraint of the substrate for catalysis, or the positioning of other residues required for enzyme activity.

In order to design and synthesize more drug like inhibitors we need to learn from the nature. Base on previous works, carbohydrates binding to proteins is often accompanied by stacking interaction with aromatic residue [8-10] Our previous work also suggests that mutating the aromatic residues in the sugar binding sites of *B. malayi* T6PP result in low binding affinity (16 fold decreased) with T6S (trehalose-6 sulfate) inhibitor [11]. These observations suggest that inhibitors which possess variously substituted hydrophobic aryl and/or alkyl groups attached to the 1, 2, 3 and 4 positions of the glucose-6-sulfate backbone might display enhanced binding to the T6PPs. This reasoning led to the selection of the carbohydrate analogs displayed in **Scheme 1** as members of the library that was prepared and screened in this effort.

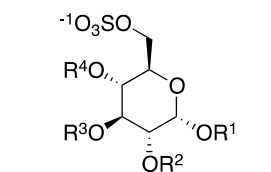
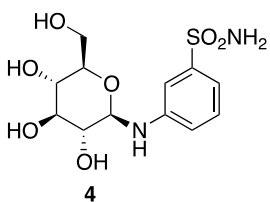
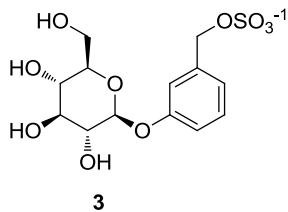
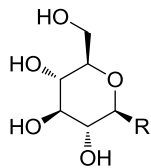
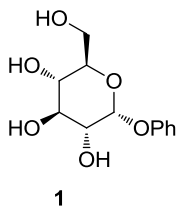


Trehalose-6-sulfate (T6S)

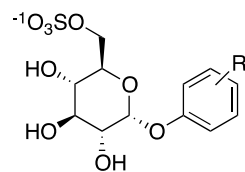
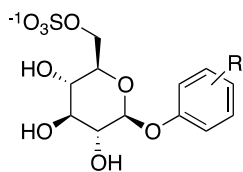
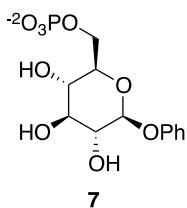
In the study described below, a structure-guided search for inhibitors of T6PPs from important target pathogens was carried out. The effort was aimed at uncovering a versatile T6PP inhibitor prototype that could be modified to target specific T6PPs of pathogens from various taxonomic groups. For this purpose, selected several members of different structural families of potential T6PP inhibitors were designed and synthesized. A determination of binding affinities of these substances was carried out.

4.3.2 Synthesis

Scheme 4.1.

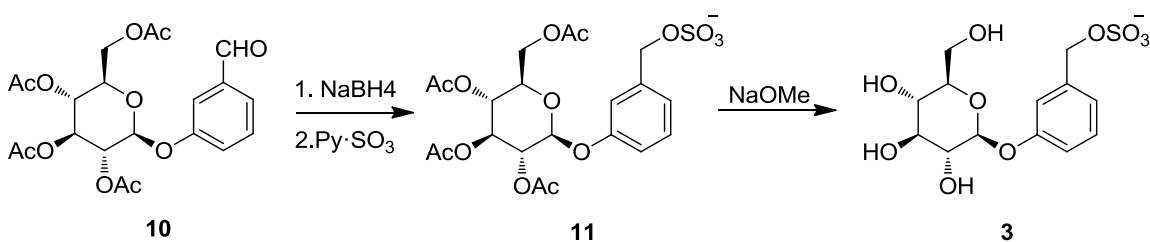


	R ¹	R ²	R ³	R ⁴
5a	H	H	H	H
5b	Me	H	H	H
5c	Ph	H	H	H
5d	Me	Bn	H	H
5e	Me	H	Bn	H
5f	Me	H	H	Bn

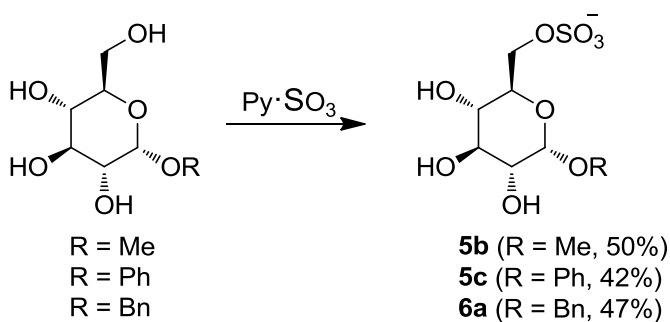


Inhibitor Preparation. Phenyl α -D-glucopyranoside (**1**) and phenyl β -D-glucopyranoside (**2a**) are commercially available substances and glucose derivatives **2b** [12], **2c** [13], **2d** [14] and **4** [15], and glucose-6-sulfate **5a** [16] were synthesized by using the referenced procedures. The routes utilized for preparation of the other members of the T6PP inhibitor library, displayed in Schemes 2-10 below and described completely in the Experimental, begin with either commercially available or previously synthesized starting materials. Each substance was shown to be >95% pure by using NMR spectroscopy and HPLC analysis.

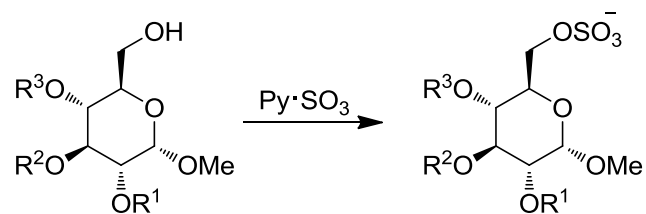
Scheme 4.2.



Scheme 4.3.



Scheme 4.4.



$R^1 = \text{Bn}, R^2 = R^3 = \text{H}$

$R^1 = R^3 = \text{H}, R^2 = \text{Bn}$

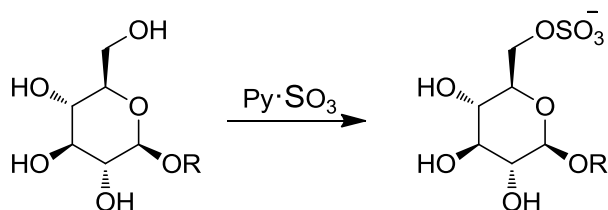
$R^1 = R^2 = \text{H}, R^3 = \text{Bn}$

5d ($R^1 = \text{Bn}, R^2 = R^3 = \text{H}$, 43%)

5e ($R^1 = R^3 = \text{H}, R^2 = \text{Bn}$, 50%)

5f ($R^1 = R^2 = \text{H}, R^3 = \text{Bn}$, 51%)

Scheme 4.5.



$R = \text{n-octyl}$

$R = 1\text{-naphthyl}$

$R = 1\text{-(1H-4-phenyl-1,2,3-triazole)}$

$R = \text{phenyl}$

$R = 4,4'\text{-biphenyl}$

$R = 4\text{-nitrophenyl}$

$R = 2\text{-formylphenyl}$

$R = 4\text{-formylphenyl}$

6b ($R = \text{n-octyl}$, 56%)

6c ($R = 1\text{-naphthyl}$, 45%)

6d ($R = 1\text{-(1H-4-phenyl-1,2,3-triazole)}$, 55%)

8a ($R = \text{phenyl}$, 49%)

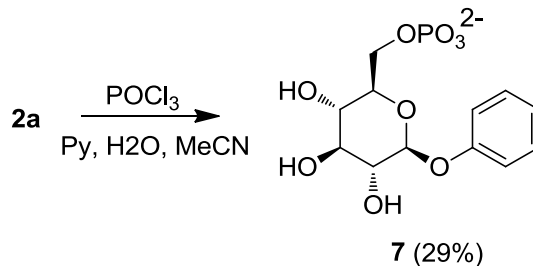
8b ($R = 4,4'\text{-biphenyl}$, 49%)

8e ($R = 4\text{-nitrophenyl}$, 31%)

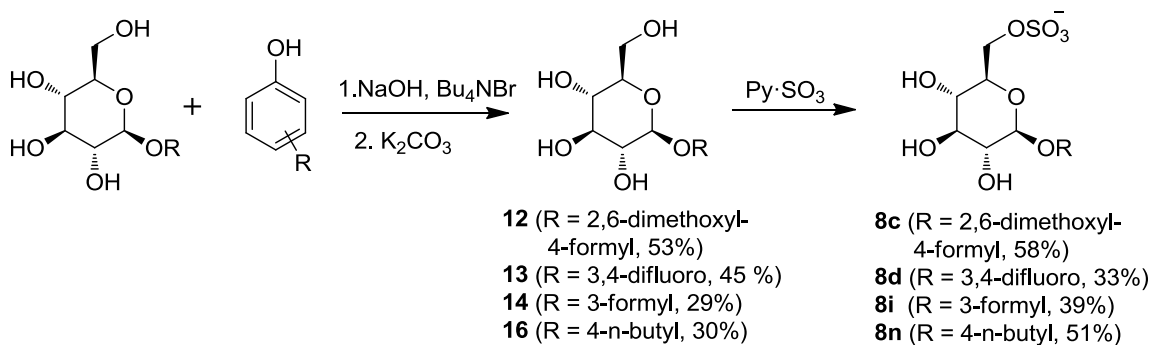
8h ($R = 2\text{-formylphenyl}$, 39%)

8j ($R = 4\text{-formylphenyl}$, 59%)

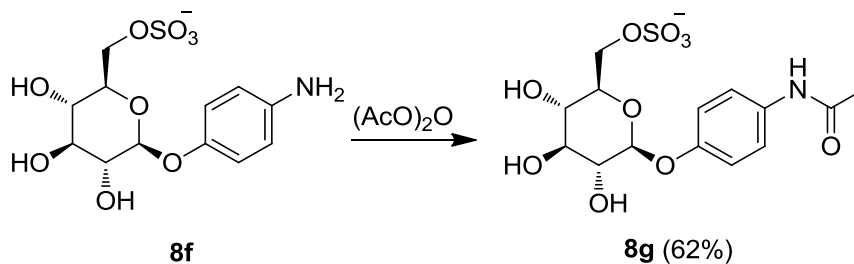
Scheme 4.6.



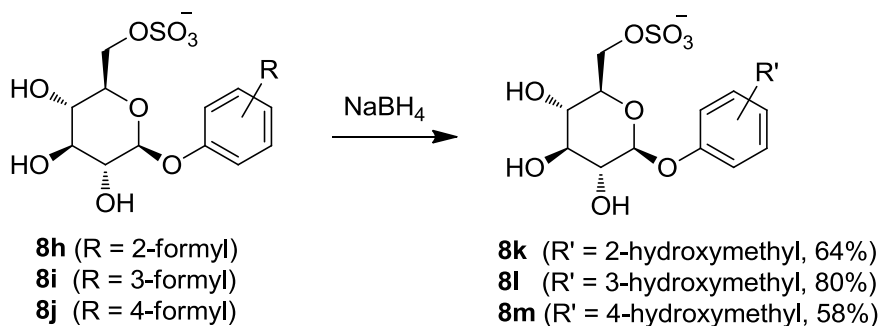
Scheme 4.7.



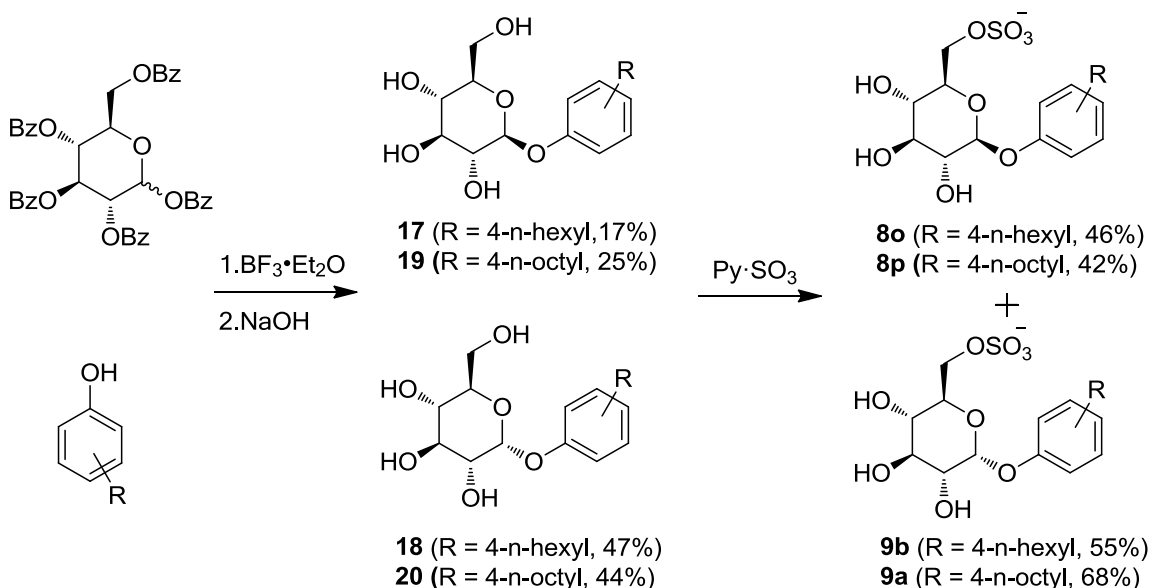
Scheme 4.8.



Scheme 4.9.



Scheme 4.10.



4.3.3 Catalytic hydrolysis of Compound 7 by T6PP

The catalytic activities of the T6PPs toward p-nitrophenyl phosphate (PNPP), a common substrate of phosphatases, glucose-6-phosphate and phenyl β -D-glucose-6-phosphate (**7**) were determined. In this series, only **7** was found to serve as a substrate for these phosphatases with k_{cat} values of 1.4×10^{-2} , 0.96×10^{-2} , 0.71×10^{-2} , $0.71 \times 10^{-2} \text{ s}^{-1}$ and or the respective Bm-T6PP, Mt-T6PP, Sb-T6PP, As-T6PP and St-T6PP. These values compare to the k_{cat} values observed for hydrolysis of T6P catalyzed by the T6PPs, which fall in the range of $4\text{-}24 \text{ s}^{-1}$, which shows that the phenyl glucopyranoside base compounds can bind to T6PPs, where the binding affinity comes from the introducing phenyl group.

Table 4.2 Steady-state kinetic constants for T6PPs-catalyzed hydrolysis of compound 7.

<u>T6PP Source</u>	<u>k_{cat} (s^{-1})</u>
<i>Brugia malayi</i>	1.4×10^{-2}
<i>Mycobacterium tuberculosis</i>	0.96×10^{-2}
<i>Shigella boydii</i>	0.71×10^{-2}
<i>Ascaris suum</i>	0.71×10^{-2}
<i>Samonella typhimurium</i>	0.41×10^{-2}

4.3.4 Inhibition measurement using High Throughput Screening

An initial evaluation of the inhibitory activities of a large number of the substances shown in Scheme 1 (see Table 1) toward T6PP catalyzed hydrolysis reactions of T6P was carried out by using a high throughput screen. For this purpose, the initial velocities were determined for reactions of T6P promoted by Bm-T6PP, Mt-T6PP, Sb-T6PP, As-T6PP and St-T6P in the presence of 1mM inhibitor (V') and absence of inhibitor (V_0). Each well of a 96-well plate contained 50 μ L of a solution containing 5-25 nM freshly purified T6PP, T6P (400 μ M for Mt-T6PP, Sb-T6PP and StT6PP, 200 μ M for Bm-T6PP and As-T6PP) and 1 mM inhibitor and buffer (25 mM HEPES pH 7.5, 50 mM NaCl, 5 mM MgCl₂, and 5% glycerol for Mt-T6PP; 50 mM HEPES pH 7.5, 25 mM NaCl, 2 mM MgCl₂, and 5% glycerol for Sb-T6PP; 50 mM Tris pH 7.5, 50 mM NaCl, 5 mM MgCl₂, 1mM DTT and 5% glycerol for As-T6PP; 25 mM Tris pH 7.5, 25 mM NaCl, 2 mM MgCl₂, 1 mM DTT for Bm-T6PP; and 50 mM HEPES pH 8.0, 25 mM NaCl, 5 mM MgCl₂, and 5%

glycerol for St-T6PP. The plate was incubated at room temperature for 5 min at which time 5 μ L of each solution in each well was transferred to individual wells of another 96 well plate, each containing containing 45 μ L the appropriate buffer. After adding 100 μ L BioMol Green (Enzo Life Sciences) to each well and incubating for 30 min absorbance of each well at 625 nm were measured using a SpectraMax i3 Multi-Mode Microplate Detection Platform. The initial velocity ratios (V'/V_0) obtained by using this procedure are given in Table 4.3.

Table 4.3. Inhibition measurement using HTS

Compound	Bm-T6PP	Mt-T6PP	Sb-T6PP	As-T6PP	St-T6PP
T6S	0.13	0.43	0.22	0.21	0.01
Trehalose	0.98	0.83	1.01	0.97	0.88
1	0.96	0.88	0.86	0.97	1
2a	1.12	0.81	0.9	1	0.87
2b	1	0.88	0.92	0.97	0.77
2c	0.99	1.04	0.92	0.81	1.09
2d	0.85	0.95	1	0.96	0.9
3	0.59	0.96	0.8	0.98	0.85
4	1.05	1.17	0.85	0.96	1
5a	0.93	0.97	0.75	0.94	0.84
5b	0.8	0.91	1	1.07	1.04
5c	0.42	1.17	0.76	0.71	0.64
5d	0.53	1.01	1	0.96	0.95
5e	0.67	1.16	0.84	1.04	0.99
5f	0.68	1.11	0.95	0.99	0.97
6a	0.07	0.83	0.74	0.86	0.47
6b	0.72	0.83	0.79	0.9	0.54
6c	0.85	0.85	0.85	0.91	0.8
6d	0.98	0.98	0.9	0.76	0.97
7	0.79	0.94	0.94	0.98	0.77
8a	0.52	0.94	0.76	0.92	0.81
8b	0.58	0.58	0.84	0.9	0.85
8c	0.55	1.09	1	0.94	0.96
8d	0.74	0.8	0.92	0.88	0.89
8e	0.64	1.27	0.77	0.83	0.68
8f	0.63	1	1.03	0.74	0.94
8g	0.87	0.94	0.88	0.9	0.85
8h	0.79	1.17	0.96	0.99	0.85
8i	1.05	0.67	0.81	0.78	0.95
8j	1	0.87	1.06	0.81	0.87
8k	0.89	0.89	0.85	0.9	0.73
8l	0.69	0.69	0.46	0.63	0.77
8m	0.68	0.85	0.67	0.76	0.79
8p	0.07	0.42	0.04	0.02	0.01

4.3.5 Competitive inhibition test

We also tested the inhibition of **8p** on Sb-T6PP using EnzChek Phosphate Assay, which turns out to be competitive inhibitor. The initial velocities (v) for T6PPs catalyzed hydrolysis of trehalose 6-phosphate ($0.5 K_m$ - $3 K_m$) at presence of different concentrations of inhibitor (0, $0.5 K_i$, $1.7 K_i$, $2.5 k_i$, $3.3K_i$) were measured at $25\text{ }^\circ\text{C}$ using EnzCheck Phosphate Assay Kit (Invitrogen). The assay solutions that contained 1 mM MgCl_2 , 0.1 mM sodium azide 1.0 unit/mL purine nucleoside phosphorylase, and 0.2 mM MESG in 50 mM Tris-HCl (pH 7.5). Absorbance changes were monitored at 360 nm ($\Delta\epsilon = 9.8\text{ mM}^{-1}\text{cm}^{-1}$).

Inhibitor: 8p, Enzyme: Sb-T6PP, Units: V: $\mu\text{M/s}$, S (T6P): μM

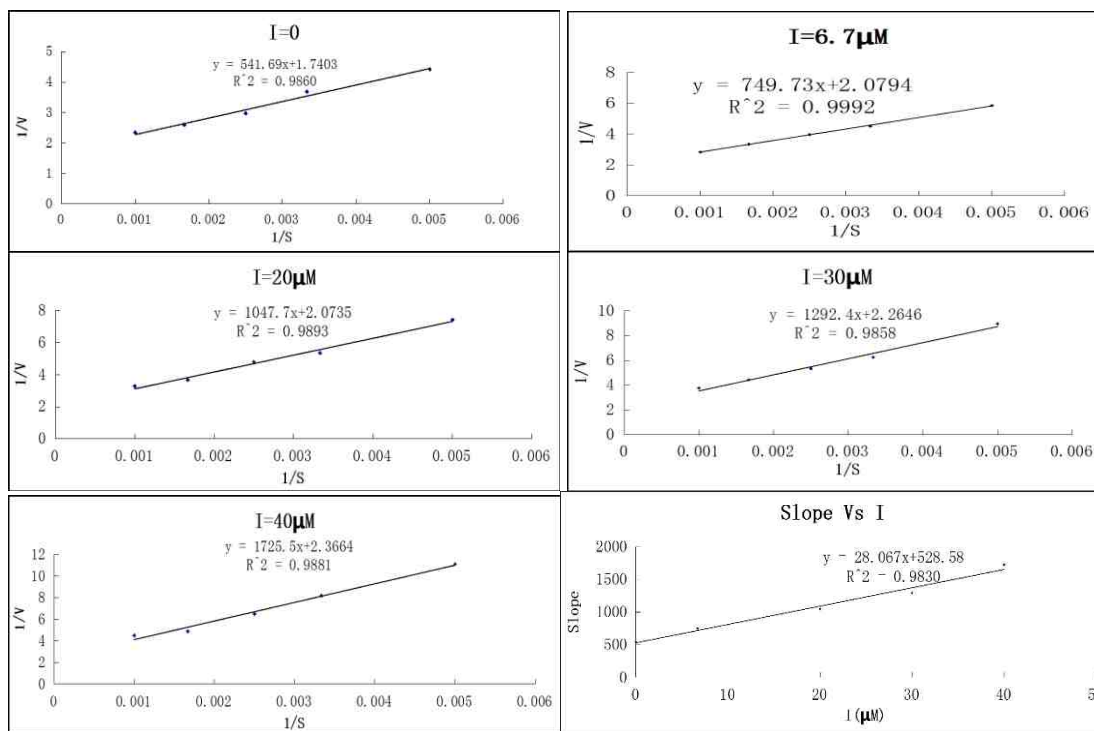


Figure 4.5. 8p's competitive inhibition on Sb-T6PP

4.3.6 Inhibition Constants

Analysis of the screening results given in Table 1 showed that the glucaose-6-sulfate derivatives **5c**, **6a**, **8a**, **8b** and **8i**, each of which contain a hydrophobic group at the glycosidic position, display high T6PP inhibitory activities. This finding prompted a more detailed investigation of the inhibition constants of these substances. For this purpose, initial velocities (v) of the T6PP catalyzed hydrolysis reactions of T6P (0.5 - $3 K_m$) at $25\text{ }^\circ\text{C}$ in the presence of different concentrations (0 , K_i , $2K_i$) of inhibitors **5c**, **6a**, **8a**, **8b** and **8i** were determined using the EnzCheck Phosphate Assay Kit (Invitrogen). In addition to enzyme (T6PP), substrate (T6P) and inhibitor, the assay solutions contain 1 mM MgCl_2 , 0.1 mM sodium azide 1.0 unit/mL purine nucleoside phosphorylase, and 0.2 mM MESG in 50 mM Tris-HCl (pH 7.5). Absorbance changes were monitored at 360 nm ($\Delta\epsilon = 9.8\text{ mM}^{-1}\text{cm}^{-1}$). Initial velocity data, measured as a function of trehalose 6-phosphate (0.5 to $5K_m$) and inhibitor (0 , K_i , $2K_i$) concentrations, were fitted using the SigmaPlot Enzyme Kinetics Module to the following equation:

$$v_o = \frac{v_{\max}[S]}{K_m \left(1 + \frac{[I]}{K_I}\right) + [S]}$$

where v_o is the initial velocity, v_{\max} the maximum velocity, $[S]$ the substrate concentration and K_m the Michaelis Menten constant calculated for trehalose 6-phosphate, $[I]$ is the inhibitor concentration and K_i is the inhibition constant. This treatment gave the K_i values listed in Table 4.4.

Because the initial screening results (Table 4.3) demonstrated that 4-octylphenyl β -D-glucose-6-sulfate (**8p**) is the most active inhibitor of the five T6PPs, the closely related 4-butyl- and 4-hexylphenyl and 4-octylphenyl- β - and -hexylphenyl and 4-octylphenyl α -D-glucopyranoside-6-sulfate, **8n**, **8o**, **9a** and **9b**, respectively, were prepared and subjected to kinetic studies. It is clear from viewing the results in Table 3 that the strategy of incorporating both a negatively charged 6-sulfate and hydrophobic glycosidic group into the glucose skeleton does lead to the design of highly active inhibitors of the T6PPs. Moreover, a comparison of the activities of **8p** and **9a** shows the spacial disposition of the glycosidic alkylphenyl group plays an important role in binding to the phosphatases.

Table 4.4. Competitive inhibition constants

Inhibitor	<i>B. malayi</i>	<i>M. tuberculosis</i>	<i>S. boydii</i>	<i>A. suum</i>	<i>S. typhimurium</i>
5c	320±30			1800±260	
6a	160±20	-	-	-	-
8a	830±100	-	-	-	-
8b	-	1600±270	-	-	-
8i	-	1700±350	-	-	-
8n	NI	NI	>400 ^f	NI	>400 ^h
8o	>200 ^a	>400 ^b	140±20	>200 ^g	>400 ⁱ
8p	61±10	>300 ^c	13±2	180±20*	120±20
9a	5.3±0.6	>300 ^d	21±3	84±10*	56±6
9b	82±10*	>400 ^e	78±9	350±30*	280±30

*: Slow-onset inhibition observed, preincubation time: 2 minutes at room temperature;

- : Did not test;

NI: No inhibition observed when T6P = K_m in the presence of 400 μ M inhibitor;

^a: 19% inhibition observed in the presence of 200 μ M **8o**;

^b: 2% inhibition observed in the presence of 400 μ M **8o**;

^c: 16% inhibition observed in the presence of 300 μ M **8p**;

^d: 36% inhibition observed in the presence of 300 μ M **9a**;

^e: 4% inhibition observed in the presence of 400 μ M **9b**;

^f: 4% inhibition observed in the presence of 400 μ M **8n**;

^g: 15% inhibition observed in the presence of 200 μ M **8o**;

^h: 5% inhibition observed in the presence of 400 μ M **8n**;

ⁱ: 4% inhibition observed in the presence of 400 μ M **8o**;

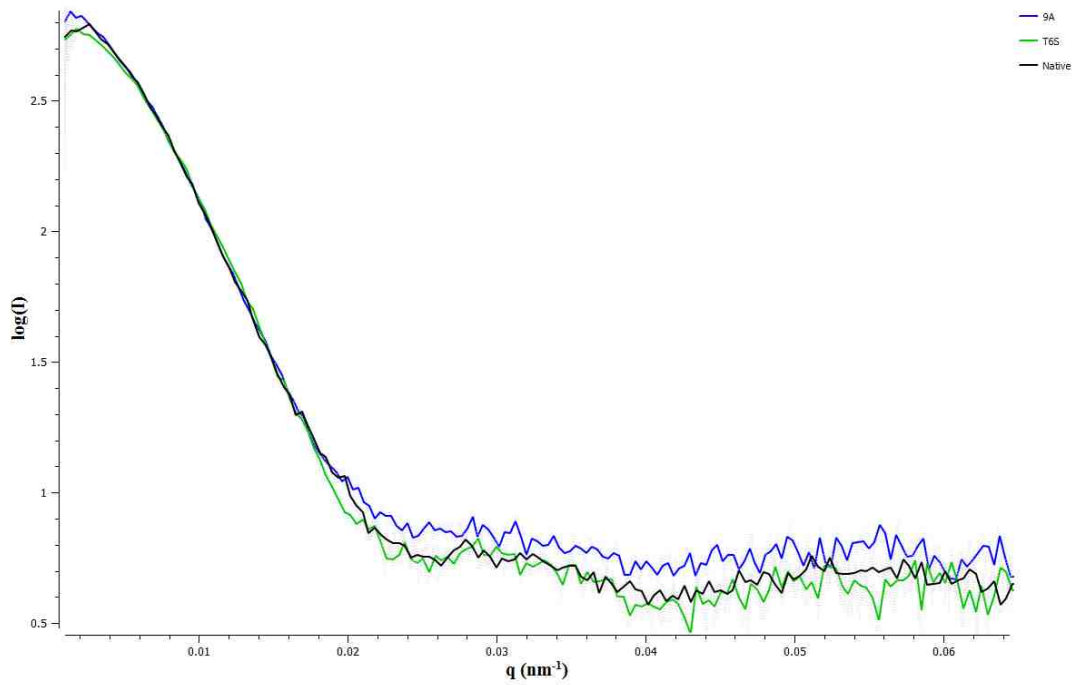
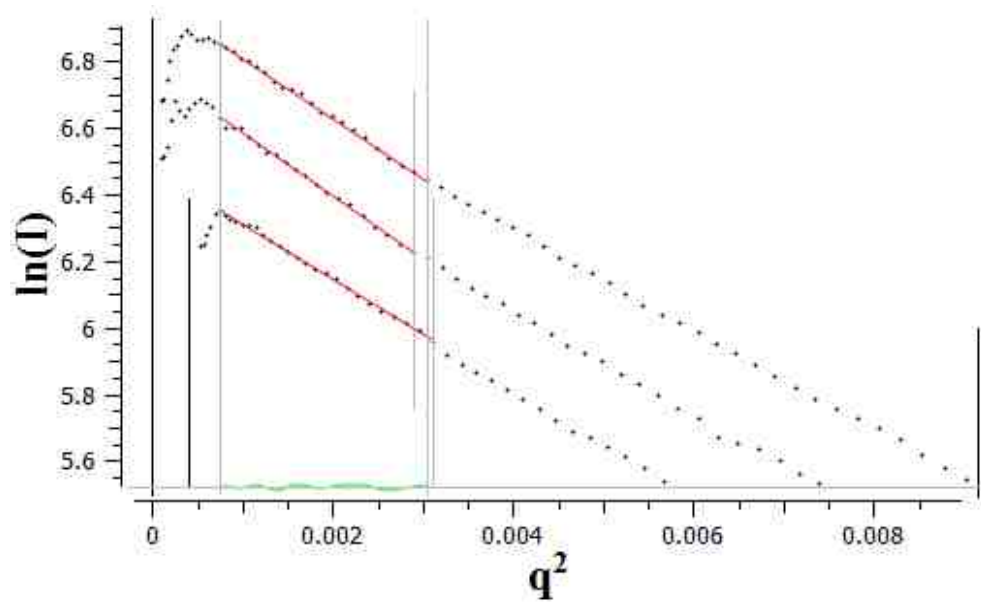
Interestingly, the inhibitors **8p**, **9a**, **9b** showed slow-onset inhibition on As-T6PP, and this phenomenon was also observed in the inhibition of Bm-T6PP by **9b**. The N-terminal MIT domain of As- and Bm-T6PP lock the enzyme conformation, such that the binding site is relatively fixed. Besides, the high flexibility of the aliphatic chain of the inhibitors result in several conformational forms, one of which makes up only a small proportion of all forms and interacts with the enzyme at the relatively fixed binding site.

4.3.7 SAXS studies

We also used Small Ange X-ray Scattering “SAXS” techniques to examine the inhibitor **9a**’s effect on T6PPs domain movement. Surprisingly, it makes the cap domain more open than its apo form (**Table 4.5, 4.6**). We hypothesize that the inhibitor may simply be sitting in the wedge formed in the open cap-core domain conformation.

Table 4.5. Calculated SAXS values for *S. boydii* T6PP w/wo ligands. R_g were calculated using Guinier region and with Parod's, d_{max} was calculated using P(r) Distribution. All values were calculated using PRIMUS.

Protein	Ligand	R_g (Guinier)	R_g (P(r) distribution)	d_{max} (nm)
<i>S. boydii</i>	---	23.50 ± 0.28	23.7	82
	T6S	22.30 ± 0.13	22.9	80
	9A	24.78 ± 0.27	24.1	84



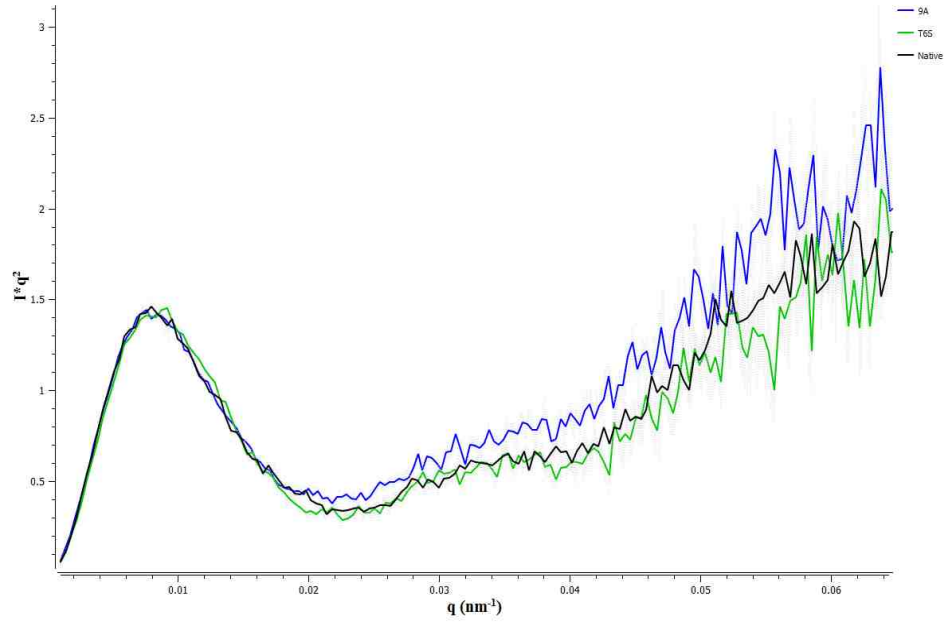
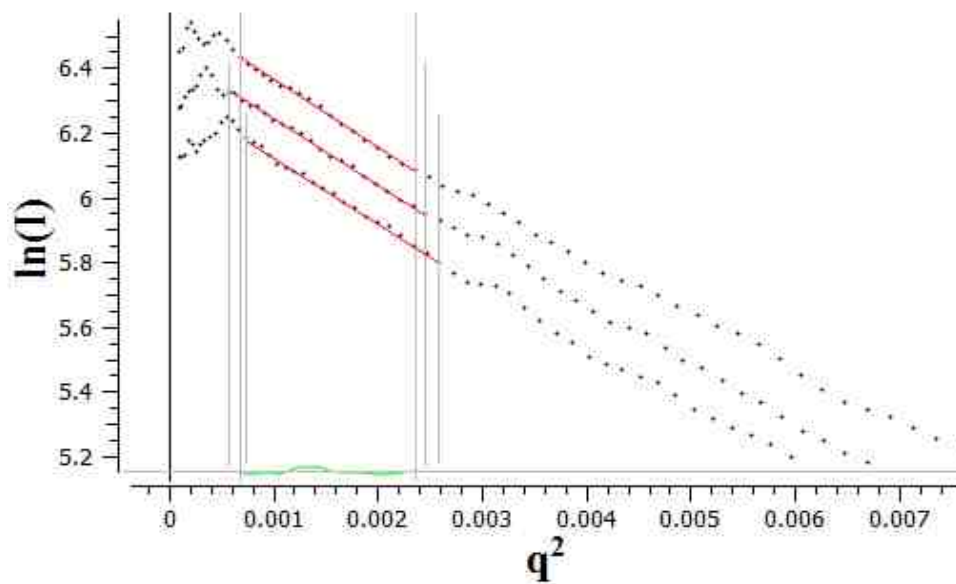
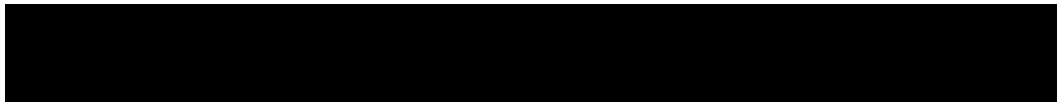
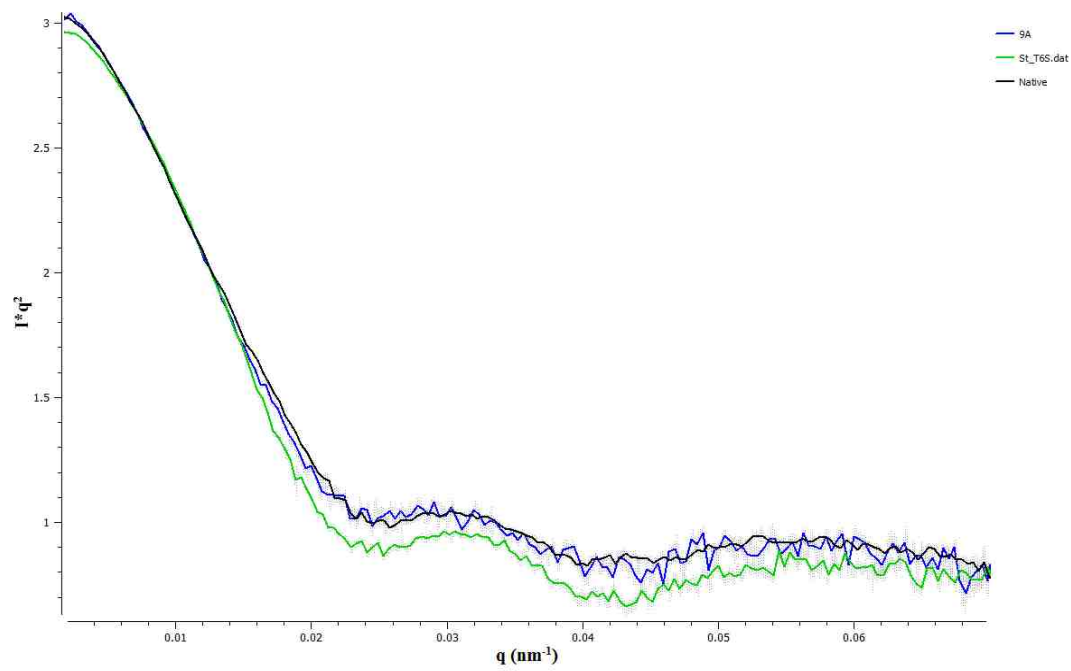
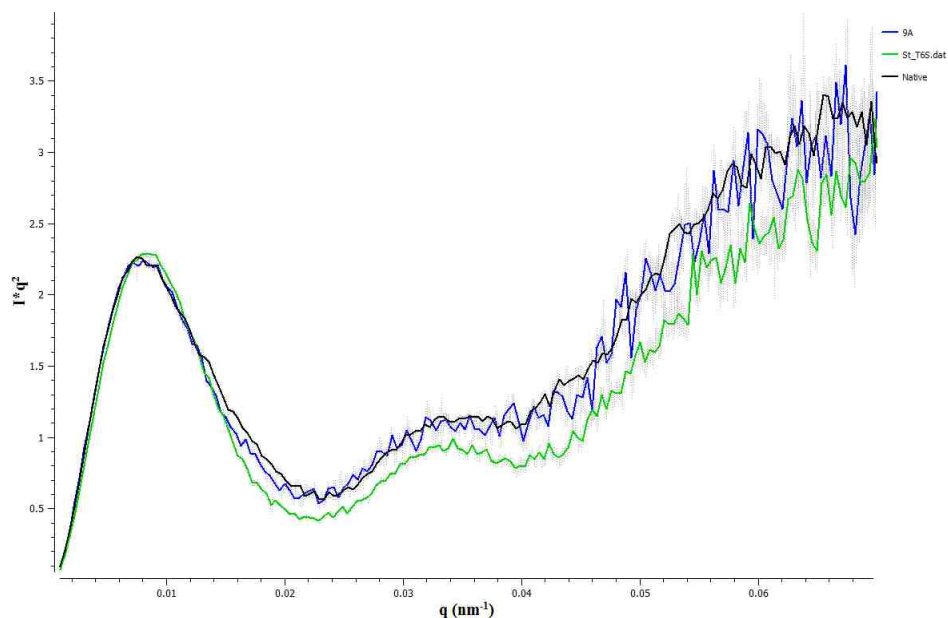


Table 4.6: Calculated SAXS values for *S. typhimurium* T6PP w/wo ligands. R_g were calculated using Guinier region and with Parod's, d_{max} was calculated using P(r) Distribution. All values were calculated using PRIMUS.

Protein	Ligand	R_g (Guinier)	R_g (P(r) distribution)	d_{max} (nm)
<i>S. typhimurium</i>	---	23.96 ± 0.09	24.8	84
	T6S	23.18 ± 0.16	23.2	81
	9A	25.16 ± 0.18	25.8	86







Tables (Table 4.5 and 4.6) and graphs (Graphs 4.6-4.11) represent each protein (*S.boydii* and *S.typhimurium*) with two ligands (T6S, and 9A) and without ligand. T6S represents the protein in the closed conformation whereas the native used as a control to investigate the conformation change upon binding ligand. Each protein was tested with 9A to investigate changes in conformation upon binding. Results suggest that when binding 9A observable changes in conformation are present although the change in R_g and d_{max} suggest a larger increase in size compared to both native and T6S liganded. The results conclude that substrate binds to the proteins and because changes in R_g are in the direction of cap movement suggest that binding occurs in active site. The explanation for the increase in size (R_g , and d_{max}) can be explained through interference in favorable interactions

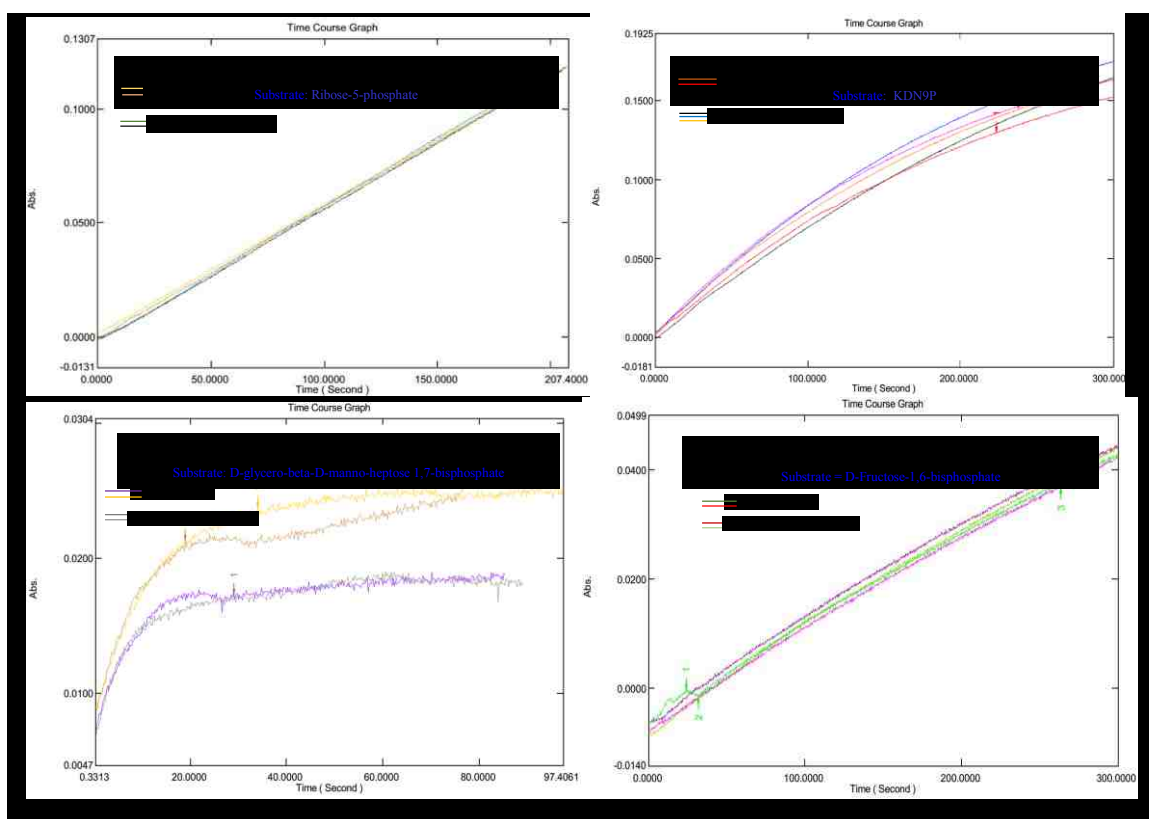
between substrate/protein (T6S-complex) or domain/domain (native complex). Although the substrate binds and interferes with catalysis; the extended conformation can be expressed by an accommodation of substrate in active site.

4.3.8 Inhibition Specificity

In order to test **9a**' inhibition specificity, we test its inhibition on several sugar phosphatases. Yibv [17], which is from *E. coli*, can hydrolyze a wide scope of sugar phosphates, substrates like glucose-6-phosphate, imido-di-phosphate, fructose-1-phosphate, ribose-5-phosphate, acetyl-phosphate, glycerol-1-phosphate, glycerol-2-phosphate. BT1713 [18], which is from *Bacteroides thetaiotaomicron*, is a 2-keto-3-deoxy-D-glycero-D-galacto-9-phosphononic acid (KDN-9-P) phosphatase in the biosynthetic pathway of the 9-carbon alpha-keto acid, 2-keto-3-deoxy-D-glycero-D-galactononic acid (KDN). It can also hydrolyze 2-keto-3-deoxy-8-phospho-d-manno-octulosonic acid (KDO-8-P), N-acetylneuraminate-9-phosphate (Neu5Ac-9-P), pNPP, glucose-6-phosphate, PEP, tyrosine phosphate, and gluconate-6-phosphate. The other enzyme that we tested is GmhB (EFI 501036) [19], from *Pseudomonas putida KT2440*, is a D,D-heptose 1,7-bisphosphate phosphatase, it can convert the D-glycero-beta-D-manno-heptose 1,7-bisphosphate intermediate into D-glycero-beta-D-manno-heptose 1-phosphate. D-Fructose-1,6-bisphosphate is also its substrate. I didn't observe any inhibition in the presence of 1/3 K_m 's substrate and 200 μ M of **9a** (Table 4.7, Figure 4.12).

Table 4.7 9a's inhibition specificity test on sugar phosphate phosphatases.

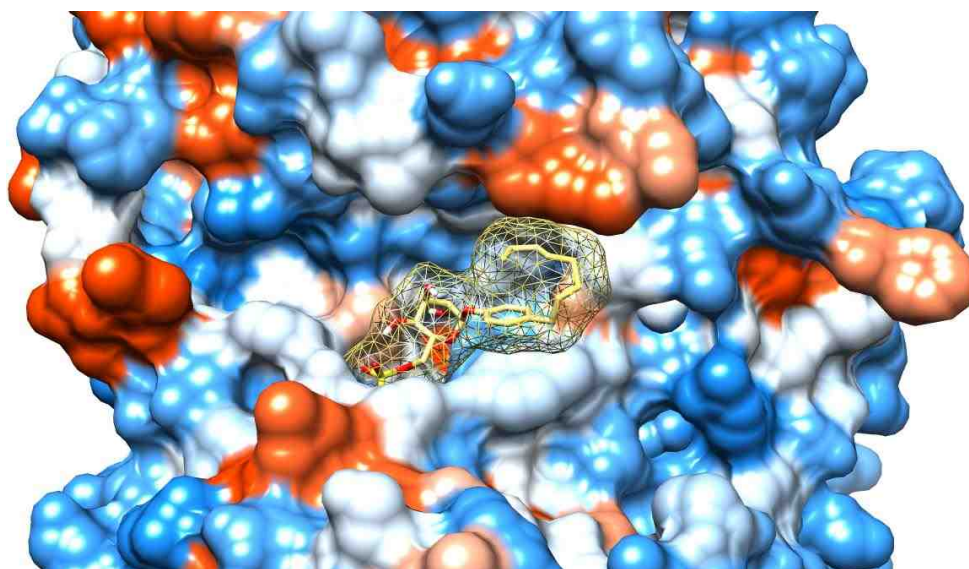
Enzyme	Substrate	Km (μM)	[S] (μM)	V_0 ([9a] = 0) ($\mu\text{M/s}$)	V_0 ([9a] = 200 μM) ($\mu\text{M/s}$)
Yibv	Ribose-5-phosphate	2400	800	0.0589/0.0582	0.0613/0.0596
BT1713	KDN9P	100	33	0.0730/0.0827	0.0740/0.0829/0.0794
GmhB (EF1 501036)	D-glycero-beta-D-manno- heptose 1,7-bisphosphate	17.6	6	0.0944/0.1178	0.0965/0.1164
GmhB (EF1 501036)	D-Fructose-1,6- bisphosphate	151	53.3	0.0166/0.0169	0.0173/0.0177



4.3.9 Molecular Modeling

To better understand the binding mode between T6PP and the newly identified inhibitors, molecular docking studies were performed on compound **9a** with Bm-T6PP by using AutoDock Vina, **9a** is the most potent (5.3 μM) within this series while displaying significant activity against Bm-T6PP. Computations were aimed at elucidating the structural requisites responsible for binding at Bm-T6PP active sites.

Bm-T6PP (PDB ID: 4OFZ) is in complex with Mg^{2+} ions required for catalytic



activity. According to docking results (**Figure 4.13**), **9a** sits in the interface of cap and catalytic domains. Where the sulfate warhead sits in the phosphate binding site, and the 4-n-Octyl phenyl hydrophobic group is sitting in the hydrophobic pocket of Bm-T6PP. This hydrophobic region widely exist in carbohydrate processing enzymes. Although the sugar molecules may be considered to be polar, the carbon atom at the five epimeric position of

the ring and at the adjacent exocyclic position form a contiguous hydrophobic region. Where nearby this region of sugar processing enzyme form a hydrophobic surface in order to stabilize the substrate binding [20].

As shown in **Figure 4.14**, the cofactor Mg^{2+} is coordinated by the carboxylate group of the loop 1 Asp (213) nucleophile, the backbone amine carbonyl of the loop 1 Asp acid/base and by the carboxylate of the Asp (424) on loop 4, and sulfate oxygen anion of the inhibitor **9a**. The Mg^{2+} functions to prevent charge repulsion between the sulfate

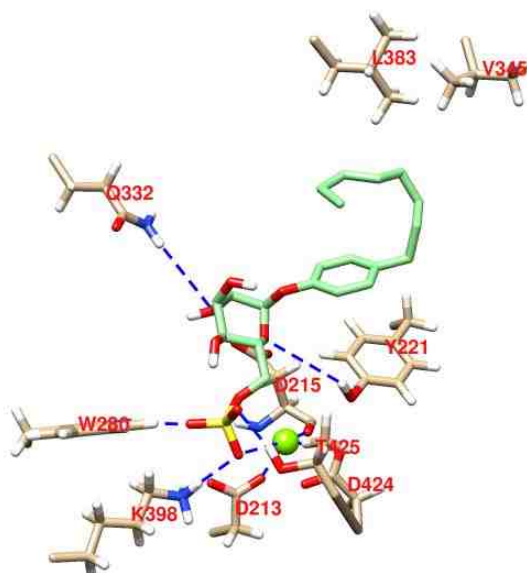


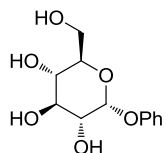
Figure 4.14. . Binding mode of compound **9a** (green) within the Bm-T6PP active site.

Warhead and the Asp 213, Asp 424. Besides coordination of the metal center, additional key interactions are established by our reference compound within the active site. The sulfate warhead forms electrostatic interaction with Lys398 and hydrogen binding with Trp280 and Thr425. More importantly, the 4-n-octyl-phenyl group of **9a** establishes

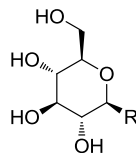
hydrophobic contacts with the hydrophobic side chains of L383, V345, Y221 and is involved in a parallel-displaced π - π interaction with Y221. The hydroxyl groups of the inhibitor **9a** are also involved in hydrogen bonding with Q332 and Y221. Overall, these results support the theory according to which bimodular inhibitor **9a** inhibit Bm-T6PP by employing the binding affinity of warhead sulfate with catalytic domain and π - π stacking interaction and hydrophobic interaction.

4.4 Material and Methods

4.4.1 Inhibitor Synthesis

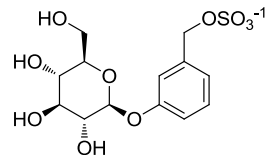
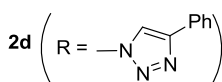
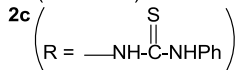


1

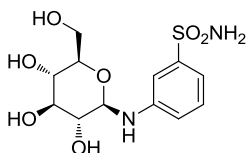


2a (R = OPh)

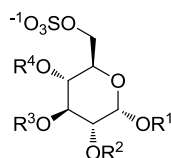
2b (R = NHPPh)



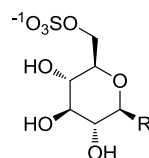
3



4



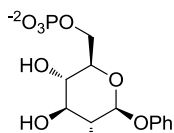
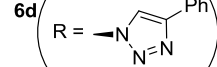
	R ¹	R ²	R ³	R ⁴
5a	H	H	H	H
5b	Me	H	H	H
5c	Ph	H	H	H
5d	Me	Bn	H	H
5e	Me	H	Bn	H
5f	Me	H	H	Bn



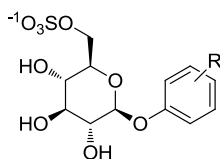
6a (R =OBn)

6b (R = O-n-octyl)

6c (R = O-1-naphthyl)



7



8a (R = H)

8b (R = 4-phenyl)

8c (R = 2,6-(MeO)₂-4-CHO)

8d (R = 3,4-F₂)

8e (R = 4-NO₂)

8f (R = 4-NH₂)

8g (R = 4-NHOAc)

8h (R = 2-CHO)

8i (R = 3-CHO)

8j (R = 4-CHO)

8k (R = 2-CH₂OH)

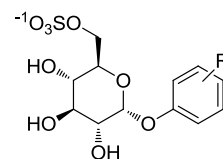
8l (R = 3-CH₂OH)

8m (R = 4-CH₂OH)

8n (R = 4-n-butyl)

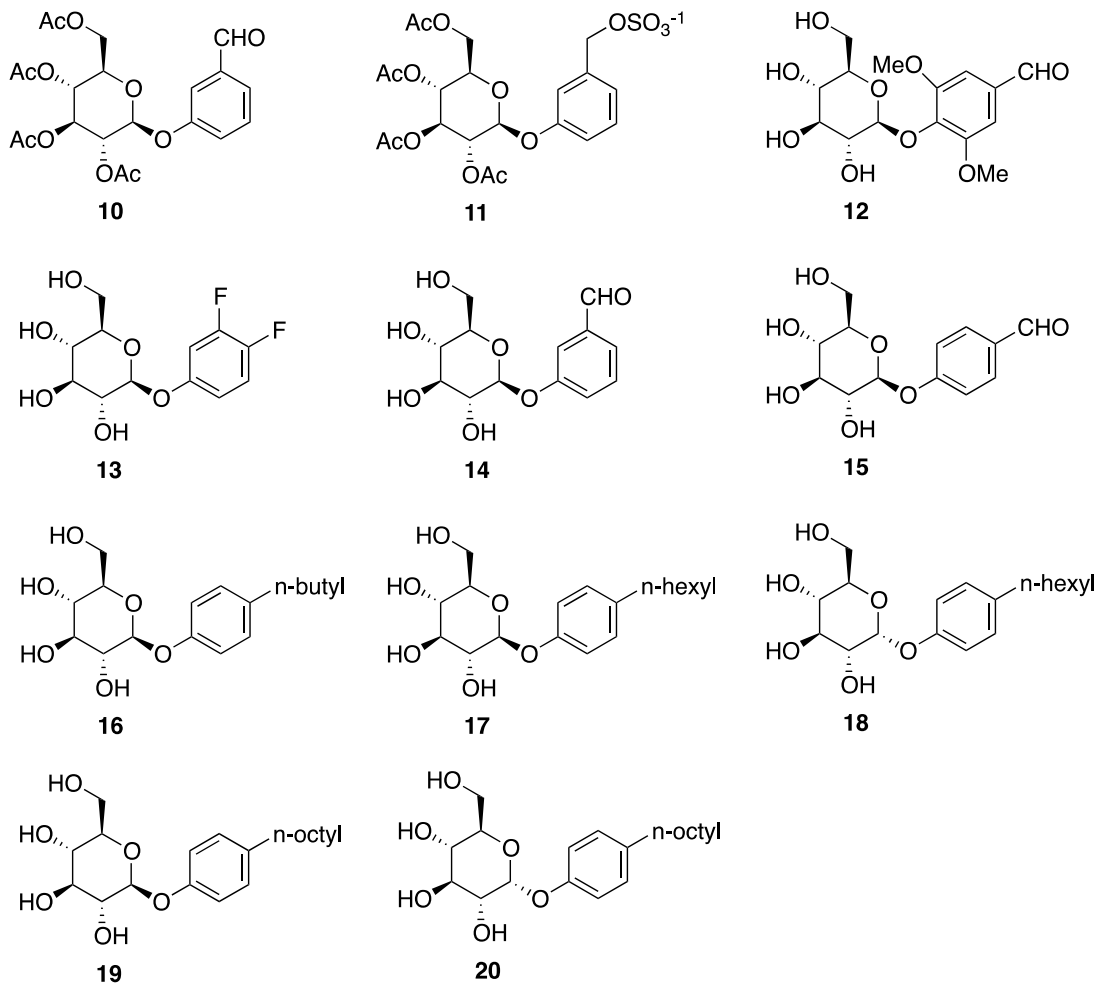
8o (R = 4-n-hexyl)

8p (R = 4-n-octyl)



9a (R = 4-n-octyl)

9b (R = 4-n-hexyl)



General. Except when specified, all solvents and reagents were purchased and used without further purification. Analytical thin-layer chromatography (TLC) was performed on silica gel plates containing F₂₅₄ fluorescence indicator and column chromatography was performed using the indicated eluants on silica gel (230-400 mesh). ¹H (300 and 500 MHz), ¹³C NMR (75 MHz and 125 MHz), and ³¹P (121.5 MHz) NMR spectra were recorded on Bruker Avance 500 and Bruker Avance III 300 spectrometers. ¹H, ¹³C and ³¹P NMR data

are reported as follows: for ^1H NMR chemical shifts are reported in ppm relative to HDO, multiplicities are given as s = singlet, d = doublet, t = triplet, q = quartet, m = multiplet, and coupling constant (J) are in Hz; ^{13}C NMR chemical shifts are reported in ppm relative to NH_4HCO_3 as a standard; ^{31}P NMR chemical shifts are reported in ppm relative to 50% aq H_3PO_4 as a standard. Phenyl α -D-glucopyranoside (**1**) and phenyl β -D-glucopyranoside (**2a**) were purchased from Carbosynth Limited. n-Octyl β -D-glucopyranoside was purchased from Sigma-Aldrich. **2b**,¹ **2c**,² **2d**,³ **4**,⁴ **5a**⁵ were synthesized by using procedures previously described in the corresponding references.

4-Sulfatomethylphenyl β -D-Glucopyranoside (3). A solution of 3-formylphenyl 2,3,4,6-O-triacetyl- β -D-glucopyranoside (**10**)⁶ (0.976 g, 2.2 mmol) in 50 mL of a 1:1 mixture of THF/EtOH containing NaBH_4 (42 mg, 1.1 mmol) was stirred at r.t. until complete disappearance of starting material occurred (TLC). The mixture was poured into ice-water, the pH was adjusted to 7.0 and extracted with chloroform. The extracts were dried and concentrated in vacuo, giving a residue that was dissolved in anhydrous DMF (4 mL). To this solution at $-20\text{ }^\circ\text{C}$ was added a solution of SO_3 .pyridine (0.7 g, 4.4 mmol) in 2 mL anhydrous DMF. The resulting solution was stirred at r.t. for 12 h and concentrated in vacuo, giving a residue that was subjected to silica gel chromatograph (10:1 to 5:1 DCM/MeOH) to give 3-sulfatomethylphenyl 2,3,4,6-O-triacetyl- β -D-glucopyranoside (**11**) (0.857 g, 73%). ^1H NMR (300 MHz, CDCl_3) 7.14 (t, $J = 8.1$, 1H), 6.98-6.96 (m, 2H), 6.82-6.79 (m, 1H), 5.22-5.00 (m, 4H), 4.91 (s, 2H), 4.18 (dd, $J_1 = 12.6$, $J_2 = 5.4$, 1H), 4.07-4.02 (m, 1H), 3.85-3.79 (m, 1H), 1.95 (s, 3H), 1.93 (s, 3H), 1.92 (s, 3H), 1.91 (s, 3H). ^{13}C NMR

(300 MHz, CDCl₃) 170.4, 169.9, 169.3, 169.2, 156.6, 138.5, 129.3, 122.7, 116.4, 116.0, 98.6, 72.5, 71.7, 70.9, 68.9, 68.0, 61.7, 20.5, 20.5, 20.4.

Following addition sodium (38 mg, 1.64 mmol) to 70 mL of anhydrous methanol, a solution of **11** (768 mg, 1.6 mmol) in anhydrous methanol (4.5 mL) was added dropwise. After stirring at r.t. for 2 h, the mixture was neutralized with solid carbon dioxide, and concentrated in vacuo, giving a residue that was subjected to silica gel chromatography to give 0.485 g (78%) of **3**. ¹H NMR (300 MHz, CD₃OD) 7.30 (t, *J* = 8.1, 1H), 7.21-7.20 (m, 1H), 7.10-7.06 (m, 2H), 5.01 (s, 2H), 4.95 (d, *J* = 6.9, 1H), 3.93 (dd, *J*₁ = 12.0, *J*₂ = 1.2, 1H), 3.74 (dd, *J*₁ = 12.0, *J*₂ = 4.5, 1H), 3.50-3.47 (m, 4H). ¹³C NMR (75 MHz, CD₃OD) 159.1, 139.4, 130.4, 122.8, 117.3, 102.3, 78.0, 77.9, 74.9, 71.3, 70.4, 62.4. HRMS (ESI) calcd for C₁₃H₁₈O₁₀S [M-H]⁻ m/z 365.0542, found 365.0535.

Methyl α-D-Glucopyranoside-6-sulfonate (5b). To a solution of methyl α-D-glucopyranoside (0.58 g, 3.0 mmol) in anhydrous DMF (9 mL) at -20°C, was added a solution of SO₃.pyridine (0.50 g, 3.15 mmol) in 1 mL anhydrous DMF, The resulting solution was stirred at r.t. for 12 h and concentrated in vacuo, giving a residue that was subjected to silica gel chromatograph to give 0.435g (50%) of **5b**. ¹H NMR (300 MHz, CD₃OD) 4.69 (d, *J* = 3.9, 1H), 4.29 (dd, *J*₁ = 10.8, *J*₂ = 1.8, 1H), 4.16 (dd, *J*₁ = 10.8, *J*₂ = 5.7, 1H), 3.77-3.71 (m, 1H), 3.64 (t, *J* = 9.2, 1H), 3.45-3.41 (m, 1H), 3.43 (s, 3H), 3.56-3.33 (m, 1H). ¹³C NMR (75 MHz, CD₃OD) 101.2, 74.9, 73.4, 71.6, 71.53, 68.3, 55.6. HRMS (ESI) calcd for C₇H₁₄O₉S [M-H]⁻ m/z 273.0208, found 273.0278.

Phenyl α-D-Glucopyranoside-6-sulfonate (5c). This substance was prepared

starting with phenyl α -D-glucopyranoside (**1**) using the same procedure employed for the preparation of **5b**. Yield 42%. ^1H NMR (500 MHz, CD_3OD) 7.30-7.27 (m, 2H), 7.16-7.15 (m, 2H), 7.01 (t, $J = 7.5$, 1H), 5.45 (d, $J = 3.5$, 1H), 4.22 (dd, $J_1 = 10.0$, $J_2 = 4.0$, 1H), 4.17-4.15 (m, 1H), 3.88 (t, $J = 9.5$, 1H), 3.77-3.70 (m, 1H), 3.59 (dd, $J_1 = 10.0$, $J_2 = 4.0$, 1H), 3.52 (t, $J_1 = 10.0$, 1H). ^{13}C NMR (125 MHz, CD_3OD) 158.6, 130.5, 123.5, 118.3, 99.4, 74.6, 73.2, 72.5, 71.1, 67.8. HRMS (ESI) calcd for $\text{C}_{12}\text{H}_{16}\text{O}_9\text{S}$ $[\text{M-H}]^-$ m/z 335.0407, found 335.0438.

Methyl 2-O-Benzyl- α -D-glucopyranoside-6-sulfonate (5d). This substance was prepared starting with 2-O-benzyl- α -D-glucopyranoside⁷ using the same procedure employed for the preparation of **5b**. Yield 43%. ^1H NMR (300 MHz, CD_3OD) 7.46-7.41 (m, 2H), 7.40-7.32 (m, 3H), 4.80 (d, $J = 12.0$, 1H), 4.68 (d, $J = 12.0$, 1H), 4.66 (d, $J = 3.9$, 1H), 4.29 (dd, $J_1 = 7.8$, $J_2 = 2.1$, 1H), 4.17 (dd, $J_1 = 10.8$, $J_2 = 5.4$, 1H), 3.79 (t, $J = 9.3$, 1H), 3.75-3.70 (m, 1H), 3.39-3.37 (m, 1H), 3.37 (s, 3H), 3.36-3.34 (m, 1H). ^{13}C NMR (75 MHz, CD_3OD) 139.8, 129.4, 129.2, 128.8, 99.2, 80.9, 74.1, 74.0, 71.6, 71.4, 68.2, 55.5. HRMS (ESI) calcd for $\text{C}_{14}\text{H}_{20}\text{O}_9\text{S}$ $[\text{M-H}]^-$ m/z 363.0750, found 363.0738.

Methyl 3-O-Benzyl- α -D-glucopyranoside-6-sulfonate (5e). This substance was prepared starting with 3-O-benzyl- α -D-glucopyranoside⁸ using the same procedure employed for the preparation of **5b**. Yield 50%. ^1H NMR (300 MHz, CD_3OD) 7.44-7.41 (m, 2H), 7.33-7.16 (m, 3H), 4.86 (s, 2H), 4.65 (d, $J = 3.6$ Hz, 1H), 4.28 (dd, $J_1 = 10.8$, $J_2 = 1.8$, 1H), 4.16 (dd, $J_1 = 10.8$, $J_2 = 5.4$, 1H), 3.78-3.72 (m, 1H), 3.62-3.60 (m, 1H), 3.55-3.45 (m, 2H), 3.41 (s, 3H). ^{13}C NMR (75 MHz, CD_3OD) 140.5, 129.1, 129.0, 128.4, 101.4, 83.5,

76.2, 73.5, 71.7, 71.4, 68.2, 55.6. HRMS (ESI) calcd for C₇H₁₄O₉S [M-H]⁻ m/z 363.0750, found 363.0739.

Methyl 4-O-Benzyl- α -D-glucopyranoside-6-sulfonate (5f). This substance was prepared starting with 4-O-benzyl- α -D-glucopyranoside⁹ using the same procedure employed for the preparation of **5b**. Yield 51%. ¹H NMR (500 MHz, CD₃OD) 7.44-7.43 (m, 2H), 7.33-7.30 (m, 2H), 7.27-7.24 (m, 1H), 4.93-4.91 (m, 1H), 4.75 (m, 1H), 4.67 (d, *J* = 3.5, 1H), 4.25 (s, 2H), 3.81-3.75 (m, 1H), 3.45-3.43 (m, 2H), 3.40 (s, 3H). ¹³C NMR (75 MHz, CD₃OD) 139.9, 129.4, 129.2, 128.6, 101.2, 79.3, 75.9, 75.5, 73.6, 70.6, 67.8, 55.7. HRMS (ESI) calcd for C₁₄H₂₀O₉S [M-H]⁻ m/z 363.0750, found 363.0740.

Benzyl α -D-Glucopyranoside-6-sulfonate (6a). This substance was prepared from benzyl α -D-glucopyranoside¹⁰ using the same procedure described for the preparation of **5b**. Yield 47%. ¹H NMR (300 MHz, CD₃OD) 7.45-7.43 (m, 2H), 7.34-7.30 (m, 3H), 4.88 (d, *J* = 3.6, 1H), 4.77 (d, *J* = 11.7, 1H), 4.56 (d, *J* = 11.7, 1H), 4.26 (dd, *J*₁ = 10.8, *J*₂ = 3.8, 1H), 4.15 (dd, *J*₁ = 10.8, *J*₂ = 5.4, 1H), 3.83-3.80 (m, 1H), 3.72 (t, *J* = 9.3, 1H), 3.46-3.37 (m, 2H). ¹³C NMR (75 MHz, CD₃OD) 138.7, 129.3, 129.2, 128.7, 99.1, 74.7, 73.2, 71.8, 71.4, 70.3, 62.1. HRMS (ESI) calcd for C₁₃H₁₈O₉S [M-H]⁻ m/z 349.0593, found 349.0585.

n-Octyl β -D-Glucopyranoside-6-sulfonate (6b). This substance was prepared starting with n-octyl β -D-glucopyranoside using the same procedure described for the preparation of **5b**. Yield 56%. ¹H NMR (300 MHz, CD₃OD) 4.33-4.23 (m, 2H), 4.13 (dd, *J*₁ = 11.1, *J*₂ = 5.6, 1H), 3.90-3.83 (m, 1H), 3.56-3.44 (m, 2H), 3.38-3.33 (m, 2H), 3.18 (t, *J* = 7.2, 1H), 1.64-1.56 (m, 2H), 1.38-1.26 (m, 10H), 0.90 (t, *J* = 6.6, 3H). ¹³C NMR (75

MHz, CD₃OD) 104.3, 77.7, 75.9, 75.0, 71.4, 71.0, 68.2, 33.0, 30.8, 30.6, 30.4, 27.1, 23.7, 14.4. HRMS (ESI) calcd for C₁₄H₂₈O₉S [M-H]⁻ m/z 371.1376, found 371.1373.

1-Naphthyl β-D-Glucopyranoside-6-sulfonate (6c). This substance was prepared starting with 1-naphthyl β-D-glucopyranoside (purchased from Carbosynth Limited) using the same procedure described for the preparation of **5b**. Yield 45%. ¹H NMR (500 MHz, CD₃OD) 8.38-8.36 (m, 1H), 7.79-7.77 (m, 1H), 7.50-7.44 (m, 3H), 7.40-7.37 (m, 1H), 7.24-7.22 (m, 1H), 5.10 (d, *J* = 7.5, 1H), 4.39 (m, 1H), 4.21 (dd, *J*₁ = 11.0, *J*₂ = 5.5, 1H), 3.77-3.67 (m, 2H), 3.59-3.50 (m, 2H). ¹³C NMR (125 MHz, CD₃OD) 154.4, 135.8, 128.4, 127.3, 127.1, 127.0, 126.3, 123.2, 123.0, 110.6, 102.6, 77.7, 75.9, 75.0, 71.2, 68.1. HRMS (ESI) calcd for C₁₆H₁₈O₉S [M-H]⁻ m/z 385.0593, found 385.0589.

(4-Phenyl-1H-1,2,3-triazole) β-D-Glucopyranoside-6-sulfonate (6d). This substance was prepared starting with **2d** using the same procedure described for the preparation of **5b**. Yield 55%. ¹H NMR (300 MHz, D₂O) 8.35 (s, 1H), 7.68-7.65 (m, 2H), 7.46-7.42 (m, 3H), 5.74 (d, *J* = 9.0, 1H), 4.47-4.43 (m, 1H), 4.37-4.35 (m, 1H), 4.05-4.02 (m, 2H), 3.78-3.74 (m, 2H), ¹³C NMR (75 MHz, D₂O) 147.5, 129.0, 128.9, 125.6, 121.0, 87.4, 76.7, 75.7, 75.3, 72.2, 68.8. HRMS (ESI) calcd for C₁₄H₁₇N₃O₈S [M-H]⁻ m/z 386.0664, found 386.0666.

Phenyl β-D-Glucopyranoside-6-phosphate (7). To a solution of phenyl β-D-glucopyranoside (**2a**) (1.08 g, 4.0 mmol) in 5.08 mL of a 2.5:1:0.1 mixture of acetonitrile/pyridine/water at 0°C was added POCl₃ (1.6 mL, 8 mmol). The resulting solution was stirred at 0 °C for 2 h and poured onto 20 g of ice. After the ice melted, the pH

of the mixture was adjusted to 7.0 by slowly adding 1 M aqueous NaOH. The resulting solution was concentrated in vacuo, giving a residue that was subjected to silica gel chromatograph (ethyl acetate/isopropyl alcohol/H₂O/NH₃•H₂O = 5/5/2/0.2, v/v/v/v) to give **7** (0.38 g, 29%). ¹H NMR (300 MHz, D₂O) 7.42-7.37 (m, 2H), 7.16-7.12 (m, 3H), 5.13(d, *J* = 7.2, 1H), 4.08-4.06 (m, 2H), 3.68-3.59 (m, 4H). ¹³C NMR (75 MHz, D₂O) 156.5, 129.9, 123.3, 116.5, 100.2, 75.3, 75.1, 73.0, 68.7, 62.8. ³¹P NMR (121.5 MHz, D₂O) 3.32. HRMS (ESI) calcd for C₁₂H₁₇O₉P [M-H]⁻ *m/z* 335.0532, found 335.0529.

Phenyl β-D-Glucopyranoside-6-sulfonate (8a). This substance was prepared using starting with **2a** using the same procedure described for the preparation of **5b**. Yield 49%. ¹H NMR (300 MHz, CD₃OD) 7.32-7.27 (m, 2H), 7.13-7.10 (m, 2H), 7.04-6.99 (m, 1H), 4.90 (d, *J* = 7.5, 1H), 4.39 (dd, *J*₁ = 10.8, *J*₂ = 1.4, 1H), 4.19 (dd, *J*₁ = 10.8, *J*₂ = 5.7, 1H), 3.69 (t, *J* = 7.4, 1H), 3.51-3.48 (m, 3H). ¹³C NMR (75 MHz, CD₃OD) 159.1, 130.4, 123.4, 117.8, 102.3, 77.6, 75.9, 74.8, 71.2, 68.1. HRMS (ESI) calcd for C₁₂H₁₆O₉S [M-H]⁻ *m/z* 335.0437, found 335.0429.

4,4'-Biphenyl β-D-Glucopyranoside-6-sulfonate (8b). This substance was prepared starting with 4,4'-biphenyl β-D-glucopyranoside¹¹ using the same procedure described for the preparation of **5b**. Yield 49%. ¹H NMR (500 MHz, CD₃OD) 7.54-7.51 (m, 4H), 7.38-7.34 (m, 2H), 7.26-7.23 (m, 1H), 7.16-7.15 (m, 2H), 4.90 (d, *J* = 7.0, 1H), 4.37 (m, 1H), 4.14 (dd, *J*₁ = 11.0, *J*₂ = 6.0, 1H), 3.68 (t, *J* = 7.3, 1H), 3.50-3.40 (m, 3H). ¹³C NMR (125 MHz, CD₃OD) 158.6, 142.0, 136.7, 129.8, 129.0, 127.6, 118.2, 102.4, 77.7, 76.1, 74.9, 71.3, 68.2. HRMS (ESI) calcd for C₁₈H₂₀O₉S [M-H]⁻ *m/z* 411.0705, found

411.0746.

2,6-Dimethoxy-4-formylphenyl β -D-Glucopyranoside-6-sulfonate (8c). To a solution of 2,3,4,6-tetra-O-acetyl- α -D-glucopyranosyl bromide (0.824 g, 2 mmol) in CH_2Cl_2 (8 mL), containing tetrabutylammonium bromide (0.76 g, 2 mmol) and syringaldehyde (1.09 g, 6mmol) was added 8 mL of 1 M NaOH. The resulting mixture was stirred vigorously at 35 °C for 6 h. The mixture was diluted with EtOAc and the organic phase was separated, washed three times with a 1 M NaOH aqueous solution, water and brine, dried and concentrated in vacuo. The resulting residue was dissolved in 20 mL of a 1:1 mixture of THF/MeOH containing anhydrous K_2CO_3 (0.5 g). The resulting mixture was stirred for 20 h at r.t. and concentrated in vacuo, giving a residue that was subjected to silica gel chromatography to give 2,6-dimethoxy-4-formylphenyl β -D-glucopyranoside (**12**)¹⁴ (364 mg, 53%). ¹H NMR (300 MHz, $\text{CD}_3\text{OD}/\text{D}_2\text{O}$ (v/v, 1/2)) 9.91 (s, 1H), 7.39 (s, 2H), 5.24 (d, $J = 7.2$, 1H), 4.02 (s, 6H), 3.87-3.78 (m, 2H), 3.65-3.58 (m, 3H), 3.42-3.39 (m, 1H). ¹³C NMR (75 MHz, $\text{CD}_3\text{OD}/\text{D}_2\text{O}$ (v/v, 1/2)) 195.0, 154.2, 140.6, 133.6, 108.4, 103.8, 77.7, 77.0, 74.9, 70.4, 61.6, 57.2.

The target **8c** was prepared from **12** using the same procedure as described for the preparation of **5b**. Yield 58%. ¹H NMR (300 MHz, D_2O) 9.44 (s, 1H), 6.90 (s, 2H), 5.07 (d, $J = 5.7$, 1H), 4.30-4.18 (m, 2H), 3.82 (s, 6H), 3.64-3.60 (m, 4H). ¹³C NMR (75 MHz, D_2O) 194.3, 152.6, 138.8, 132.1, 107.1, 102.7, 75.4, 74.1, 73.5, 69.1, 66.8, 56.1. HRMS (ESI) calcd for $\text{C}_{15}\text{H}_{20}\text{O}_{12}\text{S}$ [$\text{M}-\text{H}$]⁻ m/z 423.0597, found 423.0599.

3,4-Difluorophenyl β -D-Glucopyranoside-6-sulfonate (8d). 3,4-Difluorophenyl β -D-glucopyranoside (**13**) was prepared using the same procedure as that for 2,6-dimethoxy-

4-formylphenyl β -D-glucopyranoside (**12**).¹² Yield 45%. ¹H NMR (300 MHz, D₂O) 7.14-7.04 (m, 1H), 7.01-6.94 (m, 1H), 6.85-6.81 (m, 1H), 4.77 (d, $J = 5.1$, 1H), 3.83 (dd, $J_1 = 12.0, J_2 = 2.0$, 1H), 3.63 (dd, $J_1 = 12.0, J_2 = 5.4$, 1H), 3.45-3.31 (m, 4H). ¹³C NMR (75 MHz, MeOD) 155.4 (d, $J_{C,F} = 6.6$), 150.90 (dd, $J_{C,F1} = 319.1, J_{C,F2} = 13.7$), 147.8 (dd, $J_{C,F1} = 313.8, J_{C,F2} = 14.0$), 118.2 (d, $J_{C,F} = 18.7$), 113.9, 107.6 (d, $J_{C,F} = 20.3$), 102.8, 78.1, 77.8, 74.1, 71.2, 62.4.

The target **8d** was prepared from **13** using the same procedure as that for **5b**. Yield 33%. ¹H NMR (300 MHz, MeOD) 7.10-7.01 (m, 1H), 6.94-6.92 (m, 1H), 6.86-6.79 (m, 1H), 4.45 (d, $J = 10.8$, 1H), 4.29-.20 (m, 1H), 4.03-3.82 (m, 2H), 3.65 (t, $J = 9.0$, 1H), 3.53-3.38 (m, 2H). ¹³C NMR (75 MHz, MeOD) 155.2 (d, $J_{C,F} = 4.7$), 150.9 (dd, $J_{C,F1} = 298.4, J_{C,F2} = 4.7$), 147.74 (dd, $J_{C,F1} = 312.2, J_{C,F2} = 12.8$), 118.3 (d, $J_{C,F} = 18.8$), 113.9, 107.8 (d, $J_{C,F} = 19.2$), 102.4, 75.8, 75.5, 73.5, 70.0, 68.0. HRMS (ESI) calcd for C₁₂H₁₄F₂O₉S [M-H]⁻ m/z 371.0248, found 371.0239.

4-Nitrophenyl β -D-Glucopyranoside-6-sulfonate (8e). This substance was prepared using the same procedure as that for **5b** starting with 4-nitrophenyl β -D-glucopyranoside.¹³ Yield 31%. ¹H NMR (300 MHz, MeOD) 8.19 (d, $J = 9.3$, 2H), 7.24 (d, $J = 9.3$, 2H), 5.08 (d, $J = 7.2$, 1H), 3.40 (dd, $J_1 = 11.1, J_2 = 1.8$, 1H), 4.17 (dd, $J_1 = 11.1, J_2 = 6.0$, 1H), 3.85-3.80 (m, 1H), 3.57-3.47 (m, 3H). ¹³C NMR (75 MHz, MeOD) 163.6, 143.7, 126.6, 117.7, 101.3, 77.3, 75.9, 74.5, 71.0, 68.0. HRMS (ESI) calcd for C₁₂H₁₅NO₁₁S [M-H]⁻ m/z 380.0288, found 380.0284.

4-Aminophenyl β -D-Glucopyranoside-6-sulfonate (8f).¹⁴ To a solution of **8e** (120

mg, 0.3 mmol) in DI water (6 mL), was added Pd(OH)₂/C (32 mg, 0.06 mmol). The resulting mixture was stirred under a H₂ atmosphere for 2 h. The mixture was filtered through Celite pad and the filtrate was concentrated in vacuo, giving **8f** (105 mg, 100%). ¹H NMR (500 MHz, D₂O) 7.06-7.03 (m, 2H), 6.91-6.88 (m, 2H), 4.98 (d, *J* = 8.0, 1H), 4.38-4.35 (m, 1H), 4.29-4.26 (m, 1H), 3.82-3.80 (m, 1H), 3.63-3.55 (m, 3H). ¹³C NMR (125 MHz, D₂O) 143.9, 132.4, 111.3, 111.0, 94.2, 68.3, 66.6, 65.8, 62.0, 59.7. HRMS (ESI) calcd for C₁₂H₁₇NO₉S [M-H]⁻ m/z 350.0546, found 350.0536.

4-Acetamidophenyl β-D-Glucopyranoside-6-sulfonate (8g).¹⁴ A mixture of **8f** (95 mg, 0.27 mmol) in 4.5 mL H₂O containing K₂CO₃ (112 mg, 0.81 mmol) was stirred at 0 °C before adding Ac₂O (77 μL, 0.81 mmol) dropwise. Following stirring at for 3 h at 0 °C, the mixture was concentrated in vacuo, giving a residue that was subjected to silica gel chromatography, to give **8g** (65 mg, 62%). ¹H NMR (300 MHz, D₂O) 7.34 (d, *J* = 8.7, 2H), 7.13 (d, *J* = 8.7, 2H), 5.08 (d, *J* = 7.2, 1H), 4.38-4.35 (m, 1H), 4.23 (dd, *J*₁ = 11.4, *J*₂ = 5.4, 1H), 3.87-3.83 (m, 1H), 3.62-3.56 (m, 3H), 2.13 (s, 3H). ¹³C NMR (75 MHz, D₂O) 172.9, 154.1, 132.0, 123.9, 117.1, 100.5, 75.3, 73.9, 72.8, 69.1, 66.8, 22.6. HRMS (ESI) calcd for C₁₄H₁₉NO₁₀S [M-H]⁻ m/z 392.0651, found 392.0645.

2-Formylphenyl β-D-Glucopyranoside-6-sulfonate (8h). This substance was prepared using the same procedure as that for **5b** starting with 2-formylphenyl β-D-glucopyranoside.¹⁵ Yield 39%. ¹H NMR (500 MHz, D₂O) 10.03 (s, 1H), 7.72-7.64 (m, 2H), 7.27-7.17 (m, 2H), 5.20 (d, *J* = 7.5, 1H), 4.38-4.35 (m, 1H), 4.26-4.23 (m, 1H), 3.87-3.86 (m, 1H), 3.69-3.58 (m, 3H). ¹³C NMR (125 MHz, D₂O) 186.1, 151.9, 130.2, 121.4, 117.6,

116.1, 108.7, 92.8, 68.3, 66.9, 65.6, 61.9, 59.7. HRMS (ESI) calcd for C₁₃H₁₆O₁₀S [M-H]⁻ m/z 363.0386, found 363.0379.

3-Formylphenyl β-D-Glucopyranoside-6-sulfonate (8i). 3-Formylphenyl β-D-glucopyranoside (**14**) was prepared from 3-hydroxybenzaldehyde and 2,3,4,6-tetra-O-acetylglucosyl bromide using the same procedure as that for **12**. Yield 29%. ¹H NMR (300 MHz, CD₃OD) 9.88 (s, 1H), 7.54-7.34 (m, 4H), 4.96 (d, *J* = 6.3, 1H), 3.88-3.84 (m, 1H), 3.67 (dd, *J*₁ = 12.0, *J*₂ = 5.1, 1H), 3.48-3.39 (m, 4H). ¹³C NMR (75 MHz, CD₃OD) 193.9, 159.5, 139.2, 131.3, 125.0, 124.1, 117.7, 102.0, 78.1, 77.8, 74.7, 71.2, 62.3.

The target **8i** was prepared from **14** substance was prepared using the same procedure as that for **5b**. Yield 39%. ¹H NMR (300 MHz, D₂O) 9.83 (s, 1H), 7.63-7.49 (m, 3H), 7.41-7.37 (m, 1H), 5.14 (d, *J* = 6.6, 1H), 4.33-4.29 (m, 1H), 4.15 (dd, *J*₁ = 11.4, *J*₂ = 5.7, 1H), 3.87-3.82 (m, 1H), 3.58-3.50 (m, 3H). ¹³C NMR (125 MHz, D₂O) 188.6, 149.8, 130.1, 123.6, 118.0, 116.4, 109.6, 92.9, 68.2, 66.8, 65.6, 61.9, 59.7. HRMS (ESI) calcd for C₁₃H₁₆O₁₀S [M-H]⁻ m/z 363.0386, found 363.0384.

4-Formylphenyl β-D-Glucopyranoside-6-sulfonate (8j). 4-Formylphenyl β-D-glucopyranoside (**15**) using a previously described procedure.¹⁶ The target **8j** was prepared starting with **15** using the same procedure as that for **5b**. Yield 59%. The precursor 4-formylphenyl β-D-glucopyranoside was synthesized by using the procedure previously described.¹⁶ ¹H NMR (300 MHz, D₂O) 9.81 (s, 1H), 7.93 (d, *J* = 8.7, 2H), 7.27 (d, *J* = 8.7, 2H), 5.30 (d, *J* = 6.9, 1H), 4.46-4.43 (m, 1H), 4.31 (dd, *J*₁ = 11.4, *J*₂ = 5.1, 1H), 4.01-3.97 (m, 1H), 3.73-3.64 (m, 3H). ¹³C NMR (75 MHz, D₂O) 188.5, 155.3, 126.1, 124.3, 110.0,

92.8, 68.8, 67.5, 66.2, 62.6, 60.3. HRMS (ESI) calcd for C₁₃H₁₆O₁₀S [M-H]⁻ m/z 363.0386, found 363.0381.

2-Hydroxymethylphenyl β-D-Glucopyranoside-6-sulfonate (8k). To a solution of 2-formylphenyl β-D-glucopyranoside-6-sulfonate (**8h**) (98 mg, 0.26 mmol) in MeOH (2 mL) at 0°C, was added NaBH₄ (40 mg, 1.03 mmol) The mixture was warmed to room temperature and stirred for 1 h, The diluted with water, and concentrated in vacuo giving a residue that was subjected to silica gel chromatography, giving **8k** (61 mg, 64%). ¹H NMR (500 MHz, D₂O) 7.38-7.35 (m, 2H), 7.22-7.21 (m, 1H), 7.15-7.12 (m, 1H), 5.10 (d, *J* = 7.5, 1H), 4.73-4.65 (m, 2H), 4.35-4.32 (m, 1H), 4.23-4.20 (m, 1H), 3.83-3.82 (m, 1H), 3.65-3.55 (m, 3H). ¹³C NMR (125 MHz, D₂O) 122.6, 122.4, 122.2, 116.3, 108.3, 93.5, 68.3, 66.7, 65.7, 61.9, 59.7, 52.1. HRMS (ESI) calcd for C₁₃H₁₈O₁₀S [M-H]⁻ m/z 365.0548, found 365.0540.

3-Hydroxymethylphenyl β-D-Glucopyranoside-6-sulfonate (8l). This substance was prepared from 3-formylphenyl β-D-glucopyranoside-6-sulfonate (**8i**) using the same procedure as that for **8k**. Yield 80%. ¹H NMR (500 MHz, D₂O) 7.37-7.36 (m, 1H), 7.10-7.07 (m, 3H), 5.10 (d, *J* = 4.5, 1H), 4.61-4.59 (m, 2H), 4.36-4.34 (m, 1H), 4.20 (dd, *J*₁ = 11.0, *J*₂ = 5.0, 1H), 3.86-3.85 (m, 1H), 3.61-3.56 (m, 3H). ¹³C NMR (125 MHz, D₂O) 126.2, 123.0, 119.5, 114.9, 108.6, 108.1, 93.1, 68.2, 66.7, 65.7, 62.0, 59.7, 56.4. HRMS (ESI) calcd for C₁₃H₁₈O₁₀S [M-H]⁻ m/z 365.0548, found 365.0538.

4-Hydroxymethylphenyl β-D-Glucopyranoside-6-sulfonate (8m). This substance was prepared from 4-formylphenyl β-D-glucopyranoside-6-sulfonate (**8j**) using the same

procedure as that for **8k**. Yield 58%. ¹H NMR (500 MHz, D₂O) 7.35-7.33 (m, 2H), 7.12-7.10 (m, 2H), 5.09 (d, *J* = 4.5, 1H), 4.56-4.55 (m, 2H), 4.34-4.32 (m, 1H), 4.22-4.20 (m, 1H), 3.84-3.83 (m, 1H), 3.58-3.54 (m, 3H). ¹³C NMR (125 MHz, D₂O) 149.0, 127.8, 122.1, 109.5, 93.1, 68.2, 66.7, 65.7, 61.9, 59.7, 56.2. HRMS (ESI) calcd for C₁₃H₁₈O₁₀S [M-H]⁻ *m/z* 365.0548, found 365.0538.

4-n-Butylphenyl β-D-Glucopyranoside-6-sulfonate (8n). 4-n-Butylphenyl β-D-glucopyranoside (**16**) was prepared from 4-n-butylphenol using the same procedure as that for **12**. Yield 30% in two steps. ¹H NMR (300 MHz, CD₃OD) 7.18-7.07 (m, 4H), 4.98 (d, *J* = 7.2, 1H), 3.98-3.94 (m, 1H), 3.80 (dd, *J*₁ = 11.1, *J*₂ = 4.5, 1H), 3.61-3.53 (m, 4H), 2.59 (t, *J* = 7.7, 2H), 1.62-1.57 (m, 2H), 1.40-1.33 (m, 2H), 0.96 (t, *J* = 7.4, 3H). ¹³C NMR (75 MHz, CD₃OD) 156.6, 138.2, 130.3, 117.6, 102.2, 77.5, 77.3, 74.5, 70.9, 62.1, 35.5, 34.8, 23.0, 14.2.

The target **8n** was prepared from **16** using the same procedure as that for **5b**. Yield 51%. ¹H NMR (300 MHz, D₂O/CD₃OD (v/v, 1/1)) 7.21-7.06 (m, 4H), 4.99 (d, *J* = 6.9, 1H), 4.39-4.35 (m, 1H), 4.24 (dd, *J*₁ = 11.1, *J*₂ = 5.1, 1H), 3.78-3.77 (m, 1H), 3.59-3.56 (m, 3H), 2.59 (t, *J* = 7.7, 2H), 1.63-1.53 (m, 2H), 1.40-1.30 (m, 2H), 0.93 (t, *J* = 7.4, 3H). ¹³C NMR (75 MHz, D₂O/CD₃OD (v/v, 1/1)) 156.1, 138.8, 130.4, 117.6, 102.1, 76.7, 75.1, 74.1, 70.4, 67.8, 35.2, 34.4, 22.7, 14.2. HRMS (ESI) calcd for C₁₆H₂₄O₉S [M-H]⁻ *m/z* 391.1063, found 391.1075.

4-n-Hexylphenyl β-D-Glucopyranoside (17) and 4-n-Hexylphenyl α-D-Glucopyranoside (18).¹⁷ To a solution of penta-O-benzoyl-D-glucose (2.8 g, 4 mmol) and

4-n-hexylphenol (1.42 g, 8 mmol) in dichloromethane (28 ml) under argon at 0 °C was added BF₃·Et₂O (1.67 mL, 13.2 mmol). The mixture was stirred at 50 °C for 48 h, diluted with water (30 mL) and stirred for 15 min. The mixture was diluted with dichloromethane (60 mL), washed with water, brine, and concentrated in vacuo, giving a residue that was dissolved in THF/MeOH (100 mL/20 mL) and cooled to 0 °C. A 3N solution of aq NaOH (9.52 mL) was added and the mixture was stirred for 9 h at room temperature, diluted with water (40 mL), neutralized with AG 50W-X8 resin (Bio-Rad), filtered, and concentrated *in vacuo*, giving a residue that was subjected to silica gel chromatography, giving 4-n-hexylphenyl β-D-glucopyranoside (**17**) (237 mg, 17%) and 4-n-hexylphenyl α-D-glucopyranoside (**18**) (639 mg, 47%).

17: ¹H NMR (300 MHz, CDCl₃/CD₃OD (v/v, 1/1)) 7.59-7.45 (m, 4H), 5.39 (d, *J* = 6.9, 1H), 4.39-4.26 (m, 2H), 4.06-4.04 (m, 3H), 3.93-3.92 (m, 1H), 3.04 (t, *J* = 7.7, 2H), 2.07-2.05 (m, 2H), 1.84-1.79 (m, 6H), 1.38 (t, *J* = 6.6, 3H). ¹³C NMR (75 MHz, CDCl₃/CD₃OD (v/v, 1/1)) 155.1, 137.0, 129.0, 116.3, 100.8, 76.1, 75.9, 73.1, 69.4, 61.0, 34.8, 31.4, 31.4, 28.6, 22.3, 13.6.

18: ¹H NMR (300 MHz, CDCl₃/CD₃OD (v/v, 1/1)) 7.36-7.29 (m, 4H), 5.75 (d, *J* = 3.6, 1H), 4.19 (t, *J* = 9.3, 1H), 4.10-3.98 (m, 3H), 3.93-3.82 (m, 2H), 2.81 (t, *J* = 7.7, 2H), 1.86-1.84 (m, 2H), 1.58-1.57 (m, 6H), 1.56 (t, *J* = 6.6, 3H). ¹³C NMR (300 MHz, CDCl₃/CD₃OD (v/v, 1/1)) 154.7, 136.8, 129.0, 116.6, 97.7, 73.4, 72.2, 71.6, 69.3, 60.7, 34.8, 31.4, 31.3, 28.6, 22.3, 13.6.

4-n-Hexylphenyl β-D-Glucopyranoside-6-sulfonate (80). This substance was prepared from 4-n-hexylphenyl β-D-glucopyranoside (**17**) using the same procedure as that

for **5b**. Yield 46 %. ¹H NMR (300 MHz, D₂O/CD₃OD (v/v, 1/1)) 7.19-7.09 (m, 4H), 4.99 (d, *J* = 6.6, 1H), 4.43-4.40 (m, 1H), 4.29 (dd, *J*₁ = 11.1, *J*₂ = 5.4, 1H), 3.80-3.76 (m, 1H), 3.65-3.57 (m, 3H), 2.60 (t, *J* = 7.5, 2H), 1.65-1.60 (m, 2H), 1.38-1.35 (m, 6H), 0.95 (t, *J* = 6.6, 3H). ¹³C NMR (75 MHz, CDCl₃/CD₃OD (v/v, 1/1)) 156.6, 138.3, 130.2, 117.7, 102.4, 77.0, 75.4, 74.4, 70.7, 67.9, 35.8, 32.6, 32.5, 29.6, 23.4, 14.4. HRMS (ESI) calcd for C₁₈H₂₈O₉S [M-H]⁻ m/z 419.1376, found 419.1388.

4-n-Hexylphenyl α-D-Glucopyranoside-6-sulfonate (9b). This substance was prepared from 4-n-hexylphenyl α-D-glucopyranoside (**18**) using the same procedure as that for **5b**. Yield 55 %. ¹H NMR (300 MHz, CD₃OD) 7.12-7.05 (m, 4H), 5.44 (d, *J* = 3.6, 1H), 4.29-4.17 (m, 2H), 3.94-3.88 (m, 2H), 3.65-3.52 (m, 2H), 2.56 (t, *J* = 7.7, 2H), 1.61-1.54 (m, 2H), 1.33-1.31 (m, 6H), 0.91 (t, *J* = 6.6, 3H). ¹³C NMR (75 MHz, CD₃OD) 156.5, 138.0, 130.2, 118.2, 99.5, 74.5, 73.1, 72.3, 71.1, 67.8, 36.0, 32.8, 29.9, 23.2, 14.4. HRMS (ESI) calcd for C₁₈H₂₈O₉S [M-H]⁻ m/z 419.1376, found 419.1375.

4-n-Octylphenyl β-D-Glucopyranoside (19) and 4-n-Octyl phenyl α-D-Glucopyranoside (20).¹⁷ These substances were prepared using the same procedure as those for 4-n-hexylphenyl β-D-glucopyranoside (**17**) and 4-n-hexylphenyl α-D-glucopyranoside (**18**).

19: Yield 25 %. ¹H NMR (300 MHz, CD₃OD) 7.03-6.92 (m, 4H), 4.80 (d, *J* = 6.6, 1H), 3.84-3.80 (m, 1H), 3.64 (dd, *J*₁ = 11.4, *J*₂ = 3.6, 1H), 3.40-3.35 (m, 4H), 2.47 (t, *J* = 7.5, 2H), 1.54-1.48 (m, 2H), 1.24-1.23 (m, 10H), 0.83 (t, *J* = 6.3, 3H). ¹³C NMR (75 MHz, CD₃OD) 157.2, 137.9, 130.2, 117.7, 102.5, 78.0, 77.9, 74.9, 71.3, 62.5, 36.1, 33.0, 32.9,

30.6, 30.4, 30.2, 23.7, 14.4.

20: Yield 44 %. ¹H NMR (300 MHz, CD₃OD) 7.10-7.09 (m, 4H), 5.46 (d, *J* = 3.6, 1H), 3.90 (t, *J* = 9.3, 1H), 3.77-3.71 (m, 3H), 3.59 (dd, *J*₁ = 9.6, *J*₂ = 3.6, 1H), 3.47 (t, *J* = 9.2, 1H), 2.57 (t, *J* = 7.7, 2H), 1.62-1.58 (m, 2H), 1.33-1.32 (m, 10H), 0.92 (t, *J* = 6.8, 3H). ¹³C NMR (75 MHz, CD₃OD) 156.7, 138.0, 130.2, 118.2, 99.6, 74.9, 74.2, 73.3, 71.5, 62.3, 36.1, 33.0, 32.9, 30.6, 30.4, 30.3, 23.7, 14.4.

4-n-Octylphenyl β-D-Glucopyranoside-6-sulfonate (8p). This substance was prepared from 4-n-octylphenyl β-D-glucopyranoside (**19**) using the same procedure as that for **5b**. Yield 42 %. ¹H NMR (300 MHz, D₂O) 6.97-6.90 (m, 4H), 4.72 (d, *J* = 6.3, 1H), 4.30-4.27 (m, 1H), 4.17-4.13 (m, 1H), 3.61-3.43 (m, 4H), 2.37 (t, *J* = 7.1, 2H), 1.44-1.43 (m, 2H), 1.24-1.23 (m, 10H), 0.88 (t, *J* = 6.2, 3H). ¹³C NMR (75 MHz, D₂O) 155.2, 137.3, 129.3, 117.3, 101.7, 75.2, 73.8, 72.8, 68.7, 66.3, 35.0, 31.9, 31.5, 29.5, 29.4, 22.6, 13.9. HRMS (ESI) calcd for C₂₀H₃₂O₉S [M-H]⁻ *m/z* 447.1689, found 447.1693.

4-n-Octylphenyl α-D-Glucopyranoside-6-sulfonate (9a). This substance was prepared from 4-n-octylphenyl α-D-glucopyranoside (**20**) using the same procedure as that for **5b**. Yield 68 %. ¹H NMR (300 MHz, D₂O) 6.96-6.83 (m, 4H), 5.38 (d, *J* = 3.6, 1H), 4.28-4.19 (m, 1H), 3.96-3.90 (m, 2H), 3.76-3.59 (m, 3H), 2.3 (t, *J* = 7.7, 2H), 1.43-1.42 (m, 2H), 1.24-1.23 (m, 10H), 0.87 (t, *J* = 6.6, 3H). ¹³C NMR (75 MHz, D₂O) 154.8, 136.7, 129.1, 117.0, 97.8, 72.8, 71.2, 70.5, 68.7, 66.2, 35.0, 31.9, 31.6, 29.6, 29.5, 22.7, 13.9. HRMS (ESI) calcd for C₂₀H₃₂O₉S [M-H]⁻ *m/z* 447.1689, found 447.1695.

4.4.2 References for Inhibitor Synthesis

1. Bridiau, N.; Benmansour, M.; Legoy, M. D.; Maugard T. One-pot stereoselective synthesis of β -N-aryl-glycosides by N-glycosylation of aromatic amines: application to the synthesis of tumor-associated carbohydrate antigen building blocks. *Tetrahedron* **2007**, *63*(19), 4178-4183.
2. Somsak, L.; Felföldi, N.; Kónya, B.; Hüse, C.; Telepo, K.; Bokor, É.; Czifrák K. Assessment of synthetic methods for the preparation of N- β -d-glucopyranosyl- N'-substituted ureas, -thioureas and related compounds. *Carbohydrate Research* **2008**, *343*(12), 2083-2093.
3. Bokor, É.; Docsa, T.; Gergely, P.; Somsák L. Synthesis of 1-(d-glucopyranosyl)- 1,2,3-triazoles and their evaluation as glycogen phosphorylase inhibitors. *Bioorg. Med. Chem.* **2010**, *18*(3), 1171-1180.
4. Winum, J.-Y.; Casini, A.; Mincione, F.; Starnotti, M.; Montero, J.-L.; Scozzafava A.; Supuran C. T. Carbonic anhydrase inhibitors: N-(p-sulfamoylphenyl)- α -D-glycopyrano-sylamines as topically acting antiglaucoma agents in hypertensive rabbits. *Bioorg. Med. Chem. Lett.* **2004**, *14*, 225–229.
5. Guiseley, K. B.; Ruoff, P. M. Monosaccharide Sulfates. I. Glucose 6-Sulfate. Preparations, Characterization of the Crystalline Potassium Salt, and Kinetic Studies. *J. Org. Chem.* **1961**, *26* (4), 1248–1254.
6. Miura M.; Wu H. Glycosylated carboranylporphyrins for use in boron neutron capture therapy, photodynamic therapy, and as tumor imaging agents. *U.S. Pat. Appl. Publ.* **2008**, US 20080279781 A1 20081113

7. Zhou, Y.; Lia, J.; Zhan, Y.; Pei, Z.; Dong, H. Halide promoted organotin-mediated carbohydrate benzylation: mechanism and application. *Tetrahedron* **2013**, *69*(13), 2693-2700.
8. Liao, B. B.; Milgram, B. C.; Shair, M. D. Total Syntheses of HMP-Y1, Hibarimicinone, and HMP-P1. *J. Am. Chem. Soc.* **2012**, *134* (40), 16765–16772.
9. Tani, S.; Sawadi, S.; Kojima, M.; Akai, S.; Sato, K.-i. A novel method for regioselective ring-opening reduction of 4,6-O-benzylidene hexopyranoside derivatives using CoCl₂ and BH₃·THF. *Tetrahedron Letters*, **2007**, *48*(17), 3103-3104.
10. Pearce, O. M. T.; Varki, A. Chemo-enzymatic synthesis of the carbohydrate antigen N-glycolylneuraminic acid from glucose. *Carbohydrate Research*, **2010**, *345*(9), 1225–1229.
11. Dai X.; Wu S.; Yang W. Chemical synthesis process for preparing gastrodin and its analogous henolic glycoside formula (I). *Zhuanli Shenqing Gongkai Shuomingshu*, **2003**, 1428345.
12. Kröger, L.; Thiem, J. Synthesis and evaluation of glycosyl donors with novel leaving groups for transglycosylations employing b-galactosidase from bovine testes. *Carbohydrate Research*, **2007**, *342*(3-4), 467–481.
13. Green, D. E.; Ferreira, C. L.; Stick, ■; Patrick, B. O.; Adam, M. J.; Orvig, C. Carbohydrate-Bearing 3-Hydroxy-4-pyridinonato Complexes of Gallium(III) and Indium(III). *Bioconjugate Chemistry*, **2005**, *16*(6), 1597-1609.

14. Sasaki, K.; Nishida, Y.; Kambara, M.; Uzawa, H.; Takahashi, T.; Suzuki, T.; Suzuki, Y.; and Kobayashi, K. Design of N-acetyl-6-sulfo- β -D-glucosaminide-based inhibitors of influenza virus sialidase. *Bioorganic & Medicinal Chemistry*, **2004**, *12*(6), 1367–1375.
15. Loganathan, D.; Trivedi, G. K. Phase-transfer-catalyzed d-glucosylation: Synthesis of benzoylated aryl β -d-glucopyranosides and β -d-glucopyranosyl-substituted cinnamates. *Carbohydrate Research*, **1987**, *162*(1), 117–125.
16. Wen, H.; Lin, C.; Que, L.; Ge, H.; Ma, L.; Cao, R.; Wan, Y.; Peng, W.; Wang, Z.; Song, H. Synthesis and biological evaluation of helacid analogues as novel acetylcholinesterase inhibitors. *European Journal of Medicinal Chemistry*, **2007**, *43*(1):166-73
17. France, R. R.; Compton, R. G.; Davis, B. G.; Fairbanks, A. J.; Rees, N. V.; Wadhawan, J. D. Selective electrochemical glycosylation by reactivity tuning. *Org. Biomol. Chem.*, **2004**, *2*, 2195-2202.

4.5 Site-Directed Mutagenesis

Site directed mutagenesis was carried out using a PCR-based strategy with the WT-Mt-T6PP/pET-15-TEV plasmid and commercial primers. Reaction solutions also contained dNTP (Invitrogen) and Deep Vent DNA polymerase. The PCR was carried out using the Techgene thermal cycler manufactured by TECHNE. The PCR products were treated with DpnI for 1 h at 37°C to remove the wild type plasmid before transformation of T7 Express I^q Competent *E. coli* (High Efficiency) cells. The sequence of the mutated gene was confirmed by DNA sequencing carried out by GENEWIZ, Inc. The plasmid was

prepared using a QIAprep Spin Miniprep kit (Qiagen). The expression levels of the genes encoding T6PP mutants were examined by SDS-PAGE analysis of the cellular protein.

4.5 References

1. Avonce, N.; Mendoza-Vargas, A.; Morett, E. and Iturriaga, G. Insights on the evolution of trehalose biosynthesis. *BMC Evolutionary Biology*, 2006, 6, 109.
2. Murphy, H.N., Stewart, G.R., Mischenko, V.V., Apt, A.S., Harris, R. and McAlister, M.S., et al. The OtsAB pathway is essential for trehalose biosynthesis in *Mycobacterium tuberculosis*. *J Biol Chem*, **2005**, 280, 14524–14529.
3. Song, X.S., Li, H.P., Zhang, J.B., Song, B., Huang, T., Du, X.M., Gong, A.D., Liu, Y.K., Feng, Y.N., Agboola, R.S., Liao, Y.C. Trehalose 6-phosphate phosphatase is required for development, virulence and mycotoxin biosynthesis apart from trehalose biosynthesis in *Fusarium graminearum*. *Fungal Genet Biol.*, 2014, 63, 24-41.
4. Kormish, J.D., McGhee, J.D. The *C. elegans* lethal gut-obstructed *gob-1* gene is trehalose- 6-phosphate phosphatase. *Dev. Biol.*, **2005**, 287, 35–47.
5. Sears, P.; Wong, C.-H. Carbohydrate Mimetics: A New Strategy for Tackling the Problem of Carbohydrate-Mediated Biological Recognition. *Angew. Chem. Int. Ed.* **1999**, 38, 2300 – 2324.
6. Wu, C.-Y.; Wong, C.-H. Chemistry and glycobiology. *Chem. Commun.* **2011**, 47, 6201–6207.

7. N'Go, I., Golten, S.; Ard, A.; CaÇada, J.; Jimnez-Barbero, J.; Linclau, B.; and P. Vincent, S. Tetrafluorination of Sugars as Strategy for Enhancing Protein–Carbohydrate Affinity: Application to UDP-Galp Mutase Inhibition. *Chem. Eur. J.* **2014**, *20*, 106–112
8. Pratap, J.V.; Jeyaprakash, A.A.; Rani, G.P.; Sekar, K.; Surolia, A.; and Vijayan, M. Crystal structures of Artocarpin, a moraceae lectin with mannose specificity, and its complex with methyl- α -D-mannose: Implications to the generation of carbohydrate specificity. *J. Mol. Biol.* **2002**, *317*, 237–247.
9. Rao, K.N.; Suresh, C.G.; Katre, U.V.; Gaikwad, S.M.; and Khan, M.I. Two orthorhombic crystal structures of a galactose-specific lectin from *Artocarpus hirsutain* complex with methyl- α -D-galactose. *Acta Crystallogr. D Biol. Crystallogr.* **2004**, *60*, 1404–1412.
10. Rao, K. N., Kumaran, D., Seetharaman, J., Bonanno, J. B., Burley, S. K., and Swaminathan, S. Crystal structure of trehalose-6-phosphate phosphatase–related protein: Biochemical and biological implications, *Protein Science*, **2006**, *15*, 1735–1744.
11. Farelli, J. D.; Galvin, B. D.; Li, Z.; Liu, C.; Aono, M.; Garland, M.; Hallett, O. E.; Causey, T. B.; Ali-Reynolds, A.; Saltzberg, D. J.; Carlow, C. K.; Dunaway-Mariano, D.; Allen, K.N. *PLoS Pathog.*, **2014**, *10*(7), e1004245.
12. Bridiau, N.; Benmansour, M.; Legoy, M. D.; Maugard T. One-pot stereoselective synthesis of β -N-aryl-glycosides by N-glycosylation of aromatic amines:

- application to the synthesis of tumor-associated carbohydrate antigen building blocks. *Tetrahedron* **2007**, *63*(19), 4178-4183.
13. Somsak, L.; Felföldi, N.; Kónya, B.; Hüse, C.; Telepo, K.; Bokor, É.; Czifrák, K. Assessment of synthetic methods for the preparation of N-β-d-glucopyranosyl- N'-substituted ureas, -thioureas and related compounds. *Carbohydrate Research* **2008**, *343*(12), 2083-2093.
 14. Bokor, É.; Docsa, T.; Gergely, P.; Somsák, L. Synthesis of 1-(d-glucopyranosyl)-1,2,3-triazoles and their evaluation as glycogen phosphorylase inhibitors. *Bioorg. Med. Chem.* **2010**, *18*(3), 1171–1180.
 15. Winum, J.-Y.; Casini, A.; Mincione, F.; Starnotti, M.; Montero, J.-L.; Scozzafava, A.; Supuran, C. T. Carbonic anhydrase inhibitors: N-(p-sulfamoylphenyl)-α-D-glyco-pyrano-sylamines as topically acting antiglaucoma agents in hypertensive rabbits. *Bioorg. Med. Chem. Lett.* **2004**, *14*, 225–229.
 16. Guiseley, K. B.; Ruoff, P. M. Monosaccharide Sulfates. I. Glucose 6-Sulfate. Preparations, Characterization of the Crystalline Potassium Salt, and Kinetic Studies. *J. Org. Chem.* **1961**, *26*(4), 1248–1254.
 17. Roberts, A.; Lee, S.Y.; McCullagh, E.; Silversmith, R.E.; Wemmer, D.E. YbiV from *Escherichia coli* K12 is a HAD phosphatase. *Proteins*, **2005**, *58*(4), 790–801.
 18. Lu, Z.; Wang, L.; Dunaway-Mariano, D.; Allen, K.N. Structure-function analysis of 2-keto-3-deoxy-D-glycero-D-galactonononate-9-phosphate phosphatase defines

specificity elements in type C0 haloalkanoate dehalogenase family members. *J Biol Chem.* **2009**, *284*(2), 1224–33.

19. The Enzyme Function Initiative (EFI)

http://kiemlicz.med.virginia.edu/efi/space_tree/view/501036

CHAPTER FIVE

IRREVERSIBLE INHIBITION OF HAD FAMILY MEMBER

TREHALOSE-6-PHOSPHATE PHOSPHATASE WITH ACTIVE SITE

DIRECTED BIOMODULAR INHIBITORS

5.1 Abstract

Molecules that bind selectively to a given drug target and then undergo a rapid chemoselective reaction to form a covalent conjugate have utility in drug development. The design of these molecules to generate irreversible inhibitors for biological research and drug discovery is an important challenge in carbohydrate chemistry. Herein a library of known Trehalose-6-phosphate phosphatase (T6PP) inhibitors with nucleophilic warheads was conceived of by structure-based design principles and was chemically synthesized. When bound in T6PP active site, the aryl sulfonyl fluorides of **26** react rapidly and chemoselectively with highly conserved Lys residues which located in cap domain. Our results suggest that development of broad-range anthelmintic and antibacterial therapeutics employing targeting this highly conserved Lys may be possible.

5.2. Introduction

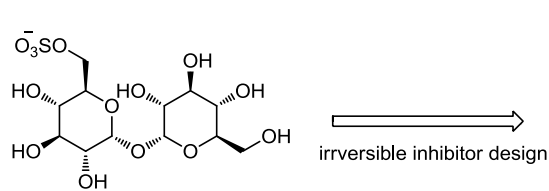
Trehalose, a natural α -linked disaccharide formed by an α,α -1,1-glucoside bond between two α -glucose units, is synthesized and stored in a wide variety of organisms such

as bacteria, plants, fungi and invertebrates to support cell survival by functioning as a fuel, a metabolic regulator or a protectant against environmental stress [1-3]. Unlike these other organisms, humans are unable to produce trehalose but can utilize trehalose through a trehalase enzyme [4-6]. Five different trehalose biosynthetic pathways are known to exist [7], one of which, the OtsA/B pathway is common among pathogenic bacteria and fungi as well as in parasitic nematodes. The OtsA/B pathway, which utilizes glucose and glucose-6-phosphate to generate trehalose-6-phosphate catalyzed by trehalose synthase, then hydrolyzed to trehalose by trehalose-6-phosphate phosphatase (T6PP). Previously reported *otsA* and *otsB* gene knockout (or knockdown) experiments have shown that both pathway enzymes are essential for *Mycobacterium tuberculosis*'s growth in laboratory culture and for its virulence in a mouse model [8]. The T6P synthase and phosphatase are also required for trehalose production in the filamentous fungus *Fusarium graminearum*, however only the T6PP proved to be indispensable for development and virulence [9]. It is also required for cell wall integrity and fungal virulence in the human fungal pathogen *Aspergillus fumigatus* [10]. Disruption of the TPS2Gene which encode Trehalose-6-Phosphate Phosphatase Decreases *Candida albicans*'s Infectivity [11]. Silencing of *tpp* gene in *Caenorhabditis elegans* and *Brugia malayi* caused the arrested growth of larvae revealed that the T6PP is essential, however only when the T6P synthase-encoding gene is functional [12, 13].

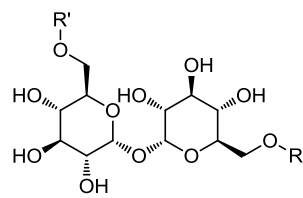
Based on these findings we concluded that trehalose synthesizing pathogens are likely to be vulnerable to the action of small molecule inhibitors of their T6PPs. Moreover, the ranking of potential drug targets for the parasitic nematode *Brugia malayi* placed T6PP

among the most attractive candidates [14]. T6PP belongs to HADSF, its active site is formed by substrate-induced association of a mobile cap domain with the catalytic site of the Rossmann-fold catalytic domain. For phosphatase-specific targeting, one end of the inhibitor is to be optimized for complementation of the catalytic site common to each phosphatase, and the other end optimized to complement the interfaced region of the cap domain, unique to each phosphatase. Phosphate-like functional groups were screened for binding affinity to the catalytic site by using trehalose as the carrier; the sulfate group proved to be most effective (Chapter 3). The ability of trehalose-6-sulfate to induce cap closure was examined by SAXS, and shown to occur in the bacterial T6PP, but not in the nematode T6PP. The X-ray structure determined for the nematode T6PP is consistent with restricted cap movement. Organic groups, attached to glucose-6-sulfate, were then screened for binding affinity towards the cap domain, with promising results for future lead inhibitor development (Chapter 4). In general, to design inhibitors for carbohydrate processing proteins is challenging, since carbohydrates themselves do not bind to proteins with great affinity, for which the monomeric K_D values are typically in the micromolar to millimolar range [15-17]. This low affinity is likely due to the extensive hydrophilic character of these polyhydroxylated compounds. In order to overcome this limitation, we turn onto use irreversible inhibitor design strategy. Compared to reversible inhibitors, irreversible inhibitors has important and potentially advantageous consequences for drug pharmacodynamics in which the level and frequency of dosing relates to the extent and duration of the resulting pharmacological effect. In particular, when covalent modification of a drug target is irreversible, the restoration of pharmacological activity requires re-

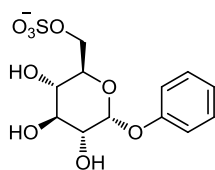
synthesis of the protein target. Some highly nucleophilic warheads, which are widely used in irreversible inhibitor design, were attached to one of highest ranking reversible inhibitors we have synthesized (**Scheme 5.2**), they were screened for their inactivation activities. An irreversible inhibitor which has fluorosulfonylbenzoate group can inactivate all the T6PPs we tested. It is possible that the fluorosulfonylbenzoate can selectively react with active residues in the interface between cap and core domains of the T6PPs. To directly demonstrate that inhibitor **26** inactivates the T6PPs by covalent modification, we analyzed T6PPs treated with or without **26** using mass spectrometry. It shows that this compound lead to covalent labelling of the enzyme within the enzyme substrate binding site residues. This results are promising for the discovery of broad-range anthelmintic and antibacterial drugs.



Ki: up to 49 μ M

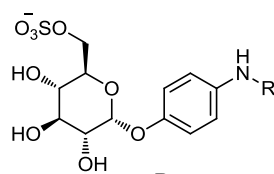


- | R | R' |
|--------------------------------------|------------------------------------|
| 4 H | SO ₂ CH=CH ₂ |
| 5 SO ₂ CH=CH ₂ | SO ₂ CH=CH ₂ |
| 6 SO ₂ CH=CH ₂ | SO ₃ ⁻ |
| 9 H | P=O(F)Et |

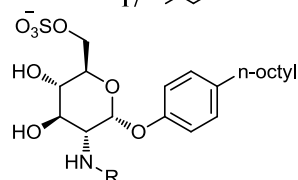


Ki: up to 160 μ M

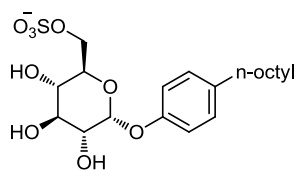
irreversible inhibitor design



- R
- 13
 - 14
 - 15
 - 16
 - 17

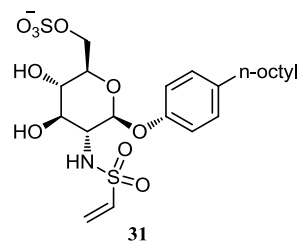


- R
- 26
 - 28
 - 30



Ki: up to 5.3 μ M

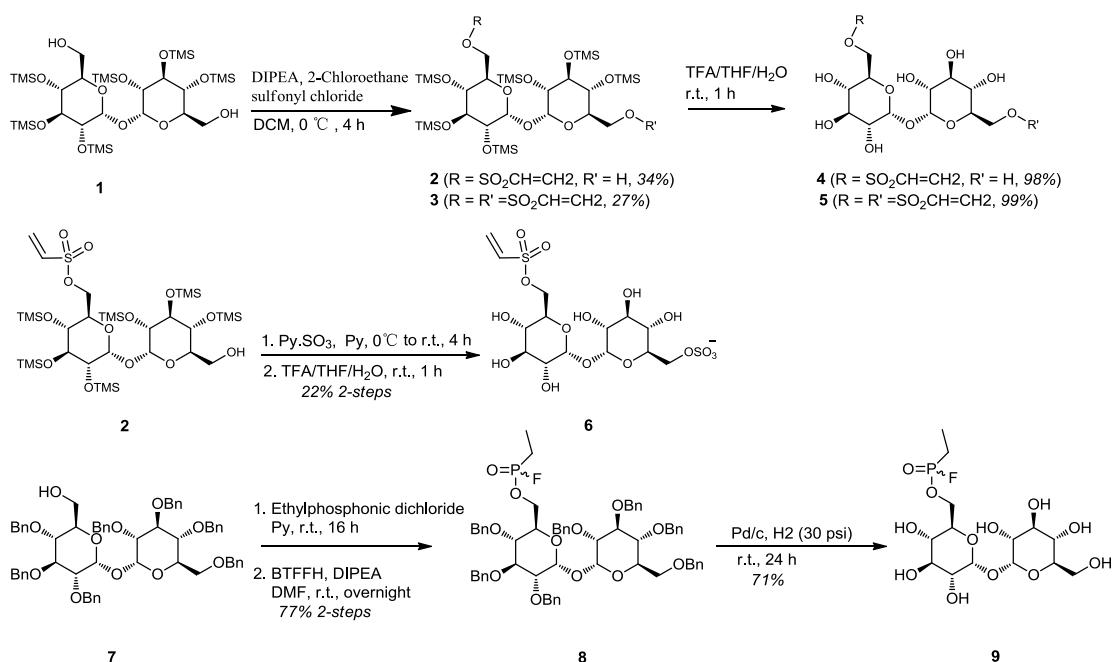
irreversible inhibitor design

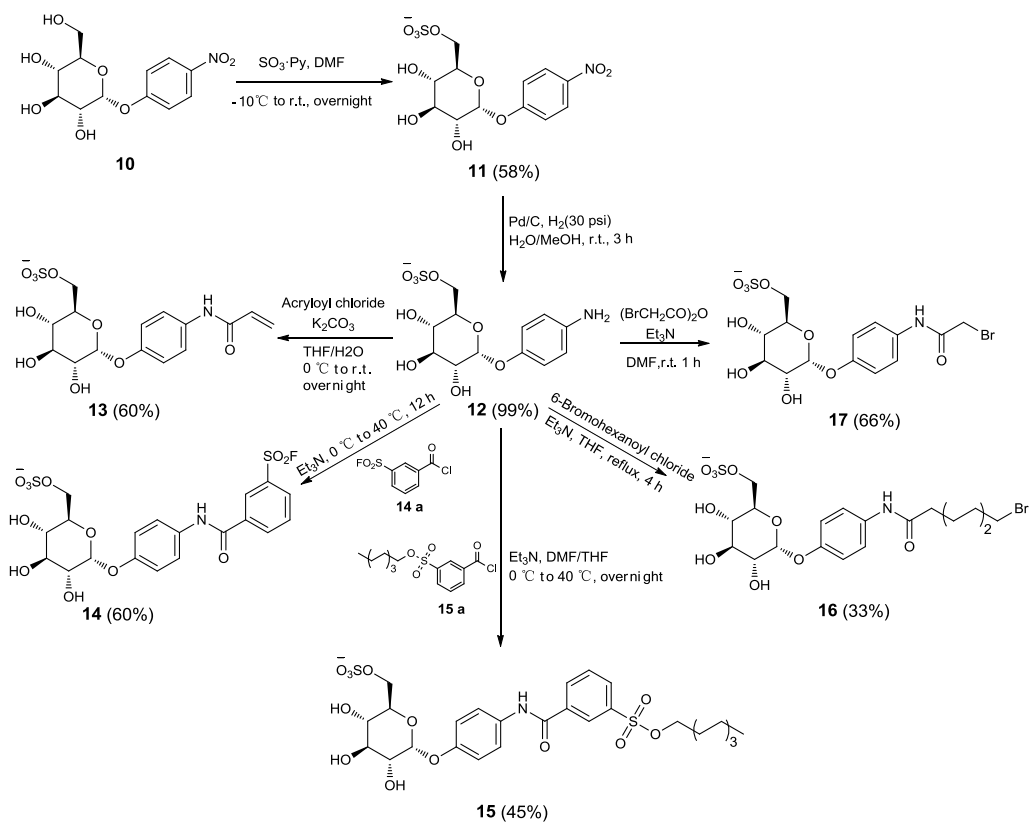


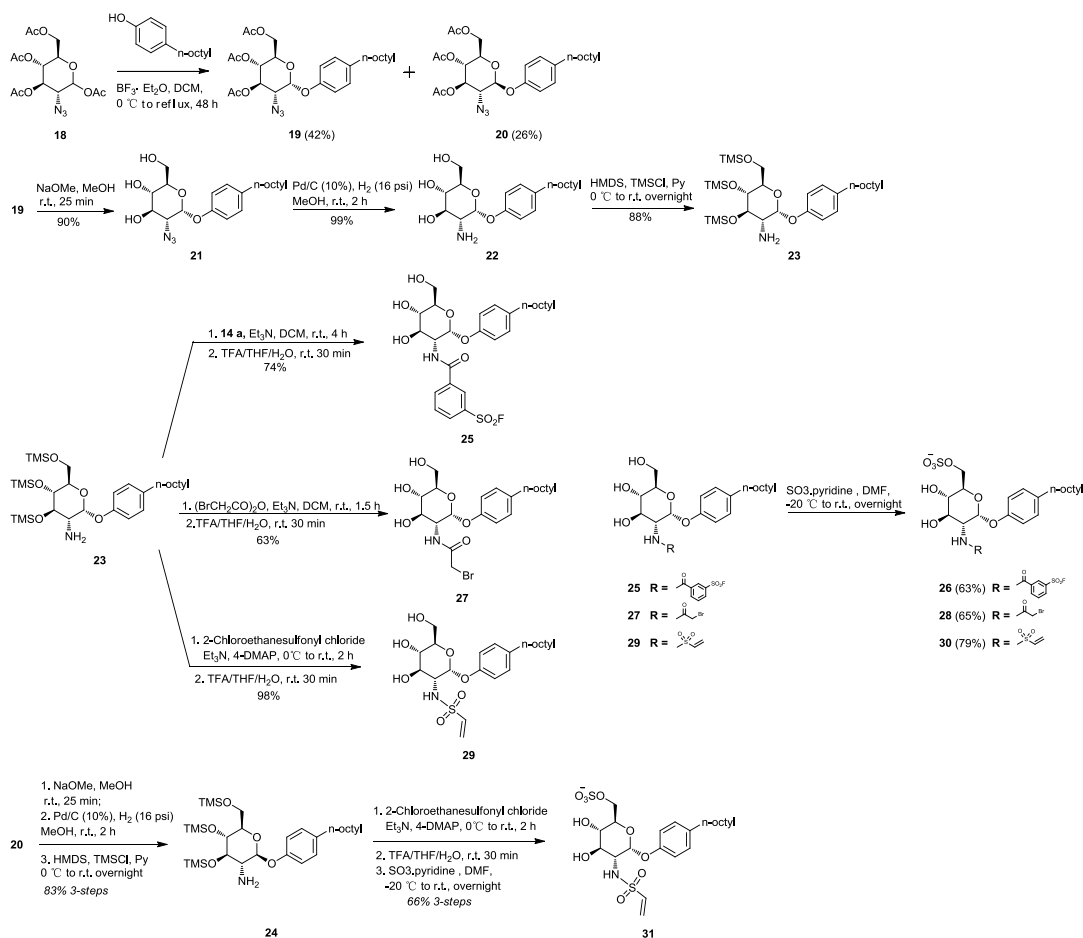
5.3. Results

5.3.1 Synthesis of T6PP irreversible inhibitors

The routes utilized for preparation of the members of the T6PP irreversible inhibitor library, displayed in **Schemes 5.3-5.5** below and described completely in the Experimental, begin with either commercially available or previously synthesized starting materials. Each substance was shown to be >95% pure by using NMR spectroscopy.








5.3.2 Biological activity of irreversible inhibitors

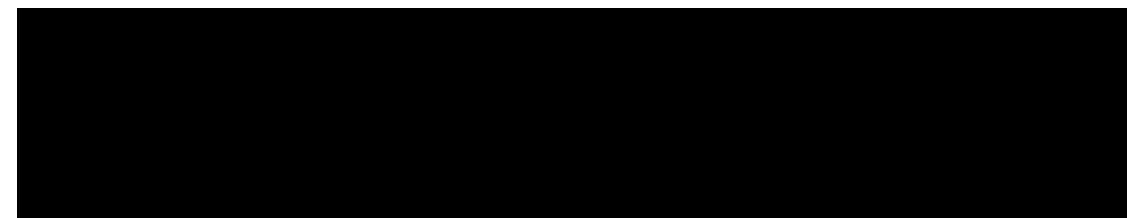
5.3.2.1 Screening the irreversible inhibitors' inactivation and inhibition activities on T6PPs

In order to get their inhibitory information, I set up a HTS assay to screen the inhibitors on the T6PPs. In general, In an incubation reaction mixture containing: T6PP,

with inhibitor or without inhibitor (control), it was incubated at room temperature for half hour, then took 5 μ L of this reaction mixture to a 96 well plate, each well contains 45 μ L reaction mixture: buffer, [T6P] = K_m . The reaction mixture was sit at room temperature for 5 min, then 100 μ L biomol green dye (Enzo Life science). And the resulting mixture was incubated at room temperature for 30 min to allow development of the green color, and measured OD_{620nm} on a microtiter-plate reader. The percentage inactivation was calculated using the ratio of OD_{620nm}' / OD_{620nm}, where OD_{620nm}' is the absorption of the reaction mixture with inhibitor, and the OD_{620nm} is the absorption without inhibitor. The inhibition constants were measured using Enzchek phosphate assay kit (Life Technologies). For the quick inhibition constants measurements, when the initial reaction rate with K_i inhibitor is half of that rate without inhibitor when the substrate concentration is K_m . The following is their inhibitory results:



		1 mM		> 1 mM	0.04 mM			0.02 mM		0.1 mM	0.02 mM	
> 1 mM	> 1 mM		> 1 mM		0.2 mM					> 0.2 mM	0.2 mM	
	> 1 mM			None	None	> 1 mM	> 1 mM	None	0.4 mM	0.4 mM	0.2 mM	0.05 mM
None	None	None		0.5 mM	0.017 mM		0.33 mM		0.017 mM	0.008 mM	0.033 mM	0.013 mM
None					0.08 mM	> 2 mM	0.4 mM	> 1 mM	0.1 mM	0.1 mM		0.01 mM



As we can see in **table 5.1**, some inhibitors are neither reversible inhibitors nor irreversible inhibitors, such as: **5, 6, 9**. Inhibitor **4** can selectively inactivate Mt-T6PP, however, it shows low binding affinity to this enzyme. Inhibitors **13, 14, 16, 17, 28, 30, 31** show moderate inactivation activities on some of the T6PPs, they may selectively react with some poorly conserved residues in T6PPs. Both **15** and **26** can inactivate T6PPs we have tested, however, inhibitor **15** shows poor binding affinity on Mt-T6PP. Then inhibitor **26** was selected for further characterization of its inactivation mechanism.

5.3.2.2 Kinetic analysis of T6PPs inactivation by 26.

In general, the action of a target-specific covalent inhibitor can be described by the mechanism shown below:

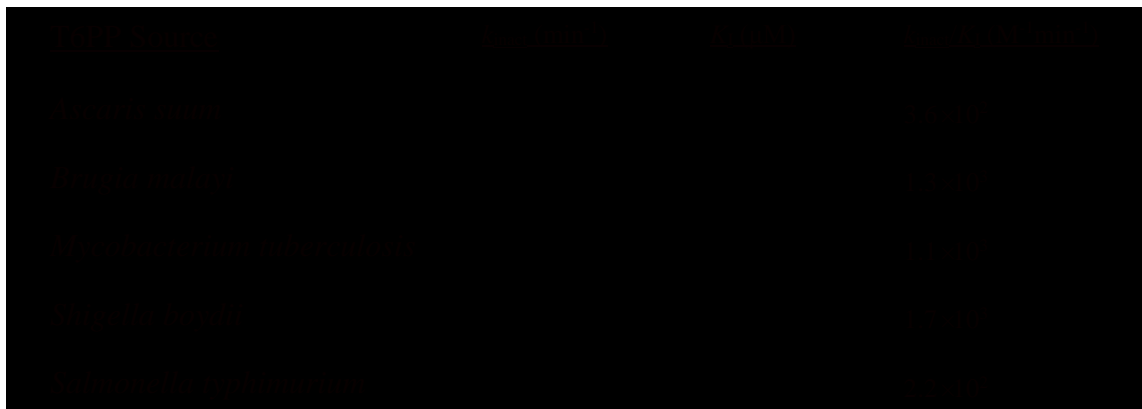


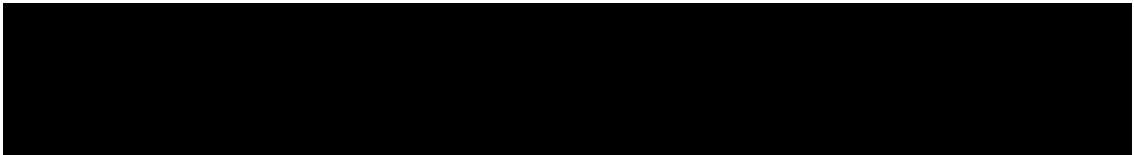
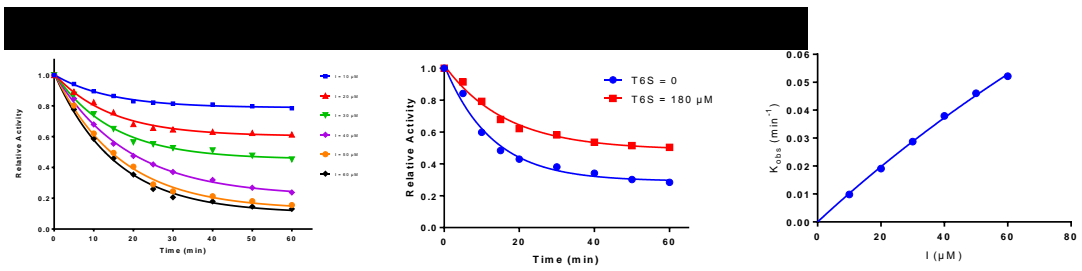
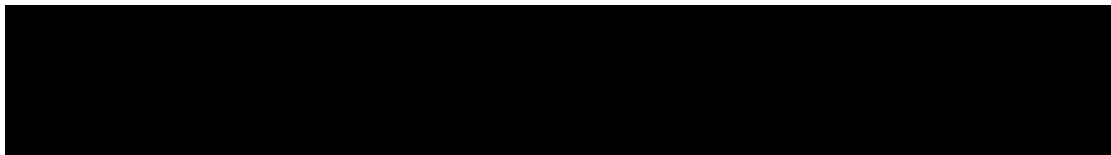
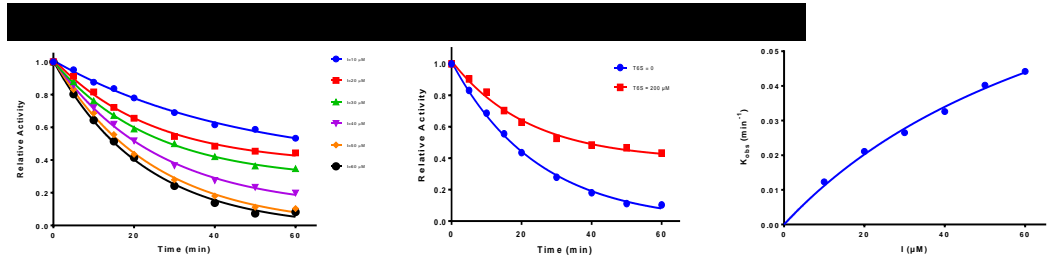
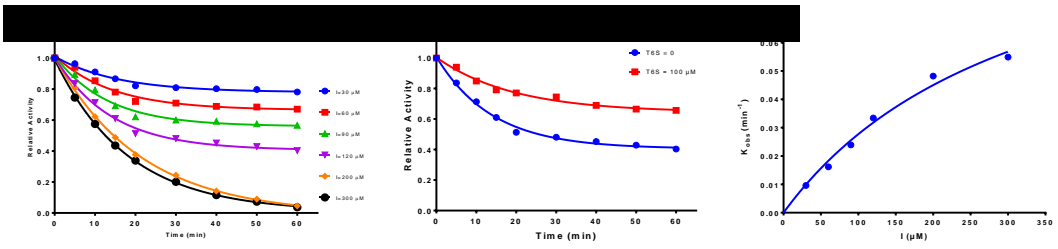
It occurs at two steps in the inhibition: the first step is the compound (**I**) binds to the target protein (**E**) non-covalently, and places its moderately reactive electrophile close to a specific nucleophile on the protein; the second step is that the resulting complex (**E·I**) then undergoes specific bond formation, which gives rise to the inhibited complex (**E-I**).

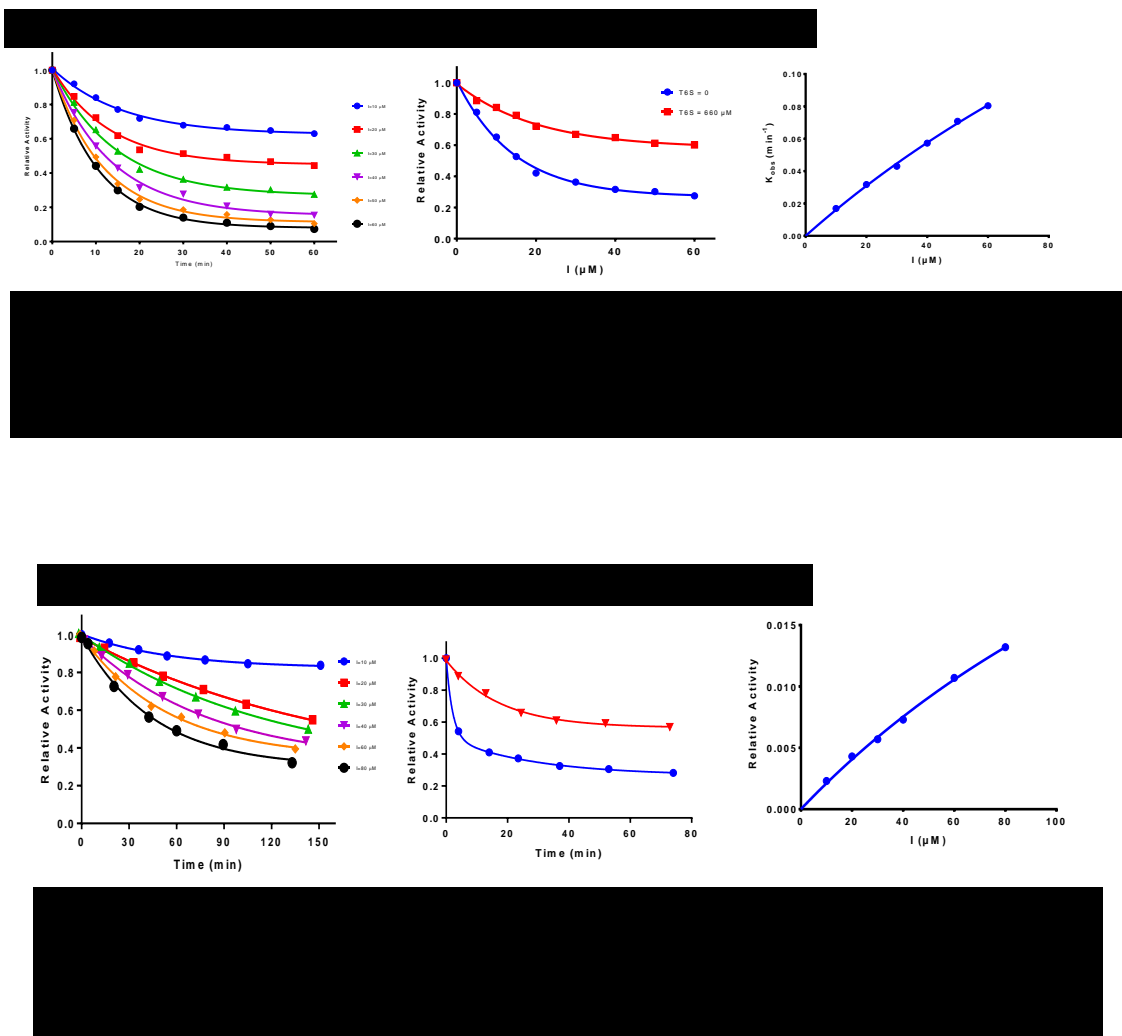
Incubation of **26** with T6PPs, results in a time- and concentration-dependent loss of phosphatase activity (**Figs 5.1-5, a**). The simplest kinetic scheme consistent with the data

is reversible binding of the inactivator to the enzyme active site to give a Michaelis complex (E·I). The stability of this complex is governed by a dissociation constant (K_i) and a chemical inactivation step (K_{inact}) (scheme 7). Extensive dialysis and buffer exchange of the reaction mixture failed to restore enzyme activities, which also suggests the inactivation of the T6PPs by **26** is irreversible. We also found that the rate of inactivation decreased in the presence of the competitive inhibitor trehalose-6-sulfate (**Figs 5.1-5, b**), indicating the inactivation is driven by action occurring at the enzymatic active site, these results also suggest that **26** inactivation action involves at least two steps: binding to the T6PPs active site, followed by covalent modification of active site residue(s). Analysis of pseudo-first-order rate constant (Appendix A5.10) as a function of inhibitor concentration reveals a hyperbolic curve, yielding values for the binding constant K_i and inactivation rate constant k_{inact} (**Table 5.2**).

Table 5.2. Kinetic analyses T6PPs' inactivation by **26** at 25 °C and pH 7.5.



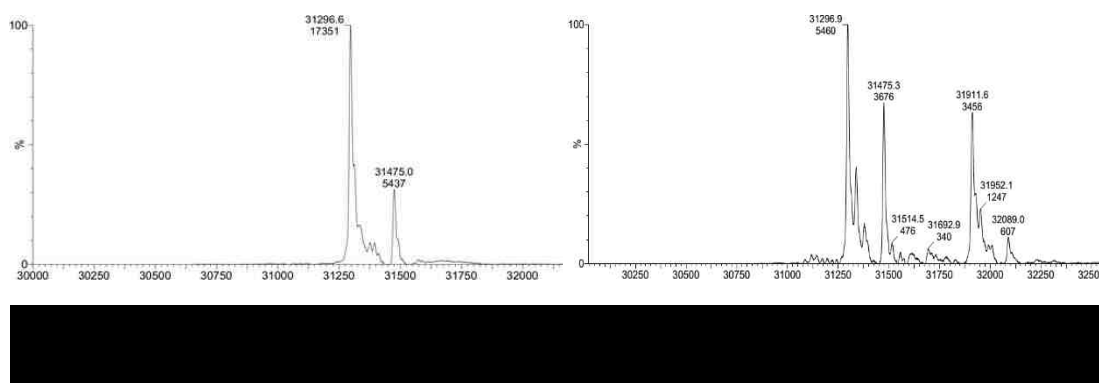
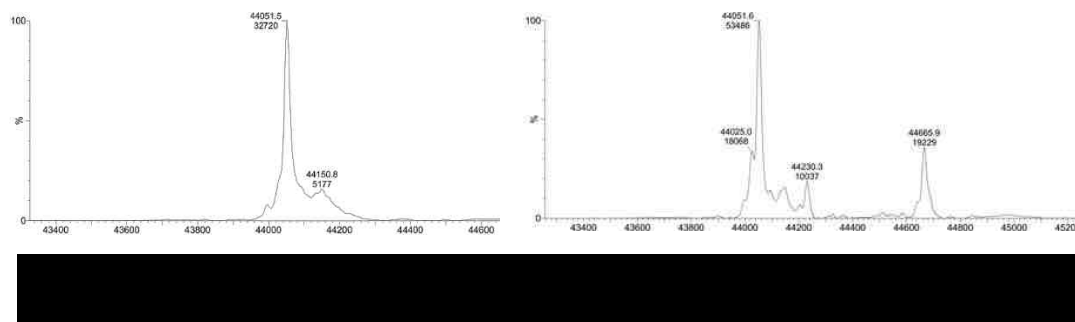




5.3.2.3 Mass spectrometry analysis of T6PPs inactivation by **26**.

In order to directly demonstrate that inhibitor **26** inactivates the T6PPs by covalent modification, I analyzed T6PPs treated with or without **26** using mass spectrometry. In the case of Mt-T6PP, the mass of unmodified Mt-T6PP measured by ESI mass spectrometer was 44052 Da (**Figure 5.6**, left), which is consistent with the theoretical value (44051 Da).

Mt-T6PP treated with **26** showed an altered mass of 44666 Da (**Figure 5.6**, right). This corresponds to a mass difference of 614 Da (**Table 5.2**), consistent with the formation of a sulfide covalent adduct between Mt-T6PP and **26** (The theoretical mass shift is 614 Da).



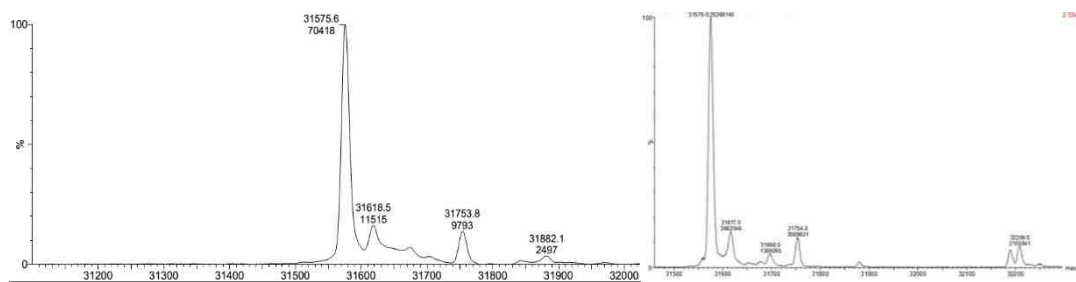
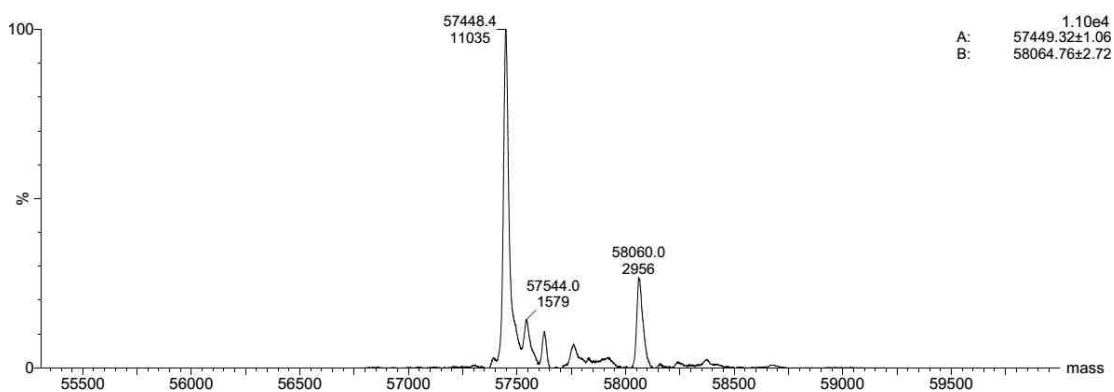


Table 5.3. Mass of covalent modification of T6PPs by **26**

<u>T6PP Source (Theoretical Mass (Da))</u>	<u>Unmodified (Da)</u>	<u>Modified (Da)</u>	<u>Mass Difference (Da)</u>
<i>Brugia malayi</i> (57450)	57448	58060	612
<i>Mycobacterium tuberculosis</i> (44052)	44052	44666	614
<i>Shigella boydii</i> (31298)	31297, 31475 ^a	31912, 32089 ^a	615, 616 ^a
<i>Salmonella typhimurium</i> (31577)	31576, 31754 ^a	32191, 32209 ^a	615, 615 ^a

^a: The protein has been modified by alpha-N-6-phosphogluconoylation of a "his tag" with an extra mass of 178 Da in the fusion protein.

5.3.3. Identification of modified residues by compound 26.

In order to explore the mechanism of T6PPs inactivation mediated by compound 26, we need to determine which residue reacted with the sulfonyl fluoride of compound 26. Based on the binding model of Bm-T6PP with T6P substrate in Figure 5.10 [18], there are several residues which may interact with the substrate D336, R337, K334, Q332, and Y221. However, the residue Y221 is far away from the trehalose unit, it is difficult for it to contact with sulfonyl fluoride group of compound 26. As previously reported, sulfonyl fluoride can modify reactive serines, context-specific threonine, lysine, tyrosine, cysteine and histidine residues [19]. Thus residue K334 is highly possible to be modified by compound 26. In

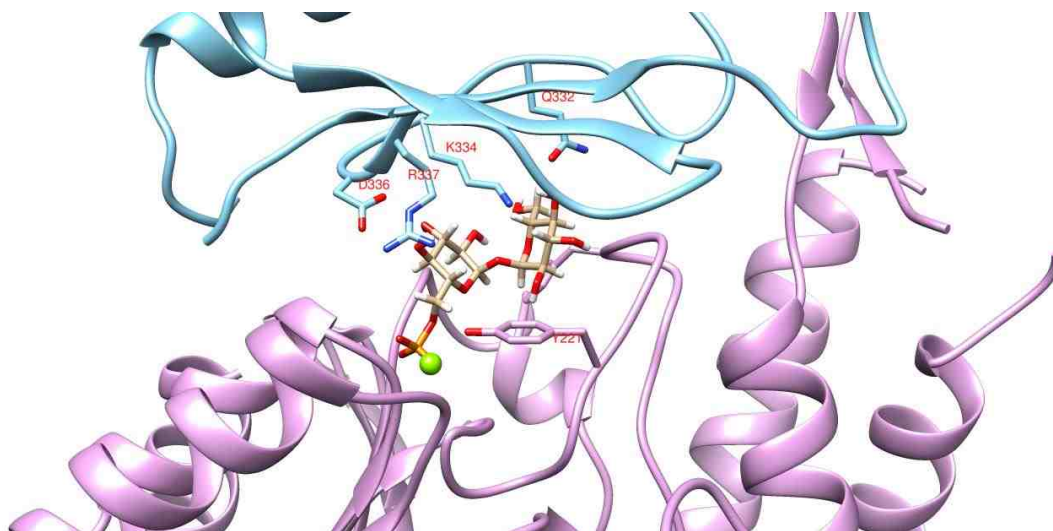


Figure 5.10 Substrate interacting residues in *B. malayi* analyzed by mutagenesis and kinetic.

Order to confirm this hypothesis, we analyzed Bm-T6PP-K334A mutant [18] treated with or without 26 using mass spectrometry. The results shown in **Figure 5.11** indicate that compound 26 is unable to modify Bm-T6PP-K334A mutant, consistent with the formation

of a covalent adduct between Bm-T6PP and **26** involving the Lys334 residue.

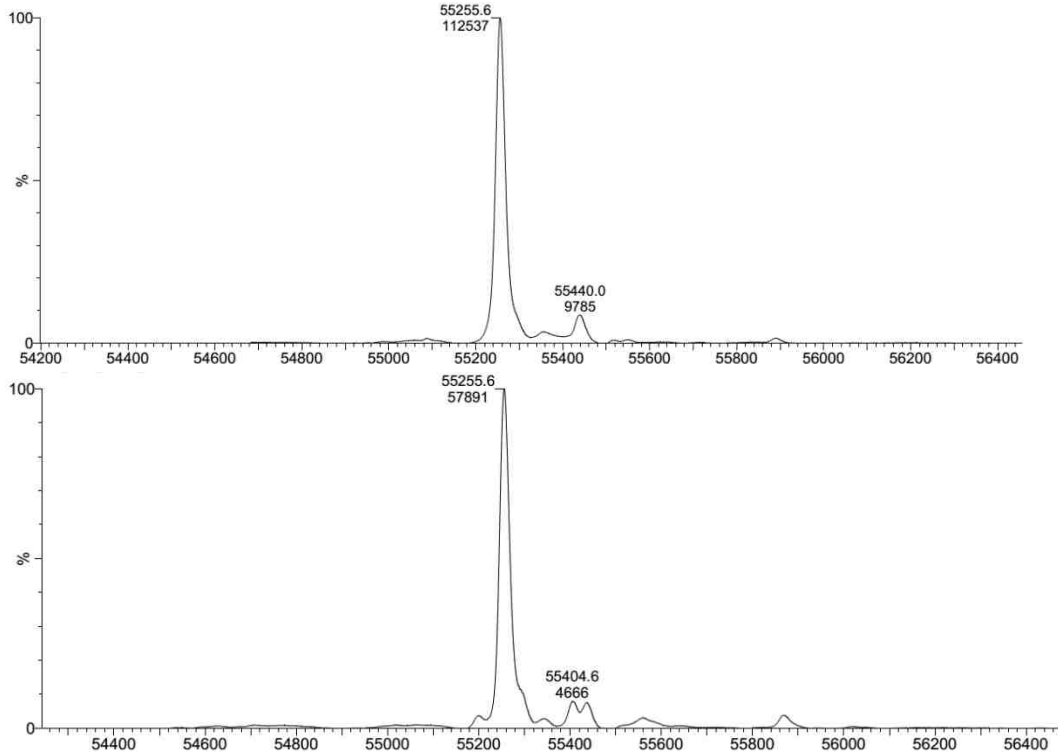


Figure 5.11 Mass spectrometry analysis of the Bm-T6PP Lys334 to Ala mutant (1 μ M) in the presence and absence of 20 μ M **26** under the same incubation conditions used for the wild type enzyme. The ESI mass spectra of Bm-T6PP-K334A treated with (bottom) or without (top) **26**.

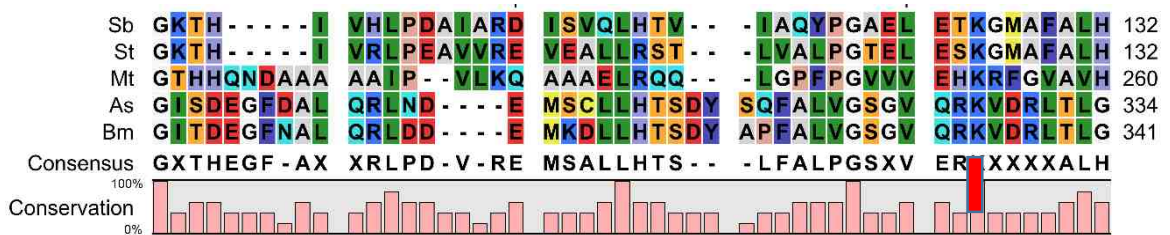


Figure 5.12 Sequence alignments of nematode and bacteria T6PP enzymes. Sb (*Shigella boydii*); St (*Salmonella typhimurium*); Mt (*Mycobacterium tuberculosis*); Bm (*Brugia malayi*); As (*Ascaris suum*). The Lys highlighted in red is highly conserved.

Interestingly, Lys334 in Bm-T6PP is highly conserved in nematode and bacteria

T6PPs base on the sequence alignments(**Figure 5.12**). In order to further confirm that compound **26** selectively react with highly conserved Lys in T6PPs, we analyzed Mt-T6PP-K253A mutant (chapter 3) treated with or without **26** using mass spectrometry (**Figure 5.13**). We got the same results as for Bm-T6PP-K253A, the mutant Mt-T6PP-K253A could be modified by compound **26** under the same incubation conditions used for the wild type enzyme.

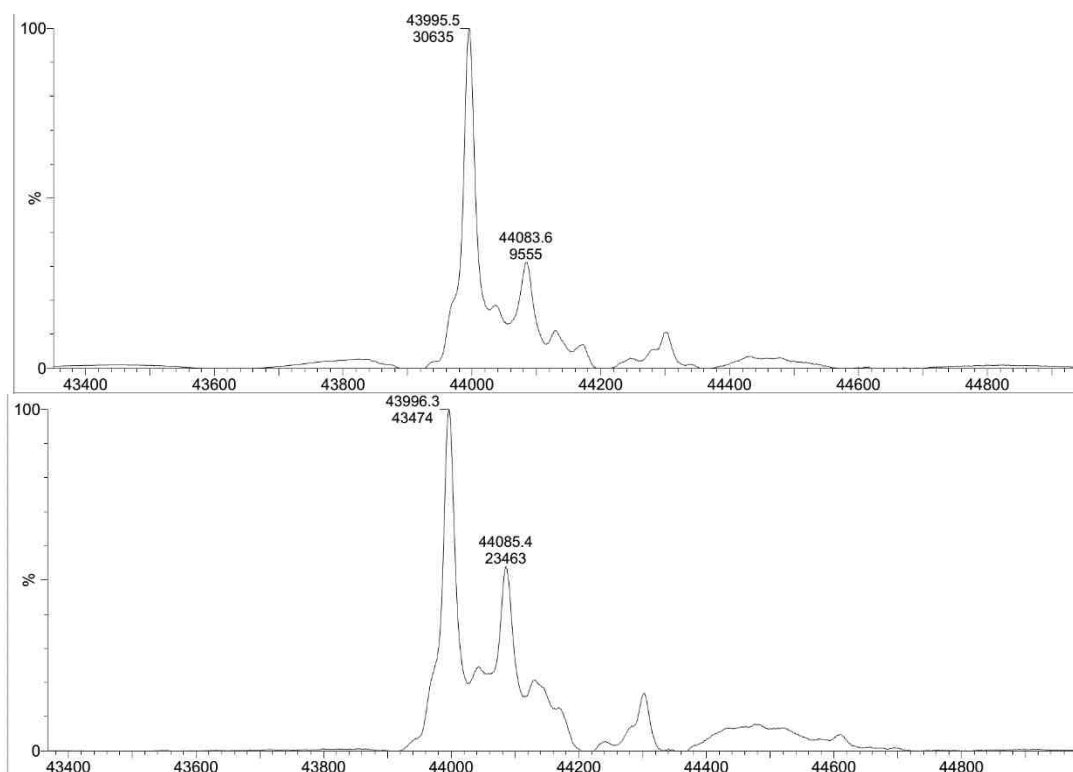
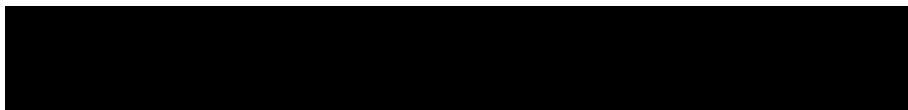
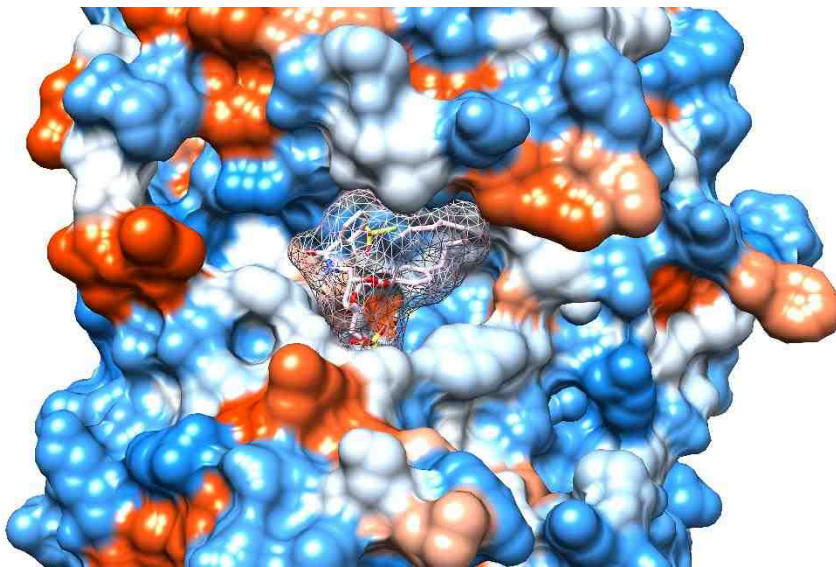


Figure 5.13 Mass spectrometry analysis of the Mt-T6PP Lys253 to Ala mutant (1 μ M) in the presence and absence of 20 μ M **26** under the same incubation conditions used for the wild type enzyme. The ESI mass spectra of Mt-T6PP-K253A treated with (bottom) or without (top) **26**.

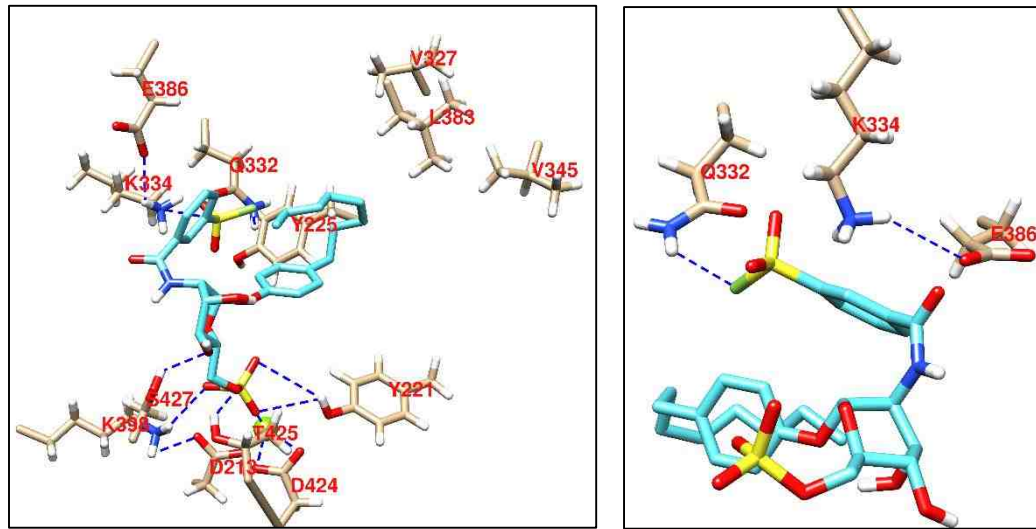
5.3.4. Molecular Modeling

In order to better to understand how the compound **26** inactivate, molecular docking

studies were performed on this compound with Bm-T6PP by using AutoDock Vina. Bm-T6PP (PDB ID: 4OFZ) is in complex with Mg^{2+} ions required for catalytic activity. According to docking results (**Figure 5.14**), **26** sits in the interface of cap and catalytic domains. The phosphate mimic sulfate group sits in the phosphate binding site, and the 4-



n-Octyl phenyl hydrophobic group is sitting in the hydrophobic pocket of Bm-T6PP.



From **Figure 5.15**, we can see the cofactor Mg^{2+} is coordinated by the carboxylate group of the loop 1 Asp213 nucleophile and Asp424 on loop 4, and sulfate oxygen anion of the inhibitor **26**. The Mg^{2+} functions to prevent charge repulsion between the sulfate and the Asp213, Asp424. Besides coordination of the metal center, additional key interactions are established by compound **26** within the active site. The sulfate warhead forms hydrogen binding with Lys398 and Tyr221 and Thr425. And the 4 position hydroxyl group can interact with Ser427 via hydrogen bond. More importantly, the 4-n-octyl-phenyl group of **26** establishes hydrophobic contacts with the hydrophobic side chains of Leu383, Val 345, Tyr 221 and Tyr225 in order to increase the binding affinity. In the cap domain, there are several hydrogen bond formed with the sulfonyl fluoride warhead group (Figure 5.14, right). In the inactivation reaction, Lys334 was deprotonated by Glu383, and then

nucleophilic attack sulfonyl fluoride which was activated by Gln332 via hydrogen bonding (Figure 5.16) to form covalent adduct.

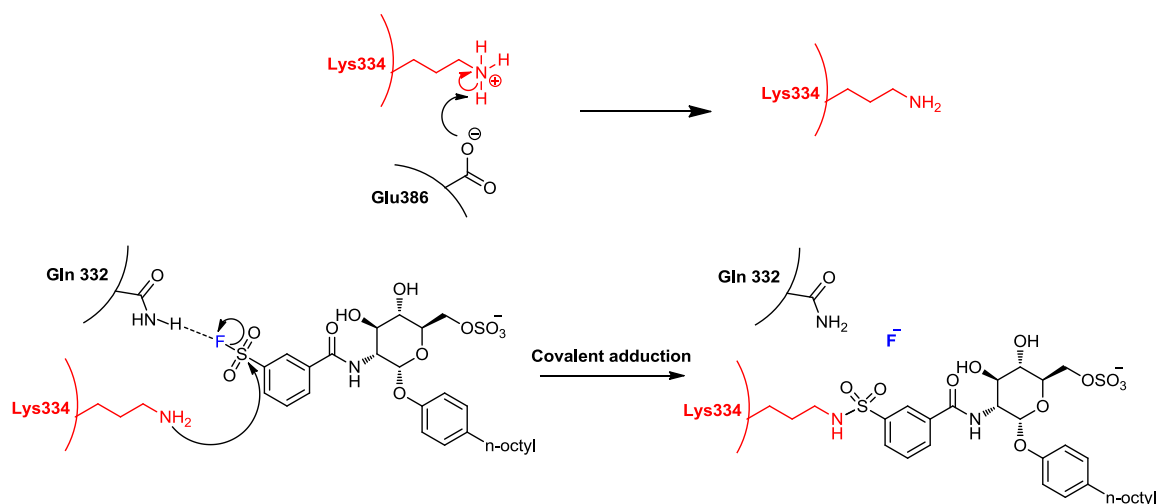
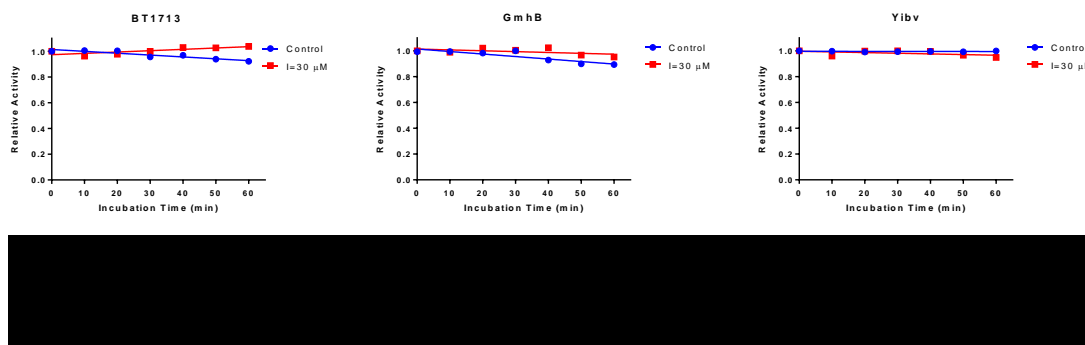


Figure 5.16. Proposed mechanism of **26** mediated Bm-T6PP inactivation.

5.3.4 Inactivation specificity of **26**.

In order to test the inactivation specificity by **26**, I tested its inactivation activities on several sugar phosphatases. Yibv [19], which is from *E. coli*, can hydrolyze a wide scope of sugar phosphates, substrates like glucose-6-phosphate, imido-di-phosphate, fructose-1-phosphate, ribose-5-phosphate, acetyl-phosphate, glycerol-1-phosphate, glycerol-2-phosphate. BT1713 [20], which is from *Bacteroides thetaiotaomicron*, is a 2-keto-3-deoxy-D-glycero-D-galacto-9-phosphononic acid (KDN-9-P) phosphatase in the biosynthetic pathway of the 9-carbon alpha-keto acid, 2-keto-3-deoxy-D-glycero-D-galactononic acid (KDN). It can also hydrolyze 2-keto-3-deoxy-8-phospho-d-manno-octulosonic acid (KDO-8-P), N-acetylneuraminic acid-9-phosphate (Neu5Ac-9-P), pNPP, glucose-6-phosphate,

PEP, tyrosine phosphate, and gluconate-6-phosphate. The other enzyme that we tested is GmhB (EFI 501036) [21], from *Pseudomonas putida* KT2440, is a D,D-heptose 1,7-bisphosphate phosphatase, it can convert the D-glycero-beta-D-manno-heptose 1,7-bisphosphate intermediate into D-glycero-beta-D-manno-heptose 1-phosphate. D-Fructose-1,6-bisphosphate is also its substrate. I didn't observe significant inactivation in the presence of 30 eq of **26** (Figure 5.17).



5.5 Conclusion

Trehalose -6-phosphate phosphatase involved in the biosynthesis of trehalose, one of the important molecule that exist in a wide variety of organisms to support cell survival by functioning as a fuel, a metabolic regulator or a protectant against environmental stress. T6PP is a potential drug target in pathogenic bacteria and fungi as well as in parasitic nematodes. Here, we describe the discovery of a novel class of covalent inhibitors that broadly inhibit T6PP through the generation of a reactive sulfonyl fluoride group within their T6P substrate binding site. Until the discovery of this compound, there were no generally applicable irreversible inhibitors for T6PP. The reactive sulfonyl fluoride

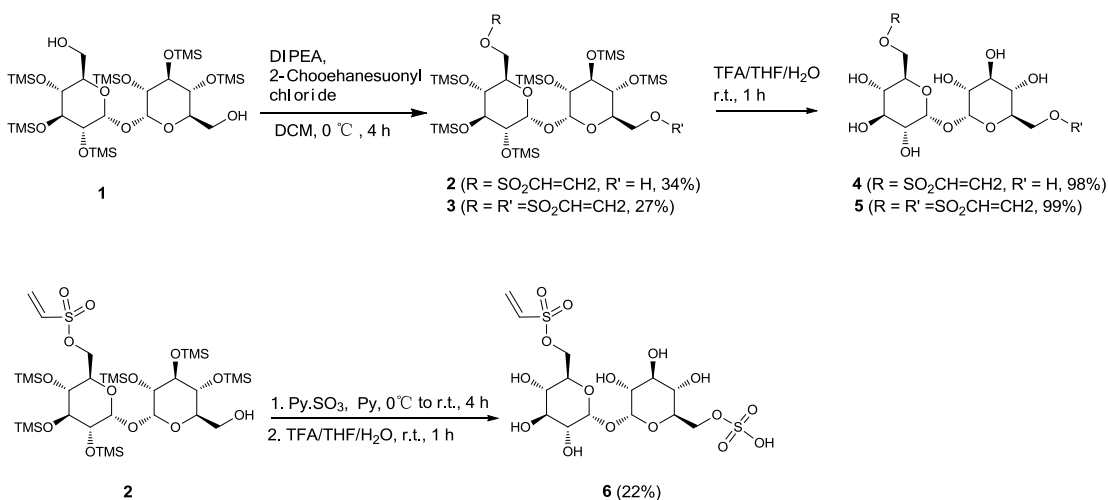
primarily remain localized within the interface between the core and cap domains (substrate binding site), since its inactivation activity decreased in the presence of reversible competitive T6PP inhibitor T6S. No significant inactivation on other sugar phosphatases were observed show that this inhibitor has its selective inhibition on T6PPs. This inhibitor will serve as powerful research tools for further exploration of T6PP drug target. In addition, these inhibitors will serve as starting points for the generation of T6PP-selective inhibitors through systematic modification of their aryl substituents to take advantage of the unique active site topologies of T6PPs. These observation highlight the potential for developing broad-range anthelmintic and antibacterial therapeutics employing targeting this highly conserved Lys may be possible.

5.5 Material and Methods

5.5.1 Inhibitor Synthesis

General. Except when specified, all solvents and reagents were purchased and used without further purification. Analytical thin-layer chromatography (TLC) was performed on silica gel plates containing F₂₅₄ fluorescence indicator and column chromatography was performed using the indicated eluants on silica gel (230-400 mesh). ¹H (300 MHz), ¹³C NMR (75 MHz), and ³¹P (121.5 MHz) NMR spectra were recorded on Bruker Avance III 300 spectrometers. ¹H, ¹³C and ³¹P NMR data are reported as follows: for ¹H NMR chemical shifts are reported in ppm relative to H₂O, multiplicities are given as s = singlet, d = doublet, t = triplet, q = quartet, td = triplet of doublets, br = broad signal, m = multiplet, and coupling constant (*J*) are in Hz; ¹³C NMR chemical shifts are reported in ppm relative

to NH_4HCO_3 as a standard; ^{31}P NMR chemical shifts are reported in ppm relative to 50% aq H_3PO_4 as a standard.



6-O-vinyl sulfonate-2,3,4,2',3',4'-hexakis-O-(trimethylsilyl)- α,α -trehalose (2) and **6,6' Di-O-vinyl sulfonate-2,3,4,2',3',4'-hexakis-O-(trimethylsilyl)- α,α -trehalose (3).**

To a solution of **1**¹ (1.2 g, 1.55 mmol) in anhydrous dichloromethane (9 mL) at 0 °C was added DIPEA (1.2 g, 9.3 mmol). 2-chloroethane-sulfonyl chloride (0.33 g, 1.86 mmol) was added over half hour. The resulting solution was stirred at 0 °C for 4 h and concentrated in vacuo, giving a residue that was subjected to silica gel chromatograph to give 0.52 g (34%) of **2** and 0.41 g (27%) of **3**.

2: ^1H NMR (300 MHz, CDCl_3) 6.55 (dd, $J_1 = 9.6$ Hz, $J_2 = 16.8$ Hz, 1H), 6.40 (d, $J = 16.8$ Hz, 1H), 6.11 (dd, $J_1 = 9.6$ Hz, $J_2 = 4.4$ Hz, 1H), 4.89 (d, $J = 3.0$ Hz, 2H), 4.20-4.19 (m, 2H), 4.03-4.0 (m, 1H), 3.91-3.89 (m, 3H), 3.72-3.68 (m, 2H), 3.50-3.40 (m, 4H), 1.73 (br, 1H), 0.17-0.12 (m, 54H). ^{13}C NMR (75 MHz, CDCl_3) 132.7, 130.1, 94.9, 94.7, 73.5, 73.2, 72.9, 72.6, 71.6, 71.5, 70.8, 69.6, 61.7, 1.13, 1.07, 0.98, 0.28, 0.21.

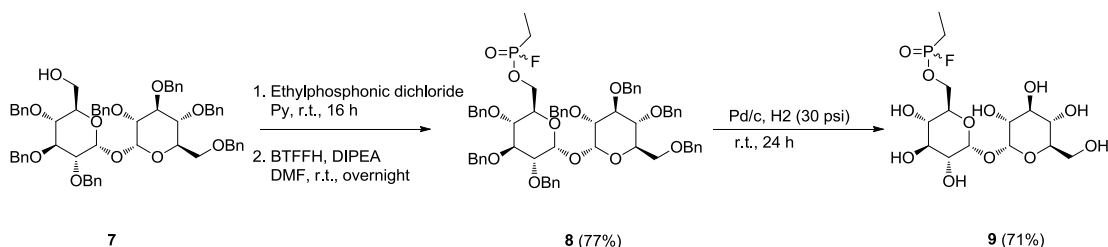
3: ¹H NMR (300 MHz, CDCl₃) 6.54 (dd, $J_1 = 9.6$ Hz, $J_2 = 16.5$ Hz, 2H), 6.40 (d, $J = 16.5$ Hz, 2H), 6.13 (d, $J = 9.6$ Hz, 2H), 4.88 (d, $J = 3.0$ Hz, 2H), 4.20-4.19 (m, 4H), 4.03-3.98 (m, 2H), 3.86 (t, $J = 9.0$ Hz, 2H), 3.45-3.40 (m, 4H), 0.16-0.12 (m, 54H). ¹³C NMR (75 MHz, CDCl₃) 132.6, 130.2, 94.8, 73.4, 72.6, 71.6, 70.9, 69.5, 1.15, 1.07, 0.29.

6-O-vinyl sulfonate- α,α -trehalose (4). **2** (200 mg, 0.21 mmol) was dissolved in a mixture of TFA/THF/H₂O (8/17/3, V/V/V, 2.5 mL), The resulting solution was stirred at r.t. for 1 h and concentrated in vacuo, giving a residue that was subjected to silica gel chromatograph to give 108 mg (98%) of **4**. ¹H NMR (300 MHz, D₂O) 6.80 (dd, $J_1 = 10.2$ Hz, $J_2 = 16.5$ Hz, 1H), 6.50 (d, $J = 16.5$ Hz, 1H), 6.37 (d, $J = 10.2$ Hz, 1H), 5.19 (d, $J = 3.9$ Hz, 1H), 5.16 (d, $J = 3.9$ Hz, 1H), 4.44-4.43 (m, 2H), 4.07-4.0 (m, 1H), 3.87-3.73 (m, 5H), 3.67-3.60 (m, 2H), 3.51-3.43 (m, 2H). ¹³C NMR (75 MHz, D₂O) 133.1, 130.5, 93.6, 93.4, 72.5, 72.3, 72.2, 70.9, 70.8, 69.7, 69.6, 69.1, 60.5. HRMS (ESI⁺) calcd for C₁₄H₂₄O₁₃S [M+Na]⁺ m/z 455.0830, found 455.0836.

6,6' Di-O-vinyl sulfonate- α,α -trehalose (5). This substance was prepared from **3** using the same procedure as that for **4**. Yield 99 %. ¹H NMR (300 MHz, D₂O) 6.79 (dd, $J_1 = 9.9$ Hz, $J_2 = 16.8$ Hz, 2H), 6.50 (d, $J = 16.8$ Hz, 2H), 6.36 (d, $J = 9.9$ Hz, 2H), 5.16 (d, $J = 3.6$ Hz, 2H), 4.44-4.43 (m, 4H), 4.14-4.02 (m, 2H), 3.83 (t, $J = 9.6$ Hz, 2H), 3.64 (dd, $J_1 = 3.6$ Hz, $J_2 = 10.2$ Hz, 2H), 3.48 (t, $J = 9.6$ Hz, 2H). ¹³C NMR (75 MHz, D₂O) 133.1, 130.5, 93.8, 72.4, 70.7, 69.8, 69.6, 69.1. HRMS (ESI⁺) calcd for C₁₆H₂₅O₁₅S₂ [M+Na]⁺ m/z 545.0611, found 545.0613.

6-O-vinyl sulfonate-6'-sulfate- α,α -trehalose (6). To a solution of compound **3** (640 mg, 0.74 mmol) in anhydrous pyridine (20 mL) at 0 °C, was added a solution of

SO₃.pyridine (141 mg, 0.89 mmol) in 1 mL anhydrous pyridine, The resulting solution was warmed to room temperature and stirred for 12 h, then concentrated in vacuo, the resulting residue was dissolved in a mixture of TFA/THF/H₂O (8/17/3, V/V/V, 1 mL), The resulting solution was stirred at r.t. for 1 h and concentrated in vacuo giving a residue that was subjected to silica gel chromatograph to give 82 mg (22%) of **6**. ¹H NMR (300 MHz, D₂O) 6.80 (dd, *J*₁ = 9.9 Hz, *J*₂ = 16.5 Hz, 1H), 6.52 (d, *J* = 16.5 Hz, 1H), 6.38 (d, *J* = 9.9 Hz, 1H), 5.20 (d, *J* = 3.6 Hz, 1H), 5.16 (d, *J* = 3.6 Hz, 1H), 4.47-4.44 (m, 2H), 4.28-4.25 (m, 2H), 4.08-4.00 (m, 2H), 3.85 (t, *J* = 9.6 Hz, 2H), 3.67 (dd, *J*₁ = 3.6 Hz, *J*₂ = 9.9 Hz, 2H), 3.55-3.46 (m, 2H). ¹³C NMR (75 MHz, D₂O) 133.1, 130.5, 93.8, 93.7, 72.4, 72.3, 70.7, 70.3, 69.8, 69.6, 69.3, 69.2, 66.9. HRMS (ESI⁺) calcd for C₁₄H₂₃O₁₆S₂ [M]⁺ m/z 511.0428, found 511.0411.



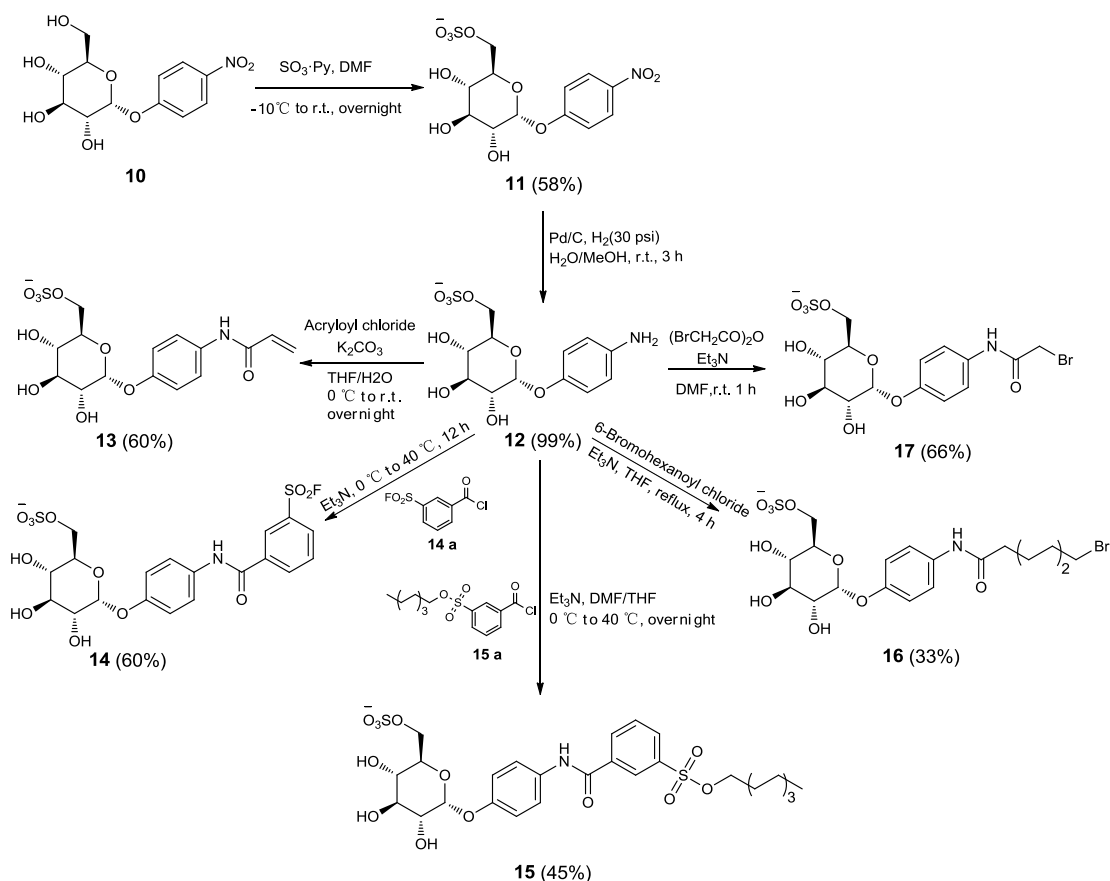
6-O-(Ethylphosphorylfluoro)-2,3,4,2',3',4,6'-hepta-O-benzyl- α,α -D-trehalose

(8).³ To a solution of compound **7**² (0.47 g, 0.48 mmol) in anhydrous pyridine (10 mL), was added ethylphosphonic dichloride (0.71 g, 4.8 mmol). The resulting solution was stirred at r.t. overnight. The reaction mixture was concentrated under reduced pressure and the resulting residue was dissolved in a mixture of dichloromethane and H₂O (5 mL/10

mL), and stirred at r.t. for 1 hour, then acidified with 1 N HCl, and extracted with dichloromethane, dried over Na₂SO₄ and concentrated in vacuo, giving a residue, which was dissolved in anhydrous DMF under argon atmosphere, and fluoro-N,N,N',N'-bis(tetramethylene) formamidinium hexafluorophosphate (466 mg, 1.48 mmol) was added. Then DIPEA (190 mg, 1.48 mmol) was added, the resulting mixture was stirred overnight at room temperature and concentrated in vacuo, giving a residue that was subjected to silica gel chromatograph to give 387 mg (77%) of **8**. ¹H NMR (300 MHz, CDCl₃) 7.38-7.16 (m, 35H), 5.26 (d, *J* = 3.3 Hz, 1H), 5.24 (d, *J* = 3.9 Hz, 1H), 5.06 (d, *J* = 8.4 Hz, 1H), 5.02 (d, *J* = 8.4 Hz, 1H), 4.96-4.84 (m, 4H), 4.80-4.41 (m, 8H), 4.23-4.04 (m, 6H), 3.76-3.69 (m, 1H), 3.65 (dd, *J*₁ = 9.6 Hz, *J*₂ = 3.6 Hz, 1H), 3.60-3.52 (m, 3H), 3.45-3.40 (m, 1H), 1.96-1.81 (m, 2H), 1.30-1.15 (m, 3H). ¹³C NMR (75 MHz, CDCl₃) 138.9, 138.6, 138.4, 138.1, 138.0, 137.9, 128.5, 128.2, 128.2, 128.1, 127.9, 127.8, 127.6, 127.5, 94.7, 94.5, 94.2, 94.0, 81.9, 81.9, 81.6, 81.5, 79.5, 77.8, 77.4, 77.0, 75.8, 75.7, 75.3, 75.2, 73.6, 73.2, 73.1, 72.8, 70.9, 69.6 (d, *J*_{C,P} = 4.4 Hz), 68.2, 65.2 (d, *J*_{C,P} = 17.3 Hz), 65.1 (d, *J*_{C,P} = 17.5 Hz), 17.8 (dd, *J*_{C,P} = 146.0 Hz, *J*_{C,F} = 25.4 Hz), 17.7 (dd, *J*_{C,P} = 144.5 Hz, *J*_{C,F} = 25.4 Hz), 6.3, 6.2. ³¹P NMR (121.5 MHz, D₂O) 33.9 (d, *J*_{P,F} = 1071.5 Hz), 33.3 (d, *J*_{P,F} = 1077.9 Hz).

6-O-(Ethylphosphorylfluoro- α,α -D-trehalose (9)). Compound **8** (367 mg, 0.34 mmol) was dissolved in ethanol (35 mL). Pd/C (10% w/w, 700 mg) was added and the resulting suspension was stirred under an atmosphere of hydrogen (30 psi) at room temperature for 24 h. The catalyst Pd/C was removed by filtration and the reaction was concentrated in vacuo, giving a residue that was subjected to silica gel chromatograph to give 107 mg (71%) of **9**. ¹H NMR (300 MHz, D₂O) 5.20 (d, *J* = 3.6 Hz, 1H), 5.16 (d, *J* =

3.6 Hz, 1H), 4.45-4.39 (m, 2H), 4.01-3.96 (m, 1H), 3.88-3.71 (m, 5H), 3.66-3.60 (m, 2H), 3.51 (dd, $J_1 = 9.6$ Hz, $J_2 = 2.7$ Hz, 1H), 3.43 (t, $J = 9.6$ Hz, 1H), 2.18-2.05 (m, 2H), 1.34-1.04 (m, 3H). ^{13}C NMR (75 MHz, D_2O) 93.6, 93.5, 93.4, 72.6, 72.4, 72.3, 72.2, 71.0, 70.9, 70.5, 70.4, 69.7, 69.2, 69.1, 69.0, 66.1, 66.0, 60.5, 16.6 (dd, $J_{\text{C,P}} = 138.6$ Hz, $J_{\text{C,F}} = 18.4$ Hz), 16.5 (dd, $J_{\text{C,P}} = 140.2$ Hz, $J_{\text{C,F}} = 18.0$ Hz), 5.0, 4.9. ^{31}P NMR (121.5 MHz, D_2O) 38.9 (d, $J_{\text{P,F}} = 1075.6$ Hz), 38.7 (d, $J_{\text{P,F}} = 1078.2$ Hz). HRMS (ESI^+) calcd for $\text{C}_{14}\text{H}_{26}\text{FO}_{12}\text{P}$ $[\text{M}+\text{Na}]^+$ m/z 459.1044, found 459.1028.



4-Nitrophenyl α -D-glucopyranoside-6-sulfate (11). To a solution of 4-Nitrophenyl α -D-glucopyranoside (4.0 g, 13.3 mmol) in anhydrous DMF (40 mL) at -20 °C, was added a

solution of SO₃·pyridine (2.2 g, 14 mmol) in 4 mL anhydrous DMF, The resulting solution was stirred at r.t. for 12 h and concentrated in vacuo, giving a residue that was subjected to silica gel chromatograph to give 2.92 g (58%) of **11**. ¹H NMR (300 MHz, CD₃OD) 8.23 (d, *J* = 9.3 Hz, 2H), 7.34 (d, *J* = 9.3 Hz, 2H), 5.64 (d, *J* = 3.6 Hz, 1H), 4.18-4.16 (m, 2H), 3.86 (t, *J* = 9.3 Hz, 1H), 3.76 (td, *J*₁ = 9.9 Hz, *J*₂ = 3.6 Hz, 1H), 3.65 (dd, *J*₁ = 9.9 Hz, *J*₂ = 3.6 Hz, 1H), 3.50 (t, *J* = 9.9 Hz, 1H). ¹³C NMR (75 MHz, CD₃OD) 163.6, 144.1, 126.7, 118.1, 99.3, 74.5, 73.2, 72.9, 71.1, 67.8.

4-Aminophenyl α-D-glucopyranoside-6-sulfate (12). Compound **11** (2.4 g, 6.31 mmol) was dissolved in methanol/H₂O mixture (50 mL/25 mL). Pd/C (10% w/w, 300 mg) was added and the resulting suspension was stirred under an atmosphere of hydrogen (30 psi) at room temperature for 3 h. The catalyst Pd/C was removed by filtration and the reaction was concentrated in vacuo, giving a residue that was subjected to silica gel chromatograph to give 2.2 g (99%) of **12**. ¹H NMR (300 MHz, D₂O) 7.07 (d, *J* = 8.7 Hz, 2H), 6.88 (d, *J* = 8.7 Hz, 1H), 5.45 (d, *J* = 3.6 Hz, 1H), 4.27-4.25 (m, 2H), 4.10-4.06 (m, 1H), 3.92 (t, *J* = 9.6 Hz, 1H), 3.74 (dd, *J*₁ = 9.9 Hz, *J*₂ = 3.6 Hz, 1H), 3.59 (dd, *J*₁ = 9.9 Hz, *J*₂ = 9.0 Hz, 1H). ¹³C NMR (75 MHz, D₂O) 150.3, 140.5, 119.1, 118.1, 98.5, 72.9, 71.0, 70.5, 69.1, 66.8.

4-Acrylamino phenyl α-D-glucopyranoside-6-sulfate (13). Compound **12** (105.3 mg, 0.3 mmol) was dissolved in a THF/H₂O mixture (1 mL/2 mL) and cooled to 0 °C. Acryloyl chloride (54.3 mg, 0.6 mmol) and K₂CO₃ (165.6 mg, 1.2 mmol) were added, the resulting solution was warmed to room temperature and stirred overnight. The reaction was concentrated in vacuo, giving a residue that was subjected to silica gel chromatograph to

give 73 mg (60%) of **13**. ¹H NMR (300 MHz, D₂O) 7.48 (d, *J* = 9.0 Hz, 2H), 7.22 (d, *J* = 9.0 Hz, 2H), 6.45 (dd, *J*₁ = 17.1 Hz, *J*₂ = 9.9 Hz, 1H), 6.33 (dd, *J*₁ = 17.1 Hz, *J*₂ = 1.8 Hz, 1H), 5.88 (dd, *J*₁ = 9.9 Hz, *J*₂ = 1.8 Hz, 1H), 5.62 (d, *J* = 3.6 Hz, 1H), 4.25-4.24 (m, 2H), 4.05-4.00 (m, 1H), 3.92 (t, *J* = 9.6 Hz, 1H), 3.77 (dd, *J*₁ = 9.9 Hz, *J*₂ = 3.6 Hz, 1H), 3.59 (dd, *J*₁ = 9.9 Hz, *J*₂ = 9.2 Hz, 1H). ¹³C NMR (75 MHz, D₂O) 166.7, 153.5, 131.8, 130.2, 128.2, 123.4, 117.8, 97.5, 72.7, 70.8, 70.4, 68.9, 66.7. HRMS (ESI⁻) calcd for C₁₅H₁₈NO₁₀S [M]⁻ m/z 404.0651, found 404.0651.

4-(3-(Flurosulfonyl)benzoylamino)phenyl α-D-Glucopyranoside-6-sulfate (14).

Freshly prepared **14a**⁴ (66.6 mg, 0.3 mmol) in THF (366 μL) was added dropwise to the stirred solution of compound **12** (116 mg, 0.33 mmol) and trimethylamine (104 μL, 0.75 mmol) in anhydrous THF (8 mL) at 0 °C under argon atmosphere. The resulting solution was stirred at 40 °C for 12 h and concentrated in vacuo, giving a residue that was subjected to silica gel chromatograph to give 97 mg (60%) of **14**. ¹H NMR (300 MHz, CD₃OD) 8.62 (d, *J* = 1.5 Hz, 1H), 8.44 (d, *J* = 7.8 Hz, 1H), 8.27 (d, *J* = 7.8 Hz, 1H), 7.90 (t, *J* = 7.8 Hz, 1H), 7.66 (dd, *J*₁ = 6.9 Hz, *J*₂ = 2.1 Hz, 2H), 7.22 (dd, *J*₁ = 6.9 Hz, *J*₂ = 2.1 Hz, 2H), 5.46 (d, *J* = 3.6 Hz, 1H), 4.22-4.21 (m, 2H), 3.91-3.85 (m, 2H), 3.61 (dd, *J*₁ = 9.6 Hz, *J*₂ = 3.6 Hz, 1H), 3.52 (dd, *J*₁ = 9.9 Hz, *J*₂ = 9.0 Hz, 1H). ¹³C NMR (75 MHz, CD₃OD) 165.7, 155.8, 138.3, 135.9, 135.0, 134.1, 132.0, 131.6, 128.6, 123.8, 118.7, 99.8, 74.7, 73.2, 72.6, 71.3, 67.9. HRMS (ESI⁻) calcd for C₁₉H₁₉FNO₁₂S₂ [M]⁻ m/z 536.0333, found 536.0333.

tert-Butyl 3-((octyloxy)sulfonyl)benzoate.⁵ To a solution of 1-octanol (916 mg, 7.05 mmol) in anhydrous dichloromethane (2 mL), DIPEA (546 mg, 4.23 mmol) and DMAP (17.2 mg, 0.1 mmol) was added at 0 °C under argon atmosphere. *tert*-Butyl 3-

(chlorosulfonyl) benzoate⁵ (390 mg, 1.41 mmol) in anhydrous dichloromethane (1 mL) was added dropwise and stirred for 30 min at 0 °C. The reaction mixture was warmed to room temperature and stirred for 24 h and concentrated in vacuo, giving a residue that was subjected to silica gel chromatograph to give 370 mg of tert-butyl 3-((octyloxy)sulfonyl)benzoate (71 %). ¹H NMR (300 MHz, CDCl₃) 8.48 (s, 1H), 8.26 (d, *J* = 7.8 Hz, 1H), 8.05 (d, *J* = 7.8 Hz, 1H), 7.62 (t, *J* = 7.8 Hz, 1H), 4.08 (t, *J* = 6.6 Hz, 2H), 1.70-1.58 (m, 2H), 1.61 (s, 9H), 1.32-1.20 (m, 10 H), 0.86 (t, *J* = 6.8 Hz, 3H). ¹³C NMR (75 MHz, CDCl₃) 163.9, 137.0, 134.5, 133.6, 131.4, 129.4, 128.8, 82.6, 71.4, 31.8, 29.2, 29.0, 28.3, 25.5, 22.7, 14.2.

3-((Octyloxy)sulfonyl)benzoic acid.⁵ To a solution of tert-Butyl 3-((octyloxy)sulfonyl)benzoate (300 mg, 0.81 mmol) in anhydrous dichloromethane (11 mL), TFA (3.7 mL) was added. After stirring for 1 h at room temperature, the mixture was concentrated in vacuo to give 245 mg of 3-((octyloxy)sulfonyl)benzoic acid (98%). ¹H NMR (300 MHz, CDCl₃) 8.65 (s, 1H), 8.40 (d, *J* = 7.5 Hz, 1H), 8.16 (d, *J* = 7.5 Hz, 1H), 7.71 (t, *J* = 7.5 Hz, 1H), 4.11 (t, *J* = 6.8 Hz, 2H), 1.70-1.65 (m, 2H), 1.26-1.20 (m, 10 H), 0.86 (t, *J* = 6.8 Hz, 3H). ¹³C NMR (75 MHz, CDCl₃) 169.6, 136.8, 135.2, 132.4, 131.0, 129.8, 129.5, 71.8, 31.7, 29.0, 28.9, 25.3, 22.6, 14.0.

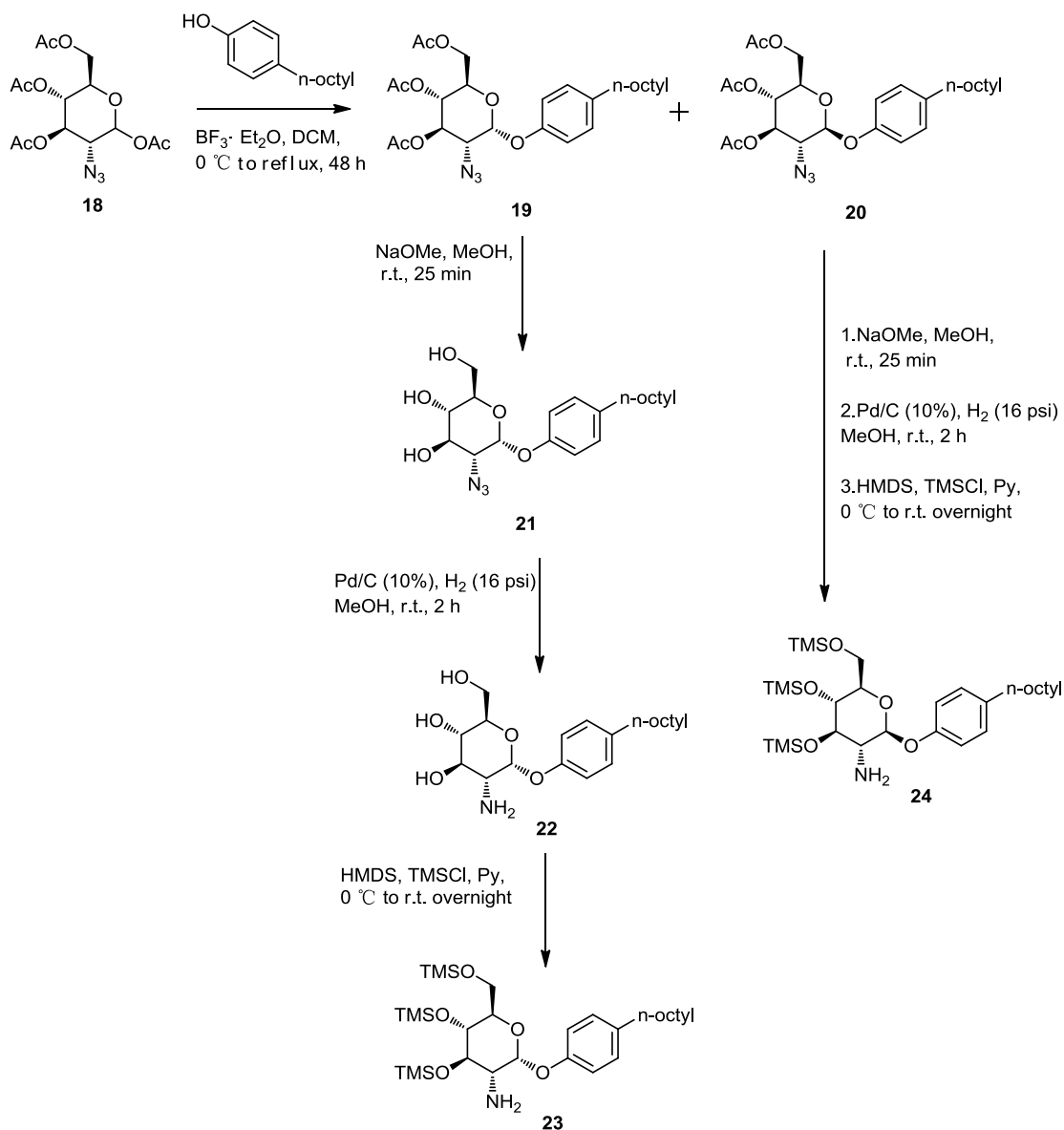
Octyl 3-(chlorocarbonyl)benzenesulfonate (15a). 3-((octyloxy)sulfonyl) benzoic acid (254 mg, 0.81 mmol) was dissolved in thionyl chloride (6 mL). The reaction mixture was heated under reflux for 4 h. The solvent was evaporated and then co-evaporated with anhydrous toluene to give unstable **15a**, which was dissolved in anhydrous THF (1 mL) to make 0.81 M solution.

4-(3-((octyloxy)sulfonyl)benzoylamino)phenyl α -D-Glucopyranoside-6-sulfate (15). Freshly prepared **15a** (370 μ L, 0.81M, 0.3 mmol) was added dropwise to the stirred solution of compound **12** (116 mg, 0.33 mmol) and trimethylamine (104 μ L, 0.75 mmol) in anhydrous THF (6 mL) at 0 °C under argon atmosphere. The resulting solution was stirred at 40 °C for 12 h and concentrated in vacuo, giving a residue that was subjected to silica gel chromatograph to give 86.5 mg (45%) of **15**. ^1H NMR (300 MHz, D_2O) 8.30 (s, 1H), 8.11 (d, $J=7.8$ Hz, 1H), 7.85 (d, $J=7.8$ Hz, 1H), 7.59 (t, $J=7.8$ Hz, 1H), 7.32 (d, $J=8.4$ Hz, 2H), 6.98 (d, $J=8.4$ Hz, 2H), 5.41 (d, $J=3.0$ Hz, 1H), 4.26-4.23 (m, 1H), 4.10-4.07 (m, 1H), 4.00 (t, $J=6.6$ Hz, 2H), 3.93-3.87 (m, 2H), 3.66-3.55 (m, 2H), 1.55-1.45 (m, 2H), 1.09-1.05 (m, 10 H), 0.72 (t, $J=6.6$ Hz, 3H). ^{13}C NMR (75 MHz, D_2O) 164.9, 153.8, 135.8, 135.3, 132.0, 130.3, 130.0, 126.8, 123.5, 117.6, 98.0, 72.8, 71.8, 71.2, 70.6, 68.8, 66.5, 31.7, 29.0, 28.9, 28.7, 25.2, 22.5, 13.8. HRMS (ESI $^-$) calcd for $\text{C}_{27}\text{H}_{36}\text{NO}_{13}\text{S}_2$ [M] $^-$ m/z 646.1628, found 646.1660.

4-(6-Bromohexanoylamino) phenyl α -D-Glucopyranoside-6-sulfate (16). A solution of compound **12** (105.3 mg, 0.3 mmol), 6-bromohexanoyl chloride (64.1 mg, 0.3 mmol), triethylamine (209 μ L, 1.5 mmol) in anhydrous THF (15 mL) was heated under reflux for 4 h under argon atmosphere. The reaction mixture was cooled to room temperature and concentrated in vacuo, giving a residue that was subjected to silica gel chromatograph to give 52 mg (33%) of **16**. ^1H NMR (300 MHz, D_2O) 7.39 (d, $J=9.0$ Hz, 2H), 7.18 (d, $J=9.0$ Hz, 2H), 5.57 (d, $J=3.6$ Hz, 1H), 4.27-4.19 (m, 2H), 4.03-3.90 (m, 2H), 3.75 (dd, $J_1=9.9$ Hz, $J_2=3.6$ Hz, 1H), 3.66-3.56 (m, 2H), 3.50 (t, $J=6.6$ Hz, 1H), 2.40 (t, $J=7.2$ Hz, 2H), 1.90-1.77 (m, 2H), 1.75-1.64 (m, 2 H), 1.55-1.44 (m, 2 H). ^{13}C

NMR (75 MHz, D₂O) 175.4, 153.4, 131.8, 123.7, 117.7, 97.5, 72.7, 70.8, 70.4, 68.8, 66.5, 45.3, 34.7, 31.5, 26.6, 24.3. HRMS (ESI⁻) calcd for C₁₈H₂₅BrNO₁₀S [M]⁻ m/z 526.0383, found 526.0378.

4-(2-Bromoacetylamino) phenyl α -D-Glucopyranoside-6-sulfate (17). To a solution of compound **12** (70.2 mg, 0.2 mmol) and triethylamine (27.8 μ L, 0.2 mmol) in anhydrous dichloromethane (2.5 mL), was added 2-bromoacetic anhydride (114.3 mg, 0.44 mmol) in one portion. The resulting solution was stirred at room temperature for 40 min and concentrated in vacuo, giving a residue that was subjected to silica gel chromatograph to give 62 mg (66%) of **17**. ¹H NMR (300 MHz, CD₃OD) 7.54 (d, *J* = 9.0 Hz, 2H), 7.18 (d, *J* = 9.0 Hz, 2H), 5.45 (d, *J* = 3.6 Hz, 1H), 4.24-4.23 (m, 2H), 4.01 (s, 2H), 3.92-3.86 (m, 2H), 3.62 (dd, *J*₁ = 9.6 Hz, *J*₂ = 3.6 Hz, 1H), 3.54 (dd, *J*₁ = 9.6 Hz, *J*₂ = 9.0 Hz, 1H). ¹³C NMR (75 MHz, CD₃OD) 167.4, 155.5, 134.1, 122.7, 118.7, 99.7, 74.6, 73.2, 72.5, 71.2, 67.8, 29.7. HRMS (ESI⁻) calcd for C₁₄H₁₈BrNO₁₀S [M]⁻ m/z 469.9757, found 469.9748.



4-n-Octylphenyl-3,4,6-tri-O-acetyl-2-azido-2-deoxy α -D-glucopyranoside (19)
and 4-n-Octylphenyl-3,4,6-tri-O-acetyl-2-azido-2-deoxy β -D-glucopyranoside (20). To
 a solution of 1,3,4,6-tetraacetate-2-azido-2-deoxy-D-glucopyranose **18**⁶ (3.56 g, 9.54

mmol) and 4-n-octylphenol (2.36 g, 11.45 mmol) in anhydrous dichloromethane (50 ml) under argon at 0 °C was added BF₃·Et₂O (4.8 mL, 38.16 mmol). The mixture was stirred at 50 °C for 48 h, diluted with water and stirred for 15 min. The mixture was diluted with dichloromethane, washed with water, brine, and concentrated in vacuo, giving a residue that was subjected to silica gel chromatography, giving compound **19** (2.07 g, 42%) and compound **20** (1.29 g, 26%).

19: ¹H NMR (300 MHz, CDCl₃) 7.11 (d, *J* = 8.7 Hz, 2H), 7.03 (d, *J* = 8.7 Hz, 2H), 5.69 (dd, *J*₁ = 10.5 Hz, *J*₂ = 9.3 Hz, 1H), 5.58 (d, *J* = 3.6 Hz, 1H), 5.13 (dd, *J*₁ = 10.2 Hz, *J*₂ = 9.3 Hz, 1H), 4.28 (dd, *J*₁ = 12.3 Hz, *J*₂ = 4.5 Hz, 1H), 4.20-4.14 (m, 1H), 4.05 (dd, *J*₁ = 12.3 Hz, *J*₂ = 2.1 Hz, 1H), 3.44 (dd, *J*₁ = 10.5 Hz, *J*₂ = 3.6 Hz, 1H), 2.55 (t, *J* = 7.7, 2H), 2.12 (s, 3H), 2.04 (s, 3H), 2.04 (s, 3H), 1.60-1.55 (m, 2H), 1.33-1.23 (m, 10H), 0.87 (t, *J* = 6.8, 3H). ¹³C NMR (75 MHz, CDCl₃) 170.5, 170.1, 169.8, 154.1, 138.1, 129.6, 116.6, 97.0, 70.4, 68.5, 68.3, 61.7, 60.9, 35.2, 32.0, 31.7, 29.5, 29.3, 22.7, 20.8, 20.7, 20.7, 14.2.

20: ¹H NMR (300 MHz, CDCl₃) 7.11 (d, *J* = 8.7 Hz, 2H), 6.97 (d, *J* = 8.7 Hz, 2H), 5.08-4.91 (m, 2H), 4.90 (d, *J* = 8.1 Hz, 1H), 4.30 (dd, *J*₁ = 12.3 Hz, *J*₂ = 5.4 Hz, 1H), 4.14 (dd, *J*₁ = 12.3 Hz, *J*₂ = 2.4 Hz, 1H), 3.83-3.75 (m, 2H), 2.56 (t, *J* = 10.8, 2H), 2.10 (s, 3H), 2.08 (s, 3H), 2.03 (s, 3H), 1.60-1.55 (m, 2H), 1.30-1.26 (m, 10H), 0.87 (t, *J* = 6.8, 3H). ¹³C NMR (75 MHz, CDCl₃) 170.6, 170.0, 169.7, 154.8, 138.4, 129.5, 117.1, 100.9, 72.5, 72.0, 68.5, 63.6, 62.1, 35.2, 32.0, 31.7, 29.5, 29.3, 22.7, 20.8, 20.7, 14.2.

4-n-Octylphenyl-2-azido-2-deoxy α-D-glucopyranoside (21). To a solution of compound **19** (2.0 g, 3.85 mmol) in anhydrous methanol (40 mL), was added freshly prepared 0.1 M NaOMe solution in methanol (1.5 mL) dropwise. The resulting solution

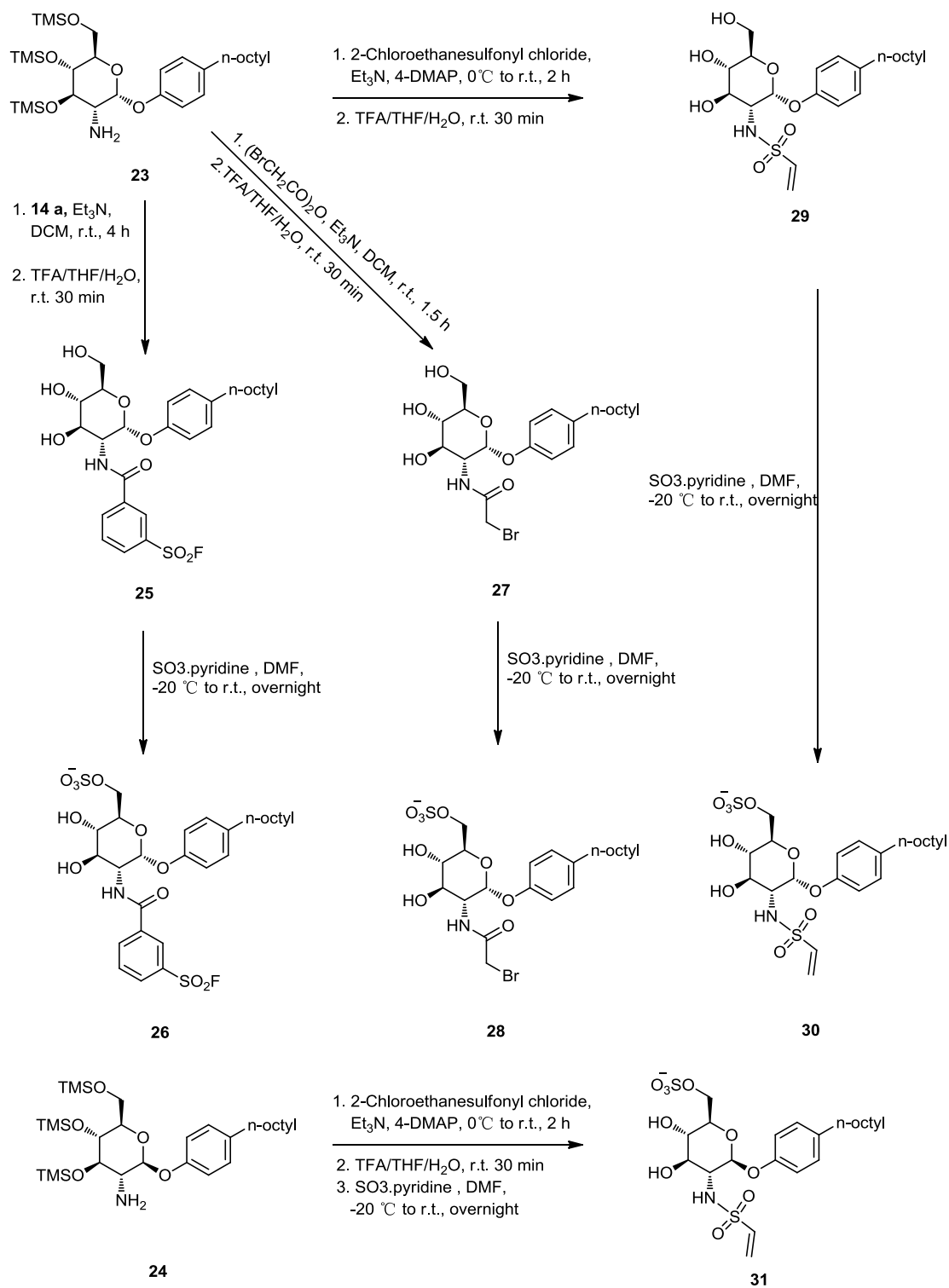
was stirred at room temperature for 25 min, then quenched with 8 drops of acetic acid and concentrated in vacuo, giving a residue that was subjected to silica gel chromatograph to give 1.36 g (90%) of **21**. ¹H NMR (300 MHz, CDCl₃) 7.07 (d, *J* = 8.7 Hz, 2H), 6.98 (d, *J* = 8.7 Hz, 2H), 5.50 (d, *J* = 3.3 Hz, 1H), 5.11 (br, 2H), 4.29-4.23 (m, 1H), 3.98-3.80 (m, 4H), 3.64 (br, 1H), 3.41 (dd, *J*₁ = 10.5 Hz, *J*₂ = 3.3 Hz, 1H), 2.53 (t, *J* = 7.8 Hz, 2H), 1.59-1.54 (m, 2H), 1.29-1.27 (m, 10H), 0.89 (t, *J* = 6.8 Hz, 3H). ¹³C NMR (75 MHz, CDCl₃) 154.5, 137.9, 129.6, 116.9, 97.7, 72.2, 71.6, 70.0, 62.7, 61.2, 35.3, 32.0, 31.8, 29.6, 29.5, 29.4, 22.8, 14.2.

4-n-Octylphenyl -2-amino-2-deoxy α-D-glucopyranoside (22). Compound **21** (912 mg, 2.32 mmol) was dissolved in methanol (66 mL). Pd/C (10% w/w, 347 mg) was added and the resulting suspension was stirred under an atmosphere of hydrogen (16 psi) at room temperature for 2 h. The catalyst Pd/C was removed by filtration and the reaction was concentrated in vacuo, giving a residue that was subjected to silica gel chromatograph to give 851 mg (99%) of **22**. ¹H NMR (300 MHz, CDCl₃) 7.11-7.09 (m, 4H), 5.46 (d, *J* = 3.6 Hz, 1H), 3.76-3.66 (m, 4H), 3.43 (t, *J* = 9.0 Hz, 1H), 2.78 (dd, *J*₁ = 9.9 Hz, *J*₂ = 3.6 Hz, 1H), 2.56 (t, *J* = 7.5 Hz, 2H), 1.61-1.57 (m, 2H), 1.33-1.30 (m, 10H), 0.91 (t, *J* = 6.8 Hz, 3H). ¹³C NMR (75 MHz, CDCl₃) 156.6, 138.2, 130.3, 118.1, 99.9, 76.0, 74.7, 71.7, 62.4, 57.2, 36.1, 33.0, 32.9, 30.6, 30.4, 30.3, 23.7, 14.4.

4-n-Octylphenyl-3,4,6-tri-O-trimethylsilyl-2-azido-2-deoxy α-D-glucopyranoside (23). To a solution of compound **22** (0.84 g, 2.29 mmol) in dry pyridine (8.4 mmol) at 0 °C, was added a mixture of hexamethyldisilazane (1.48 g, 9.16 mmol) and chlorotrimethylsilane (3.98 g, 36.64 mmol) dropwise. The resulting solution was warmed

to room temperature and stirred overnight. The reaction was concentrated in vacuo, giving a residue that was subjected to silica gel chromatograph to give 1.18 g (88%) of **23**. ¹H NMR (300 MHz, CD₃OD) 7.07 (d, *J* = 8.7 Hz, 2H), 6.99 (d, *J* = 8.7 Hz, 2H), 5.39 (d, *J* = 3.3 Hz, 1H), 3.76-3.66 (m, 4H), 3.58 (t, *J* = 8.7 Hz, 1H), 2.75 (dd, *J*₁ = 9.6 Hz, *J*₂ = 3.6 Hz, 1H), 2.54 (t, *J* = 7.8 Hz, 2H), 1.60-1.55 (m, 2H), 1.30 (br, 2H) 1.30-1.27 (m, 10H), 0.88 (t, *J* = 6.8 Hz, 3H), 0.24 (s, 9H), 0.18 (s, 9H), 0.08 (s, 9H). ¹³C NMR (75 MHz, CD₃OD) 155.2, 137.0, 129.3, 117.2, 99.6, 78.0, 73.7, 72.0, 62.0, 57.1, 35.3, 32.1, 31.8, 29.6, 29.4, 22.8, 14.3, 1.6, 1.0, -0.1.

4-n-Octylphenyl-3,4,6-tri-O-trimethylsilyl-2-azido-2-deoxy β -D-glucopyranoside (24). The target **24** was prepared starting with compound **20** using the same procedure as that for **23**. Yield 83% over three steps. ¹H NMR (300 MHz, CDCl₃) 7.06 (d, *J* = 8.7 Hz, 2H), 6.97 (d, *J* = 8.7 Hz, 2H), 4.69 (d, *J* = 7.8 Hz, 1H), 3.82 (dd, *J*₁ = 11.4 Hz, *J*₂ = 2.1 Hz, 1H), 3.73 (dd, *J*₁ = 11.4 Hz, *J*₂ = 4.8 Hz, 1H), 3.61 (t, *J* = 9.0 Hz, 1H), 3.45 (t, *J* = 9.0 Hz, 1H), 3.32-3.27 (m, 1H), 2.93 (dd, *J*₁ = 9.3 Hz, *J*₂ = 8.1 Hz, 1H), 2.54 (t, *J* = 7.7 Hz, 2H), 1.61-1.51 (m, 4H), 1.32-1.24 (m, 10H), 0.88 (t, *J* = 6.8 Hz, 3H), 0.23 (s, 9H), 0.18 (s, 9H), 0.08 (s, 9H). ¹³C NMR (75 MHz, CDCl₃) 156.0, 137.3, 129.3, 117.4, 103.0, 79.2, 77.4, 71.7, 62.2, 58.0, 35.3, 32.1, 31.8, 29.7, 29.5, 29.4, 22.8, 14.3, 1.4, 1.0, -0.1.



4-n-Octylphenyl-2-(3-(fluorosulfonyl)benzoylamino)-2-deoxy α -D-Glucopyranoside (25). To a solution of compound **23** (150 mg, 0.257 mmol), triethylamine (71.2 μ L, 0.514 mmol) in anhydrous dichloromethane (15 mL), was added a solution of **14a** (97 mg, 0.437 mmol) in anhydrous dichloromethane (2 mL) dropwise at room temperature. The resulting mixture was stirred for 4 h and concentrated in vacuo, giving a residue that was dissolved in a mixture of TFA/THF/H₂O (0.4 mL/2.85 mL/0.15 mL) and stirred for 25 min at room temperature. The reaction mixture was concentrated in vacuo, giving a residue that was subjected to silica gel chromatograph to give 103 mg (74%) of **25**. ¹H NMR (300 MHz, CD₃OD/CDCl₃ (1/1, v/v)) 9.3 (d, *J* = 7.8 Hz, 1H), 8.6 (s, 1H), 8.33 (d, *J* = 7.8 Hz, 1H), 8.22 (d, *J* = 7.8 Hz, 1H), 7.83 (t, *J* = 7.8 Hz, 1H), 7.10-7.03 (m, 4H), 5.60 (d, *J* = 3.6 Hz, 1H), 4.33-4.26 (m, 1H), 4.11 (dd, *J*₁ = 10.8 Hz, *J*₂ = 8.7 Hz, 1H), 3.85-3.74 (m, 3H), 3.59 (t, *J* = 9.2 Hz, 1H), 2.53 (t, *J* = 7.5 Hz, 2H), 1.60-1.54 (m, 2H), 1.29-1.27 (m, 10H), 0.89 (t, *J* = 6.6 Hz, 3H). ¹³C NMR (75 MHz, CD₃OD/CDCl₃ (1/1, v/v)) 168.3, 156.8, 138.4, 137.8, 135.9, 134.6 (d, *J*_{C,F} = 25.2 Hz), 132.0, 131.5, 130.4, 128.7, 118.1, 98.3, 74.6, 72.2, 72.2, 62.4, 56.6, 36.1, 33.0, 32.8, 30.5, 30.3, 30.2, 23.7, 14.4.

4-n-Octylphenyl-2-(3-(fluorosulfonyl)benzoylamino)-2-deoxy α -D-Glucopyranoside-6-sulfate (26) This substance was prepared starting with compound **25** using the same procedure employed for the preparation of **11**. Yield 63%. ¹H NMR (300 MHz, CD₃OD) 9.05 (d, *J* = 8.1 Hz, 1H), 8.57 (s, 1H), 8.34 (d, *J* = 7.8 Hz, 1H), 8.23 (d, *J* = 7.8 Hz, 1H), 7.85 (t, *J* = 7.8 Hz, 1H), 7.11-7.03 (m, 4H), 5.57 (d, *J* = 3.6 Hz, 1H), 4.33-4.27 (m, 3H), 4.10 (dd, *J*₁ = 10.8 Hz, *J*₂ = 8.7 Hz, 1H), 4.03-3.97 (m, 1H), 3.66 (t, *J* = 9.5 Hz, 1H), 2.54 (t, *J* = 7.5 Hz, 2H), 1.60-1.57 (m, 2H), 1.30-1.28 (m, 10H), 0.90 (t, *J* = 6.8 Hz,

3H). ^{13}C NMR (75 MHz, DMSO- d_6) 166.0, 155.8, 137.5, 136.4, 136.1, 132.5 (d, $J_{C,F}$ = 23.2 Hz), 131.7, 131.6, 130.1, 127.8, 118.0, 97.6, 72.2, 70.9, 70.5, 66.4, 55.7, 34.9, 31.8, 31.6, 29.4, 29.2, 29.1, 22.7, 14.6. HRMS (ESI) calcd for $\text{C}_{27}\text{H}_{35}\text{FNO}_{11}\text{S}_2$ $[\text{M}]^-$ m/z 632.1636, found 632.1631.

4-n-Octylphenyl-2-(2-bromoacetyl-amino)-2-deoxy α -D-Glucopyranoside (27).

To a solution of compound **23** (160 mg, 0.27 mmol), trimethylamine (65.1 μL , 0.47 mmol) in anhydrous dichloromethane (20 mL), was added a solution of 2-bromoacetic anhydride (121.2 mg, 0.47 mmol) in anhydrous dichloromethane (2 mL) dropwise at room temperature. The resulting mixture was stirred for 1.5 h and concentrated in vacuo, giving a residue that was dissolved in a mixture of TFA/THF/ H_2O (0.4 mL/4.85 mL/0.15 mL) and stirred for 30 min at room temperature. The reaction mixture was concentrated in vacuo, giving a residue that was subjected to silica gel chromatograph to give 130 mg (98%) of **27**. ^1H NMR (300 MHz, CD_3OD) 8.57 (d, J = 8.1 Hz, 1H), 7.12-7.04 (m, 4H), 5.45 (d, J = 3.3 Hz, 1H), 4.08-4.03 (m, 1H), 3.98-3.87 (m, 3H), 3.82-3.72 (m, 3H), 3.55-3.47 (m, 1H), 2.56 (t, J = 7.5 Hz, 2H), 1.59-1.56 (m, 2H), 1.32-1.30 (m, 10H), 0.93 (t, J = 6.8 Hz, 3H). ^{13}C NMR (75 MHz, $\text{CD}_3\text{OD}/\text{CDCl}_3$ (2/1, v/v)) 167.4, 154.6, 137.6, 129.3, 116.9, 96.8, 72.5, 71.7, 70.3, 61.2, 54.2, 35.0, 31.8, 31.6, 29.4, 29.2, 28.4, 22.6, 13.9.

4-n-Octylphenyl-2-(2-bromoacetyl-amino)-2-deoxy α -D-Glucopyranoside-6-sulfate (28). This substance was prepared starting with compound **27** using the same procedure employed for the preparation of **11**. Yield 65%. ^1H NMR (300 MHz, CD_3OD) 7.13-7.04 (m, 4H), 5.42 (d, J = 3.6 Hz, 1H), 4.25-4.23 (m, 2H), 4.06 (dd, J_1 = 10.8 Hz, J_2 = 3.3 Hz, 1H) 3.98-3.86 (m, 4H), 3.58 (dd, J_1 = 9.9 Hz, J_2 = 9.0 Hz, 1H), 2.57 (t, J = 7.7

Hz, 2H), 1.62-1.57 (m, 2H), 1.33-1.30 (m, 10H), 0.91 (t, $J = 6.8$ Hz, 3H). ^{13}C NMR (75 MHz, $\text{CD}_3\text{OD}/\text{D}_2\text{O}$ (5/1, v/v)) 170.2, 156.4, 138.6, 130.4, 118.5, 98.4, 72.4, 72.1, 71.3, 67.7, 55.7, 35.9, 32.8, 32.6, 30.3, 30.2, 30.0, 28.7, 23.5, 14.4. HRMS (ESI) calcd for $\text{C}_{22}\text{H}_{33}\text{BrNO}_9\text{S} [\text{M}]^-$ m/z 566.1059, found 566.1069.

4-n-Octylphenyl-2-(vinylsulfonylamino)-2-deoxy α -D-Glucopyranoside (29). To a solution of compound **23** (130 mg, 0.22 mmol), triethylamine (92 μL , 0.66 mmol), 4-DMAP (2.7 mg, 0.022 mmol) in anhydrous dichloromethane (1.5 mL), was added 2-chloroethanesulfonyl chloride (51 mg, 0.31 mmol) dropwise over 30 min at 0 $^\circ\text{C}$. The resulting mixture was warmed to room temperature and stirred for 2 h. The reaction was diluted dichloromethane, washed with water and dried over Na_2SO_4 and concentrated in vacuo, giving a residue that was dissolved in a mixture of TFA/THF/ H_2O (0.4 mL/2.85 mL/0.15 mL) and stirred for 30 min at room temperature. The reaction mixture was concentrated in vacuo, giving a residue that was subjected to silica gel chromatograph to give 92 mg (92%) of **29**. ^1H NMR (300 MHz, CD_3OD) 7.12-7.05 (m, 4H), 6.77 (dd, $J_1 = 16.5$ Hz, $J_2 = 10.2$ Hz, 1H), 6.17 (d, $J = 16.5$ Hz, 1H), 5.82 (d, $J = 10.2$ Hz, 1H), 5.45 (d, $J = 3.6$ Hz, 1H), 3.85-3.70 (m, 4H), 3.47 (t, $J = 8.3$ Hz, 1H), 3.38-3.33 (m, 1H), 2.55 (t, $J = 7.5$ Hz, 2H), 1.61-1.56 (m, 2H), 1.32-1.29 (m, 10H), 0.90 (t, $J = 6.8$ Hz, 3H). ^{13}C NMR (75 MHz, CD_3OD) 156.5, 139.0, 138.3, 130.3, 125.2, 118.3, 99.7, 74.3, 72.7, 72.0, 62.3, 59.3, 36.1, 33.0, 32.9, 30.5, 30.4, 30.3, 23.7, 14.2.

4-n-Octylphenyl-2-(vinylsulfonylamino)-2-deoxy α -D-Glucopyranoside-6-sulfate (30). This substance was prepared starting with compound **28** using the same procedure employed for the preparation of **11**. Yield 79%. ^1H NMR (300 MHz, CD_3OD)

7.16-7.08 (m, 4H), 6.80 (dd, $J_1 = 16.5$ Hz, $J_2 = 10.2$ Hz, 1H), 6.21 (d, $J = 16.5$ Hz, 1H), 5.87 (d, $J = 10.2$ Hz, 1H), 5.44 (d, $J = 3.3$ Hz, 1H), 4.26-4.24(m, 2H), 3.95-3.90 (m, 1H), 3.86 (dd, $J_1 = 10.5$ Hz, $J_2 = 9.0$ Hz, 1H), 3.57 (dd, $J_1 = 9.9$ Hz, $J_2 = 9.0$ Hz, 1H), 3.39 (dd, $J_1 = 10.5$ Hz, $J_2 = 3.6$ Hz, 1H), 2.59 (t, $J = 7.7$ Hz, 2H), 1.64-1.60 (m, 2H), 1.36-1.33 (m, 10H), 0.93 (t, $J = 6.8$ Hz, 3H). ^{13}C NMR (75 MHz, CD_3OD) 156.6, 138.9, 138.4, 130.3, 125.3, 118.4, 99.8, 72.4, 71.7, 67.8, 59.2, 36.1, 33.0, 32.8, 30.5, 30.4, 30.3, 23.7, 14.4. HRMS (ESI $^-$) calcd for $\text{C}_{22}\text{H}_{34}\text{NO}_{10}\text{S}_2$ [M] $^-$ m/z 536.1624, found 536.1638.

4-n-Octylphenyl-2-(vinylsulfonylamino)-2-deoxy β -D-Glucopyranoside-6-sulfate (31). This substance was prepared starting with compound **24** using the same procedure employed for the preparation of **30**. Yield 66% over 3 steps. ^1H NMR (300 MHz, CD_3OD) 7.14 (d, $J = 8.4$ Hz, 2H), 7.04 (d, $J = 8.4$ Hz, 2H), 6.88 (dd, $J_1 = 16.5$ Hz, $J_2 = 10.2$ Hz, 1H), 6.19 (d, $J = 16.5$ Hz, 1H), 5.87 (d, $J = 10.2$ Hz, 1H), 4.96 (d, $J = 8.1$ Hz, 1H), 4.42 (dd, $J_1 = 10.8$ Hz, $J_2 = 1.5$ Hz, 1H), 4.21 (dd, $J_1 = 10.8$ Hz, $J_2 = 5.7$ Hz, 1H), 3.72-3.67 (m, 1H), 3.52-3.42 (m, 2H), 3.40-3.36 (m, 1H), 2.60 (t, $J = 7.5$ Hz, 2H), 1.64-1.61 (m, 2H), 1.36-1.27 (m, 10H), 0.94 (t, $J = 6.6$ Hz, 3H). ^{13}C NMR (75 MHz, CD_3OD) 156.8, 140.0, 138.1, 130.3, 124.2, 117.7, 101.0, 76.2, 75.8, 71.7, 68.1, 61.1, 36.1, 33.0, 32.8, 30.5, 30.4, 30.3, 23.7, 14.4. HRMS (ESI $^-$) calcd for $\text{C}_{22}\text{H}_{34}\text{NO}_{10}\text{S}_2$ [M] $^-$ m/z 536.1624, found 536.1634.

5.5.2 Reference for synthesis

1. Sarpe, V. A.; Kulkarni, S. S. Synthesis of Maradolipid. *J. Org. Chem.* **2011**, *76*, 6866–6870.

2. Berndt, F.; Sajadi, M.; Ernsting, N. P.; Mahrwald, R. Covalent linkage of N-methyl-6-oxyquinolinium betaine to trehalose. *Carbohydr Res.* **2011**, *346*, 2960–2964.
3. Barry, C. S.; Backus, K. M.; Barry, III, C. E.; Davis, B. G. ESI-MS Assay of M. tuberculosis Cell Wall Antigen 85 Enzymes Permits Substrate Profiling and Design of a Mechanism-Based Inhibitor. *J. Am. Chem. Soc.*, **2011**, *133* (34), 13232–13235.
4. Grimster, N. P.; Connelly, S.; Baranczak, A.; Dong, J.; Krasnova, L. B.; Sharpless, K. B.; Powers, E. T.; Wilson, I. A.; Kelly, J. W. Aromatic Sulfonyl Fluorides Covalently Kinetically Stabilize Transthyretin to Prevent Amyloidogenesis while Affording a Fluorescent Conjugate. *J. Am. Chem. Soc.*, **2013**, *135* (15), 5656–5668.
5. Masuya, T.; Murai, M.; Ifuku, K.; Morisaka, H.; Miyoshi, H. Site-Specific Chemical Labeling of Mitochondrial Respiratory Complex I through Ligand-Directed Tosylate Chemistry. *Biochemistry*, **2014**, *53* (14), 2307–2317.
6. Yan, R.-B.; Yang, F.; Wu, Y.; Zhang, L.-H. and Ye, X.-S. An efficient and improved procedure for preparation of triflyl azide and application in catalytic diazotransfer reaction. *Tetrahedron Letters*, **2005**, *46*, 8993–8995.

5.5.3 Expression and Purification of T6PPs.

All T6PPs mentioned were expressed in E.coli and purified as described in **chapter 2**.

5.5.4 Kinetic Characterization of T6PPs Inactivation by 26.

Time and Concentration Dependence of T6PP Inactivation by 26. T6PP inactivation by 26 was studied at 25 °C and in the buffer containing: 50 mM Tris pH 7.5,

50 mM NaCl, 5 mM MgCl₂, 1 mM DTT. Incubating enzyme with various concentrations of inactivator **26** in the buffer mentioned above and periodically measuring the activity of the enzyme by removing an aliquot (5μL) of the inactivation stock solution and adding it to EnzChek phosphate assay reaction mixture, which contains 1 mM MgCl₂, 0.1 mM sodium azide 1.0 unit/mL purine nucleoside phosphorylase, and 0.2 mM MESG in 50 mM Tris-HCl (pH 7.5). The enzyme activity was measured by using EnzChek phosphate assay kit which was described in chapter 4 in detail. The *pseudo*-first-order rate constant for inactivation (k_{obs}) (Appendix A5.10) was derived from the slope of the plot of $\ln(v_t/v_0)$ vs t , where v_t is the velocity of the trehalose-6-phosphate hydrolysis reaction catalyzed by T6PP incubated with **26** for time (t) and v_0 is the velocity of the trehalose-6-phosphate hydrolysis reaction catalyzed by T6PP in buffer. The resulting k_{obs} values were plotted against **26** concentration. The data were fitted by using Graphpad Prism 6 to the equation $k_{\text{obs}} = (k_{\text{inact}}[I]/(K_I + [I]))$ to obtain K_I and k_{inact} values.

Trehalose-6-Sulfate (T6S) Partially Protect T6PP from Inhibitor 26 Mediated Inactivation. The effect of T6S, a reversible and competitive T6PP inhibitor, on inhibitor **26**-mediated T6PP inactivation was studied at 25 °C in a pH 7.0 buffer containing: 50 mM Tris pH 7.5, 50 mM NaCl, 5 mM MgCl₂, 1 mM DTT. T6PP was incubated with **26** in the presence or absence of T6S respectively. At appropriate time intervals, aliquots 5μL were removed from the reaction and added into EnzChek phosphate assay reaction mixture containing: 1 mM MgCl₂, 0.1 mM sodium azide 1.0 unit/mL purine nucleoside phosphorylase, and 0.2 mM MESG in 50 mM Tris-HCl (pH 7.5) for phosphatase activity measurements.

5.5.5 ES-MS Analysis of T6PP Modification by Inhibitor 26.

T6PPs were treated with or without **26** (10-20 eq) in a buffer containing 50 mM Tris pH 7.5, 50 mM NaCl, 5 mM MgCl₂, 1 mM DTT at room temperature for 30 minutes. Then the reaction mixture were transferred to amicon ultra centrifugal filters and exchanged with buffer 50 mM Tris 7.5 four times and concentrated for Mass spectrometry.

5.6 References

1. Thevelein, J.M. Regulation of trehalose mobilization in fungi. *Microbiol Rev*, **1984**, *48*, 42–59.
2. Crowe, J.H., Hoekstra, F.A., and Crowe, L.M. Anhydrobiosis. *Annu Rev Physiol*, **1992**, *54*, 579–599.
3. Singer, M.A., and Lindquist, S. Thermotolerance in *Saccharomyces cerevisiae*: the Yin and Yang of trehalose. *Trends Biotechnol*, **1998**, *16*, 460–468.
4. Ishihara, R., Taketani, S., Sasai-Takedatsu, M., Adachi, Y., Kino, M., Furuya, A., et al. ELISA for urinary trehalase with monoclonal antibodies: a technique for assessment of renal tubular damage. *Clin Chem*, **2000**, *46*, 636–643.
5. Murray, I.A., Coupland, K., Smith, J.A., Ansell, I.D., and Long, R.G. Intestinal trehalase activity in a UK population: establishing a normal range and the effect of disease. *Br J Nutr*, **2000**, *83*, 241–245.
6. Gancedo, C., and Flores, C.L. The importance of a functional trehalose biosynthetic pathway for the life of yeasts and fungi. *FEMS*, **2004**, *Yeast Res4*, 351–359.
7. Avonce, N.; Mendoza-Vargas, A.; Morett, E. and Iturriaga, G. Insights on the

- evolution of trehalose biosynthesis. *BMC Evolutionary Biology*, **2006**, *6*, 109.
8. Murphy, H.N., Stewart, G.R., Mischenko, V.V., Apt, A.S., Harris, R. and McAlister, M.S., et al. The OtsAB pathway is essential for trehalose biosynthesis in *Mycobacterium tuberculosis*. *J Biol Chem*, **2005**, *280*, 14524–14529.
 9. Song, X.S., Li, H.P., Zhang, J.B., Song, B., Huang, T., Du, X.M., Gong, A.D., Liu, Y.K., Feng, Y.N., Agboola, R.S., Liao, Y.C. Trehalose 6-phosphate phosphatase is required for development, virulence and mycotoxin biosynthesis apart from trehalose biosynthesis in *Fusarium graminearum*. *Fungal Genet Biol.*, **2014**, *63*, 24-41.
 10. Puttikamonku, S., Willger, S.D., Grah, N., Perfect, J. R., Movahed, N., Bothner, B., Park, S., Paderu, P., Perlin, D. S. and Cramer Jr, R. A. Trehalose 6-phosphate phosphatase is required for cell wall integrity and fungal virulence but not trehalose biosynthesis in the human fungal pathogen *Aspergillus fumigatus*. *Molecular Microbiology*, **2010**, *77*(4), 891–911.
 11. Dijk, V.P., Rop, D.L., Szlufcik, K., Ael, V.E., Thevelein, J.M. Disruption of the *Candida albicans* TPS2 gene encoding trehalose-6-phosphate phosphatase decreases infectivity without affecting hypha formation. *Infect Immun.*, **2002**, *70*(4), 177–282.
 12. Kormish, J.D., McGhee, J.D. The *C. elegans* lethal gut-obstructed gob-1 gene is trehalose- 6-phosphate phosphatase. *Dev. Biol.*, **2005**, *287*, 35–47.
 13. Kushwaha, S., Singh P.K., Shahab, M., Pathak, M., Bhattacharya, S.M. In vitro silencing of *Brugia malayi* trehalose-6-phosphate phosphatase impairs

- embryogenesis and in vivo development of infective larvae in jirds. *PLoS Negl Trop Dis*, **2012**, 6(8):e1770. doi:10.1371/journal.pntd.0001770.
14. Pellerone F., Archer S., Behm C., Grant W., Lacey M., et al. Trehalose metabolism genes in *Caenorhabditis elegans* and filarial nematodes. *Int J Parasitol*, **2003**, 33, 1195–1206.
 15. Sears, P.; Wong, C.-H. Carbohydrate Mimetics: A New Strategy for Tackling the Problem of Carbohydrate-Mediated Biological Recognition. *Angew. Chem. Int. Ed.* **1999**, 38, 2300–2324.
 16. Wu, C.-Y., Wong, C.-H. Chemistry and glycobiology. *Chem. Commun.* **2011**, 47, 6201–6207.
 17. N'Go, I., Golten, S., Ardá, A., Cañada, J., Jiménez-Barbero, J., Linciau, B., and P. Vincent, S. Tetrafluorination of Sugars as Strategy for Enhancing Protein–Carbohydrate Affinity: Application to UDP-Galp Mutase Inhibition. *Chem. Eur. J.* **2014**, 20, 106–112.
 18. Farelli, J. D.; Galvin, B. D.; Li, Z.; Liu, C.; Aono, M.; Garland, M.; Hallett, O. E.; Causey, T. B.; Ali-Reynolds, A.; Saltzberg, D. J.; Carlow, C. K.; Dunaway-Mariano, D.; Allen, K.N. *PLoS Pathog.*, **2014**, 10(7), e1004245.
 19. Roberts, A., Lee, S.Y., McCullagh, E., Silversmith, R.E., Wemmer, D.E. YbiV from *Escherichia coli* K12 is a HAD phosphatase. *Proteins*, **2005**, 58(4), 790–801.
 20. Lu, Z., Wang, L., Dunaway-Mariano, D., Allen, K.N. Structure-function analysis of 2-keto-3-deoxy-D-glycero-D-galactononate-9-phosphate phosphatase

defines specificity elements in type C0 haloalkanoate dehalogenase family members. *J Biol Chem.* **2009**, 284(2), 1224–33.

21. The Enzyme Function Initiative (EFI)

http://kiemlicz.med.virginia.edu/efi/space_tree/view/501036.

APPENDIX

A.1 Published Collaborative Work

A.1.1 Covalent docking predicts substrates for haloalkanoate dehalogenase superfamily phosphatases.

London N, Farelli JD, Brown SD, Liu C, Huang H, Korczynska M, Al-Obaidi NF, Babbitt PC, Almo SC, Allen KN, Shoichet BK.

Abstract

Enzyme function prediction remains an important open problem. Though structure-based modeling, such as metabolite docking, can identify substrates of some enzymes, it is ill-suited to reactions that progress through a covalent intermediate. Here we investigated the ability of covalent docking to identify substrates that pass through such a covalent intermediate, focusing particularly on the haloalkanoate dehalogenase superfamily. In retrospective assessments, covalent docking recapitulated substrate binding modes of known cocrystal structures and identified experimental substrates from a set of putative phosphorylated metabolites. In comparison, noncovalent docking of high-energy intermediates yielded nonproductive poses. In prospective predictions against seven enzymes, a substrate was identified for five. For one of those cases, a covalent docking prediction, confirmed by empirical screening, and combined with genomic context analysis, suggested the identity of the enzyme that catalyzes the orphan phosphatase reaction in the riboflavin biosynthetic pathway of *Bacteroides*.

A.1.2 Structure of the trehalose-6-phosphate phosphatase from *Brugia malayi* reveals key design principles for anthelmintic drugs.

Farelli JD, Galvin BD, Li Z, Liu C, Aono M, Garland M, Hallett OE, Causey TB, Ali-Reynolds A, Saltzberg DJ, Carlow CK, Dunaway-Mariano D, Allen KN.

Abstract

Parasitic nematodes are responsible for devastating illnesses that plague many of the world's poorest populations indigenous to the tropical areas of developing nations. Among these diseases is lymphatic filariasis, a major cause of permanent and long-term disability. Proteins essential to nematodes that do not have mammalian counterparts represent targets for therapeutic inhibitor discovery. One promising target is trehalose-6-phosphate phosphatase (T6PP) from *Brugia malayi*. In the model nematode *Caenorhabditis elegans*, T6PP is essential for survival due to the toxic effect(s) of the accumulation of trehalose 6-phosphate. T6PP has also been shown to be essential in *Mycobacterium tuberculosis*. We determined the X-ray crystal structure of T6PP from *B. malayi*. The protein structure revealed a stabilizing N-terminal MIT-like domain and a catalytic C-terminal C2B-type HAD phosphatase fold. Structure-guided mutagenesis, combined with kinetic analyses using a designed competitive inhibitor, trehalose 6-sulfate, identified five residues important for binding and catalysis. This structure-function analysis along with computational mapping provided the basis for the proposed model of the T6PP-trehalose 6-phosphate complex. The model indicates a substrate-binding mode wherein shape

complementarity and van der Waals interactions drive recognition. The mode of binding is in sharp contrast to the homolog sucrose-6-phosphate phosphatase where extensive hydrogen-bond interactions are made to the substrate. Together these results suggest that high-affinity inhibitors will be bi-dentate, taking advantage of substrate-like binding to the phosphoryl-binding pocket while simultaneously utilizing non-native binding to the trehalose pocket. The conservation of the key residues that enforce the shape of the substrate pocket in T6PP enzymes suggest that development of broad-range anthelmintic and antibacterial therapeutics employing this platform may be possible.

A.1.3 An improved method for the large scale preparation of α, α' -trehalose-6-phosphate.

Liu C, Mariano PS.

Abstract

An improved method was developed for the efficient, large-scale synthesis of α, α' -trehalose-6-phosphate starting with α, α' -trehalose. In the sequence, octa-trimethylsilylation of α, α' -trehalose is followed by selective removal of the 6-*O*-trimethylsilyl protecting group. Reaction of the mono-alcohol with $(\text{PhO})_2\text{POCl}$ is then followed by simultaneous hydrogenolysis and per-desilylation to generate α, α' -trehalose-6-phosphate, free of contamination by inorganic phosphate.

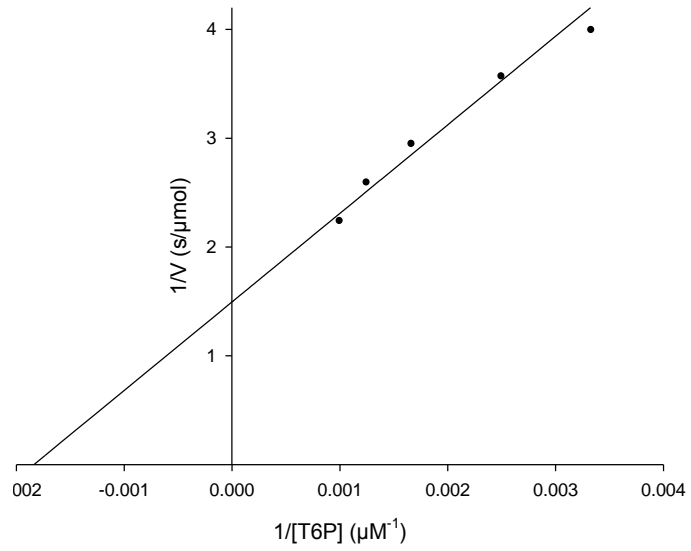
A.1.4 Panoramic view of a superfamily of phosphatases through substrate profiling.

Huang H, Pandya C, Liu C, Al-Obaidid N, Wang M, Zheng L, Keating ST, Aono M, Loved JD, Evans B, Seidel R, Hillerich BS, Garforth S, Almo SC, Mariano PS, Dunaway-Mariano D, Allen KN, and Farelli JD.

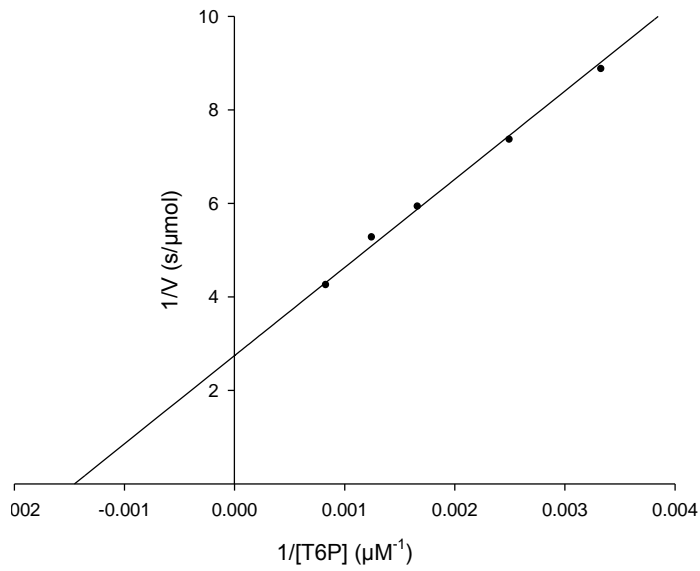
Abstract

Large-scale activity profiling of enzyme superfamilies provides information about cellular functions as well as the intrinsic binding capabilities of conserved folds. Herein, the functional space of the ubiquitous haloalkanoate dehalogenase superfamily (HADSF) was revealed by screening a customized substrate library against >200 enzymes from representative prokaryotic species, enabling inferred annotation of ~35% of the HADSF. An extremely high level of substrate ambiguity was revealed, with the majority of HADSF enzymes utilizing >5 substrates. Substrate profiling allowed assignment of function to previously unannotated enzymes with known structure, uncovered potential new pathways, and identified iso-functional orthologs from evolutionarily distant taxonomic groups. Intriguingly, the HADSF subfamily having the least structural elaboration of the Rossmann fold catalytic domain was the most specific, consistent with the concept that domain insertions drive the evolution of new functions and that the broad specificity observed in HADSF may be a relic of this process.

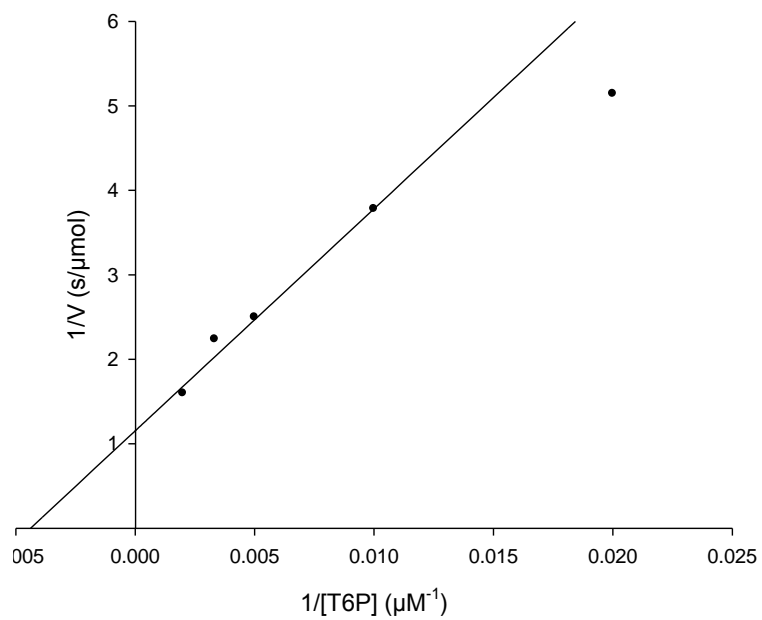
A.2 Plots in Chapter Two



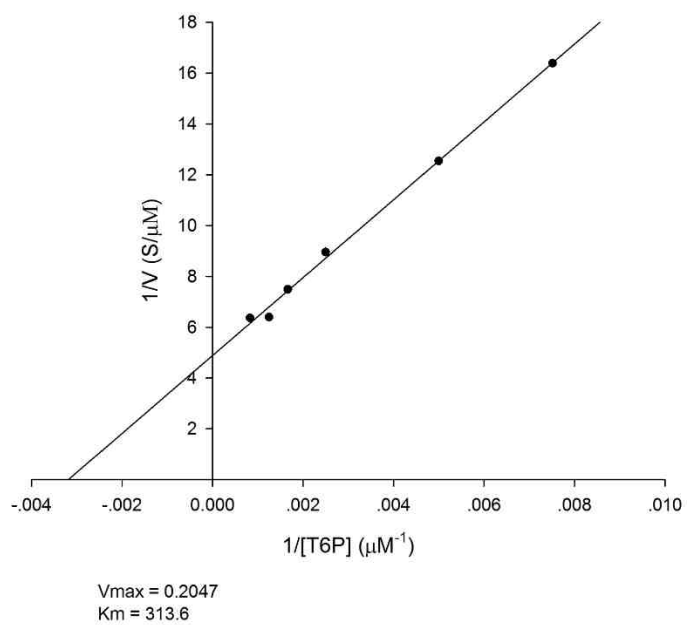
$[Mt\text{-T6PP}] = 66 \text{ nM}$; $V_{\text{max}} = 0.6687 \mu\text{M/s}$; $K_m = 544 \pm 106 \mu\text{M}$



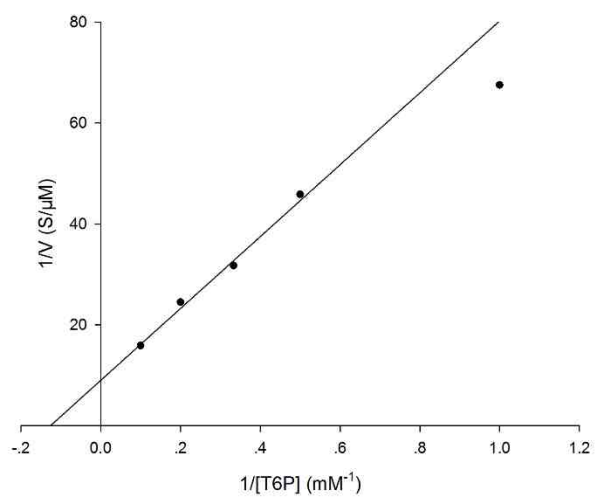
$[Sb\text{-T6PP}] = 22.8 \text{ nM}$; $V_{\text{max}} = 0.3644 \mu\text{M/s}$; $K_m = 687 \pm 73 \mu\text{M}$



[*As*-T6PP]= 240 nM; V_{\max} = 0.8667 μM/s; K_m = 228 ±72 μM



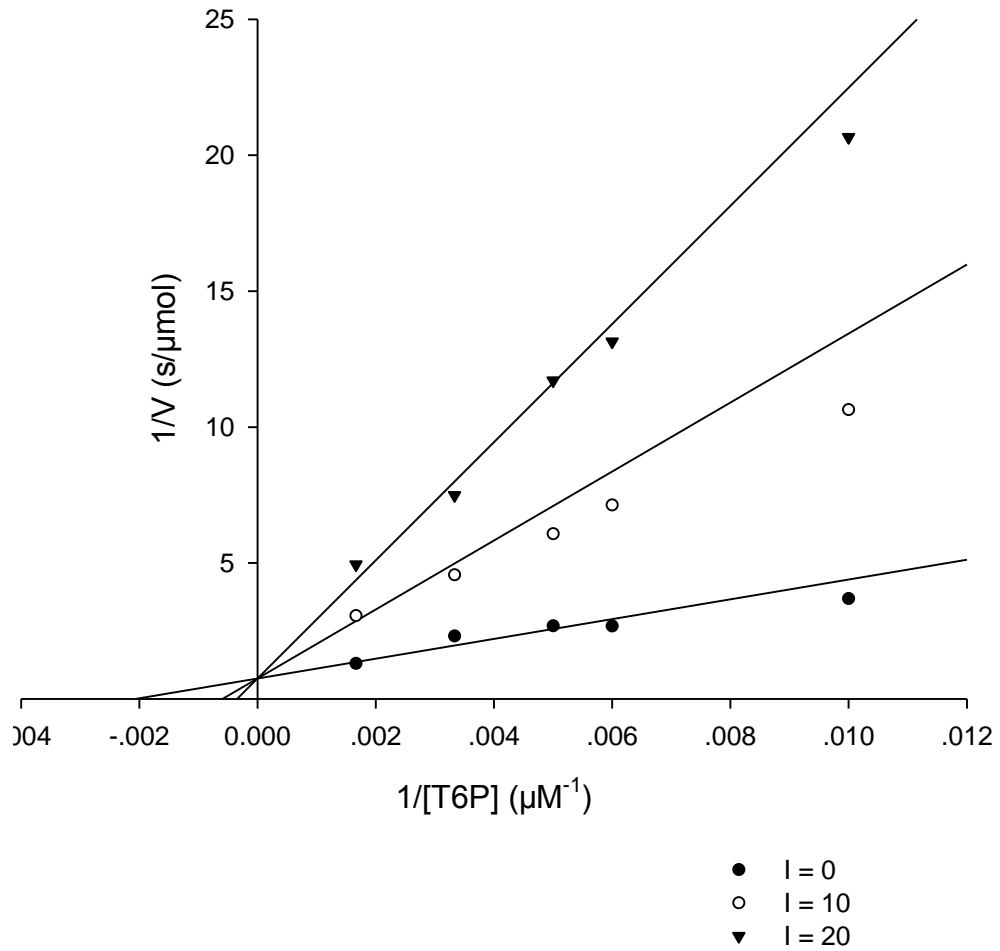
[*St*-T6PP]= 33 nM; V_{\max} = 0.2047 μM/s; K_m = 314 ±43 μM



Enzyme: Mt-T6PP(50 μ M); Substrate: α -D-Glucose-1-phosphate;

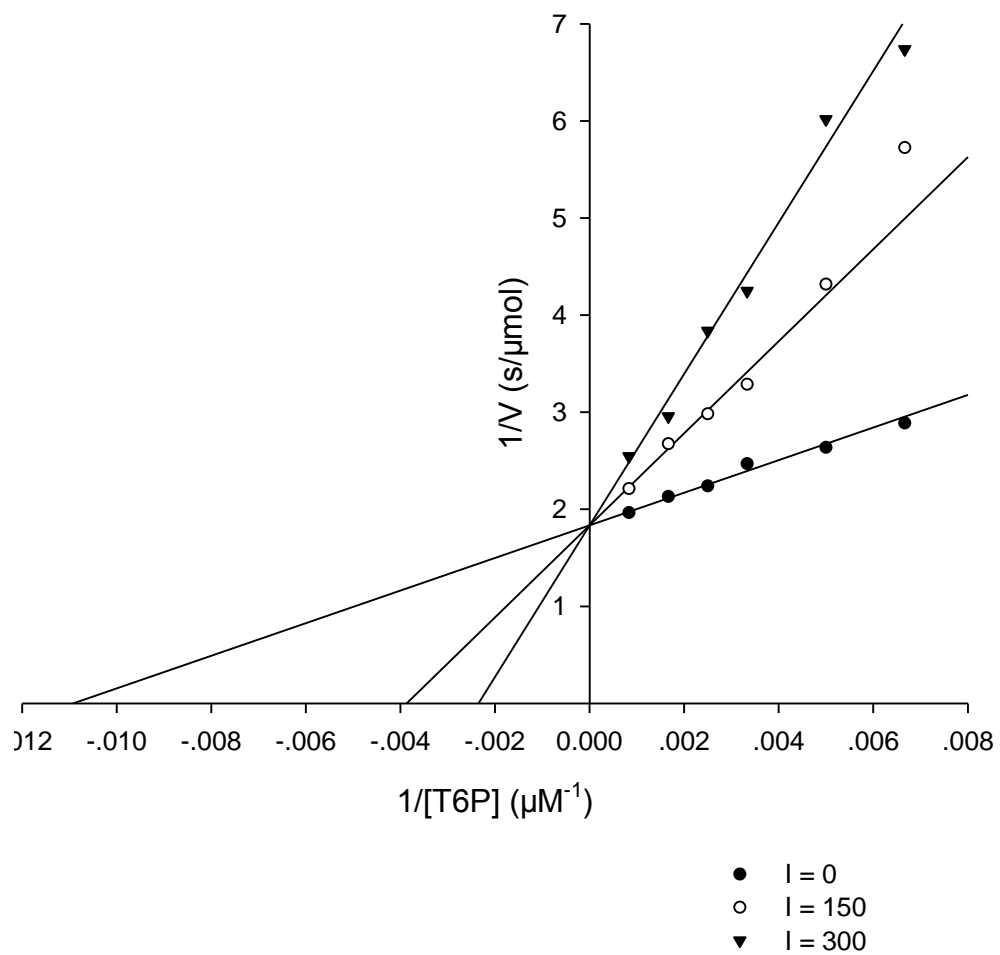
k_{cat} : 0.0022 ± 0.0002 S^{-1} K_m : 8 ± 1 mM ; k_{cat}/K_m : 0.28 $M^{-1}S^{-1}$.

A.3 Plots in Chapter Three



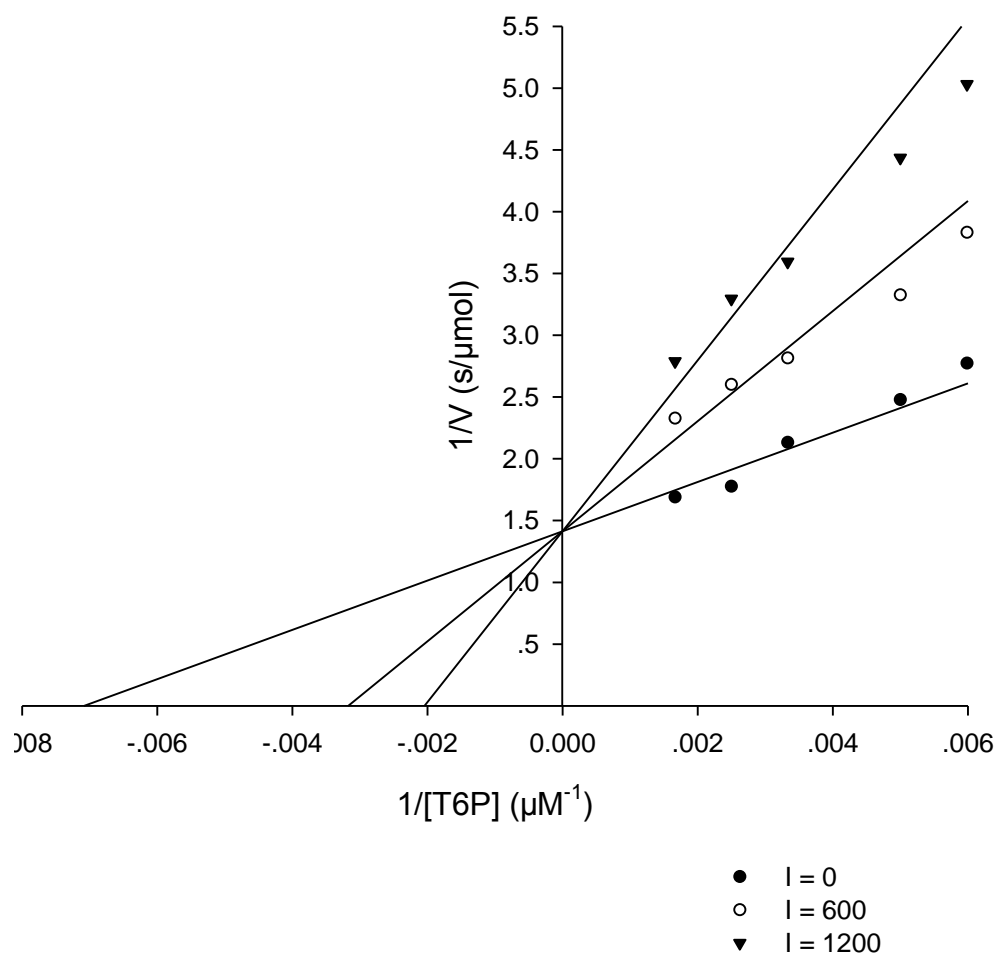
$[Bm\text{-T6PP}] = 20 \text{ nM}; K_i = 4.0 \pm 0.6 \text{ }\mu\text{M}$

Bm-T6PP with T6P and inhibitor K_2WO_4



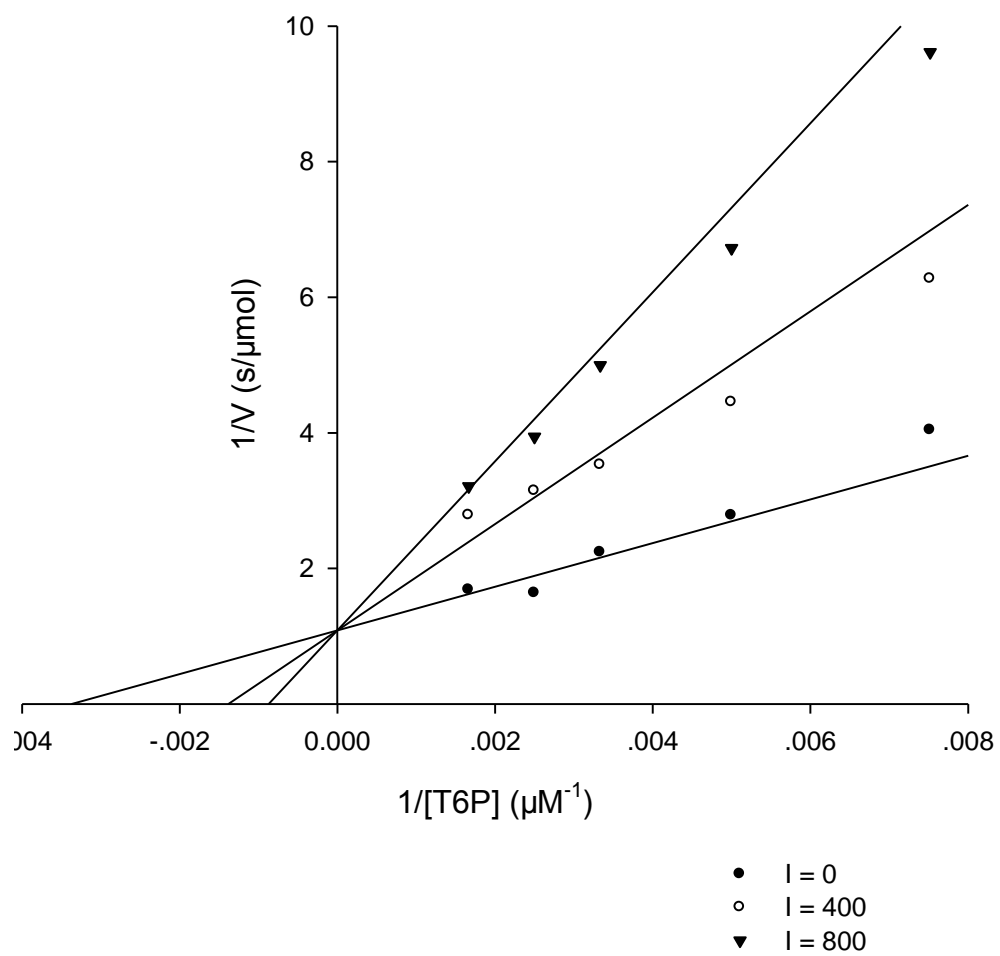
$[Bm-T6PP] = 20 \text{ nM}; K_i = 82 \pm 7 \text{ } \mu\text{M}$

Bm-T6PP with T6P and inhibitor **compound 1**



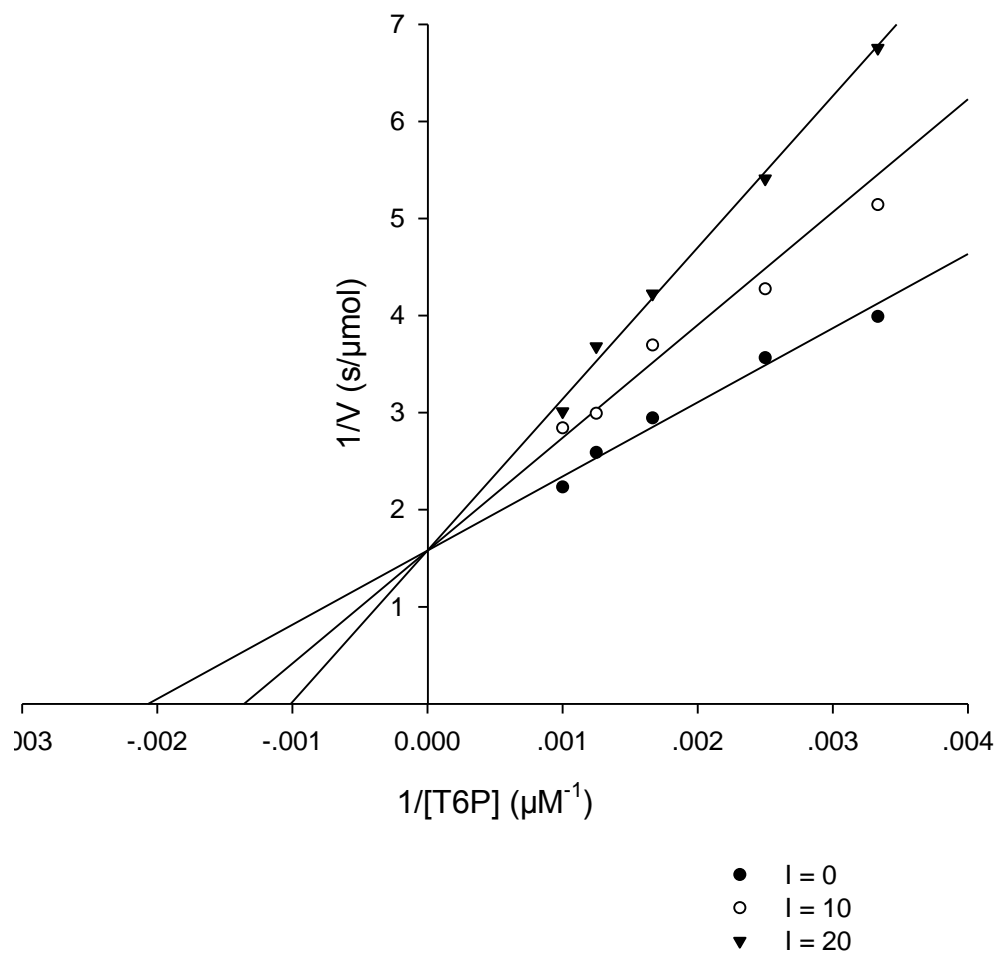
$[Bm-T6PP] = 20 \text{ nM}; K_i = 487 \pm 85 \text{ } \mu\text{M}$

Bm-T6PP with T6P and inhibitor **compound 2**



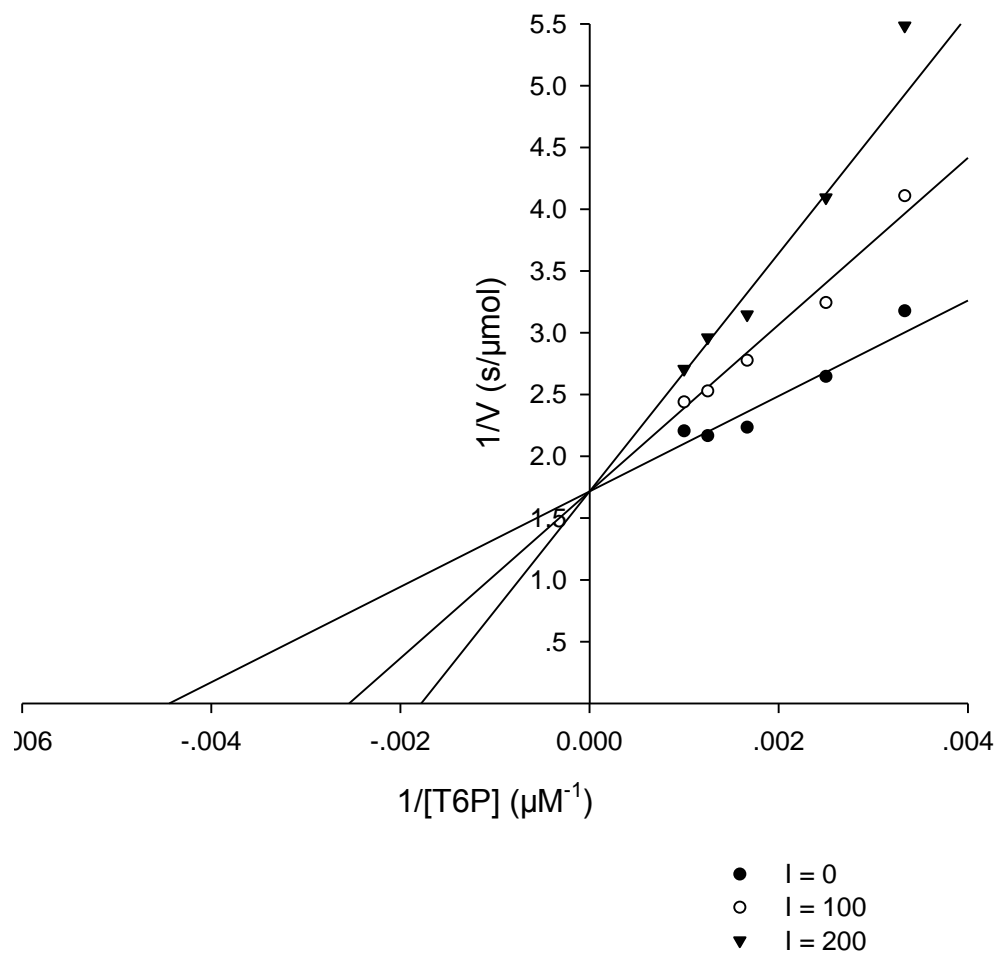
$[Bm-T6PP] = 20 \text{ nM}; K_i = 279 \pm 53 \text{ } \mu\text{M}$

Bm-T6PP with T6P and inhibitor **compound 3**



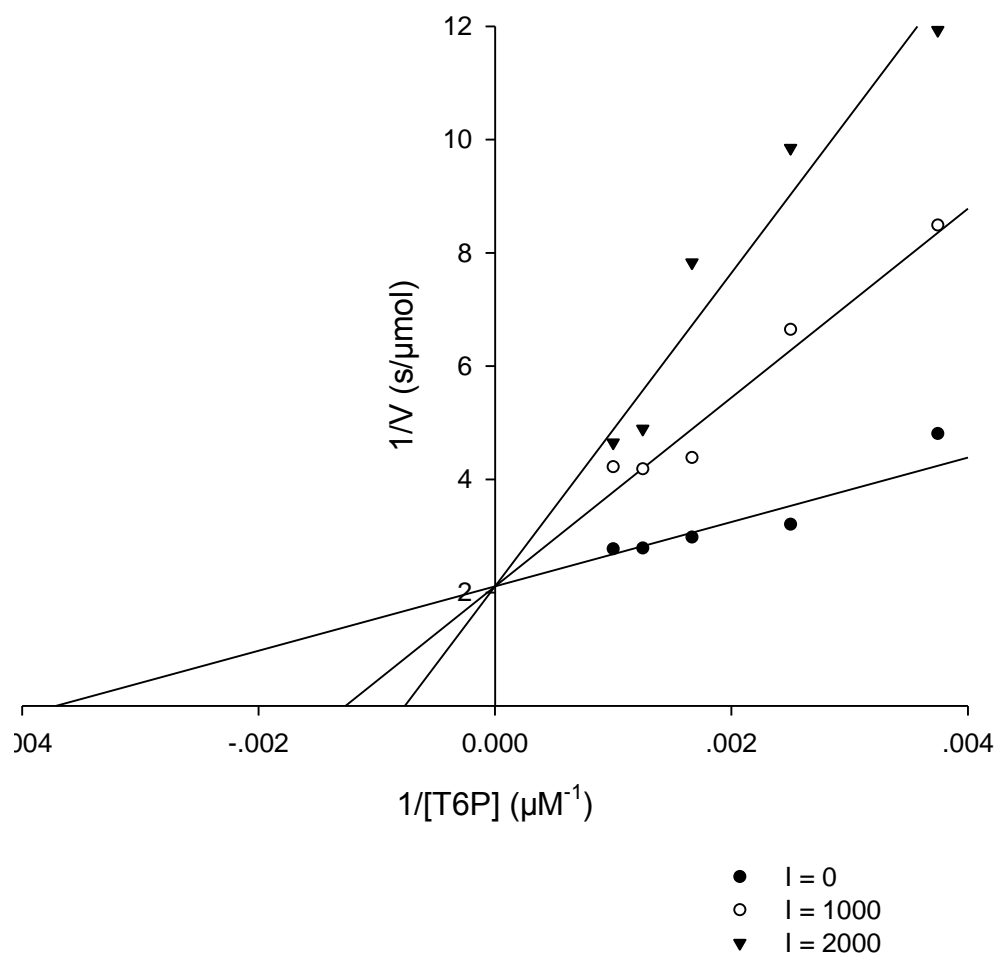
$[Mt\text{-}T6PP] = 66 \text{ nM}; K_i = 19 \pm 2 \text{ } \mu\text{M}$

Mt-T6PP with T6P and inhibitor K_2WO_4



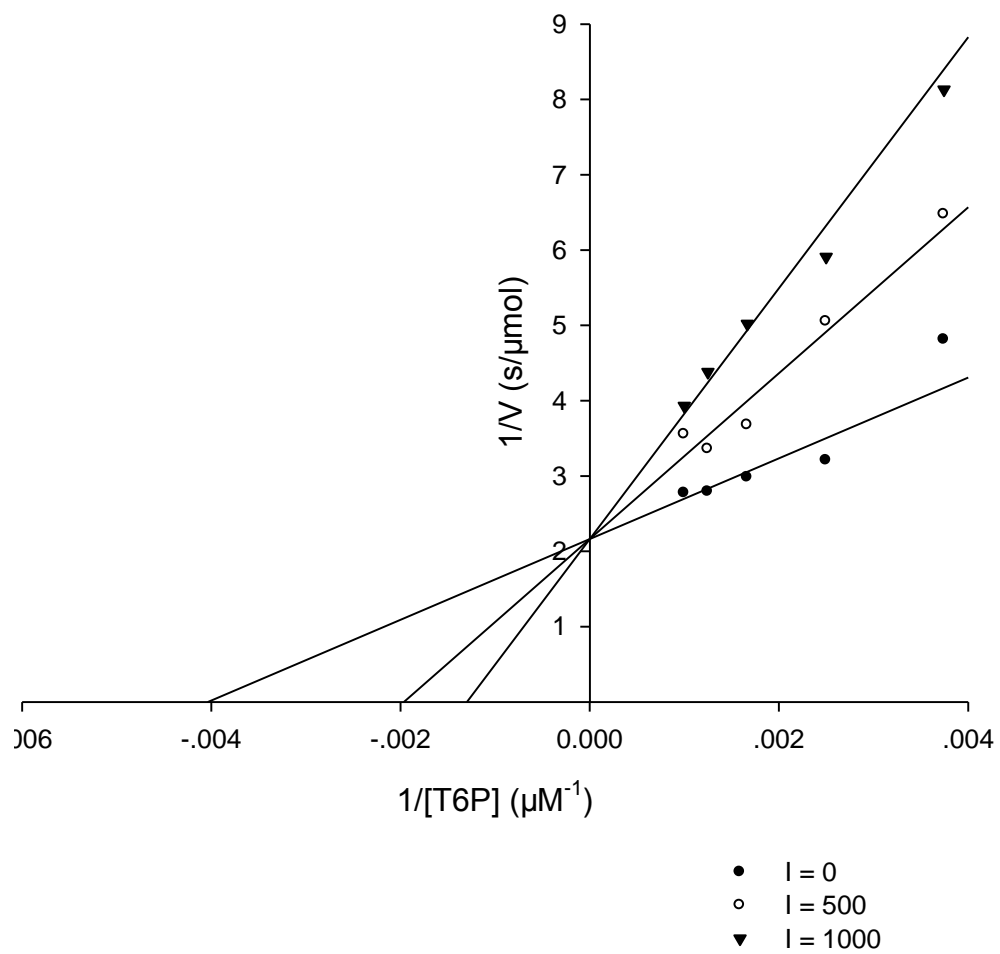
$[Mt-T6PP] = 66 \text{ nM}; K_i = 130 \pm 20 \text{ } \mu\text{M}$

Mt-T6PP with T6P and inhibitor **compound 1**



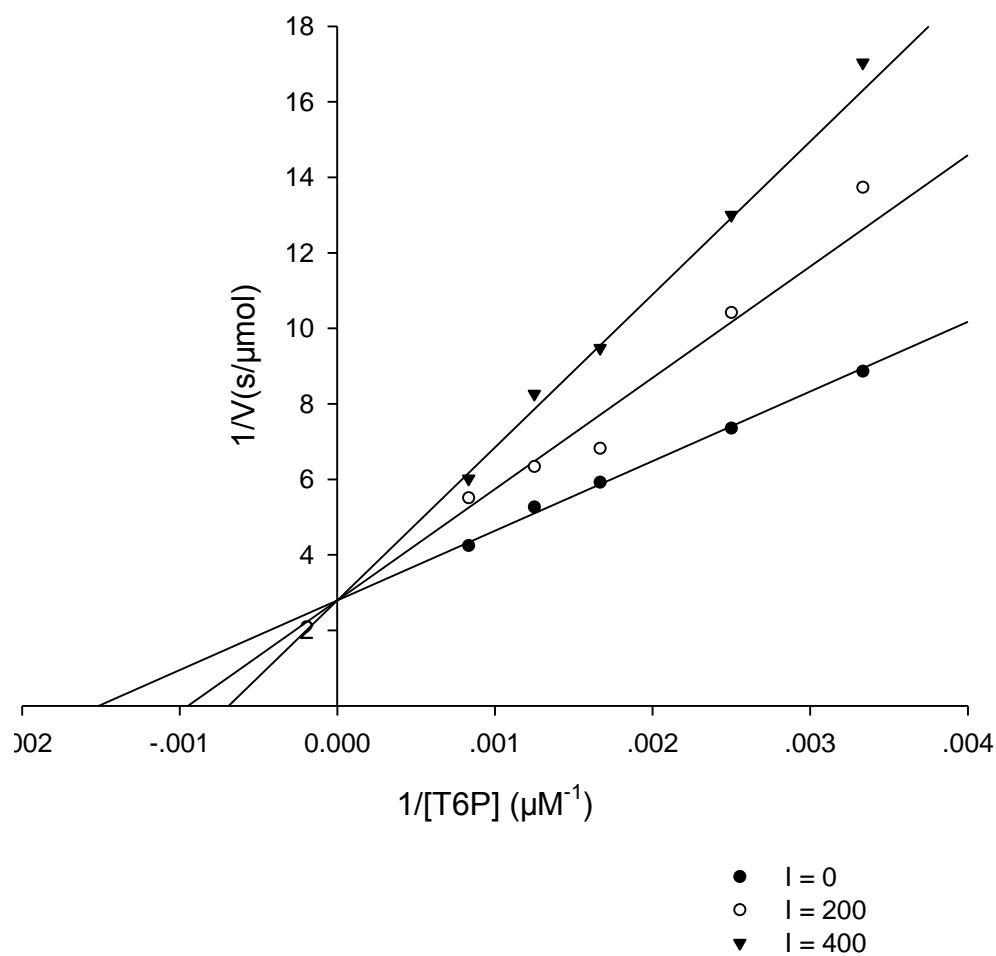
$[Mt-T6PP] = 33 \text{ nM}; K_i = 517 \pm 19 \text{ } \mu\text{M}$

Mt-T6PP with T6P and inhibitor **compound 2**



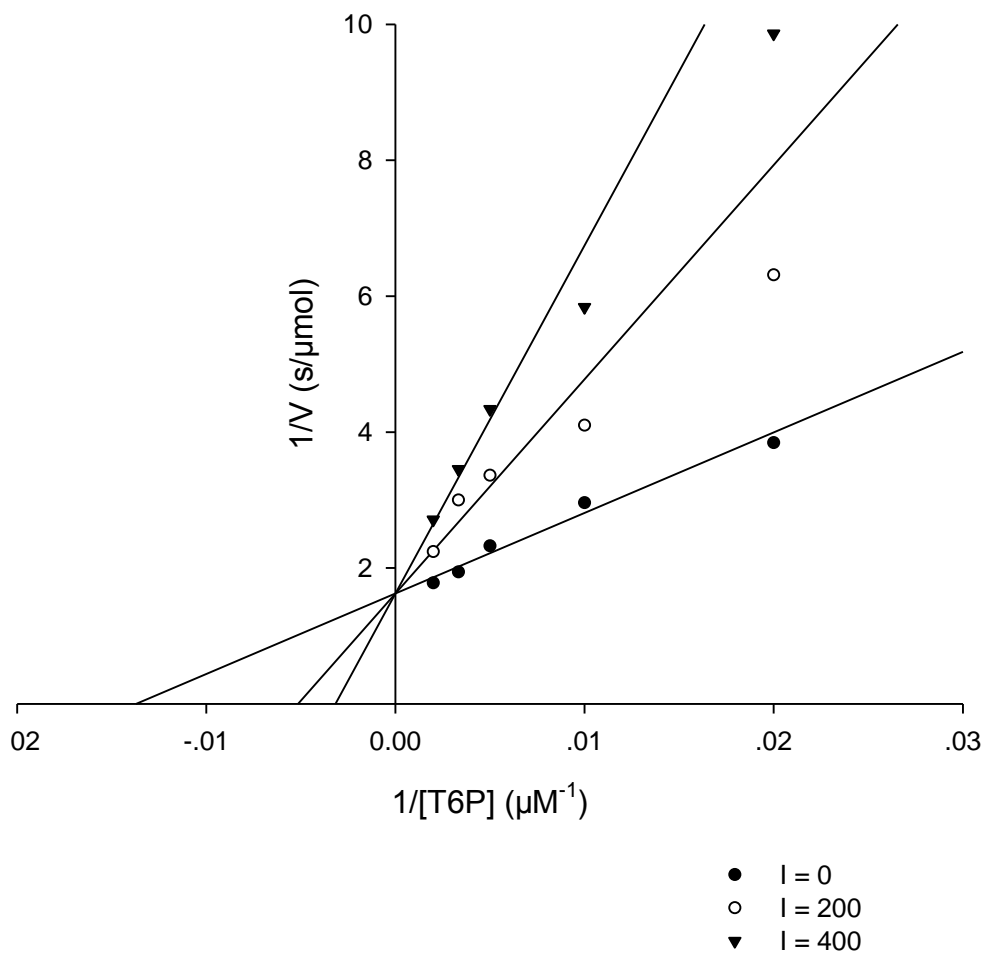
$[Mt-T6PP] = 33 \text{ nM}; K_i = 474 \pm 94 \text{ } \mu\text{M}$

Mt-T6PP with T6P and inhibitor **compound 3**



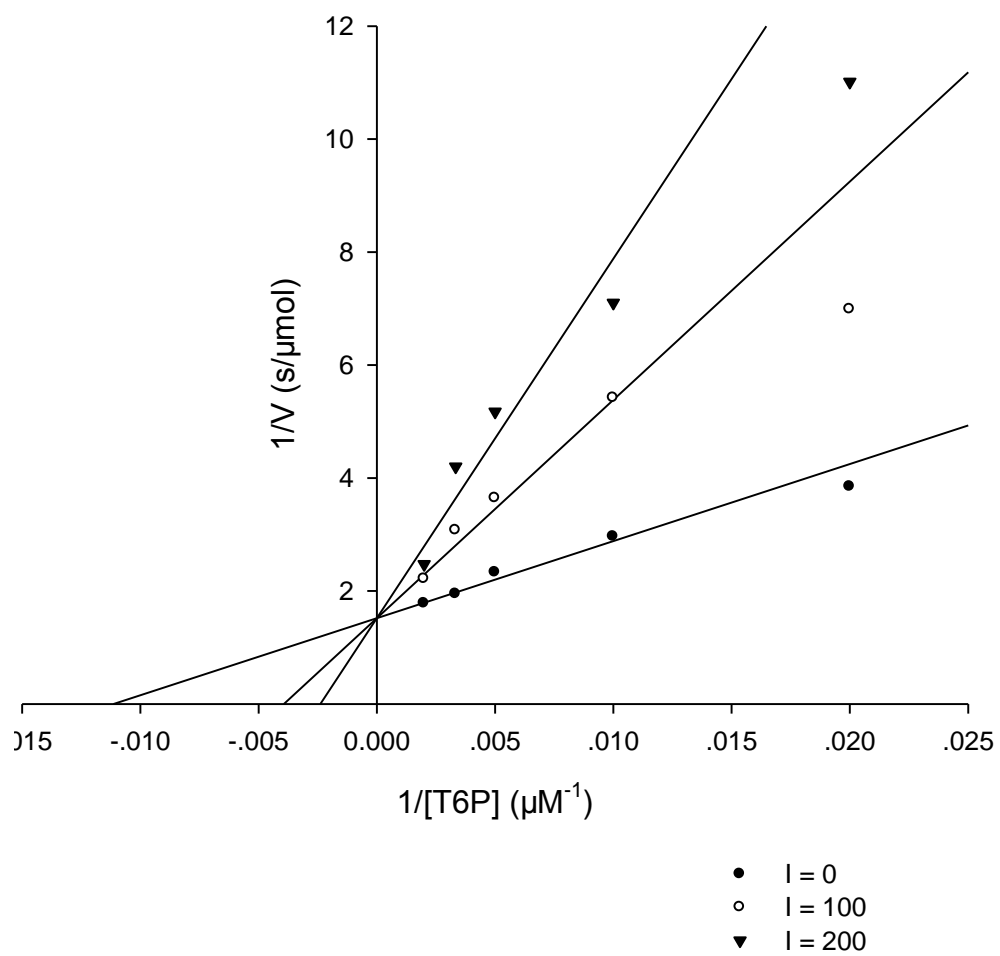
$[Sb\text{-T6PP}] = 22.8 \text{ nM}; K_i = 334 \pm 37 \text{ }\mu\text{M}$

Sb-T6PP with T6P and inhibitor **compound 1**



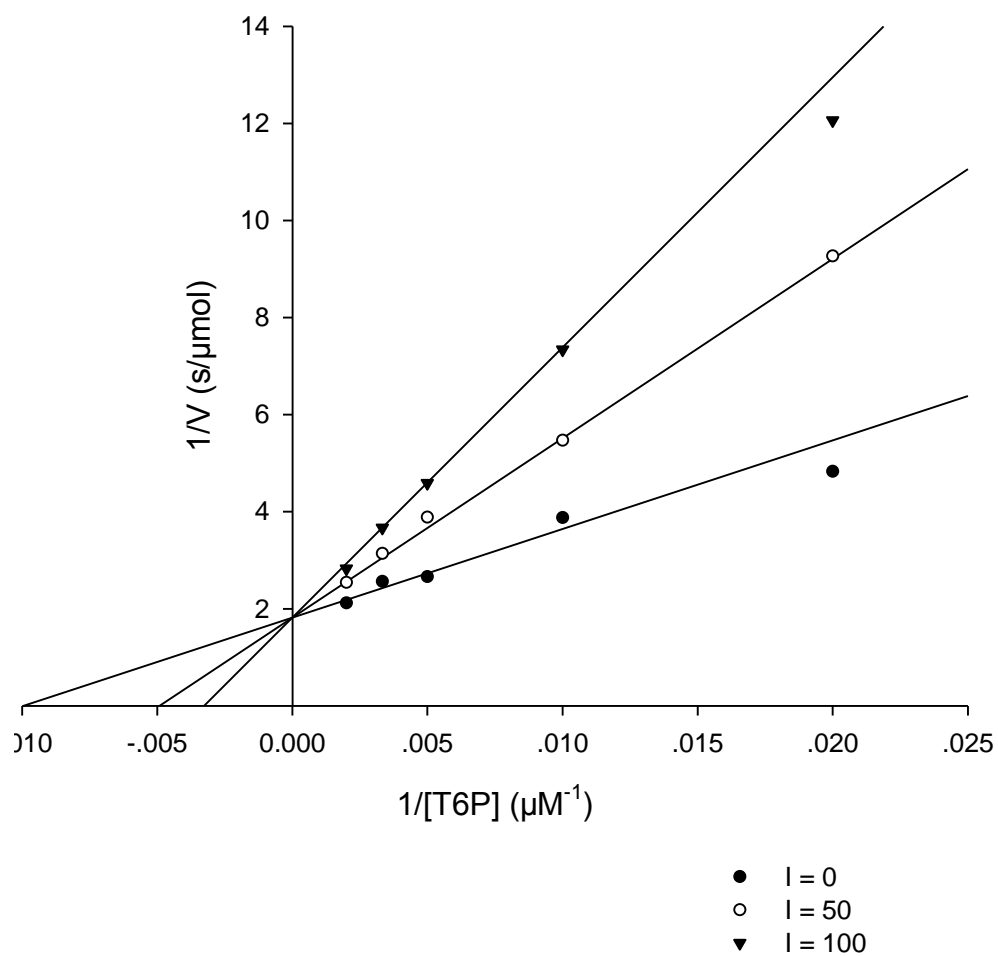
$[As\text{-}T6PP] = 9.4 \text{ nM}; K_i = 120 \pm 20 \mu\text{M}$

As-T6PP with T6P and inhibitor K_2WO_4



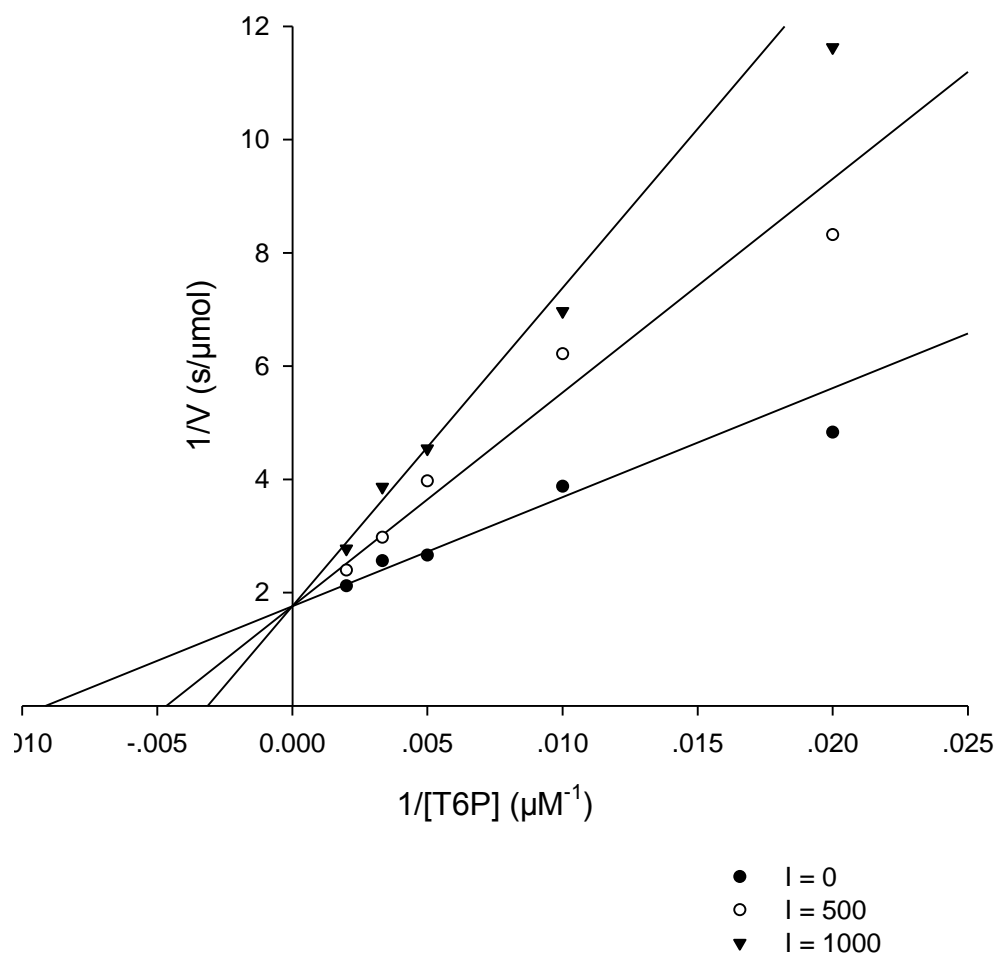
$[As-T6PP] = 9.4 \text{ nM}; K_i = 55 \pm 9 \text{ } \mu\text{M}$

As-T6PP with T6P and inhibitor Na_3VO_4



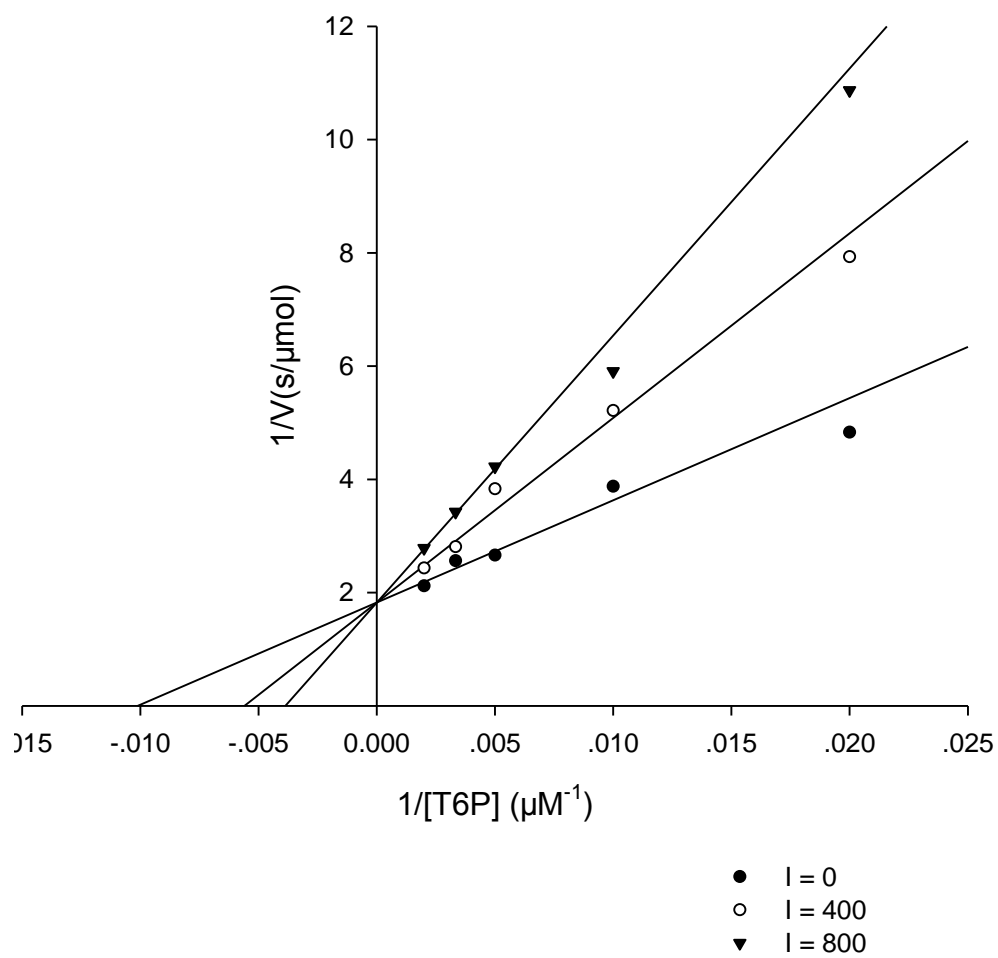
$[As-T6PP] = 9.4 \text{ nM}; K_i = 49 \pm 5 \text{ } \mu\text{M}$

As-T6PP with T6P and inhibitor **compound 1**



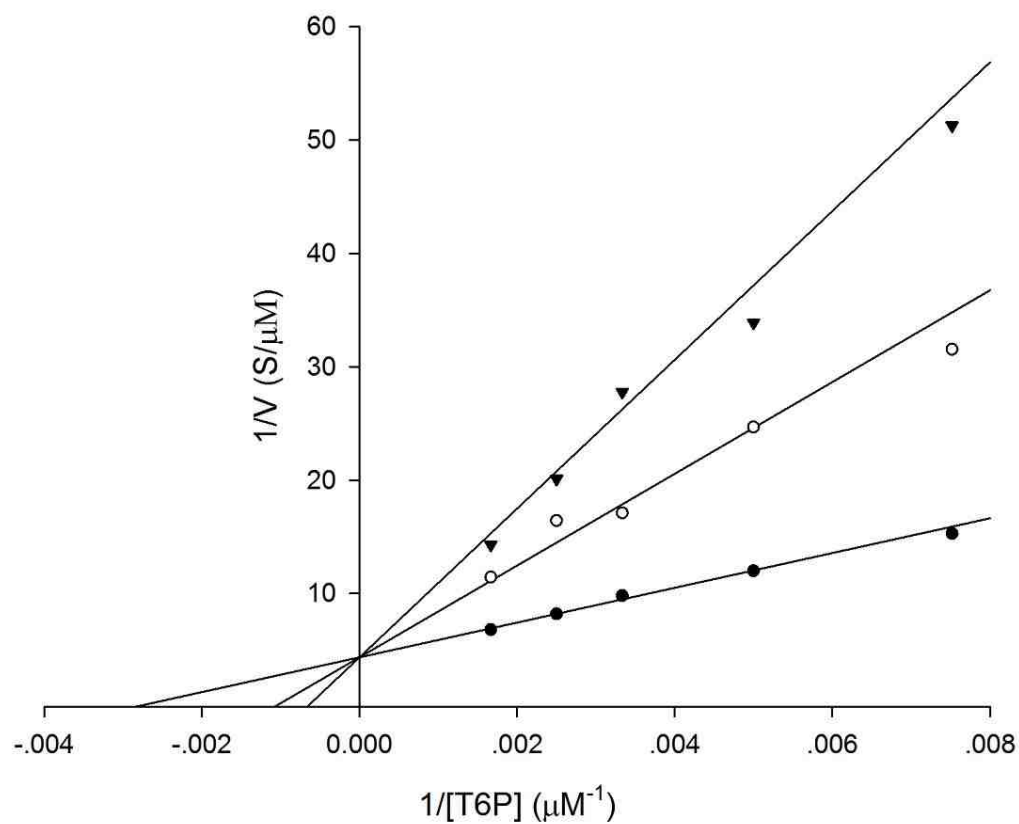
$[As-T6PP] = 9.4 \text{ nM}; K_i = 522 \pm 78 \text{ } \mu\text{M}$

As-T6PP with T6P and inhibitor **compound 2**



$[As-T6PP] = 9.4 \text{ nM}; K_i = 496 \pm 71 \text{ } \mu\text{M}$

As-T6PP with T6P and inhibitor **compound 3**



$V_{max} = 0.2282$
 $K_m = 349.7$
 $K_i = 182.8$

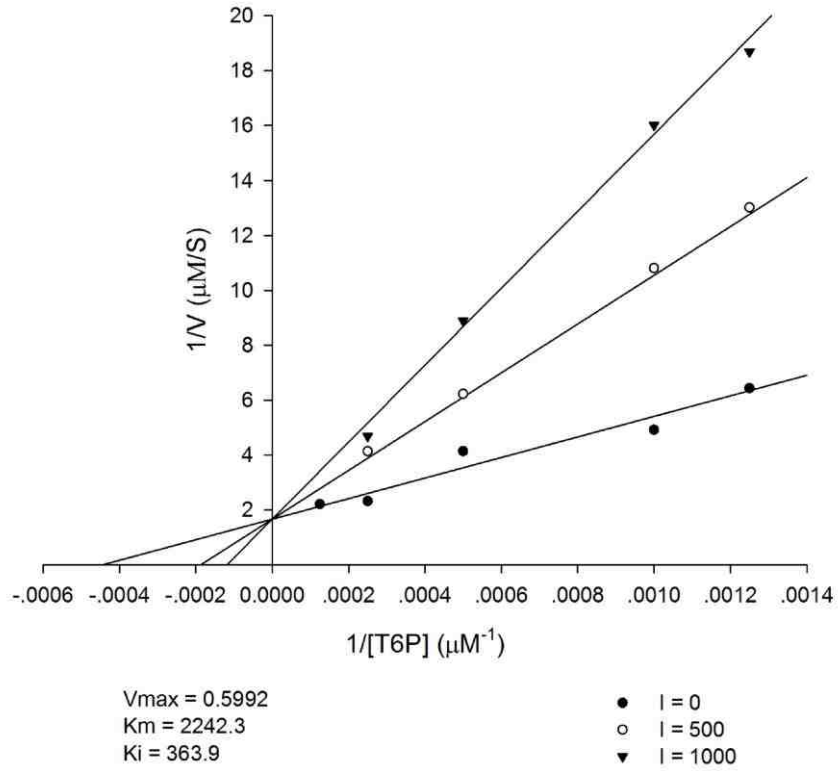
● I = 0
 ○ I = 300
 ▼ I = 600

$[S_t\text{-T6PP}] = 33 \text{ nM}; K_i = 183 \pm 15 \text{ } \mu\text{M}$

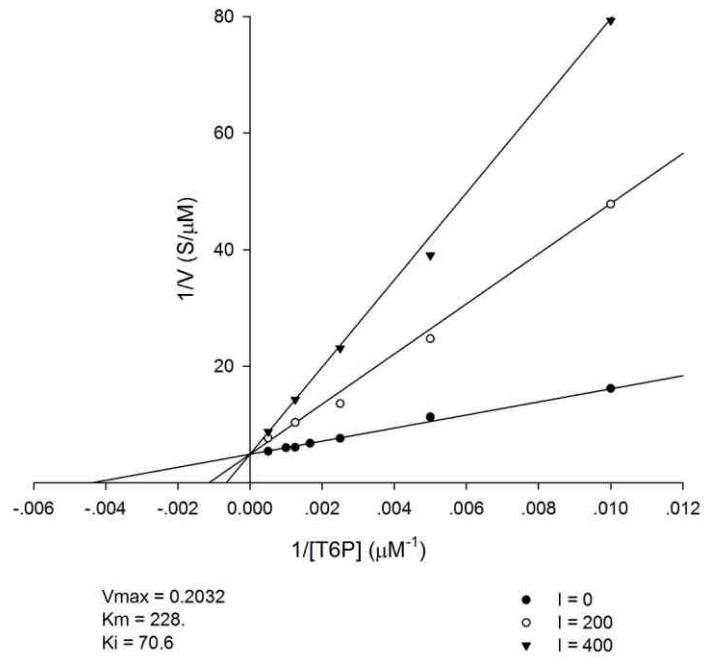
Sb-T6PP with T6P and inhibitor **compound 1**

A. 4 Plots in Chapter Four

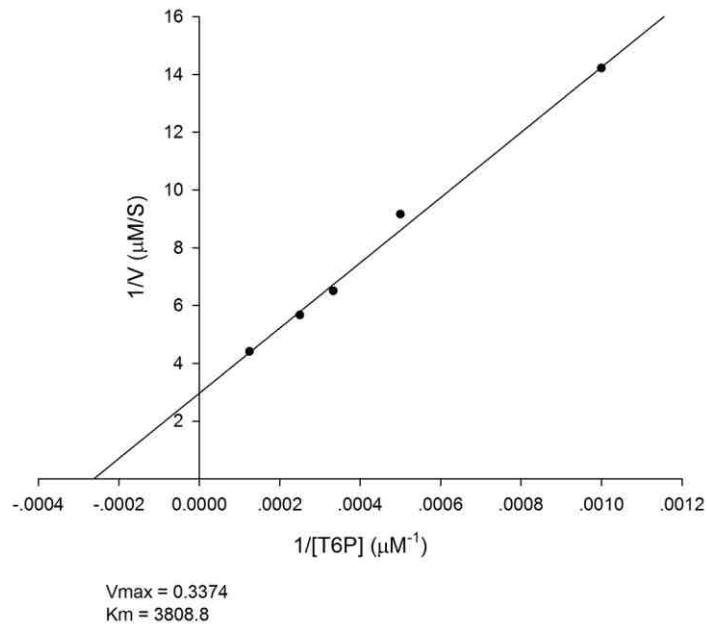
A.4.1 Bm-T6PP kinetic Plots in Table 4.1



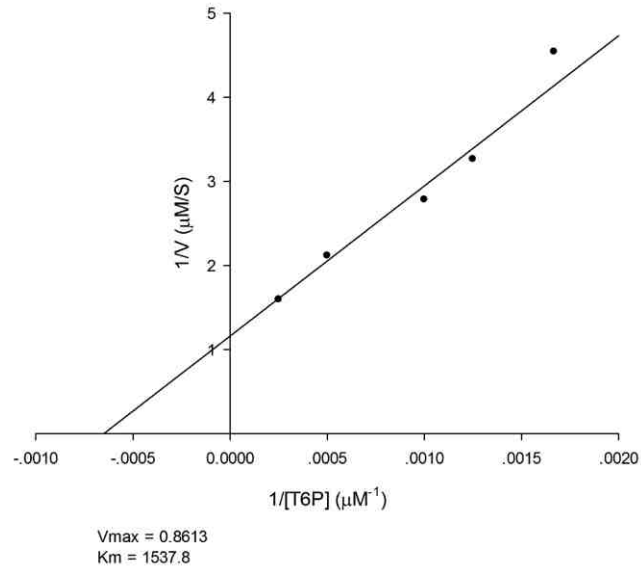
Bm-F148A, $k_{\text{cat}} = 0.28 \pm 0.02 \text{ s}^{-1}$, $K_{\text{m}} = 2200 \pm 400 \mu\text{M}$, $K_{\text{i}} = 360 \pm 70 \mu\text{M}$.



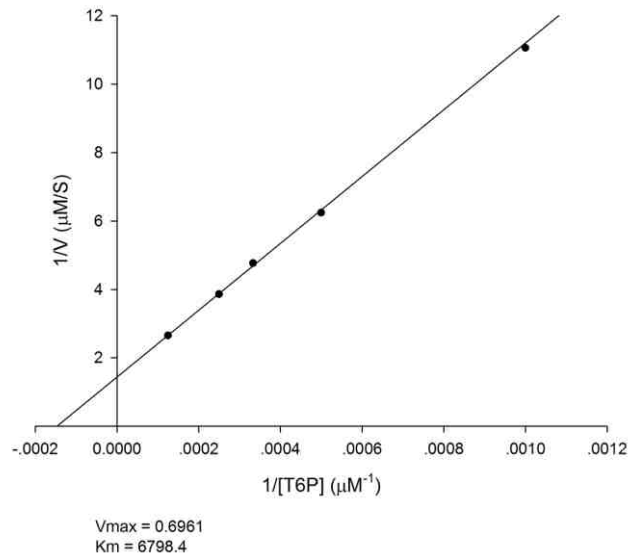
Bm-E157A, $k_{cat} = 25 \pm 0.6 \text{ s}^{-1}$, $K_m = 230 \pm 20 \text{ } \mu\text{M}$, $K_i = 71 \pm 6 \text{ } \mu\text{M}$.



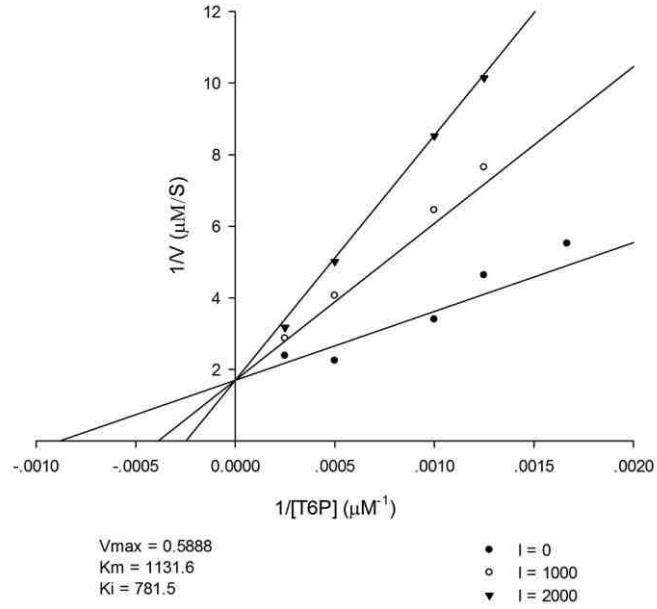
Bm-R187A, $k_{cat} = 0.11 \pm 0.01 \text{ s}^{-1}$, $K_m = 3800 \pm 400 \text{ } \mu\text{M}$, $K_i > 4 \text{ mM}$.



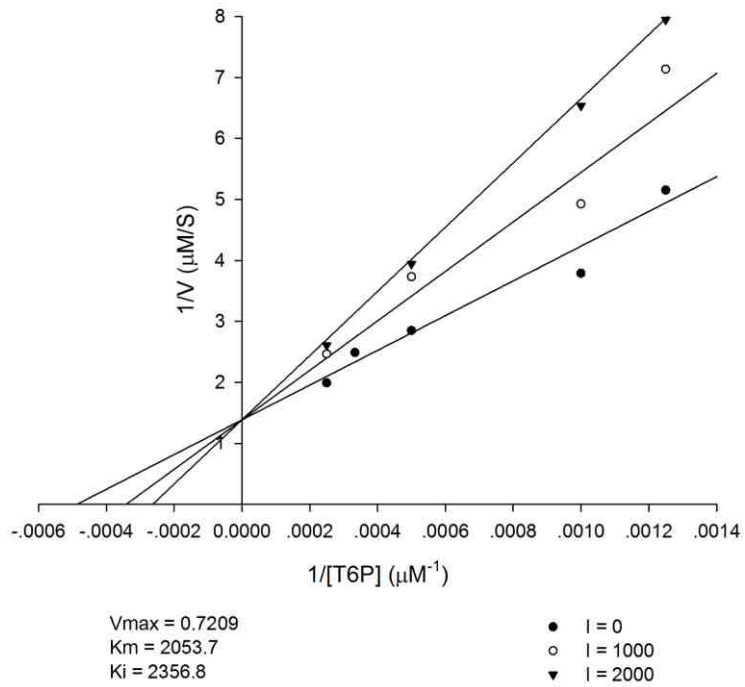
Bm-E251A, $k_{cat} = 0.99 \pm 0.06 \text{ s}^{-1}$, $K_m = 1500 \pm 200 \text{ } \mu\text{M}$, $K_i > 4 \text{ Mm}$.



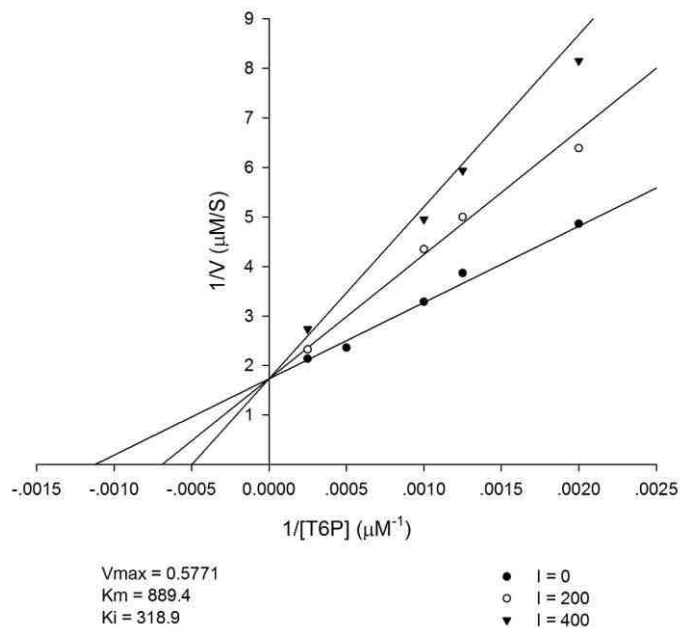
Bm-K253A, $k_{cat} = 0.098 \pm 0.002 \text{ s}^{-1}$, $K_m = 6800 \pm 300 \text{ } \mu\text{M}$, $K_i > 4 \text{ Mm}$.



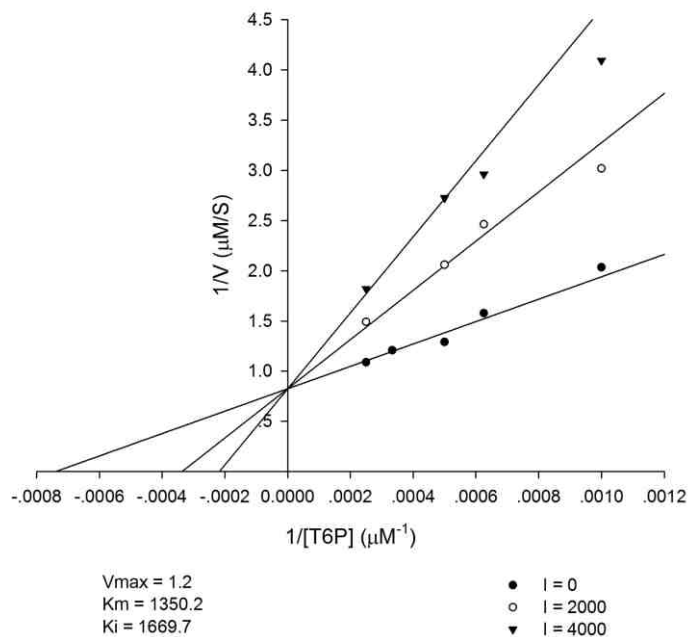
Bm-H260A, $k_{cat} = 0.28 \pm 0.03 \text{ s}^{-1}$, $K_m = 1100 \pm 300 \text{ } \mu\text{M}$, $K_i = 780 \pm 170 \text{ } \mu\text{M}$.



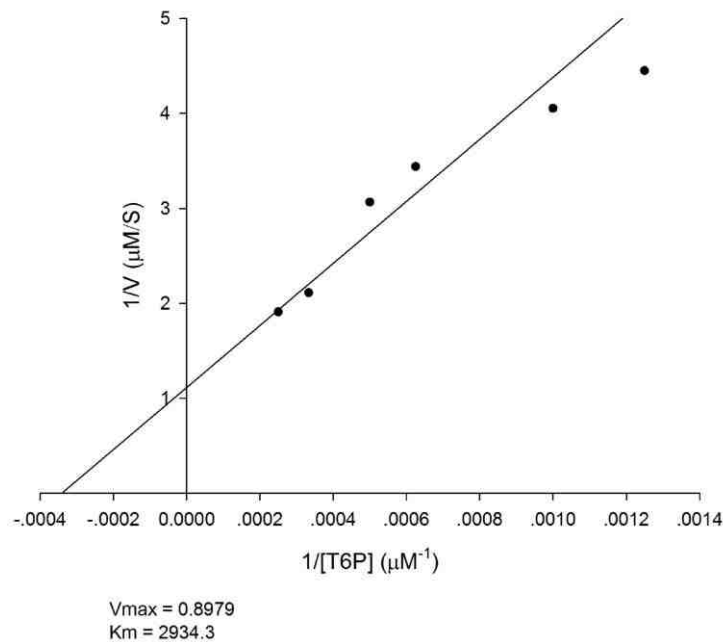
Bm-R262A, $k_{cat} = 0.13 \pm 0.01 \text{ s}^{-1}$, $K_m = 2100 \pm 300 \text{ } \mu\text{M}$, $K_i = 2400 \pm 500 \text{ } \mu\text{M}$.



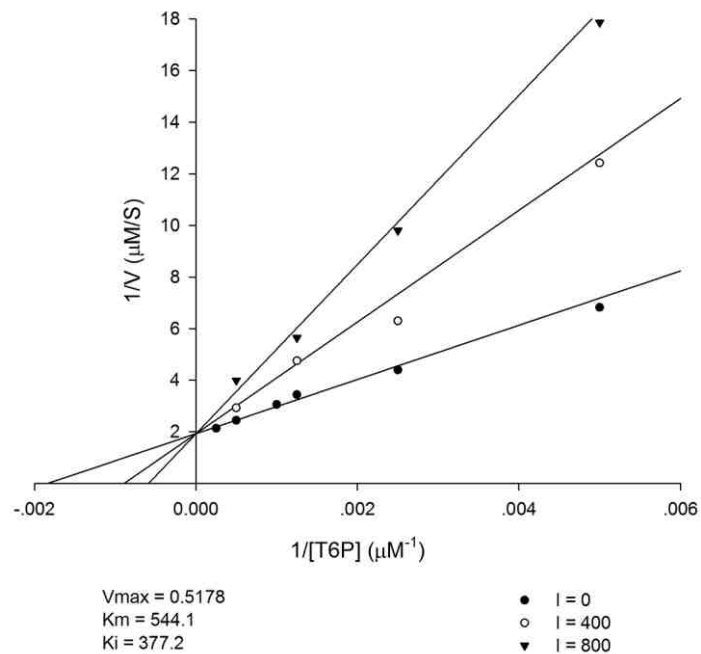
Bm-N263A, $k_{cat} = 23 \pm 0.7 \text{ s}^{-1}$, $K_m = 890 \pm 70 \text{ } \mu\text{M}$, $K_i = 320 \pm 40 \text{ } \mu\text{M}$.



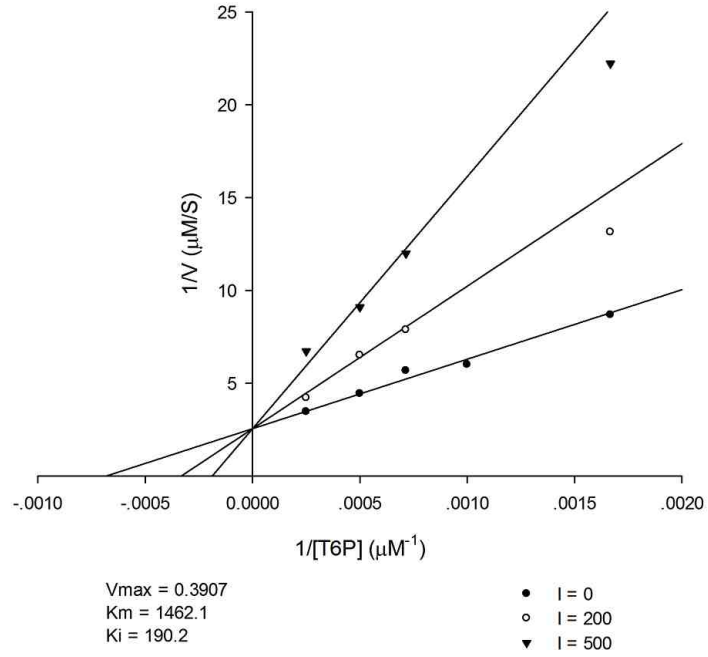
Bm-T288A, $k_{cat} = 11 \pm 0.6 \text{ s}^{-1}$, $K_m = 1400 \pm 200 \text{ } \mu\text{M}$, $K_i = 1700 \pm 200 \text{ } \mu\text{M}$.



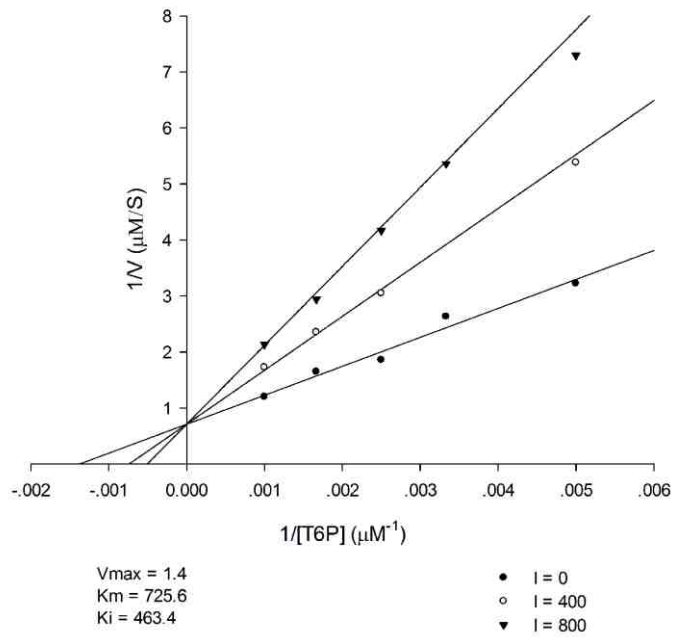
Bm-R291A, $k_{cat} = 0.39 \pm 0.07 \text{ s}^{-1}$, $K_m = 2900 \pm 900 \text{ } \mu\text{M}$, $K_i > 4 \text{ mM}$.



Bm-E292A, $k_{cat} = 15 \pm 0.5 \text{ s}^{-1}$, $K_m = 540 \pm 60 \text{ } \mu\text{M}$, $K_i = 380 \pm 50 \text{ } \mu\text{M}$.

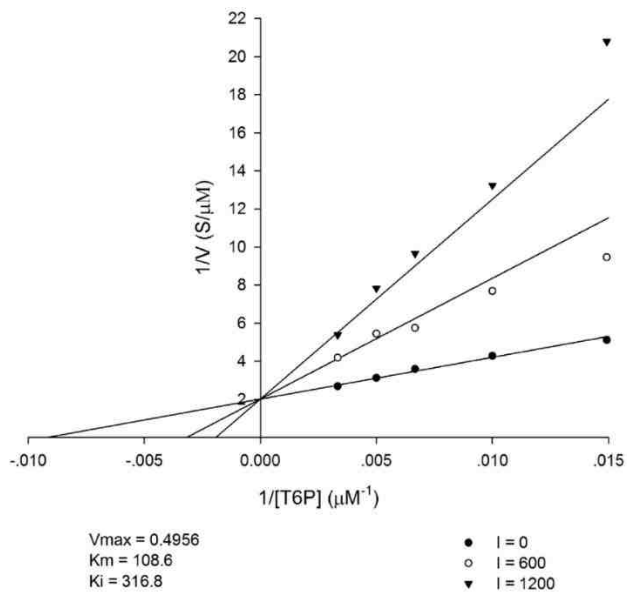


Bm-E295A, $k_{cat} = 0.16 \pm 0.01 \text{ s}^{-1}$, $K_m = 1500 \pm 200 \text{ } \mu\text{M}$, $K_i = 190 \pm 20 \text{ } \mu\text{M}$.

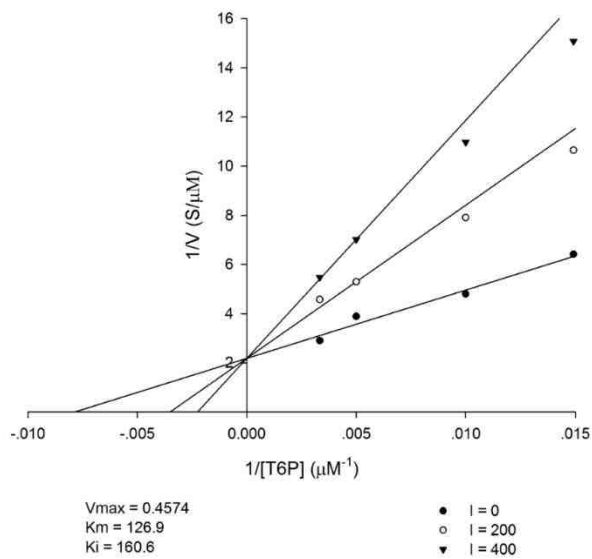


Bm-R297A, $k_{cat} = 3 \pm 0.2 \text{ s}^{-1}$, $K_m = 730 \pm 90 \text{ } \mu\text{M}$, $K_i = 460 \pm 40 \text{ } \mu\text{M}$.

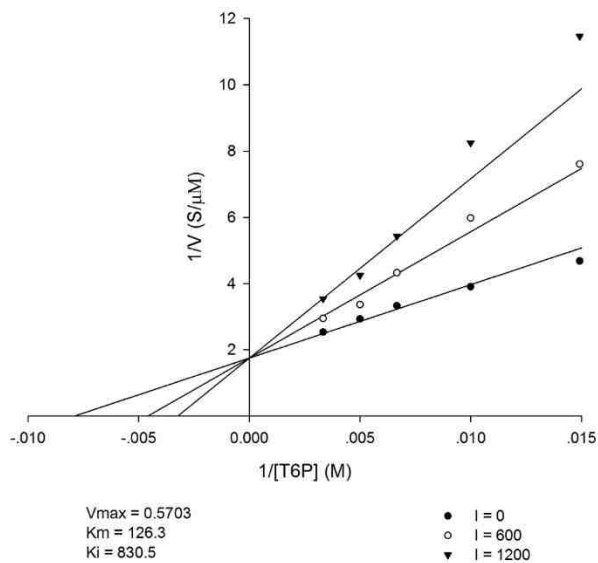
A.4.2 Bm-T6PP kinetic Plots in Table 4.4



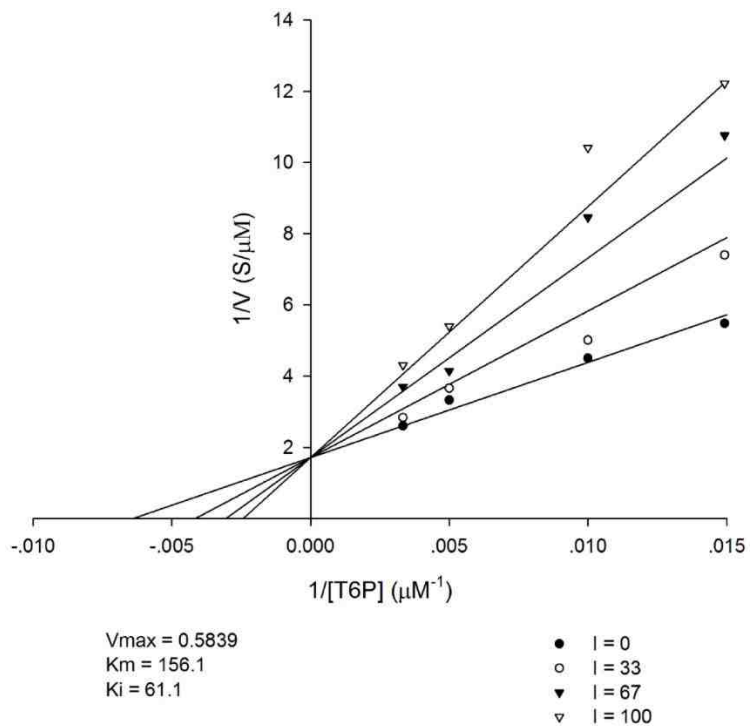
Enzyme: *Bm*-T6PP, Inhibitor: **5c**, $K_i = 320 \pm 30 \mu\text{M}$.



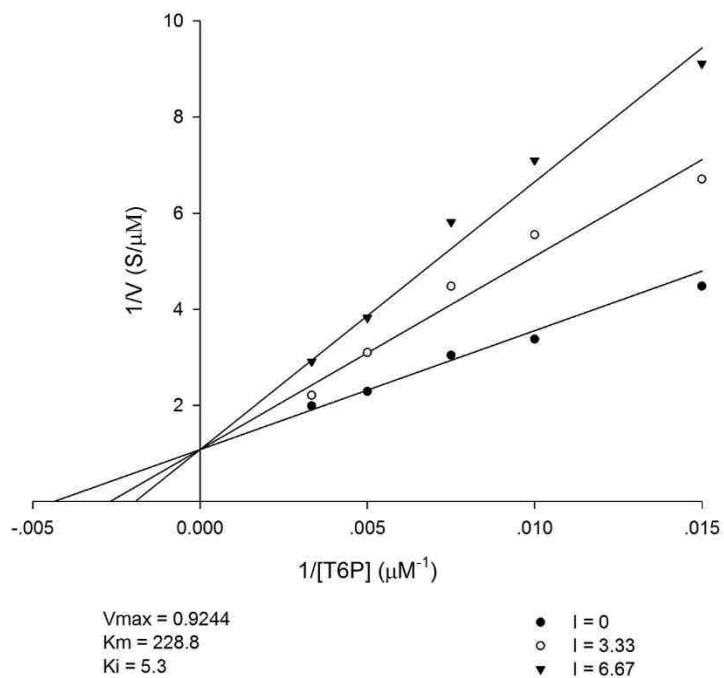
Enzyme: *Bm*-T6PP, Inhibitor: **6a**, $K_i = 160 \pm 20 \mu\text{M}$.



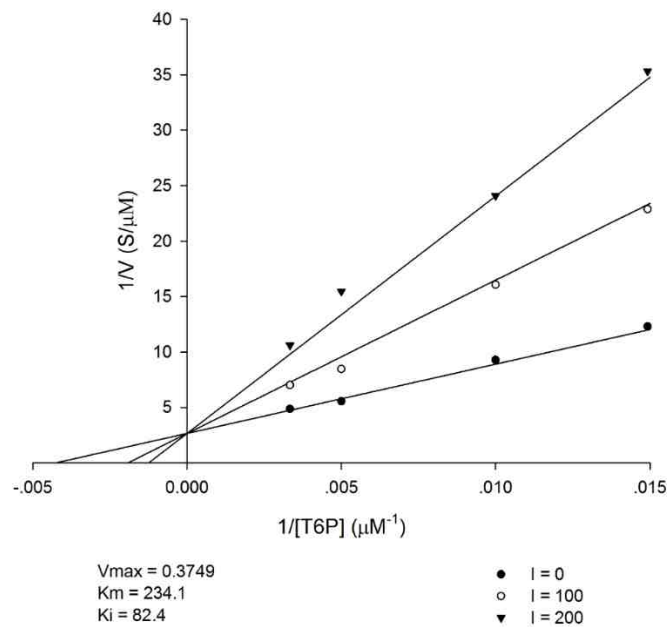
Enzyme: *Bm*-T6PP, Inhibitor: **8a**, $K_i = 830 \pm 100 \mu\text{M}$.



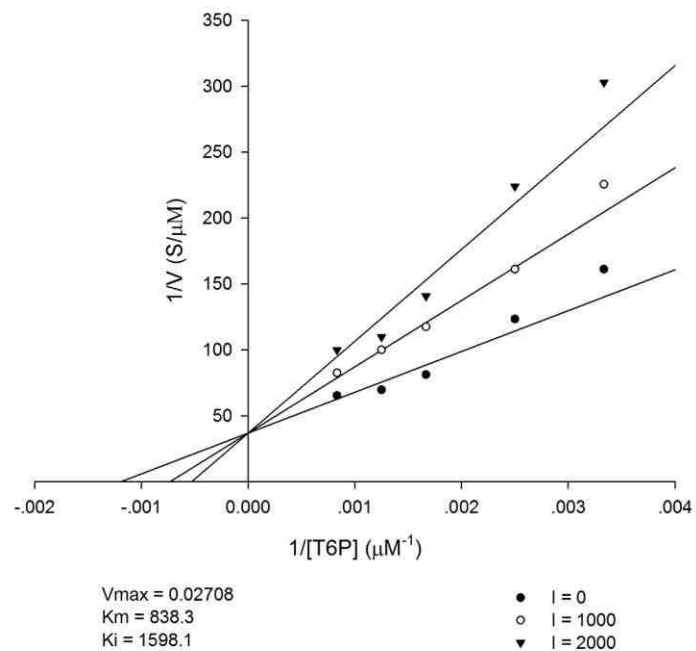
Enzyme: *Bm*-T6PP, Inhibitor: **8p**, $K_i = 61 \pm 10 \mu\text{M}$.



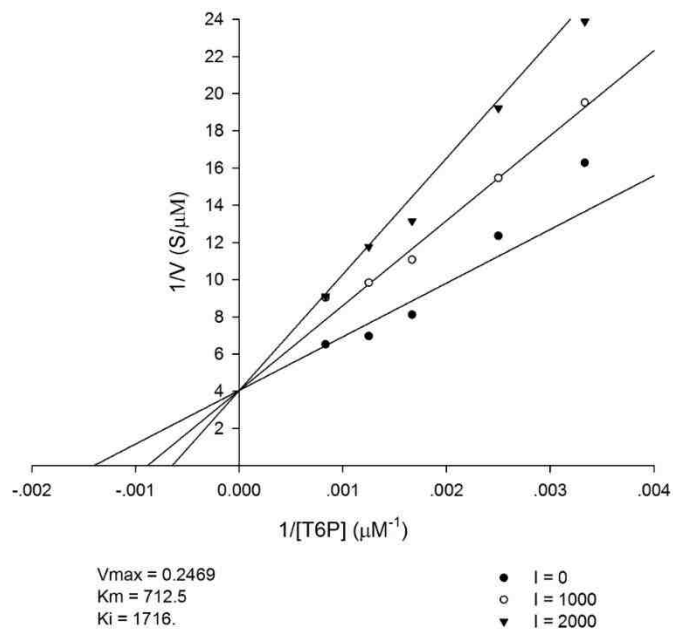
Enzyme: *Bm*-T6PP, Inhibitor: **9a**, $K_i = 5.3 \pm 0.6 \mu\text{M}$.



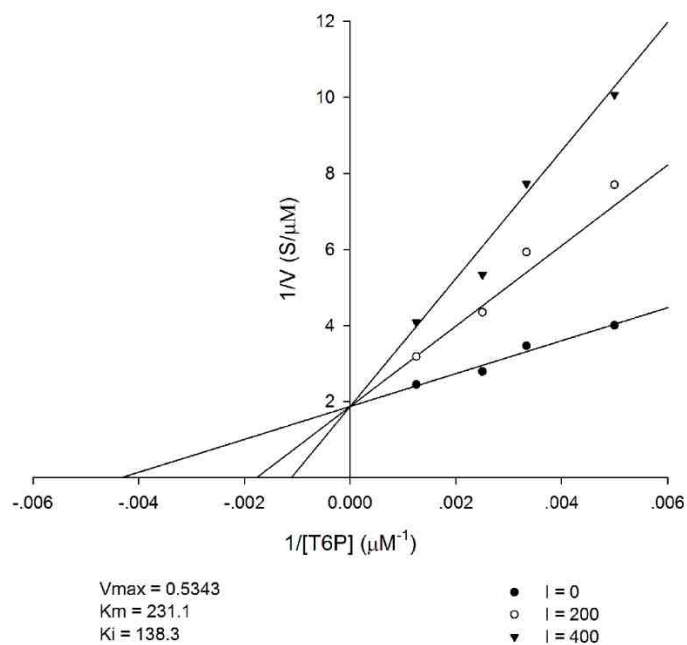
Enzyme: *Bm*-T6PP, Inhibitor: **9b**, $K_i = 82 \pm 10 \mu\text{M}$.



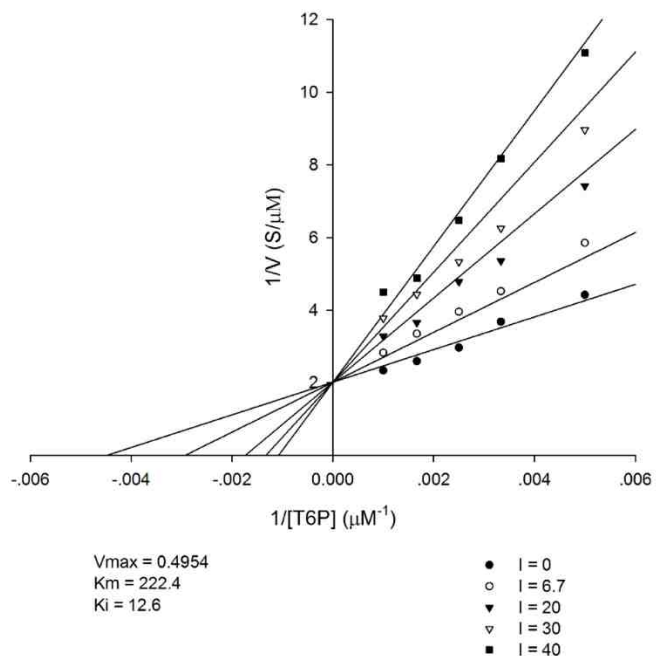
Enzyme: *Mt*-T6PP, Inhibitor: **8b**, $K_i = 1600 \pm 270 \mu\text{M}$.



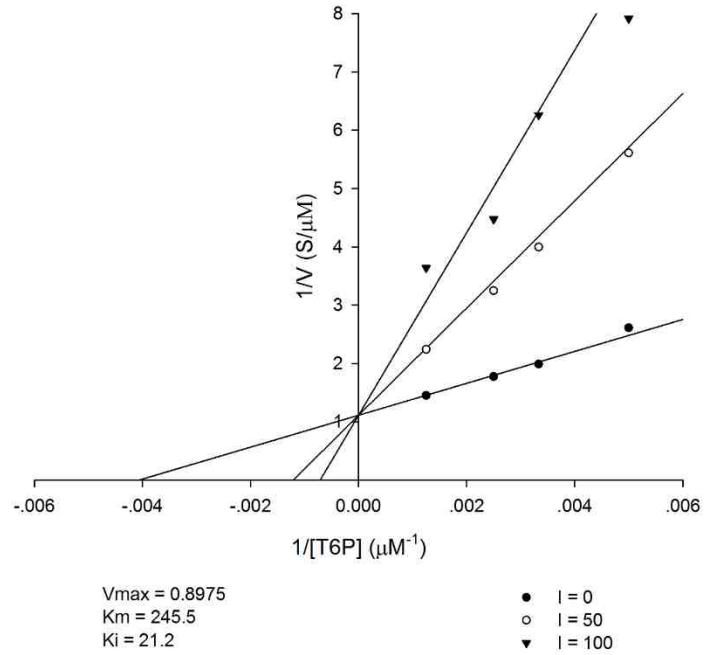
Enzyme: *Mt*-T6PP, Inhibitor: **8i**, $K_i = 1700 \pm 350 \mu\text{M}$.



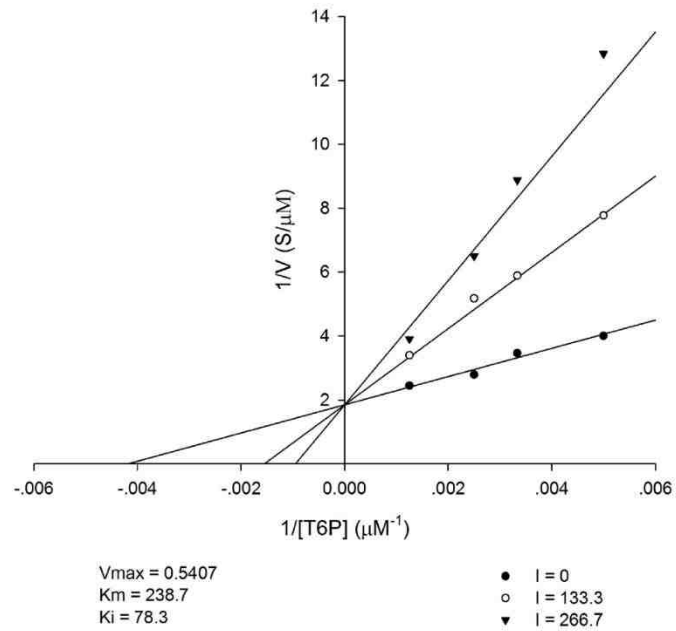
Enzyme: *Sb*-T6PP, Inhibitor: **8o**, $K_i = 140 \pm 20 \mu\text{M}$.



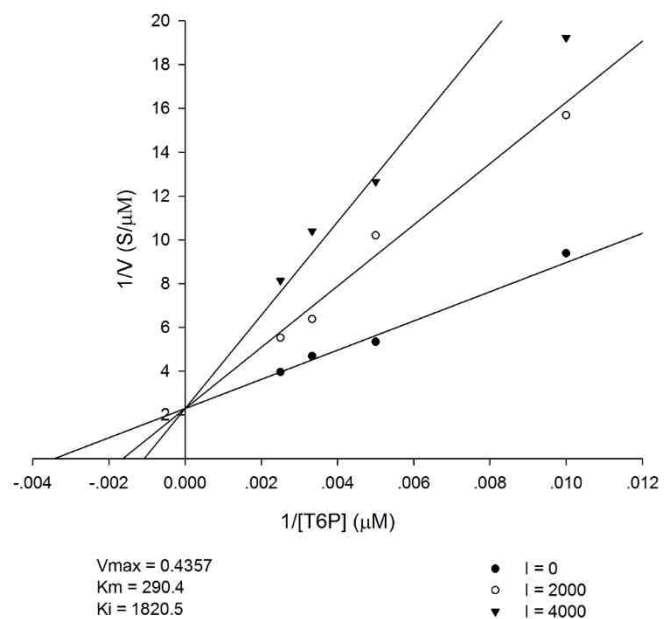
Enzyme: *Sb*-T6PP, Inhibitor: **8p**, $K_i = 13 \pm 2 \mu\text{M}$.



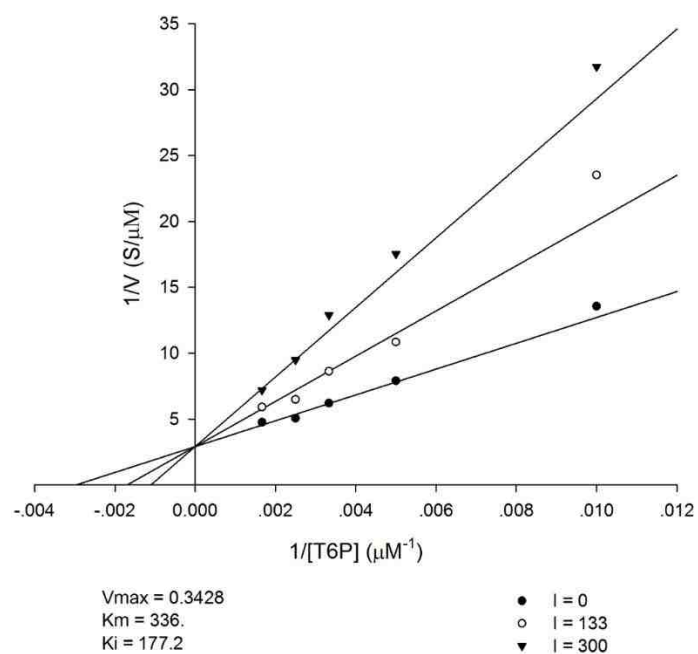
Enzyme: *Sb*-T6PP, Inhibitor: **9a**, $K_i = 21 \pm 3 \mu\text{M}$.



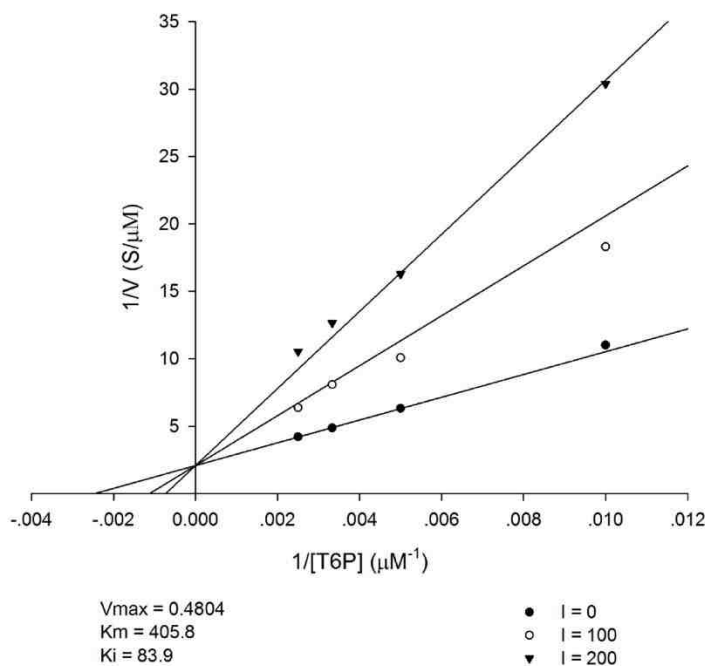
Enzyme: *Sb*-T6PP, Inhibitor: **9b**, $K_i = 78 \pm 9 \mu\text{M}$.



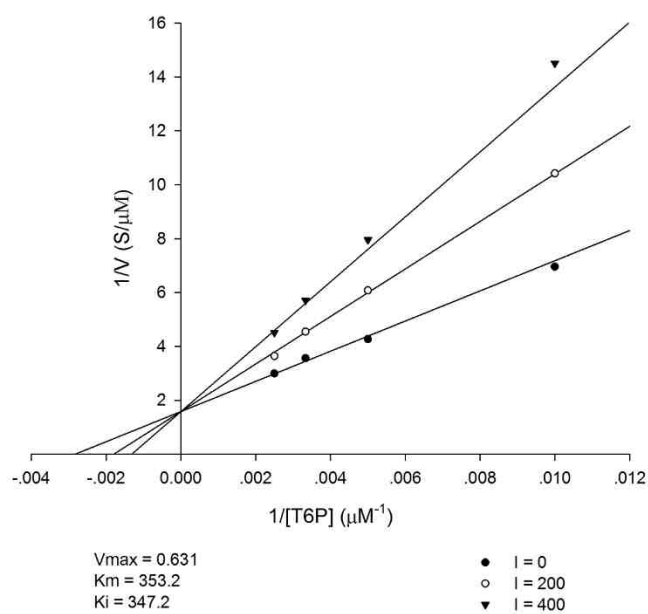
Enzyme: As-T6PP, Inhibitor: **8a**, $K_i = 1800 \pm 260 \mu\text{M}$.



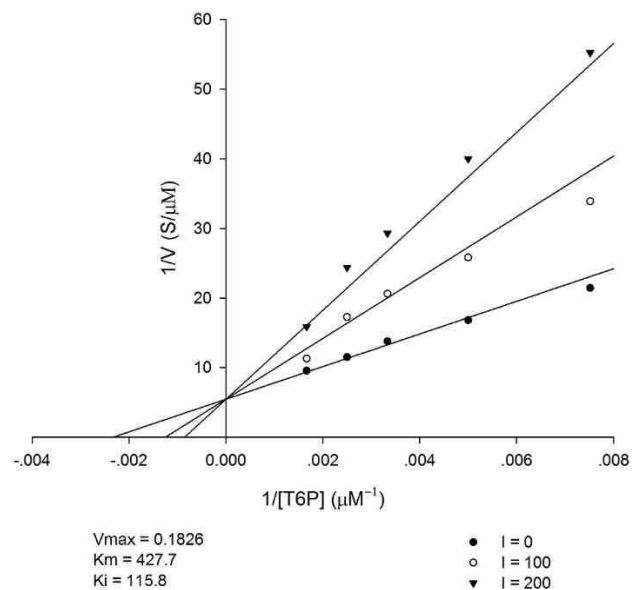
Enzyme: As-T6PP, Inhibitor: **8p**, $K_i = 180 \pm 20 \mu\text{M}$.



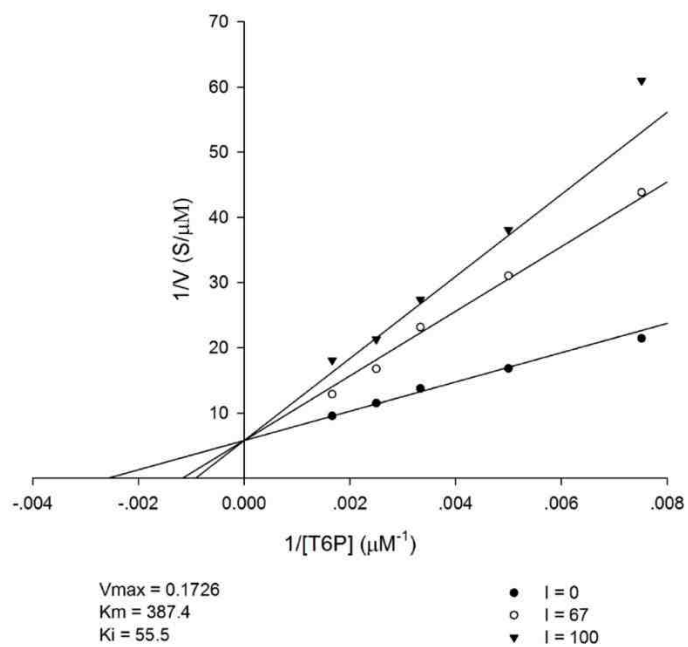
Enzyme: *As*-T6PP, Inhibitor: **9a**, $K_i = 84 \pm 10 \mu\text{M}$.



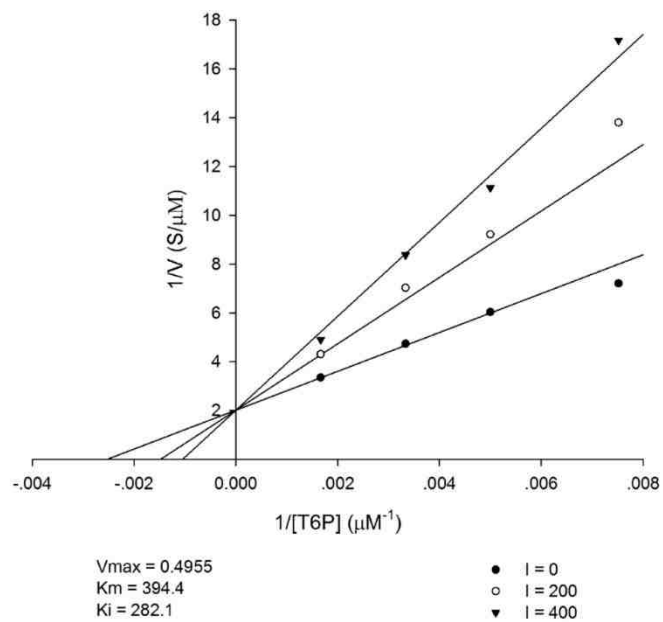
Enzyme: *As*-T6PP, Inhibitor: **9b**, $K_i = 350 \pm 30 \mu\text{M}$.



Enzyme: *St*-T6PP, Inhibitor: **8p**, $K_i = 120 \pm 20 \mu\text{M}$.



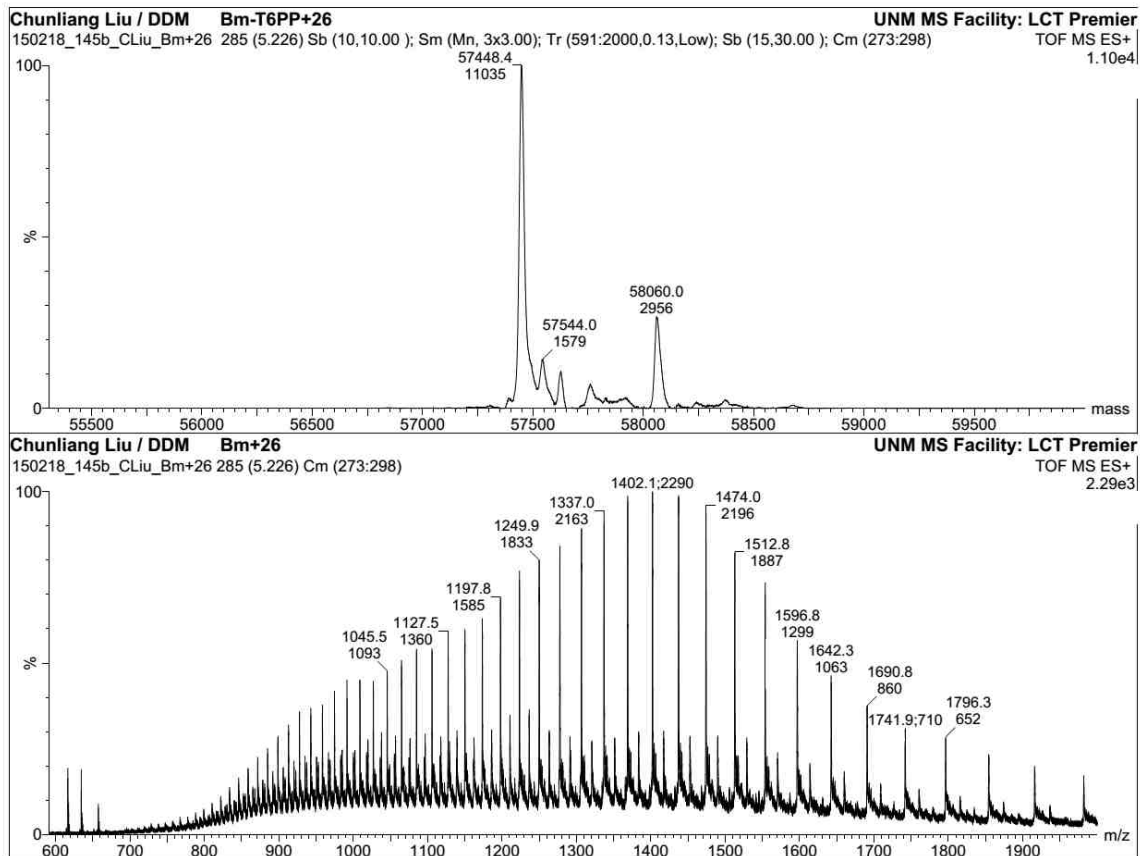
Enzyme: *St*-T6PP, Inhibitor: **9a**, $K_i = 56 \pm 6 \mu\text{M}$.



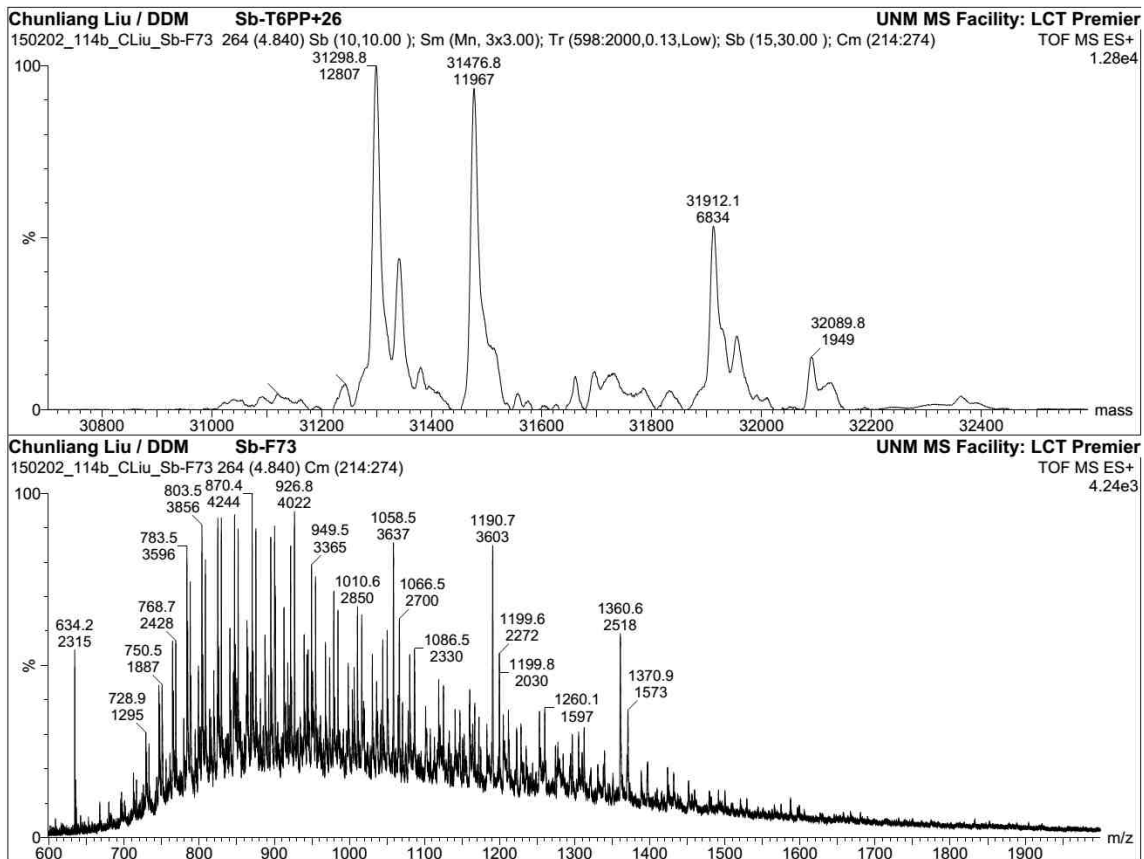
Enzyme: *St*-T6PP, Inhibitor: **9b**, $K_i = 280 \pm 30 \mu\text{M}$.

A.5 ESI mass spectra In Chapter Five

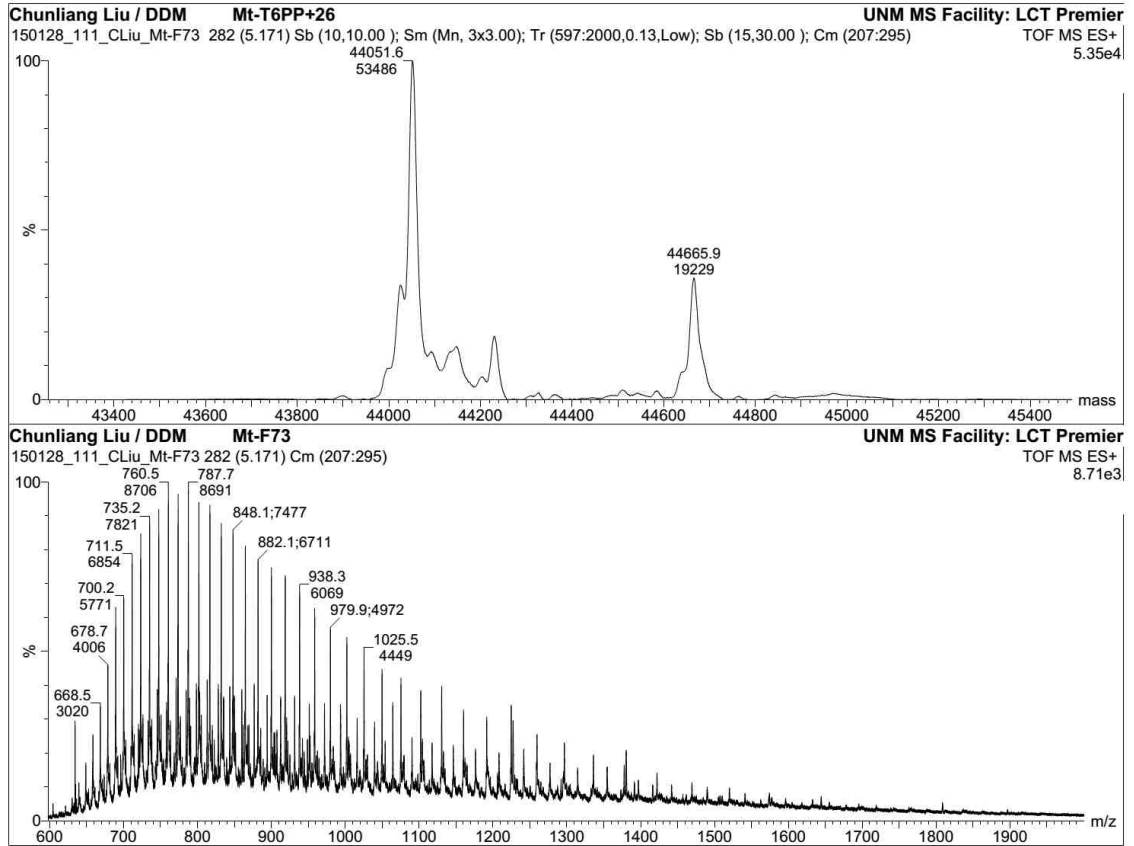
A.5.1 ESI mass spectra of Bm-T6PP treated with 26



A.5.2 ESI mass spectra of Sb-T6PP treated with 26



A.5.3 ESI mass spectra of Mt-T6PP treated with 26



A.5.4 ESI mass spectra of St-T6PP treated with 26

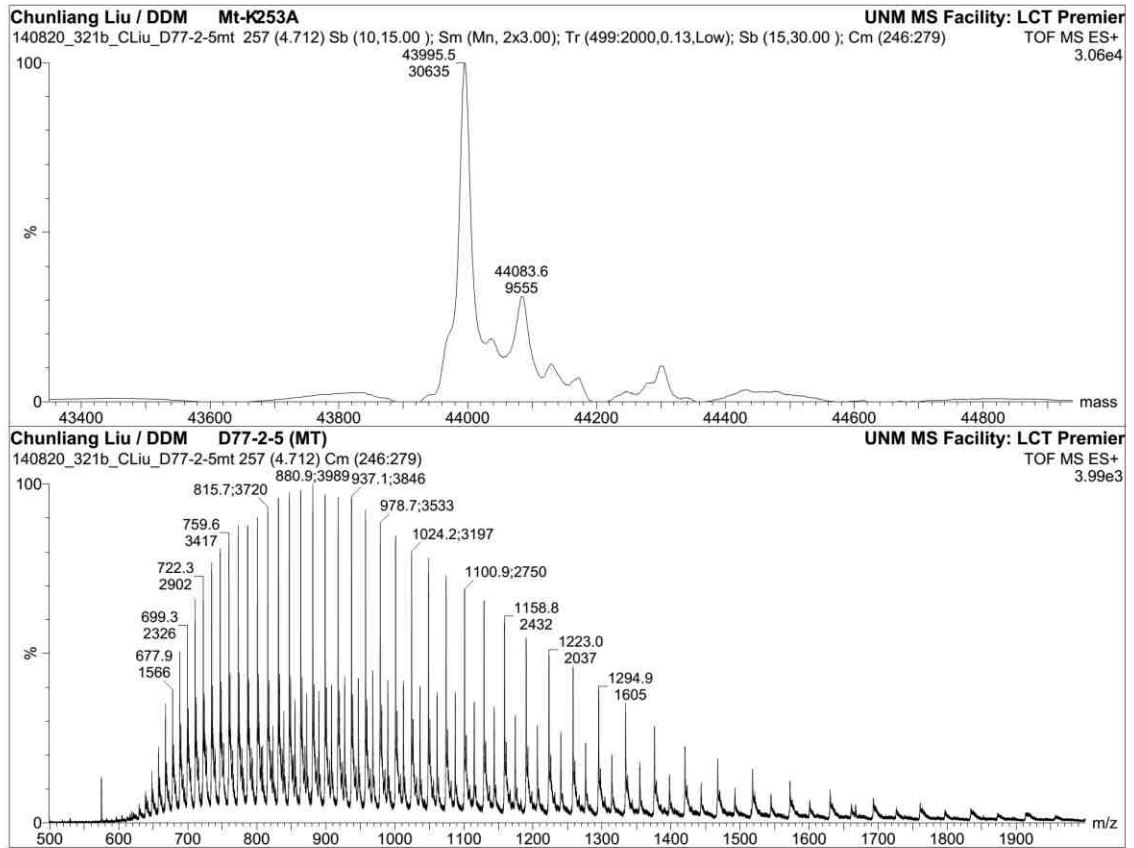


Trap CE = 4.0

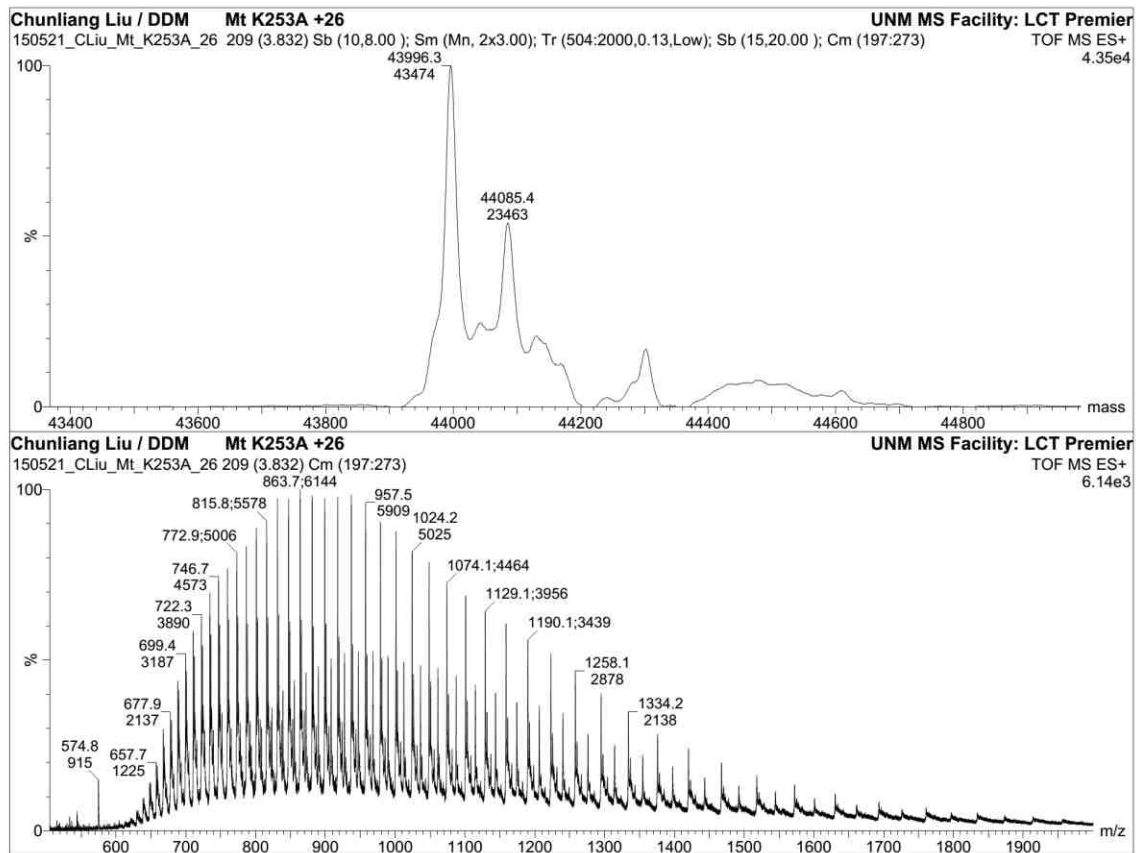
CL_UNM_St+26_intact 35 (0.667) M1 [Ev-564621.lt29] (Gs,0.100,587:2202,1.00,L50,R50); Cm (11:53)

1: TOF MS ES+
2.10e6

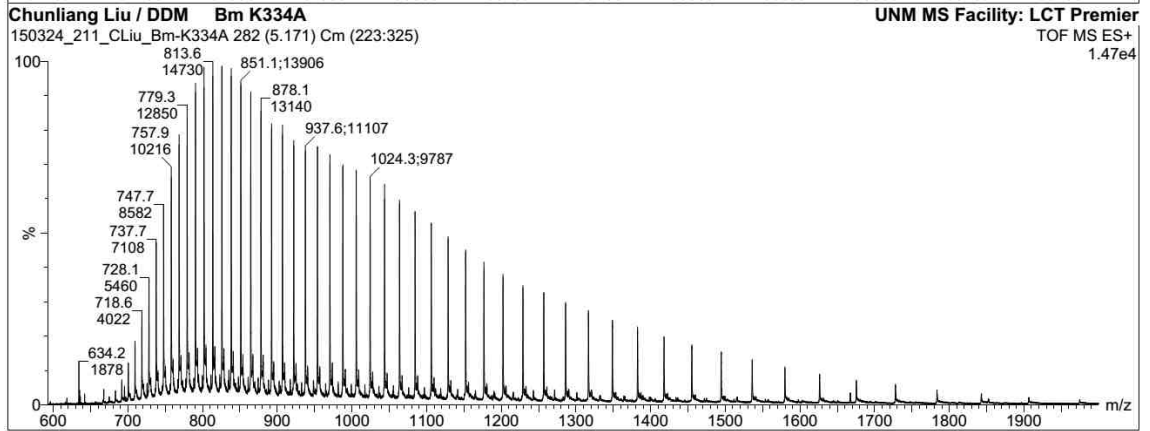
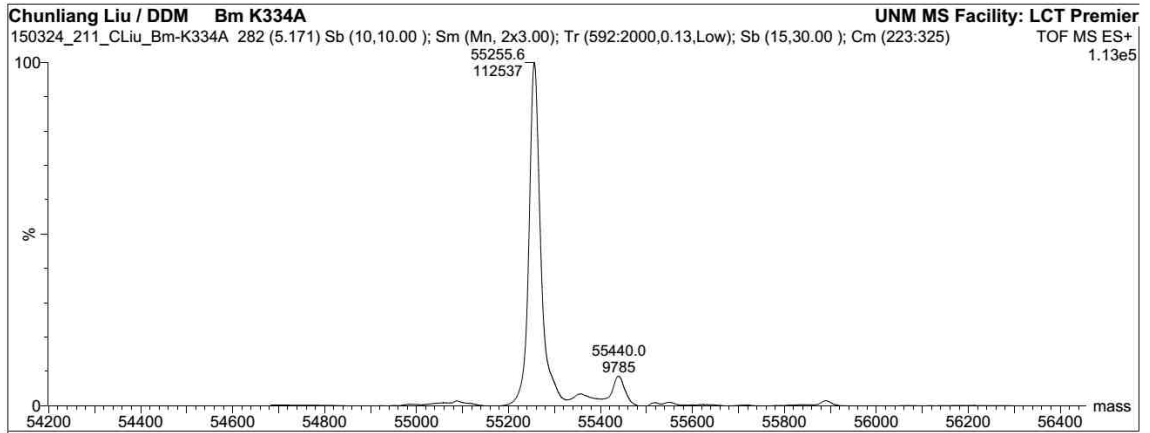
A.5.5 ESI mass spectra of Mt-T6PP-K253A



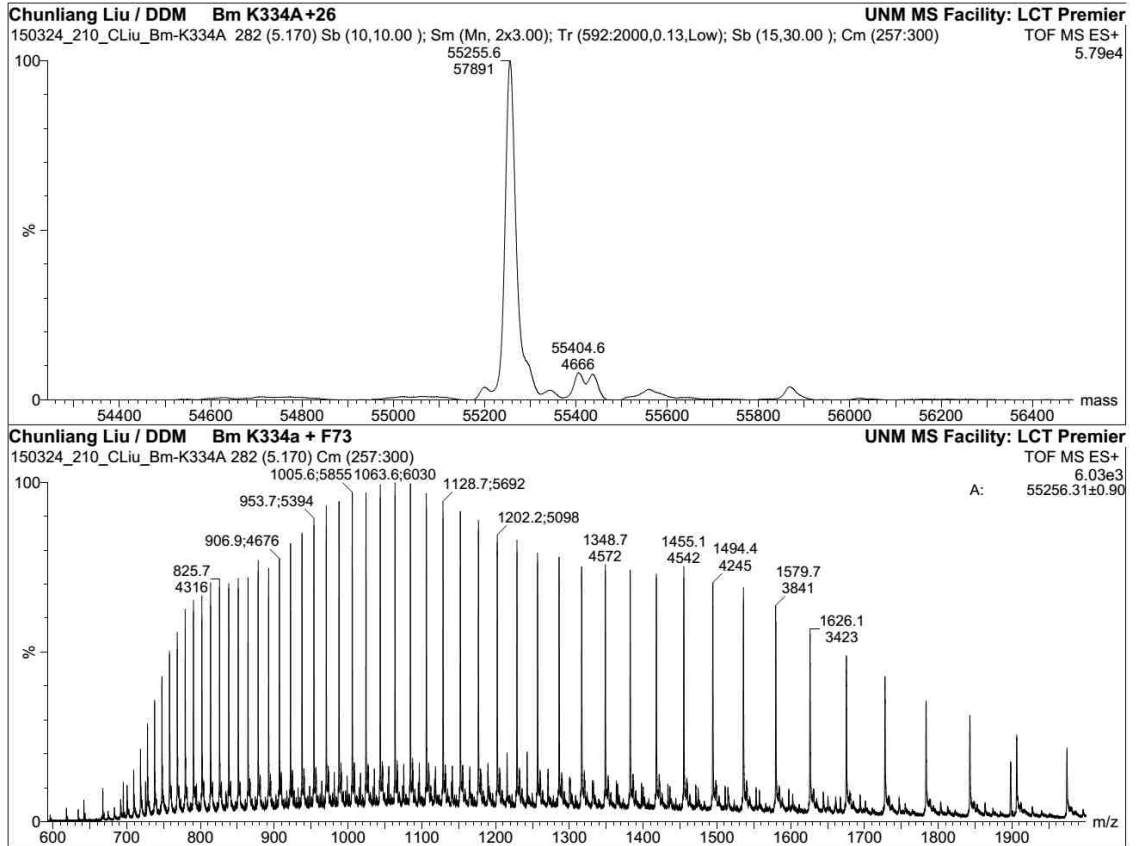
A.5.6 ESI mass spectra of Mt-T6PP-K253A treated with 26



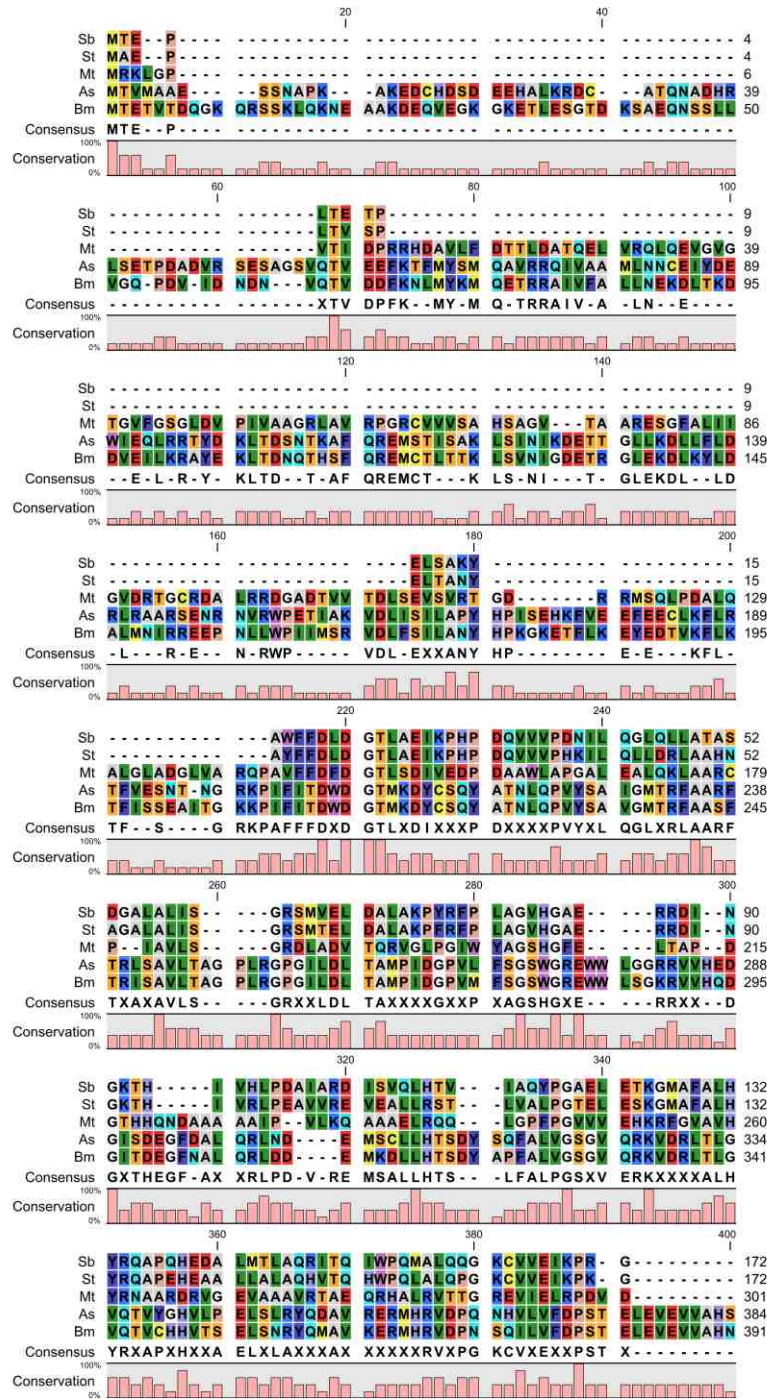
A.5.7 ESI mass spectra of Bm-T6PP-K334A



A.5.8 ESI mass spectra of Bm-T6PP-K334A treated with 26



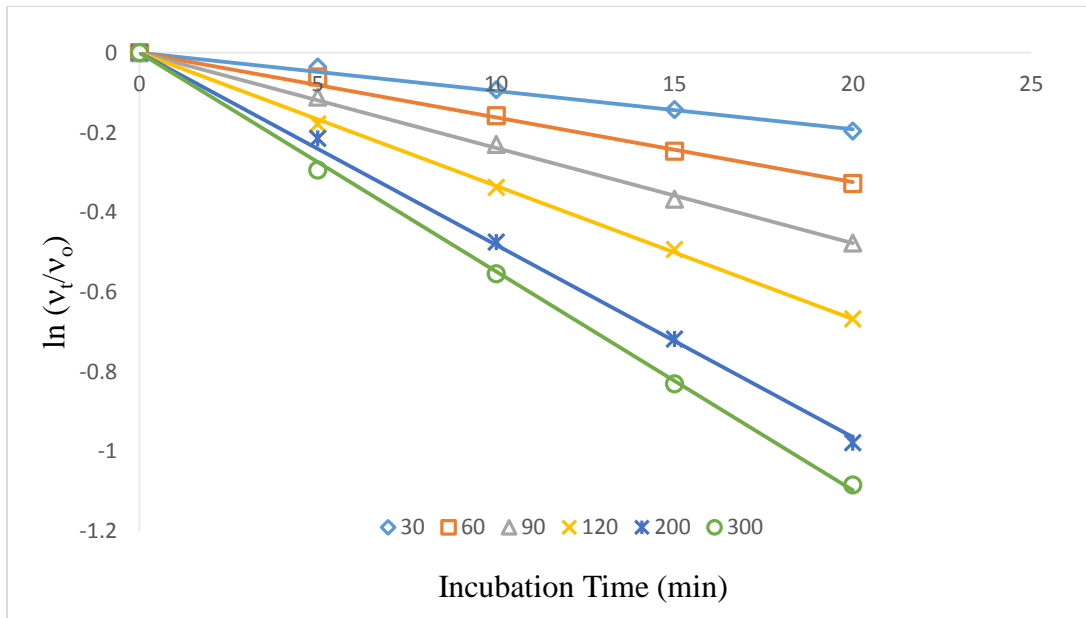
A.5.9 Sequence alignments of nematode and bacteria T6PP enzymes



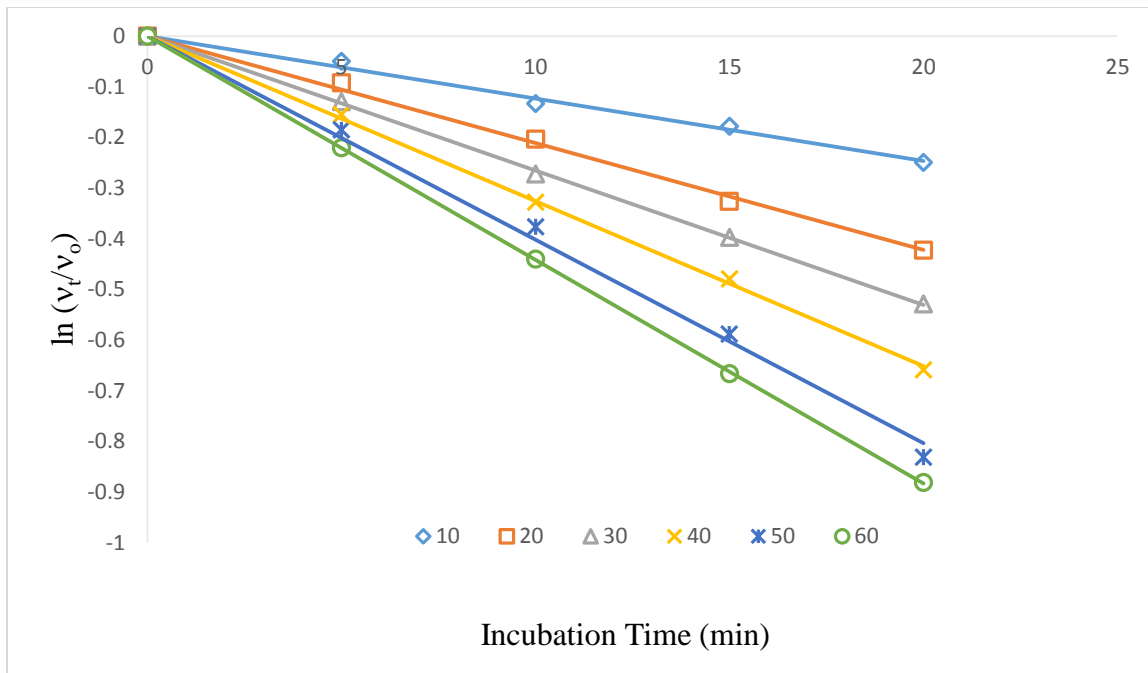


A.5.10 Plots of pseudo-first order rate constant for inactivation (k_{obs})

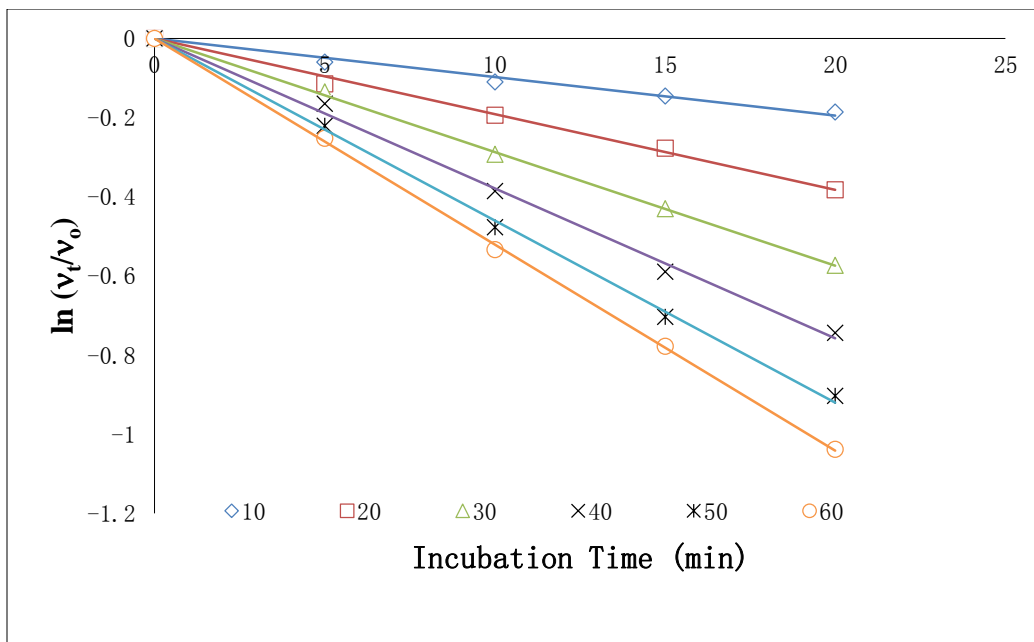
A.5.10.1 Plots of k_{obs} for 26 mediated As-T6PP inactivation.



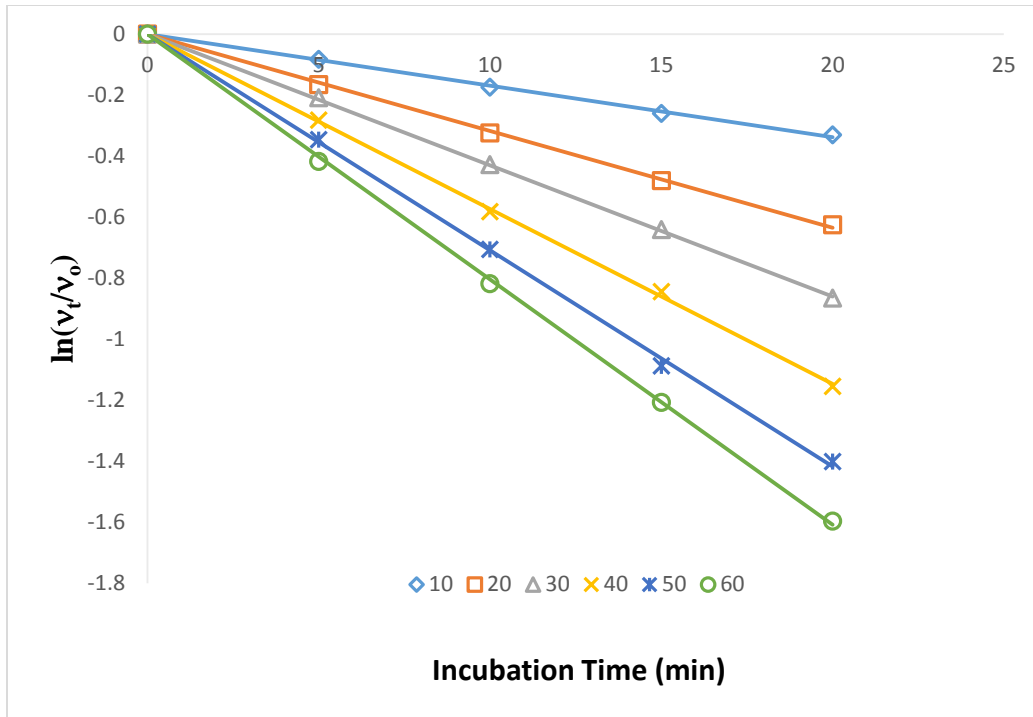
A.5.10.2 Plots of k_{obs} for **26** mediated Bm-T6PP inactivation.



A.5.10.3 Plots of k_{obs} for **26** mediated Mt-T6PP inactivation.



A.5.10.4 Plots of k_{obs} for **26** mediated Sb-T6PP inactivation.



A.5.10.5 Plots of k_{obs} for **26** mediated St-T6PP inactivation.

